Magnetic Core Losses

The PSMA-Dartmouth Studies

Pilot Project

Phase II Project

A Supplemental Report

by

Edward Herbert

Co-chairman,

PSMA Magnetics Committee

December 14, 2011

Revised January 4, 2012

Sponsored by

The Power Sources Manufacturers Association

email: power@psma.com

http://www.psma.com/

P.O. Box 418

Mendham, NJ 07945-0418

Tel: (973) 543-9660

Fax: (973) 543-6207

Table of Contents

Prologue

The study of core losses began with dissatisfaction with available SPICE models for saturable cores.

A SPICE model must work with "real" parameters, volts, current, and time. This led to questioning the use of magnetic parameters for calculating core losses. For an electrical engineer, volts, seconds and amperes are much more meaningful than webers, teslas, gauss and oersteds. A simplified representation is much easier to use and avoids errors of using unfamiliar parameters and converting them.

An early hypothesis [1] was that that square wave core loss data expressed as voltage and pulse width could be used to reconstruct low duty-ratio losses. Testing this hypothesis was the premise of the *Pilot Project*, a study sponsored by PSMA at Dartmouth under the direction of Dr. Charles Sullivan.

The *Pilot Project* showed that the "*composite waveform hypothesis"* was an improvement both for ease of use and for accuracy. However, testing with low duty-ratio waveforms showed that it was incomplete. There were unexplained additional losses per cycle with low duty-ratio waveforms.

Dr. Sullivan presented a paper at APEC2010, *Core Loss Predictions for General PWM Waveforms from a Simplified Set of Measured Data* [3]

A paper by Jonas Mühlethaler, et al, Power Electronic Systems Laboratory, ETH Zurich, Switzerland*, Improved Core Loss Calculation for Magnetic Components Employed in Power Electronic Systems*, APEC 2011, [2] attributed the additional losses to a "relaxation process," and a method of estimating the losses was given.

The *Phase II Project,* sponsored by PSMA, continued the core loss study at Dartmouth. More cores were tested and a massive amount of data was taken. The added loss per cycle with low duty-ratio waveforms was confirmed. Drilled cores with sense windings explored the possibility of flux migration, with interesting but inconclusive results.

Introduction

Objective of this report:

This supplemental report can be downloaded as a pdf document at
http://www.psma.com/coreloss/supplement.pdf

This report is supplemental, and has several purposes:

1. A brief narrative describing the Pilot Project and the Phase II Project, giving the objectives, their execution and conclusions.

2. The project reports are included as Appendix A.

3. A description of the data generated. A brief description is in the report with a more complete description as Appendix B.

4. A description of the tools used for this report. A brief description is in the body of this report, with more complete descriptions in the appendices:

   Appendix C, The Excel Tool

   Appendix D, The SPICE Tool

   Appendix E, The CAD Tool

5. Further analysis of the data. A brief description is in the body of this report, with more complete discussions in the appendices:

   Appendix F, Off-time Core loss Phenomenon

   Appendix G, Expand Data

   Appendix H, Hippo Data

   Appendix I, Drilled Core Data

   Appendix J, Simple SPICE Model

6. Identify subjects for future study.

   The "Wish List" for future projects is at the end of this section.

Summary

This report further analyzes the data from the *Pilot Project*, the *Phase II Project* and information from J. Mühlethaler's paper [2].

Key conclusions are:

1. Increased off-time does increase the energy loss per cycle, but mostly the off-time provides a window of opportunity to see and identify some loss factors while other loss factors are reduced or absent.

2. The test circuit and protocol can influence losses, including off-time losses. However, these influences are present in practical circuits as well, and they need to be identified and quantified. It is therefore not valid to dismiss them as "test rig artifacts."

3. Energy going into a magnetic core is divided between "burned energy" and "stored energy." Separating them is daunting.

    a. Burned energy probably can be quantified quite well (but not entirely) using the composite waveform hypothesis.

    b. Stored energy carried forward reduces the net input current and thus the input power and energy per cycle.

    c. The loss of stored energy significantly influences core losses. It is attributable to the core characteristics (delayed burned energy); the external circuit (or test rig); and the test protocol (waveform).

    d. Some losses may be impulses or spikes, at the switching time, and thus are analogous to switching losses.

    e. Stored energy loss is particularly difficult to quantify in a simple expression. It is unlikely to be quantifiable as a material characteristic.

4. Determining the stored energy carried forward from pulse to pulse and the loss of that stored energy is essential to improving the estimation of core loss and improving circuit performance.

5. Equations such as the familiar Steinmetz equation and its many enhancements become complicated to the extent that their general use is unlikely. At least five loss mechanisms must be accounted for as well as the influences of the external circuit and waveform.

6. It must be concluded that the *composite waveform hypothesis* is a failure, at least as applied to high frequency core losses. That it compares well with other models is pointless if its results have large errors at low duty-ratio.

7. Using the "hippo" waveform to analyze core losses may be the most significant accomplishment of the Phase II project. The hippo waveform is unlikely to be used for practical power converters, but its use for analysis is brilliant.

8. The most promising way to characterize core losses may be as an impedance.

9. Characterizing a specific core or a specific wound component is better (more accurate, easier to use) than characterizing a material.

10. An impedance model can be used for improved SPICE simulations.

A working hypothesis is that if the hysteresis loop can be faithfully reproduced using an impedance model for various waveforms, the loss estimations will be as good as the match of the areas within the hysteresis loops. Because a very important factor is the stored energy and its loss, faithfully reproducing the current during the off time of low duty-ratio waveforms is important.

Impedance models are familiar turf for an electrical engineer. Measuring them is fundamental to circuit analysis. Quantifying them both in the time and frequency domain is fundamental to stability analysis. Synthesizing them is fundamental to the design of filters and compensation networks. This expertise can be applied to modeling the magnetic core. Overkill should be avoided. A simple model may suffice for most applications.

One must not lose track of the fact that a model is an analogy. It may not reveal much about the physics of what is happening in the core.

The Pilot Project

The Pilot Project was approved by PSMA and a purchase order to Dartmouth was issued in the Spring of 2009.

The Pilot Project was constrained by the existing test equipment and by time and budget limitations. When there is mention of things not accomplished in the Pilot Project, it emphatically is not a criticism of Dartmouth. They did an outstanding job considering the constraints and significantly advanced our understanding of core losses. Things not accomplished are mentioned only as a wish list for future projects.

Objectives

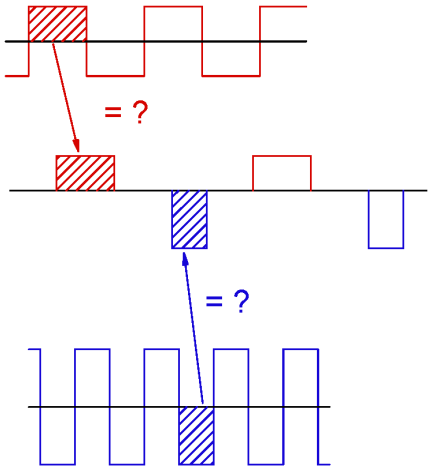

The objective of the Pilot Project was to test a hypothesis [1], later named the "*composite waveform hypothesis.*" The hypothesis was that loss data taken for a square wave excitation with a certain voltage and pulse width could be used to estimate the core loss of any excitation having rectangular pulses of the same voltage and pulse width even if the duty-ratio is lower. Further, if the excitation is not symmetrical, different square wave data could be used for the different parts of the excitation, matching pulse widths and voltage.

Data was taken on one ferrite core and one powdered metal core. The composite waveform hypothesis was partly validated, and shown to be an improvement over other approximations, both for accuracy and for ease of use.

Off-time losses

With lower duty-ratio excitation, the energy per pulse was higher than in a square-wave, and the loss per pulse increased with increasing off-time.

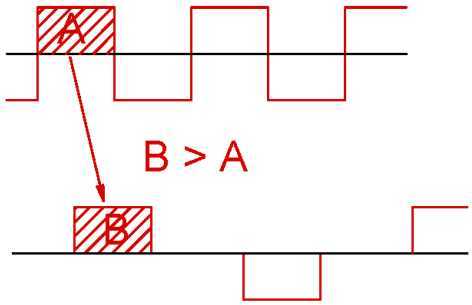

Ferrite core

The off-time effect was more pronounced in the ferrite core. The effect was quite strong, with energy increases as much as 30 percent.

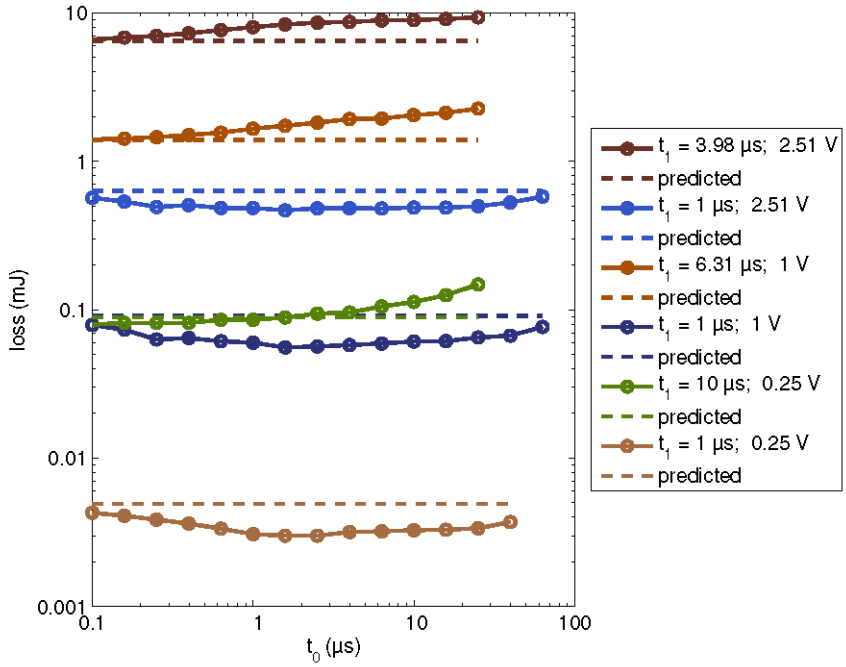

A lot of work was done taking extensive data and ensuring to the extent possible that the effect was not due to test rig anomalies.

Hysteresis loop

Losses in a core are well demonstrated as the area of its hysteresis loop, and illustrations in the Pilot Project report showed that the hysteresis loop increases in area as the off time is increased. One of the illustrations is copied and pasted below.

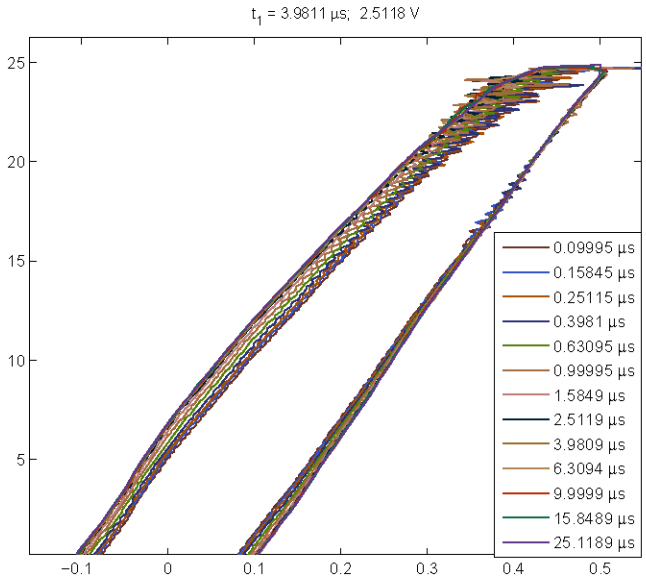

Close inspection shows that the loss per cycle increases with increased off time, but the effect is limited. Eventually, further increasing the off-time has little effect.

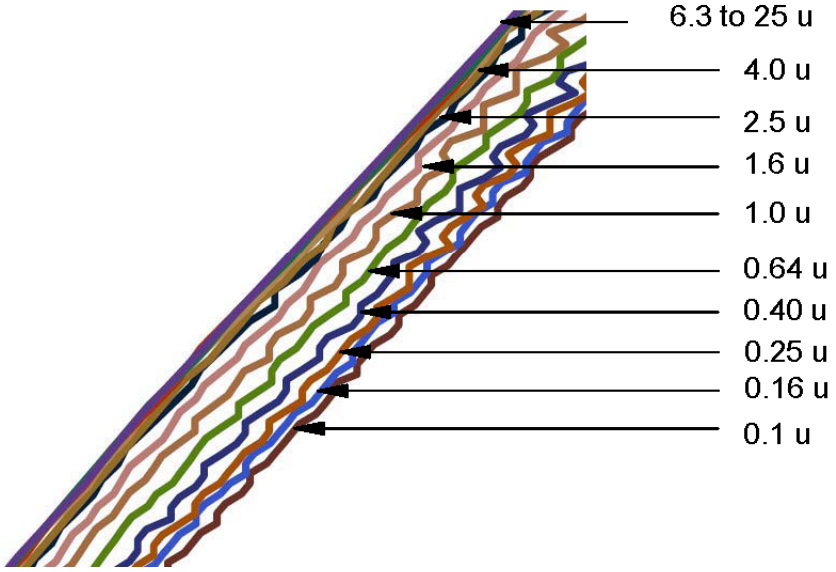

Powdered iron core

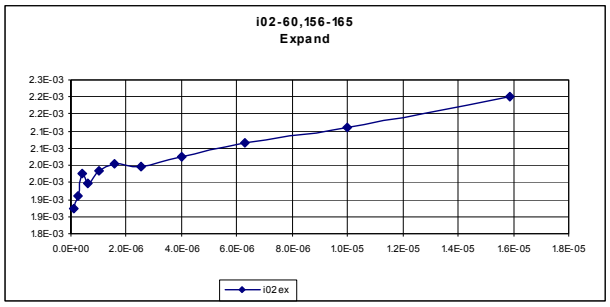

The off-tine loss effect is lower in powdered iron cores, but still significant at higher excitation levels.

Skewed and symmetric wave shapes

A lot of data was taken with skewed and asymmetrical excitation. A blocking capacitor was used, and that makes these data difficult to interpret. The excitation of a magnetic core must have balanced volt-seconds, to avoid flux walking and saturation effects, and a blocking capacitor can ensure balanced excitation. Unfortunately, it also forces balanced ampere-seconds (equal coulombs), and some wave shapes do not naturally have balanced currents.

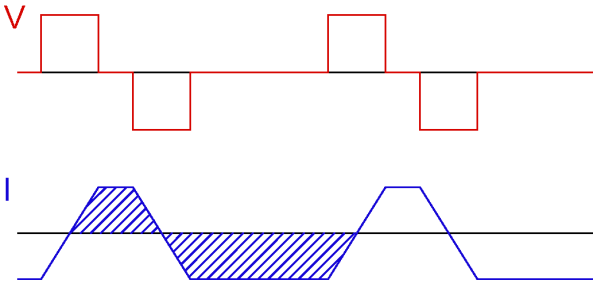

The graph above shows a generic skewed excitation and the expected current for an ideal inductor. It is obvious by inspection that the ampere-seconds are not equal if unconstrained. The conclusion is that the blocking capacitor badly distorts the current, invalidating the tests. Accordingly, no skewed data was used for this report. The case for the asymmetric waveform is not as clear. Nonetheless, I regard asymmetric test data as suspect and did not use asymmetric data either.

For further discussion, please see Appendix F, Off-time Core-loss Phenomena.

Noise

f13-010.csv

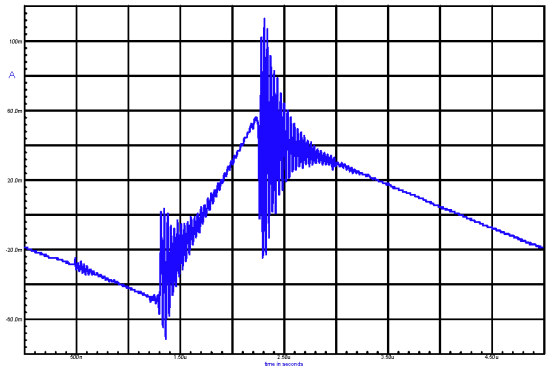

Ringing in the current measurements is a significant problem, particularly at lower excitation levels. This reflects into the hysteresis loops and other measurements. However, the flux and energy are integrated parameters, so the ringing tends to be filtered out. As an example, the loss is represented by the area of a hysteresis loop. If a ring about a nominal value has equal area, plus and minus, the net area is unchanged. While absolute accuracy may be questioned, the qualitative results probably are valid.

f13-010.csv

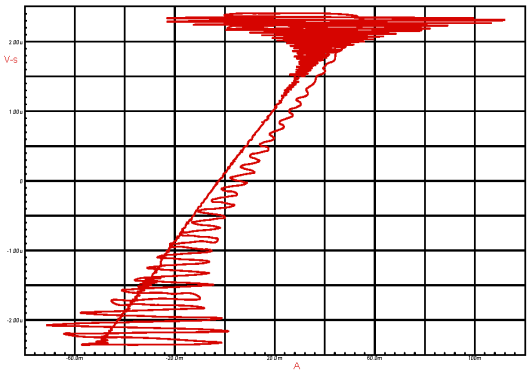

Phase II Project

The Phase II Project was approved by PSMA and a purchase order to Dartmouth was issued in the Spring of 2010.

The Phase II Project was constrained by the existing test equipment and by time and budget constraints. When there is mention of things not accomplished in the Phase II Project, it emphatically is not a criticism of Dartmouth. They did an outstanding job considering the constraints, and significantly advanced our understanding of core losses in ferrites. Things not accomplished are mentioned only as a wish list for future projects.

Objectives

The Phase II project had two principle objectives:

1. To test the composite waveform hypothesis on a variety of cores of different materials, with emphasis on ensuring that the off-time loss phenomenon was not just a test rig or test procedure artifact.

2. To test a core that had been drilled through with sense windings installed, to see if flux migration may contribute to the off-time loss phenomenon.

Largely, the Phase II project was to confirm and expand the conclusions of the Pilot project, so very similar test protocol was used

Off-time losses

The off-time losses were confirmed for a variety of different materials. See Appendix F, Off-time Core-loss Phenomena for further details.

During excitation, energy is stored in the magnetic core as $E = \frac{1}{2} I^2 * L$

A distinct decrease in the current is apparent after the voltage goes to 0 V, and the time constant appears to be consistent with the off-time loss phenomenon. Thus, the working hypothesis is that energy is dissipated during the off-time. The current of the stored energy superposes on the applied current, reducing the current and thus the input power and energy per cycle. This loss is less using square-wave excitation. As the off-time increases, the current decays, requiring more current, and thus more energy, in subsequent cycles.

Further confirmation is found in a paper by Jonas Mühlethaler [2], though his different time constant is unexplained.

A discussion of the off-time losses is in Appendix F, Off-time Core Loss Phenomenon.

Expanded waveform

There is a very good presentation of losses per cycle for expanded waveforms by material in the report. No supplement is needed for that data.

The figure below shows the expand on-time and voltages to scale for the various cores tested. The flux in µV-s is shown.

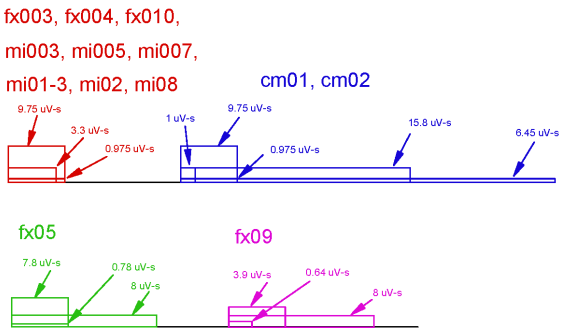

There is no expand data at all for the amorphous iron core, pt01.

The different core materials have different losses, and low loss materials have a corresponding lower loss during the off-time. These data are remarkably similar. This may raise some question whether the great similarity reveals a common external cause such as a test rig or test procedure artifact.

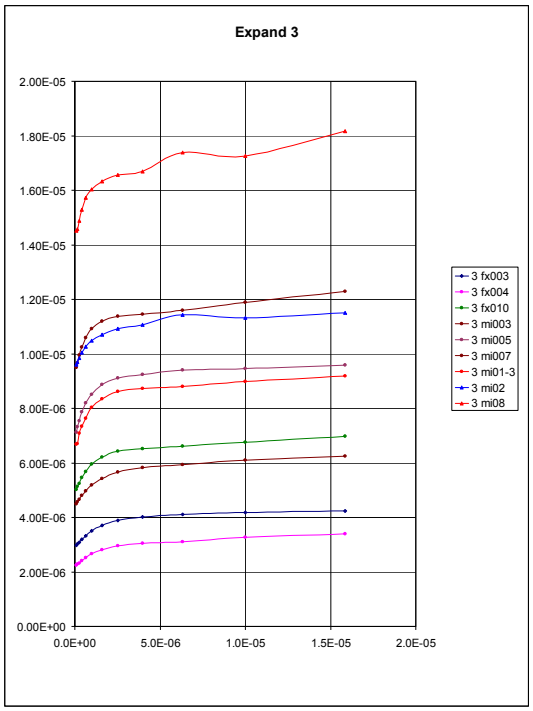

Additional graphs are in Appendix G, Expand Data. A discussion of the off-time losses in expanded waveforms is in Appendix F, Off-time Core Loss Phenomenon.

Skewed and asymmetric wave shapes

A lot of data was taken with skewed and asymmetrical excitation. A blocking capacitor was used, and that makes these data difficult to interpret. The excitation of a magnetic core must have balanced volt-seconds, to avoid flux walking and saturation effects, and a blocking capacitor can ensure balanced excitation. Unfortunately, it also forces balanced ampere-seconds (equal coulombs), and some wave shapes do not naturally have balanced currents.

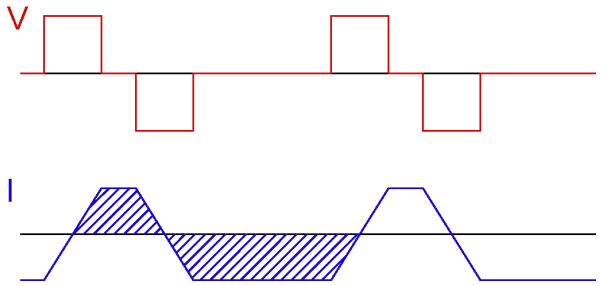

The graph above shows a generic skewed excitation and the expected current for an ideal inductor. It is obvious by inspection that the ampere-seconds are not equal if unconstrained. The conclusion is that the blocking capacitor badly distorts the current, invalidating the tests. Accordingly, no skewed data was used for this report. The case for the asymmetric waveform is not as clear. Nonetheless, I regard asymmetric test data as suspect and did not use asymmetric data either.

For further discussion, please see Appendix F, Off-time Core-loss Phenomena.

See Appendix G, Expand Data.

Hippo waveform

The introduction of the "hippo" waveform may be the most important success of the Phase II project. It is unlikely to have a practical use in power converters, but its introduction as an analytical tool is brilliant.

If a positive voltage excitation pulse is immediately followed by a negative pulse of equal magnitude and pulse width, the current ideally ramps up, then ramps down the same amount, returning to 0 A, a condition where there is no stored energy and thus no residual current carried forward to the next cycle. Thus no off-time loss is expected.

The "Hippo" waveform is very useful for analysis, because it shows the magnetizing current with no energy carried forward in the first pulse, followed by an equal and opposite pulse in which the energy carried forward is maximized. For more detail, please see Appendix F, Off-time Core loss Phenomenon and Appendix H, Hippo Data.

Blocking capacitor investigation

A quite significant change in the energy per cycle was seen when a different blocking capacitor is used. There turned out to be a simple explanation; the temperature of the core was different. Before the cause of the difference was known, exploring the difference in loss led to a much more detailed look at the data and wide ranging speculation; some of this proved to be pivotal.

There is more discussion regarding the blocking capacitor investigation in Appendix F, Off-time Core-loss Phenomena.

Drilled core tests

One hypothesis for the off time loss was that the flux in the core might change state after the excitation is removed. With approximately zero nominal volts during the off-time, the total flux would not be expected to change significantly, but the flux could migrate within the core from one region to another. The drilled core experiments showed that while there is some flux migration, the timing is such that this hypothesis is not substantiated.

The drilled core tests were proposed to see if the flux migrated in unexpected ways as excitation was applied and after it was removed. Several possibilities were considered, generally suggesting that flux might follow one path when it is dynamic, then relax to a different path under stable conditions.

One possibility was that flux might be more diffuse dynamically, then settle to a more classical radius dependent distribution at rest. To test this hypothesis, a core was drilled through so that test windings could be inserted. Originally, it was planned to drill four holes from each direction (side to side and outside to inside). A scheme was developed to allow intersecting wires to make an internal connection. If implemented, flux change (voltage) of any of 25 cross-sectional areas could be isolated.

A vendor had promised to supply the drilled core for test, but was unable to perform, so John Harris had to make arrangements himself. Drilling proved to be much more difficult that thought, so the compromise was to drill only two holes from each direction. Time and budget constraints also prevented taking data with intersecting wires.

Another hypothesis was that the extreme angle of the winding on the core might have a transverse magnetic field, causing the flux to have a spiraling path within the core during excitation, and that it might relax to a straighter (thus shorter) path while resting. To test this, it was planned to drill two intersecting holes from the outside diameter. With linear flux, there would be no flux through this probe winding, and any sensed voltage would indicate a transverse or spiral component. Unfortunately, drilling these holes proved to be too difficult and the test was never run. Since then, some winding arrangements with no transverse component have been developed and may be considered for a future test. These include some error correcting techniques borrowed from Rogowski coils.

While there is some flux migration, the timing is such that this is not a likely source of the off-time core loss phenomenon. The observed flux migration may correlate with dimensional resonance as explained well in the Phase II report. As frequencies increase, dimensional resonance may become important. On the other hand, higher frequency cores probably will have smaller dimensions and better damping due to the higher losses.

Further information is in Appendix I, Drilled Core Data.

Noise

Noise in the current waveform continues to be a problem. However flux and energy are integrated parameters, so the noise tends to be filtered out, and the qualitative results probably are valid.

Demagnitizing tests

There was some concern that remnant flux might affect the test results, so some effort was made to ensure that the core was demagnetized. This is a valid concern, as remnance caused by dc bias is known to affect losses in some cores. Testing showed no difference, tending to validate the testing done without demagnitizing procedures.

Sampling errors

The sampling scheme for both the Pilot project and the Phase II project comprised 1000 samples per cycle regardless of the period. This works well for relatively short periods. As an example, with a 40 μs period, the sampling period is 40 ns.

Some test periods are as long as 2 ms, with many in the order of 1 ms. Even with a 500 μs period, the sampling period becomes 500 ns, obscuring meaningful data at the transitions.

The sampling also is a problem with low duty-ratio waveforms, especially the hippo waveform, where there are four pulses per period. With a duty-ratio of 10 percent, there are 100 samples during active excitation. With the hippo waveform, that becomes 25 samples per pulse. At 5 percent duty-ratio, it is 12.5 samples per pulse, impossible as it must be an integer.

Sampling anomalies may account for peculiar behavior at extended periods.

Composite waveform hypothesis

The composite waveform hypothesis is reported to be more accurate and easier to use than other algorithms for core losses, particularly low duty-ratio pulses. Nonetheless, errors are commonly 30 percent and as much as 50 percent. The inescapable conclusion is that it is a failure for core loss analysis, at least at high frequencies.

Steinmetz-like equations and their application

The Steinmetz model was developed at a time when time-independent core losses dominated. At low frequencies, given a flux density, the losses were predicted fairly well regardless of the frequency, and an added correction term for frequency made the model fit quite well over a reasonable range of interest.

A failing of the Steinmetz approach is that it requires integrated parameters, so no result is possible until the cycle is done, and there is no information about what the losses are as excitation is applied and time progresses. Substituting Volts and seconds (V-s) for flux does not alter this flaw.

The Steinmetz equations and its derivatives are fundamentally a curve fitting exercise. Any formulae that spit back the loss when the parameters are entered would do as well, and one sees other expressions such as polynomials from time to time. The more constrained the range of operation, the more successful the curve fit can be.

Like Ptolemy's algorithm for celestial motion, the model can be improved with "epicycles," then "epicycles on epicycles." We tend to forget that algorithms and models are analogies and may teach very little about what is happening physically.

For years, the Steinmetz equations were patched up by using different parameters for different frequency ranges, but still the accuracy is poor. As it is patched up more and more, the expressions get increasingly complex and the number of parameters proliferates until their use is so cumbersome as to be of little use for routing application. Like Ptolemy in view of Copernicus, Galileo and Kepler, it may be time to move on.

Even with multiple patches, the ability to adapt to different excitation waveforms is poor, especially at low duty-ratios. I see no way that it could ever capture the influence of external circuit characteristics.

Simple SPICE model

A simple SPICE model is described in Appendix J, Simple SPICE Model. A modification of the model is used in the analyses of Appendix F, Off-Time Core Loss Phenomena. The accuracy is fairly good for expanded waveforms. It fails when applied to the hippo waveform, with errors of 20 percent, which is better than the composite waveform hypothesis. The hippo waveform may be a better basis upon which to construct a model, with refinements then made for other waveforms. How that will evolve is speculation at this point.

Presently, developing a SPICE model on one waveform, then refining it on others is like playing "Whac-a-mole". However, I am confident that a protocol of test waveforms can be found that will lead to an orderly identification of model component parameters. The simple model does quite well with inductors and resistors. There is an observed high frequency effect that will very likely add an R-C network. There is some suggestion that

the principle inductor may be flux-level dependent, easy enough to add to a SPICE model.

As an impedance model, the SPICE model for core loss responds appropriately to different excitation as well as external circuit parameters, as long as the parasitic impedances are included.

The blocking capacitor investigation looked at an unexplained loss variation that turned out to be a temperature dependence. Without much analysis, it is easy to see in the hysteresis loop that the principle resistor has a fairly large positive temperature coefficient and the principle inductor has a fairly small negative temperature coefficient (maybe consistent with μ going to zero a the Curie temperature.

Although just a hypothesis for now, one that is not yet well developed, I think that it has great promis.

The Reports

Composite wave-form hypothesis

User-friendly Data for Magnetic Core Loss Calculations, Edward Herbert, Canton, CT. November 10, 2008.

This document is in Appendix A, and can be downloaded at
http://www.psma.com/coreloss/eh1.pdf

Pilot Project

Testing Core Loss for Rectangular Waveforms, February 7, 2010 by Charles R. Sullivan and John H. Harris, Thayer School of Engineering at Dartmouth and Edward Herbert.

This document is in Appendix A, and can be downloaded at
http://www.psma.com/coreloss/pilot.pdf

Phase II Project

Testing Core Loss for Rectangular Waveforms, Phase II Final Report, 21 September 2011
by Charles R. Sullivan and John H.Harris;
Thayer School of Engineering at Dartmouth

This document is in Appendix A, and can be downloaded at
http://www.psma.com/coreloss/phase2.pdf

Two other important documents are:

Using the PSMA Rectangular Waveform Core Loss Data, 8 August 2011,
by John H.Harris, Thayer School of Engineering at Dartmouth.

This document is the user manual for the PSMA core loss data set. It explains the directory layout, file naming conventions, and file formats.

This document can be downloaded at
http://www.psma.com/coreloss/use2.pdf

Measuring Core Loss for Rectangular Waveforms; Draft rev 168.53; *June 18, 2011,* by John H. Harris

This document goes into much more depth about the test procedures and programs used to take the data for this project.

This document can be downloaded at
http://www.psma.com/coreloss/measure2.pdf

The Data

In general, the data is provided both as zip files, for convenient download and as expanded files, for convenient browsing.

Pilot Project Data

The data for the Pilot Project can be downloaded at
http://www.psma.com/coreloss/pilot/

There are three sub-directories,

1. Characterization-data
2. Ferrite-data
3. Powdered-iron-data

The contents of the directories and files are explained in Appendix B, The Data.

Phase II Project Data

The data for the Phase II Project can be downloaded at
http://www.psma.com/coreloss/phase2/

There are three sub-directories,

- Cores
- Sets
- Zips

The contents of the directories and files are explained in Appendix B, The Data

Using the data

For those who are familiar with SQLite, the database files may be useful (Phase II Project only). There is a good extension to the Firefox browser that I used to view the files. The coreloss.db file contains a number of calculated values determined using MatLab.

I preferred using the .csv files, partly because it is necessary for the Pilot Project data but mostly because I wanted to process the data for export to SPICE, and it is necessary to convert the negative times. It is easy to do that and to do other calculations in spreadsheets. An Excel Tool was developed for this purpose, as explained in Appendix C, The Excel Tool–Viewing the Data.

Wish list for future projects

Testing of the amorphous iron core

In the present data, there are no tests with either expanded waveforms or hippo waveforms.

Testing powdered iron cores

In the Pilot project report, it was incorrectly reported that the core loss phenomenon did not occur with powdered iron cores, so they were not included in the Phase II testing.

A closer look shows that while less, the off-time effect is present. Accordingly, powdered iron in greater variety and other cores should be added to future tests.

Testing at higher frequencies and different waveforms

This requires new test equipment.

Asymmetrical waveforms are important in practical circuits, and require voltage variation. Ideally, a fast programmable voltage source could do steps, ramps, triangles, sines and so forth.

The possibility of testing with controlled current rather than controlled voltage has been discussed. Some interesting differences might be discovered.

It is possible that test equipment from the semiconductor industry could be adapted to core testing.

Testing without a blocking capacitor

This requires new test equipment, and some provision to ensure that flux walking is not a problem

Testing the effects of test rig impedance

"Test rig artifacts" have been suggested as a problem, and test rig influences are hypothesized in this report. Until tested, this remains a hypothesis.

It probably is unwise to dismiss these effects as "test rig artifacts." The same problems may exist in real circuits, and they should be confirmed, identified and quantified.

These are further explained at the end of Appendix F, Off-time Core Loss Phenomenon.

Testing with dc bias; testing transformers with load current

This requires new test equipment.

Dc bias is known to increase core losses in ferrites.

Load current in a transformer may exacerbate some of the hypothesized test rig influences on core loss by increasing the voltage drops and inductive spikes.

Noise reduction, ac readings

The noise in the current readings is an obvious problem, and not being able to directly read true 0 may be a problem. Current probes have the known shortcoming that they require a loop be added and that they are slightly inductive.

A disk resistive current sense may be an improvement.

Testing for equal volt-seconds

There is a lot of testing for pulses of equal voltage and equal time with varying off time. This models a hysteretic converter with a constant voltage input and a varying load. As the load current becomes increasingly low, the discharge time stretches, but the hysteretic recharging time is fairly constant.

A much more common waveform in power electronics is that of a buck converter. The period usually is constant, but as the input voltage increases, the pulse-width decreases so as to maintain constant average voltage. Part of the composite waveform hypothesis was a proposed method of estimating the core losses under this excitation, and the Pilot Project report includes an example of that calculation. It is disappointing that time and budget constraints prevented taking data to see if these calculations are valid. The discovery of the off-time phenomena suggests that it is not, but we do not know by how much.

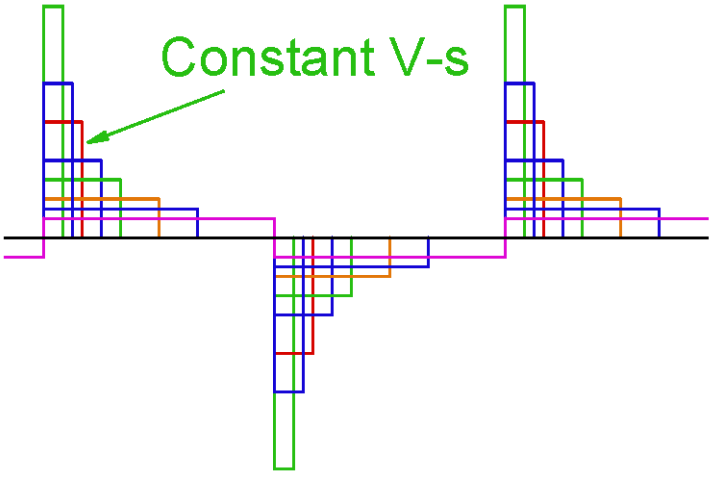

The effect of the off-time phenomena may be significant for buck converters.

Testing for segments in the drilled core experiment

There are some shortcomings in the drilled core experiments, and I hope that future testing can fill the gaps.

On the existing core, I would like to resolve the problem of the fluxes in the vertical slices not adding up correctly. I would also like to add testing of the sub-sections by using intersecting connections, as planned.

I would also like to try again to drill a core with four holes in each direction, so that 25 segments can be isolated.

Testing to avoid direct coupling to the sense winding

In making transformers, we strive for the best possible coupling between the primary and secondary, and that may use bi-filar winding, highly interleaved windings and other techniques.

In designing the sense winding for the present projects, the sense windings were located close to the drive winding for best coupling. This may have had the unfortunate effect of capturing coupling other than induction by flux change. It might be more of a problem in future tests with higher frequency.

The good correlation between the drilled core sense windings (at least the horizontal windings) and the overall sense windings suggests that this was not a problem. Some differences at the leading edge are suggestive that there might be a difference, but it is hard to distinguish from noise.

One idea is to use a sense winding that does not share factors with the drive winding, such as 5 turns and 13 turns. There may be other methods as well.

Testing for helical flux

The toroidal cores have only a few turns, so the turns cross the core at a steep angle.

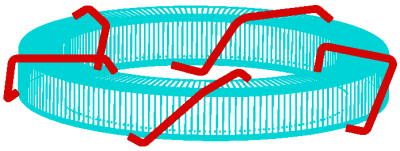

I wondered if the current crossing at a steep angle might have an angled mmf and cause the flux path to be somewhat helical circular path.

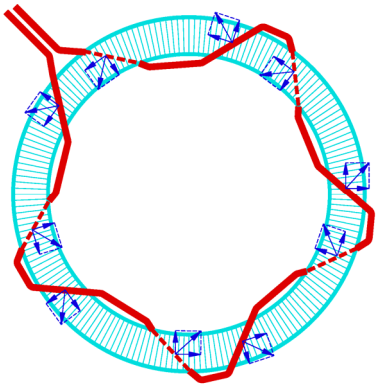

A helical path, being somewhat longer, would have longer length and less effective area. Upon removal of the excitation, it might relax to a normal circular path with shorter length and greater area. Such a path would have higher inductance.

There are two possible explanations for a current reduction. The obvious one is losses, but another is conservation of energy with increased inductance.

$$E = \tfrac{1}{2} I^2 * L$$

If L goes up, I must go down correspondingly to conserve energy. Of course, both could be happening, and L might go up for reasons that have nothing to do with helical flux paths.

This test could not be done as originally planned because it required two extra holes to be drilled in the core. Drilling proved to be much more difficult than anticipated, and this plan had to be scrapped.

There are other ways to test this idea involving winding modifications, and maybe borrowing some error correcting techniques from Rogowski coils.

Other

Other ideas will occur to me and will be added in later revisions. Others are encouraged to add to this list as well.

Appendix A–The Reports

User-friendly Data for Magnetic Core Loss Calculations, Edward Herbert, Canton, CT. November 10, 2008.

The Pilot Project Report

The Phase II Project Report

User-friendly Data for Magnetic Core Loss Calculations

Edward Herbert, Canton, CT. November 10, 2008

Introduction:

Everyone "knows" that core losses depend only upon $\widehat{B}$ and frequency. It does not matter what the excitation level and duty-cycle is, only the maximum flux density $\widehat{B}$. That is true, if the switching frequency is below 10 kHz or so. At the frequencies used in today's pulse-width-modulated (pwm) transformers, the core losses increase dramatically for low duty-cycles, as much as 10 times at 10 % duty-cycle.

Graphs of magnetic core loss data are usually for sine-wave excitation and presented in terms of maximum flux density $\widehat{B}$ and frequency f. These graphs are of questionable value for pulse-width-modulated (pwm) power converter design and decidedly not user-friendly. Graphs of core loss data for square-wave excitation, presented in terms of applied voltage and time are much more relevant to pwm power converter design and are much easier to use.

Background:

Magnetic core loss graphs from manufacturers are marginally useful for pwm power converter design. (1) They usually present loss in terms of maximum flux density $\widehat{B}$, an unfamiliar parameter of little use to the power converter designer. (2) The magnetic units used for core loss graphs are confusing and inconsistent. The likelihood of making errors is significant. (3) The graphs are for sine-wave excitation. Most pwm converters operate with square-waves having a variable duty-cycle. (4) The graphs are notoriously inaccurate. It is not unusual to see ruler-straight lines on core loss curves, with gross inaccuracies at the extremes.

Some very interesting work has been done exploring losses at increased "effective frequency." [1], [2] and [3].

Using volt-second graphs

Figure 1 shows representative core loss curves for square-wave excitation, presented as a family of constant voltage curves vs. pulse-width *t*.

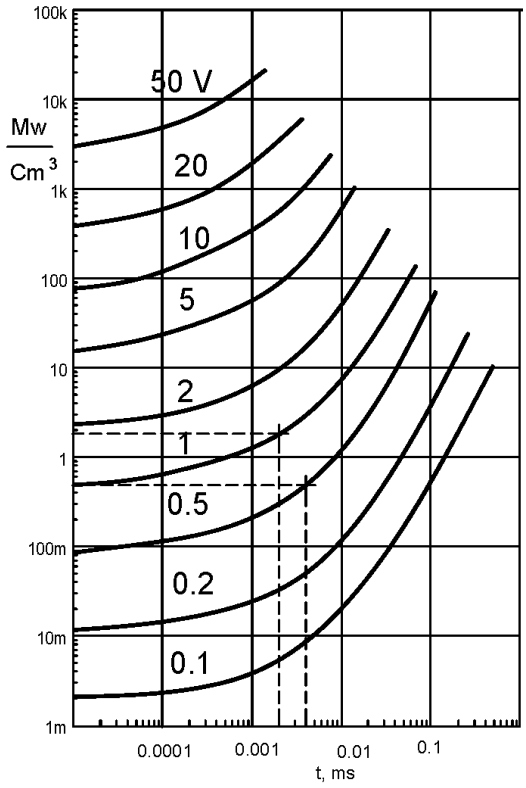

Figure 1: Representative core loss curves for constant voltage square-wave excitation vs. pulse-width.

For a graph for a magnetic material, material, the voltage is normalized and has units of volts per area-turn and the loss is in watts per volume. Core loss graphs for specific cores can include the geometric parameters, so the units are volts/turn and watts.

Low duty-cycle data

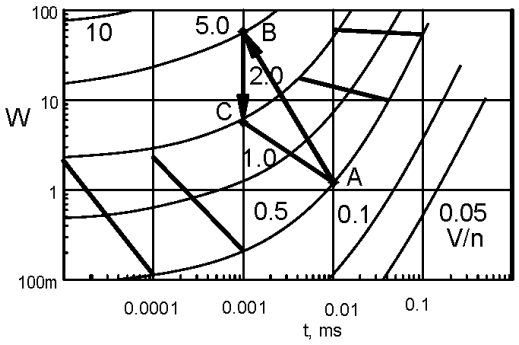

Figure 2. Curves of constant average voltage can be plotted. Note the extreme change in slope for short pulse widths (high frequency).

In figure 2, curves of constant average voltage equal to 0.5 V were plotted for several frequencies. As an example, using the technique for low duty-cycles presented below, start with the 0.5 V line and 0.01 ms, point A. That is the loss for a square wave with 0.01 ms pulse width. At 0.001 ms, to have the same average voltage, the voltage during the pulse is 5.0 V, point B, reduced by the duty-cycle 0.1, point C. The line A-C is approximately the line showing the loss for constant average voltage. This may be the most useful curve of all for a power converter designer.

The same technique is repeated to estimate the losses at constant average voltage for other starting pulse-widths (frequencies), resulting in a family of curves, shown in figure 2.

Note that at short pulse-widths (high frequency), the losses rise significantly at low duty-cycle. At longer pulse-widths, (low frequency), the duty-cycle does not much affect losses. This latter case is the classic loss characteristic taught for magnetic design.

The reader is advised that these curves were derived using Steinmetz equations applied far beyond their limits of reasonable accuracy, using many complex manipulations, each an opportunity for error. Accordingly, the graphs are qualitative at best.

However, the graphs represent a suggested form to use for plotting "real" data, from laboratory test and measurement. Real data from real tests will always trump manipulated data and approximations.

This presentation of the data is user-friendly and much more meaningful for power converter design.

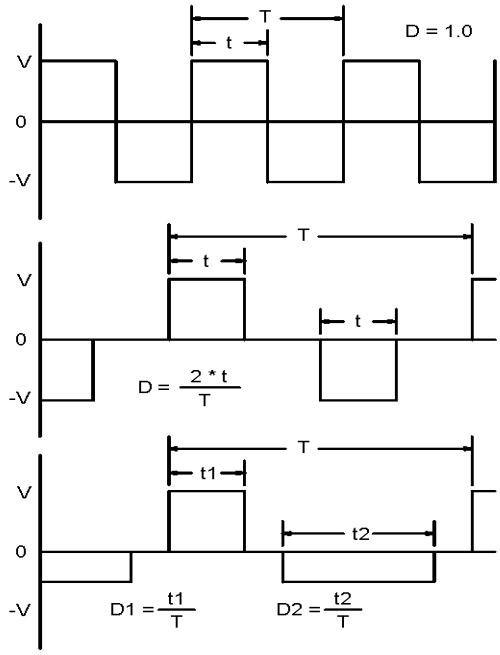

Figure 3: Times and duty-cycles defined.

Calculations

See figure 3 to define pulse-width and duty-cycle: In all cases, the pulses are repetitive steady-state pulses, as would be generated in a pwm converter at stead-state conditions.

For a square-wave excitation, *t* is the pulse-width and *T* is the period. The duty-cycle *D* is 1.0. To calculate the core losses using figure 1 for a 1 volt square-wave with a pulse-width of 2 us, follow the dashed line up from 2 us to intercept the 1 volt curve, then horizontally to intercept the vertical axis. The result is about 1.8 mw/cm^3.

For a symmetrical pulsed excitation, *t* is the pulse-width and *T* is the period. The duty-cycle *D* is 2 * *t / T*. To calculate the core loss for a 1 volt pwm wave-form having a 1 volt excitation and a 2 us pulse-width and a duty-cycle of 0.5, follow the dashed line up from 2 us to intercept the 1 volt curve, then horizontally to intercept the vertical axis. The result is multiplied by the duty-cycle 0.5 to give about 0.9 mw/cm^3.

For an asymmetrical pulsed excitation, the volt-seconds none-the-less must be equal for the pulses. T is the period, *t1* is the positive pulse-width, *t2* is the negative pulse-width. Two duty-cycles are defined, *D1 = t1 / T* and *D2 = t2 / T*.

To calculate the core loss for an asymmetrical pwm having a period of 8 us, and having a 2 us positive pulse of 1 volt and a 4 us negative pulse of 0.5 volt, first follow the dashed line up from 2 us to intercept the 1 volt curve, then horizontally to intercept the vertical axis. The result is multiplied by the duty-cycle of 0.25 to give about 0.45 mw/cm^3.

Next, follow the dashed line up from 4 us to intercept the 0.5 volt curve, then horizontally to intercept the vertical axis. The result is multiplied by the duty-cycle of 0.5 to give about 0.24 mw/cm^3. Add the partial results. The core loss is about 0.69 mw/cm^3.

Thus a method of calculating core loss is presented that does not require calculating magnetic parameters. This data and the calculations are much more relevant to power converter design, and much more user-friendly.

Saturation

Following the constant voltage curves from left to right, the volt-seconds of each point is the product of the voltage and the pulse-width. The curve ends at the volts-seconds where the core saturates. Accordingly, as long as the voltage and pulse-widths of interest are on the curve, the core will not saturate (if there is no flux walking.)

Loss data for cores and wound components

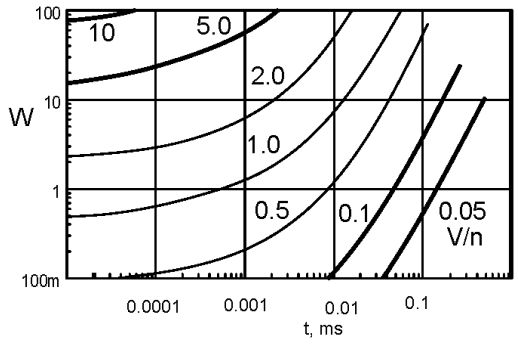

Figure 4. For a specific core, the geometric parameters can be included, so the result is read directly as watts W.

Losses for cores: A manufacturer of magnetic cores can present data for any specific core with all of the geometric

parameters included, so the user need not be concerned with effective area, effective volume and the like. Knowing the volts/turn and the pulse-widths of interest, the losses in the core can be read directly from the graph, as seen in Figure 4.

Losses for wound components: A similar graphical presentation includes the turns, allowing a designer to determine the core losses directly using only the voltage and pulse-widths.

"Remagnetization velocity"

Many papers have suggested that *dB/dt* and *B* are more relevant to core loss, leading to improved methods of calculation that have a better match to test data. None, as far as we know, has recognized *dB/dt* as voltage (with a scale factor). Yet, for most power converter designers, voltage is a much easier parameter to use and understand.

All continue to use maximum flux density $\hat{B}$ and frequency *f*. [1] uses the term "remagnetization velocity" for *dB/dt*. In [2] and [3], the more straightforward "*dB/dt*" is used.

For any expression using the flux density *B* or the maximum flux density $\hat{B}$, an equivalent expression can be written substituting volt-seconds, with an appropriate scale factor.

"Effective frequency"

[1], [2] and [3] all use the concept of "effective frequency" to account for non-sinusoidal wave-forms. Intuitively, there is a relationship between "duty-cycle" and "effective frequency," duty-cycle being analogous to the ratio of the real frequency to the effective frequency.

For any expression using frequency, an equivalent expression can substitute the inverse of the period, noting that frequency *f* equals *1 / T*, where *T* is the period. We prefer using the half-cycle period *t*, so *f* equals 1 / *2 t*.

Steinmetz equation using voltage v and the period T

The Steinmetz equation (or any other expression using $\hat{B}$ and *f*) can be expressed in terms of voltage and time.

$$P_v = C_m * f^{\alpha} * \hat{B}^{\beta}$$

Substituting $f = 1 / T$
and $\hat{B} = k * v * T$ gives

$$P_v = C_m * \left(\frac{1}{T}\right)^{\alpha} * (k * v * T)^{\beta}$$

$$P_v = C'_m * v^{\beta} * T^{(\beta-\alpha)}$$

[*T* is the period, *k* is the scale factor converting volt-seconds to $\hat{B}$, *v* is the voltage density and $C'_m = C_m * k^{\beta}$.]

This exercise is to demonstrate the equivalence of the expressions, not to suggest converting present data to the new format, particularly as we prefer using square-wave excitation. New data should be taken using voltage and pulse-width.

Graphs using converted data

To illustrate the point, we converted data mathematically to make the graphs that follow.

The starting point is the data as they are usually presented for Magnetics, Inc. F material. These data were chosen because Magnetics, Inc. also provides a family of Steinmetz constants for the F

material, as shown in the box below [6]. The frequency ranges are colored and correspond with the colors of the curves in the graphs.

Figure 5 shows a composite graph, taking the data for the F material from a data sheet (the solid lines) and superimposing on it the curves resulting from the Steinmetz calculations (the dashed lines).

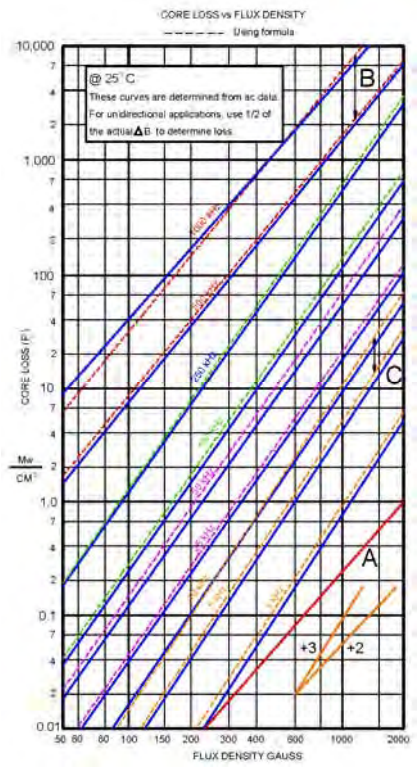

Figure 5: Core loss data for Magnetics, Inc. material F. The solid lines are from the datasheet, and the dashed lines are calculated using the Steinmetz equations.

Magnetics, Inc.'s loss expression approximation is:

$$P_L = a * f^c * \hat{B}^d \ \text{mW/cm}^3$$

[Where a, c and d are constants, f is in kHz and $\hat{B}$ is in kG.]

For each line in figure 3, the slope of the line is the exponent d, and the spacing between the lines is governed by the exponent c.

Core loss vs. frequency.

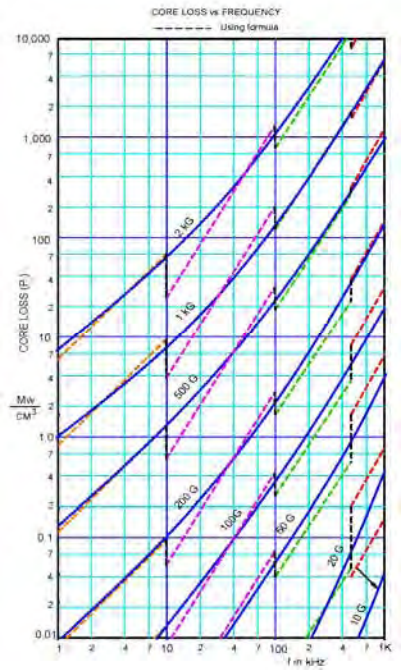

Figure 6: The data for Magnetics Inc. material F was re-plotted as a family of curves of constant flux density vs. frequency.

For Magnetics Inc.'s F material, the Steinmetz constants are given as follows.

Range	a	c	d
f ≤ 10 kHz	0.790	1.06	2.85
10 kHz ≤ f < 100 kHz	0.0717	1.72	2.66
100 kHz ≤ f < 500 kHz	0.0573	1.66	2.68
f ≥500 kHz	0.0126	1.88	2.29

The colors correspond to frequency ranges in the graphs.

First, the data was re-plotted using curves of constant $\hat{B}$ vs. *f* as in figure 6. Note the extreme discontinuities in the calculated data (dashed lines). These lines should be continuous, pointing out dramatically how poor the Steinmetz approximation is at the extremes of the frequency ranges. The solid lines are drawn free-hand in an attempt to find the best fit through the calculated data.

Excitation voltage vs. frequency

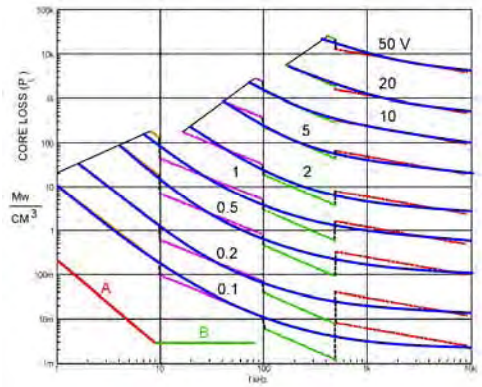

Figure 7: The data are re-plotted as a family of curves of constant excitation vs. frequency.

Next, the data is plotted in terms of voltage and frequency This required substituting volt-seconds (with a scale factor) for $\hat{B}$, but then substituting back the frequency *f* term as the inverse of the seconds. The result is a family of loss curves of the excitation voltage (in volts/turn-cm^2) vs. frequency, as shown figure 7.

Again, the dashed lines are the calculated curves, and the solid lines are a "best fit" drawn free-hand. On the upper left, the lines were ended at a flux density of 3 kG. This would be a straight line if the equations were ideal.

Voltage vs. pulse-width

The final translation is to re-plot the curves in terms of pulse-width rather than frequency. Because the pulse-width *t* is used instead of the period *T*, the scale was shifted left by 2. Only the "best fit" curves were used. The graph in figure 8 was rescaled to square up the log-log coordinates, and possible asymptotes of the curves were added. With further editing for appearance, this graph became the graph of figure 1.

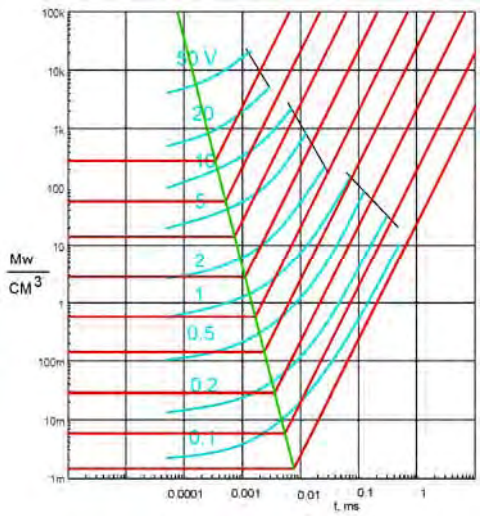

Figure 8: The curves of figure 7 were flipped left to right to invert the frequency scale to a time scale, and it was shifted left by 2 so that the scale is pulse-width *t* rather than the period *T*.

While this graph was derived from data for the Magnetics, Inc. F material, the reader is reminded that curves are based upon the Steinmetz equations applied far beyond their range of reasonable accuracy. The complexity of the calculations makes the chance of error quite significant. As such, only qualitative relationships can be inferred.

However, new data taken using square-wave constant voltage excitation and presented as a function of the pulse-width (half period) of the square-wave

will be no less accurate and valid than the data presently used, while being much more relevant to power converter design and much more "user-friendly."

Stienmetz-like equations

Rather than try to shoe-horn the Steinmetz factors into a new form, it is suggested that a new Steinmetz-like equation be defined.

$$P_v = C_x * v^{\delta} * t^{\varepsilon}$$

Find the area on the graph over which the circuit of interest will operate, and pick three points that bracket that area. For each, write the Steinmetz-like equation, with the constants as unknowns, and solve the equations simultaneously. Since solving simultaneous equations in which two of the unknowns are exponents is daunting, it is suggested to use a math program such as MathCad.

Oliver-like equations and Ridley-Nace-like equations

In [4], Christopher Oliver presents a curve fitting algorithm that is accurate over a much broader area of the graph. In [5], Dr. Ray Ridley and Art Nace do the same (but with a much different algorithm), and introduce temperature compensation as well. We see no reason why similar techniques could not be applied to voltage and pulse-width graphs as well, as the underlying physics is the same.

Conclusion

Core loss data can be taken for square-wave excitation, and presented in terms of the excitation voltage and pulse-width with no loss in accuracy.

Core loss data can also be taken and presented as curves of constant average voltage vs. pulse width, to show the consequence of low duty-cycle operation.

The resulting data are much more relevant to pwm power converter design, and are much more "user-friendly".

References

[1] Ansgar Brockmeyer, Manfred Albach, and Thomas Dürbaum, *Remagnetization Losses of Ferrite Materials used in Power Electronic Applications*, Power Conversion, May 1996 Proceedings.

[2] Jeili Li, Tarek Abdallah and Charles R. Sullivan, *Improved Calculation of Core Loss with Nonsinusoidal Waveforms*, IAS 2001.

[3] Kapil Venkatachalam, Charles R. Sullivan, Tared Abdallah and Hernán Tacca, *Accurate Prediction of Ferrite Core Loss with Nonsinusoidal Waveforms Using Only Steinmetz Parameters*, COMPEL 2002

[4] Christopher Oliver, *A new Core Loss Model*, Switching Power Magazine, Spring 2002.

[5] Dr. Ray Ridley and Art Nace, *Modeling Ferrite Core Losses*, Switching Power Magazine © Copyright 2006.

[6] Magnetics, Inc. *Ferrite Cores Design Manual and Catalog*, 2006.

Summary

In this project we have explored the feasibility of a method to generalize square-wave core-loss data to predict core loss with any common rectangular voltage waveform, proposed by Herbert [1].

The hypotheses to be tested is that, for rectangular pulses and a given magnetic core material, the core loss energy per period depends only on component pulse widths and peak voltages. We call this the *composite waveform hypothesis*. It has great intuitive appeal, and if true, it makes it convenient to decompose rectangular waveforms into such pulses for analysis. Thus, it would be be sufficient to test cores with square voltage waveforms, and then use the data to predict losses with generalized rectangular voltage waveforms.

Two important objectives of the project are to

1. Gather such square wave data for two typical core materials, one ferrite and one powdered-iron.

2. Gather additional data to determine if the composite waveform hypothesis is valid.

The square wave data were gathered for a set of data points at intervals that would be practical for manufacturers to provide for designers—five values per decade for both peak voltage and pulse width.

The validation data were measurements for non-square-wave composites of "standard" pulses from the square wave data set. We used three variations: (1) symmetric waveforms formed from a standard pulse shape with varying amounts of off-time added, increasing the period, (2) families of standard pulse shapes with set off-time, but varying the asymmetry, and (3) asymmetric waveforms with no off time, formed from two different standard pulse shapes.

It was clear from the large size of the sample space implied by this program, that an automated data gathering system would be needed, so computer control was designed in from the start. A data management system evolved that can generate a set of control input parameters for the test setup for all data points from a few global parameters, and then analyze the results.

The drive circuitry was designed to cover a wide range of flux density and frequency, consistent with budget constraints, by using existing experimental circuit boards.

The results indicate that the composite waveform hypothesis, while not perfect, performs well, and should be a significant improvement over the use of sinusoidal data for PWM design. The deviations from composite waveform model may provide valuable insight into the loss processes, and future work to characterize this behavior can likely improve the model and its value for design.

Contents

List of Figures

List of Tables

Preface

Most of the content of this report was taken from a paper to be published in the proceeding of the IEEE Applied Power Electronics Conference for 2010. I have added more detailed information the help with a practical understanding of the data gathering system and the use of the data.

John H. Harris

1 Introduction

Core-loss data published by core manufacturers is based on sinusoidal excitation, whereas most applications in switching power supplies and other types of power electronics circuits use rectangular voltage waveforms. Rectangular waveforms can be described by the voltage, period, and duty cycles of the positive and negative portions of the waveform. This leads to a wide diversity of different possible test conditions, and it is not practical for manufacturers to test all possible waveforms that might be used by customers. Approximate methods to estimate expected core loss with rectangular waveforms based on sinusoidal data [2]–[9] exist, but are difficult to use, are inherently limited in accuracy, and are not in wide use in industry.

In this project, we investigate a new approach that uses a simplified set of square-wave measurements to produce easy-to-use data that can be applied to calculate loss for any rectangular-voltage waveform. This approach is expected to provide higher accuracy than is possible starting from data based on sinusoidal waveforms, and is expected to be easier to use than existing methods for non-sinusoidal waveforms. The method can be applied to computerized optimizations or in hand calculations using graphical data. Although the data required is different from conventional sinusoidal measurements, the amount of data needed is no more than the amount of data collected in traditional loss characterization.

In order to implement and evaluate the new method, we have developed an automated excitation and data collection system under computer control. This allows rapidly gathering the proposed square-wave characterization data set, and also facilitates scanning through other rectangular waveform sets in order to assess the accuracy of the generalization from the characterization data.

Previous methods for predicting core loss with rectangular waveforms based on sinusoidal data are reviewed in Section 2. The new calculation method is described in Section 3 and the measurement system in Section 4. Measurement results are presented and used to assess the accuracy of the method in Section 5. Hysteresis loops are plotted and discussed in Section 6. A guide to applying the method in practical design is provided in Section 7. Section 8 further discusses the future application and improvement of this approach. Section 9 discusses the use of the accompanying data sets, and the appendix gives detailed information about data file formats.

2 Previous Methods for Core Loss with Non-sinusoidal Waveforms

For sinusoidal waveforms, loss is often estimated by a power law equation [10, 11]

$$\overline{P_v} = k f^{\alpha} \hat{B}^{\beta} \tag{1}$$

where $\hat{B}$ is the peak flux amplitude, $\overline{P_v}$ is the time-average power loss per unit volume, and f is the frequency of sinusoidal excitation, and k, α, and β are constants found by curve fitting. A similar equation, but without the frequency dependence, was proposed by Steinmetz in 1892 [12], and so (1) is often referred to as the Steinmetz equation.

Unfortunately, the Steinmetz equation, as well as the data provided by manufacturers of magnetic materials, is based only on sinusoidal excitation, and non-sinusoidal waveforms result in different losses [2, 3, 6]. DC bias can also significantly affect loss [13, 14, 15].

More detailed models, based on physical phenomena producing loss, have been studied [16]–[19].

However, especially for ferrites, there is not yet a clear consensus on a practical physically-based model that properly includes dynamic and nonlinear effects [6].

Initial attempts to make use of Steinmetz-equation parameters and extend the calculation to address arbitrary waveforms allowed improved loss estimates, but have significant limitations. The "modified Steinmetz equation" (MSE) [2, 3, 4] works well for waveforms with small harmonic content, but exhibits anomalies with large harmonic content [6], as does the model introduced in [5], as discussed in [7]. The "generalized Steinmetz equation" (GSE) was introduced in [6] to overcome anomalies in the MSE, and although it overcomes the problems with the MSE, it has poor accuracy in some regions [7].

A satisfactory method of using Steinmetz-equation parameters to roughly estimate loss with non-sinusoidal waveforms, the "improved generalized Steinmetz equation" (iGSE) was introduced in [7]. The same equation was independently discovered in [8, 9], where it was called the natural Steinmetz extension (NSE). Comparisons of different approaches in [25] confirm results in [7, 8, 9] showing that this method can work well in many situations.

An additional refinement introduced in [7] is to decompose a waveform that includes minor loops in the hysteresis curve, and separately analyze the loss in each minor loop. This was shown to be essential for accurately modeling such cases. An automated algorithm is described in [7] to perform this decomposition, but is unnecessary for waveforms without minor loops.

Despite these improvements, the iGSE remains an approximate prediction method, and, in particular, is dependent on the accuracy of the underlying Steinmetz model for sinusoidal loss. Unfortunately, the best-fit Steinmetz parameters are known to vary with frequency [26, 6]. For waveforms with a harmonic content over a wide frequency range, choosing the appropriate parameters can be problematic [6]. Some solutions to this problem that work for sinusoidal waveforms (e.g., [26, 27]) are not applicable with the iGSE. Summing several power-law terms is one option that can be used to better capture the wide-range frequency behavior while retaining compatibility with the general approach of the iGSE, at the price of additional complexity [8].

The approach in this project is to directly measure loss with square waveforms, rather than trying to extend data from sinusoidal loss measurements to square waveforms. The advantages relative to the iGSE and related methods are both simplicity and accuracy. The challenge to developing such a method is to be able to take data for a reasonably constrained set of parameters, and be able to use the results to predict loss for a wider range of practical waveforms. This is discussed in the next section.

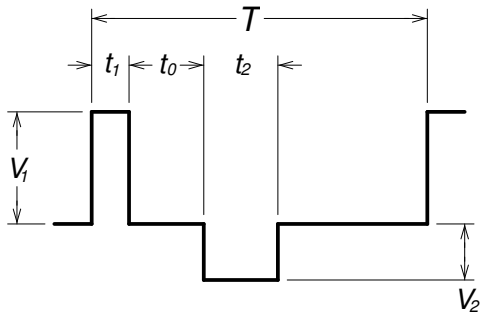

(a) Waveform parameter definitions

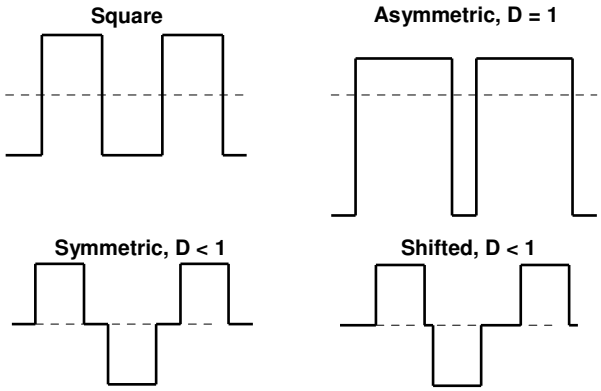

(b) Test waveform types

Figure 1: Waveforms (voltage vs. time): parameters and test waveform types. Square waves are used for characterizing materials; the other test waveforms are used to test the validity of the composite waveform hypothesis.

3 Calculating Core Loss from a Simplified Data Set

Consider a core with voltage waveforms such as those shown in Figure 1, typical of power electronics applications, applied to a winding. The flux in the core will ramp up or down during each positive or negative voltage pulse, respectively. We hypothesize that the energy loss incurred during each of these flux transitions depends only on the amplitude and duration of the pulse, and that there is no loss during periods of zero applied voltage (constant flux). If this is the case, we can decompose any of the rectangular waveform types shown in Figure 1b into a set of two pulses, calculate the energy loss associated with each pulse, and sum them to find the total energy loss per cycle. We call this hypothesis the *composite waveform hypothesis*.

If the composite waveform hypothesis proves to be a good approximation, we can predict core loss for any of the waveforms in Figure 1b if we know the loss for a square pulse as a function of its amplitude and duration. While we might estimate that loss

from sinusoidal data using one of the methods describe in Section 2 ([2]–[9]), a more accurate approach is to collect measured test data with square voltage waveforms, for which we can assume that the loss associated with each pulse is one half of the per-cycle energy loss. This requires data as a function of two parameters, such as flux amplitude and frequency, as used in conventional sinusoidal loss characterization. The parameters may also be described in terms of applied voltage per turn (corresponding to flux ramp rate) and on-time t_1 (one half the period for square waves).

The method we propose starts with characterizing a core material by measuring loss data for square waveforms. One half of the measured energy loss per cycle is the energy lost for a single pulse of the applied amplitude and on-time. If the composite waveform hypothesis is accurate, the same loss per cycle will be incurred for that applied voltage and on-time in any composite waveform. For the waveforms we consider here (Figure 1), the waveform comprises two pulses. To find the total energy loss per cycle one sums the per-pulse loss data for each of the two sets of pulse parameters (amplitude and on-time) from the corresponding square-wave measurements.

In Sections 4 and 5 we report on experimental measurements conducted for two purposes: (1) to collect square-wave data for sample cores as is necessary for this method, and (2) to assess the accuracy of the method and of the composite waveform hypothesis. We note that all of the previous methods for predicting loss with non-sinusoidal waveforms discussed in Section 2 depend on some version of the composite waveform hypothesis, even though this assumption is rarely stated. Thus, tests of this hypothesis are important for other approaches to predicting non-sinusoidal losses as well as for validating the approach proposed here.

Predictive core loss models built up from fundamental physical principals are not available for most core loss mechanisms, and so theoretical analysis of the composite waveform hypothesis is not possible. However, for core loss produced purely by classical eddy-current effects, physical models are well established, and analytical solutions exist for some geometries. It can be shown that, for classical eddy-current loss in core material layers thicker than or comparable to an electromagnetic skin depth, the composite waveform does not always hold exactly. However, it may still be a useful approximation, and may hold exactly for other types of losses. Thus experimental evaluation is needed to assess its utility.

4 Measurement System

We use a two-winding loss measurement [9] on toroidal core samples with 5 or 21 turns to match core characteristics to our drive system capabilities. The drive winding is connected to a full-bridge switching network through a $320\,\mu$F blocking capacitor (Figure 2). The gates of the four MOSFETs are controlled by an Agilent 33220A arbitrary waveform generator through a logic circuit and optically isolated gate drivers. Both the arbitrary function generator and the DC power supply feeding the bridge circuit are automatically controlled by a computer to allow synthesis of a sequence of different rectangular voltage waveforms. The principle components used in the circuit are summarized in Table 1.

The Agilent waveform generator has only one arbitrary waveform output (labeled

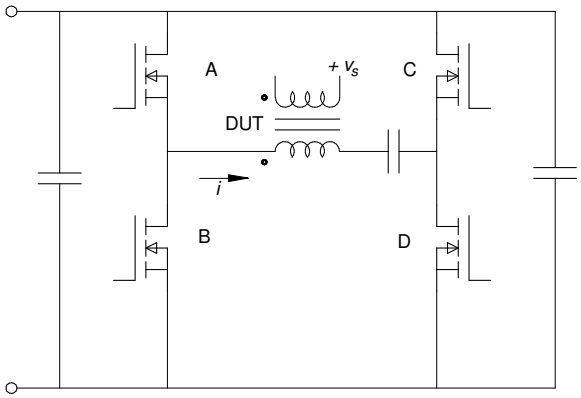

Figure 2: Full-bridge excitation circuit. The device under test, a magnetic core, is labeled DUT.

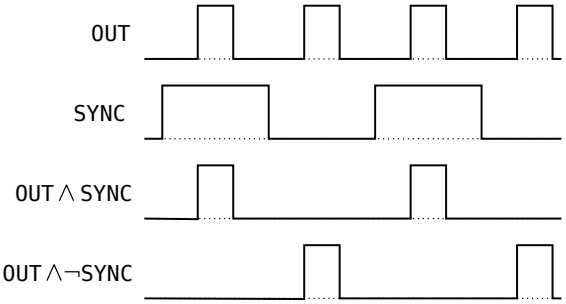

Figure 3: Decoding two drive signals from the OUT and SYNC waveform generator outputs.

OUT), but we have two phases of the bridge to be driven. We could generate a bipolar, three-level output from the arbitrary output, but then we would be using an analog representation of an essentially digital phenomenon, which introduces unnecessary trimming and level-shifting design compromises. Instead, by using a properly chosen OUT signal, gated with the generator's TTL square wave synchronization output (SYNC), we can get two independent but synchronized digital pulse trains: one is OUT ∧ SYNC, the other OUT ∧ ¬SYNC (Figure 3). This is accomplished with just a few logic gates, and can produce all of the $D < 1$ waveforms. The asymmetric $D = 1$ waveforms can be generated with the same gates by switching to the OUT signal alone (i.e., holding SYNC high). The square wave can be made several different ways; we use holding OUT high, which gives SYNC and ¬SYNC.

Dead time protection is hardwired for reliability. The dead-time circuits are hand-trimmed to get optimal waveform fidelity.

Current in the drive winding is sensed with an Agilent DSO 7104A oscilloscope with a Tektronix P 6021 wideband passive AC current probe. The AC probe avoids the

Table 1: Devices for the Drive Circuitry.

Function	Description	Value
Power supply.	Sorenson XG33-25	$33\,\mathrm{V}$, $25\,\mathrm{A}$
Switching MOSFET.	IR IRF 3706	$20\,\mathrm{V}$, $77\,\mathrm{A}$
Opto-isolated gate drive.	Avago HCPL-3180	$2.5\,\mathrm{A}$, $250\,\mathrm{kHz}$
Blocking capacitor.	AVX FFV3	$2 \times 160\,\mu\mathrm{F}$
Power supply decoupling capacitor, high capacity.	electrolytic	$2 \times 120\,\mathrm{mF}$
Power supply decoupling capacitors, low Z.	X7S surface mount	$10 \times 10\,\mu\mathrm{F}$

delay inherent in an active current probe; delay measurements verify that the delay is negligible. Flux is calculated from the voltage v_s across a sense winding. These signals are acquired by a digital storage oscilloscope under computer control to automatically collect waveforms from a sequence of measurements. After the waveforms are allowed to reach steady-state, 512 periods are averaged, and the average is recorded with 1000 points per period. Core loss and other parameters are calculated off line from the acquired data.

The core temperature was controlled by immersion in a heated oil bath. All the results reported here are for an oil-bath temperature of $80\,^{\circ}\mathrm{C}$. The automated data collection allows acquiring data for a single excitation in less than two seconds; a pause of about two seconds precedes the next excitation. Even without the oil bath, this results in very little temperature rise; with the oil bath, temperature deviations are negligible.

For verification of the test system, a large air-core toroidal transformer was constructed. This would, in principle, provide a zero-core-loss reference. However, large stray capacitance in the transformer led to excessive ringing in the waveforms and negative power dissipation numbers. Future work will develop a better reference design to allow a useful air-core test.

4.1 Data Flow

The data were generated using an automated system (Figure 4). The apparatus is controlled, via a local area network (LAN), by a program named *Coreloss*, which has a graphical user interface. It is the experimenters primary interface with the setup.

Initially, the experimenter edits a file describing a batch of runs in terms of a few general parameters, using a text editor. This is processed by a program named *Genruns*, that generates a table of run parameters defining the setup of the experimental apparatus for each run. This file can be opened from the Coreloss program and the user can execute any single run (For exploratory work, single runs can be edited before running), or all the runs can be executed sequentially and automatically. All the square wave data used to characterize a given core can be gathered in about half an hour. Further processing of the raw data is accomplished off line.

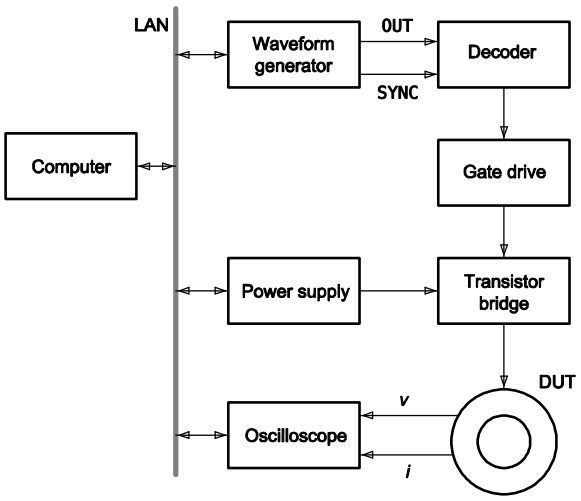

Figure 4: Block diagram of the experimental apparatus.

An experimental *run* is a data sample of one waveform shape, with a given t_1, T, V_{ps}, and perhaps other parameters, depending of the type of waveform. Experimental runs are grouped in *families*, several runs that vary one parameter while holding others constant.

A number of files are generated in the process of conducting the experiments. Figure 5 is a Petri diagram of the information flow. For the sake of data management, runs are also grouped in *sets*. A set is a batch of runs described in a single data file with the name `set-gen.dat`, where `set` is the set identifier.

The Gen-runs program reads the input data set file, and creates a file named `set-runs.dat`, a table which describes each individual run, to be read by the Coreloss program, which operates the apparatus. Each run has a run ID number. The oscilloscope, under computer control, measures the resulting voltage and current data, and records it in files named `set-run.csv`, where `run` is the run number. These CSV files are the raw data for the experiment.

There are other files that provide diagnostic information. The files names and field names and their interpretation are presented in Appendix A. The file formats are described in Appendix B.

4.2 Preferred Values

In order to make the data easier to plot and use, we chose values of voltage-per-turn and pulse width in geometric series. The software application programming interface (API) deals with integer *decilogs*—integer values of $10 \log_{10} x$ (i.e., like decibels, but not restricted to power measurements). Our reference levels are 1 volt per tune, and 1 ampere. For the present project, points were even-integer decilog values, corresponding to the sequence $x = \{1, 1.58, 2.51, 3.98, 6.31, 10\}$. Note that we chose excitation voltages to be preferred *per-turn* values, so that data could be compared for coils with

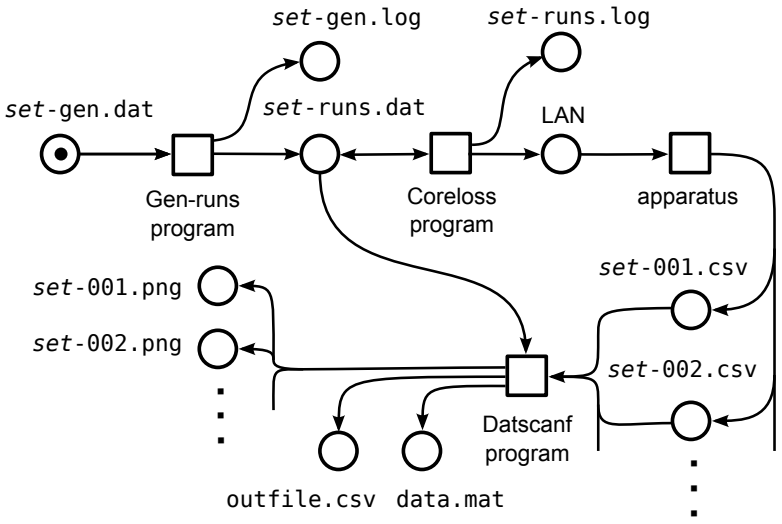

Figure 5: Petri diagram of the experiment data flow. Circles are channels (files or network), boxes are processes.

Table 2: Sample cores.

Manufacturer	Part	Material	Turns, N
Magnetics	42206-TC	R ferrite	5
Micrometals Inc.	T80-52	-52 iron powder	21

differing N—the preferred values above may be hidden behind a factor of N.

5 Experimental Results

Two sample cores were tested: one ferrite core and one powdered-iron core, as listed in Table 2.

5.1 Characterization

Figure 6 presents square-wave loss data in two different formats for the ferrite core. Figure 6a uses a format similar to that used for sinusoidal loss data on many datasheets. Figure 6b shows a Herbert curve in which core loss is plotted as a function of on-time (t_1 in Figure 1a), parameterized by the voltage per turn during that on-time [1]. The Herbert curve is convenient for use in design as discussed in Section 7; in addition, it directly illustrates the effect of period on power loss and can help guide the choice of switching frequency. Starting at a low switching frequency, increasing frequency (and thus reducing the pulse width) decreases losses, but beyond a certain frequency, further increases not only result in diminishing returns, but actually increase core losses. This

point corresponds to pulse widths of 1.5 to 3 μs for the ferrite material tested, and thus periods of 3 to 6 μs, and square-wave frequencies of 167 to 333 kHz. This is generally consistent with the behavior seen in plots of "performance factor" $B \cdot f$ for fixed power loss provided by some manufacturers [28, 29, 30]. However, the frequency beyond which performance degrades is lower in our data than in plots of performance factor for the same material (about 600 kHz [28]), presumably because of the harmonic energy content of the square-wave excitation.

Square-wave loss data for the powdered-iron core is shown in the same two formats in Figure 7, and shows similar trends though the values are different.

5.2 Verification

Additional data was collected to assess the accuracy of the method described in Section 3 for predicting loss for other waveforms using only data from square-wave measurements. The first category of these tests is experiments using asymmetric waveforms as shown in Figure 1b (upper right). The results of these experiments are plotted in Figure 8. Each curve is for fixed width and amplitude of the first pulse (fixed V_1 and t_1 as defined in Figure 1a) with the width of the second pulse (t_2) varying. The amplitude of the second pulse was adjusted for zero average voltage. The widths and amplitudes were all chosen to match data in the original characterization data set such that no interpolation was needed to predict loss, and the energy loss per cycle could be predicted from two points in the characterization data: the energy loss per cycle for a square wave of amplitude V_1 and half-period t_1 ($E_{\mathrm{sqr}}(V_1, t_1)$) and the energy loss per cycle for a square wave of amplitude V_2 and half-period t_2, as

$$E_c = \frac{1}{2}\left(E_{\mathrm{sqr}}(V_1, t_1) + E_{\mathrm{sqr}}(V_2, t_2)\right) \tag{2}$$

The measured asymmetric waveform loss is compared to loss predicted from (2) in Figure 8, showing excellent matching over a wide range of asymmetry ratios (t_1/T) and amplitudes, for both the ferrite core and the powdered iron core. This confirms that the composite waveform hypothesis is a good approximation for asymmetric waveforms.

Test results for waveforms with a zero-voltage time t_0 between pulses are shown in Figures 9 and 10. In each test, the positive and negative voltage pulses have constant amplitude and duration (as listed in the figure legend), but the zero-voltage time between pulses, t_0, is varied. In Figures 9a and 10a, the waveform is always symmetric and the overall period is expanded as t_0 is increased (marked "Symmetric, $D < 1$" in Figure 1b). In Figures 9b and 10b, the period remains constant but the waveform is skewed with one of the two zero-voltage periods shrinking as the other expands (marked "Shifted, $D < 1$" in Figure 1b).

Based on the composite waveform hypothesis (see Section 3), we would expect Figures 9a and 10a to show constant energy loss per cycle as the zero-voltage time, and thus the period, increases, with no loss occurring during the zero-voltage time. The data in Figure 9a, for the ferrite core, show significant variations as t_0 increases, as much as about 40%, in some cases increasing and in others decreasing. The data in Figure 10a, for the powdered-iron core, show much less variation, matching the expectation from

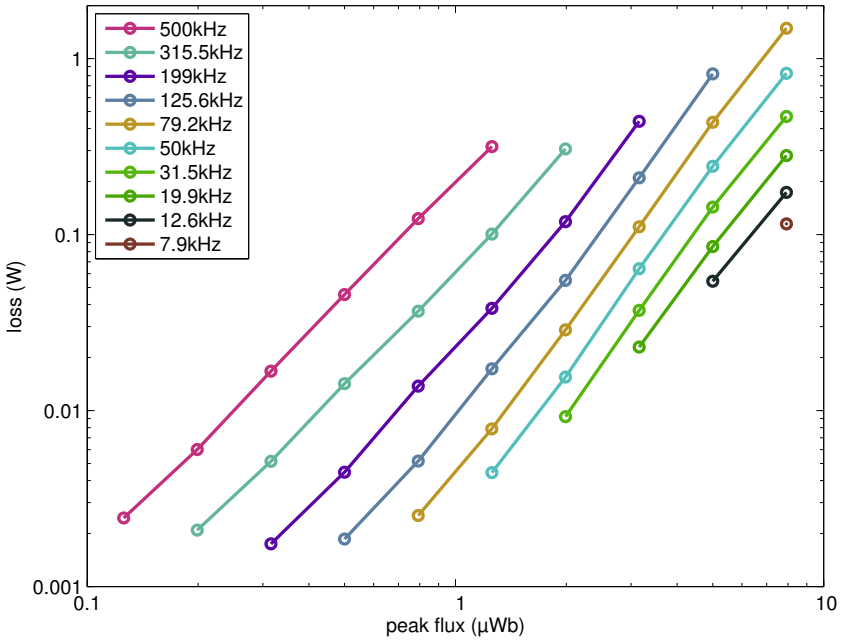

(a) Loss vs. peak flux parameterized by frequency

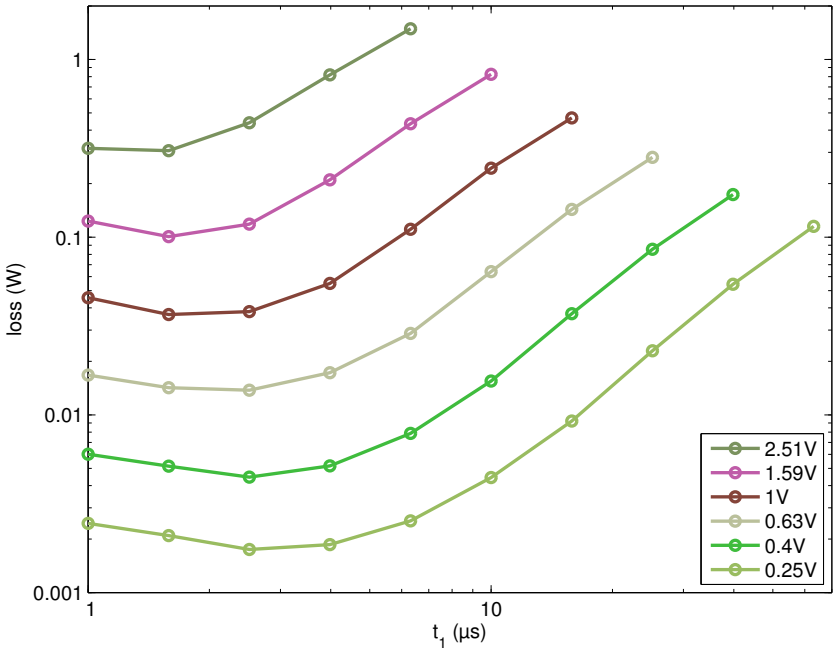

(b) Herbert curves: loss vs. on-time parameterized by voltage per turn

Figure 6: Square-wave loss data for the ferrite core in Table 2 presented in two different formats.

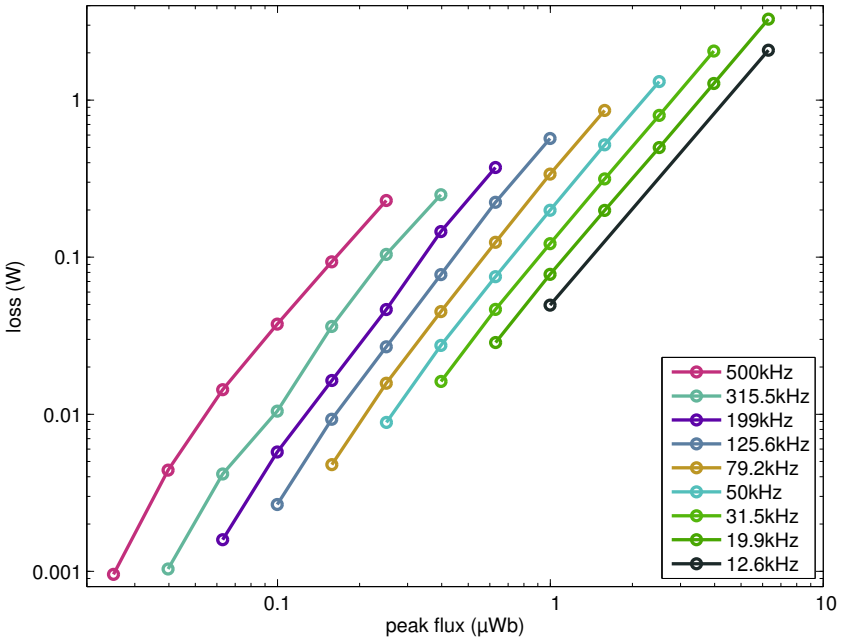

(a) Loss vs. peak flux parameterized by frequency

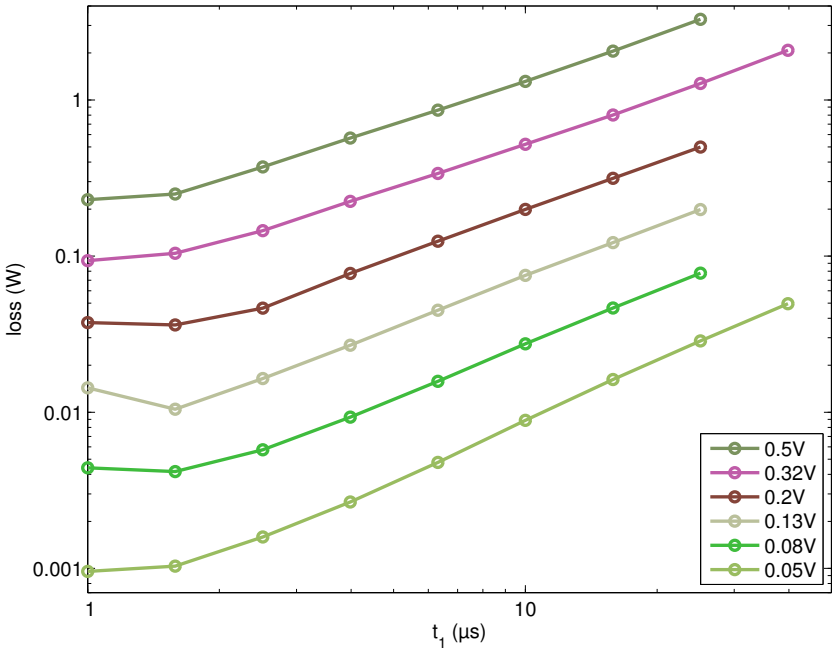

(b) Herbert curves: loss vs. on-time parameterized by voltage per turn

Figure 7: Square-wave loss data for the powdered-iron core in Table 2 presented in two different formats.

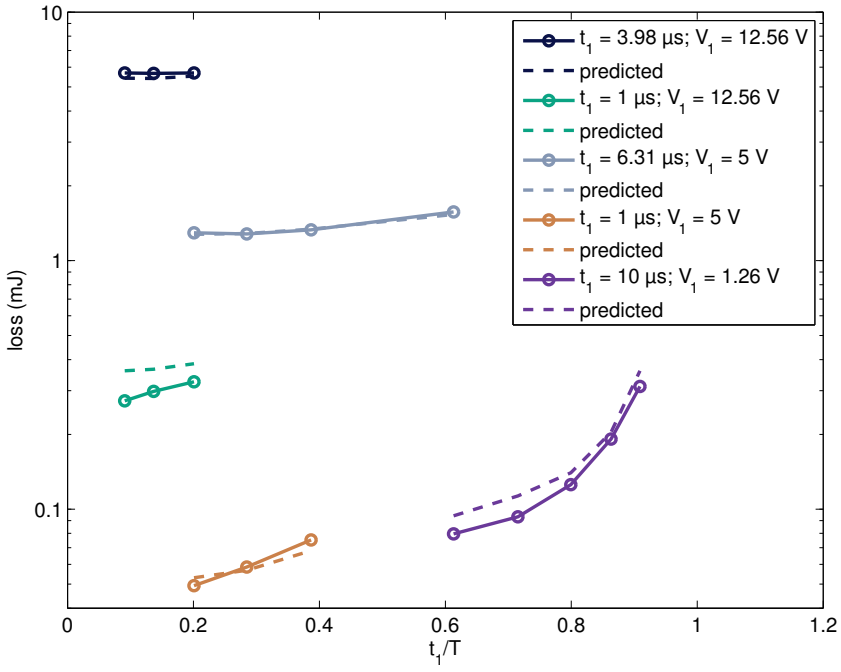

(a) Ferrite Core

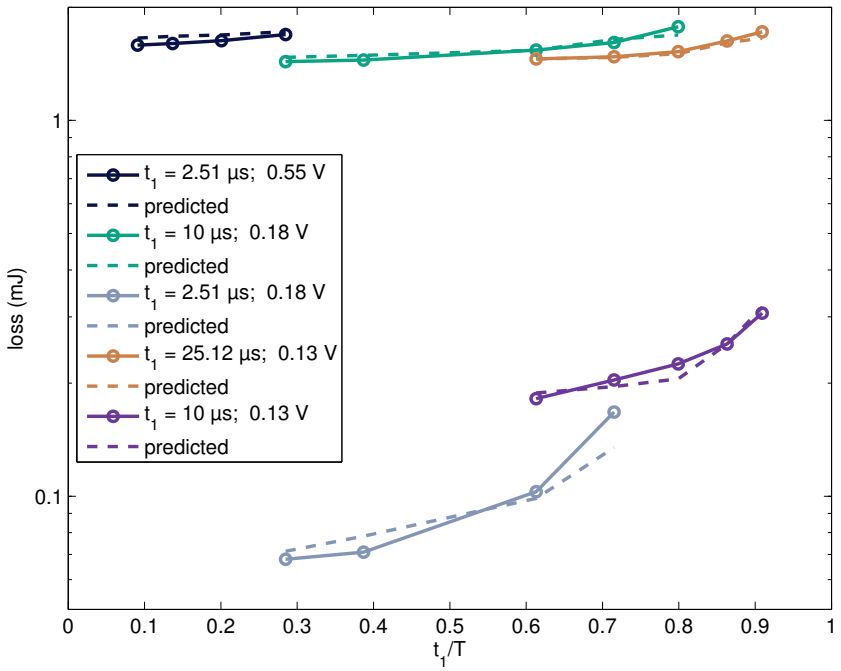

(b) Powdered-Iron Core

Figure 8: Losses with asymmetric waveforms as predicted by the proposed approach compared to measured results.

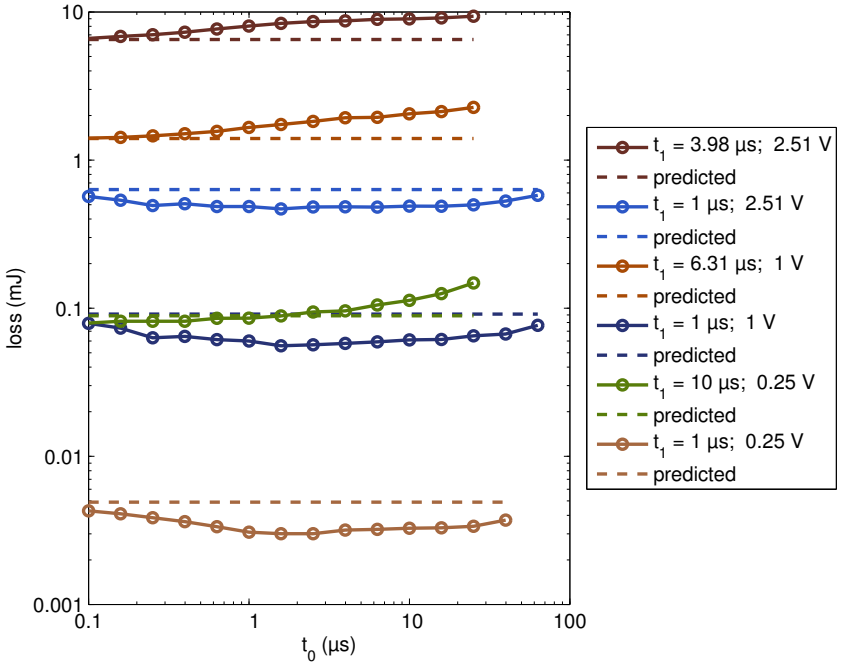

(a) Varying period

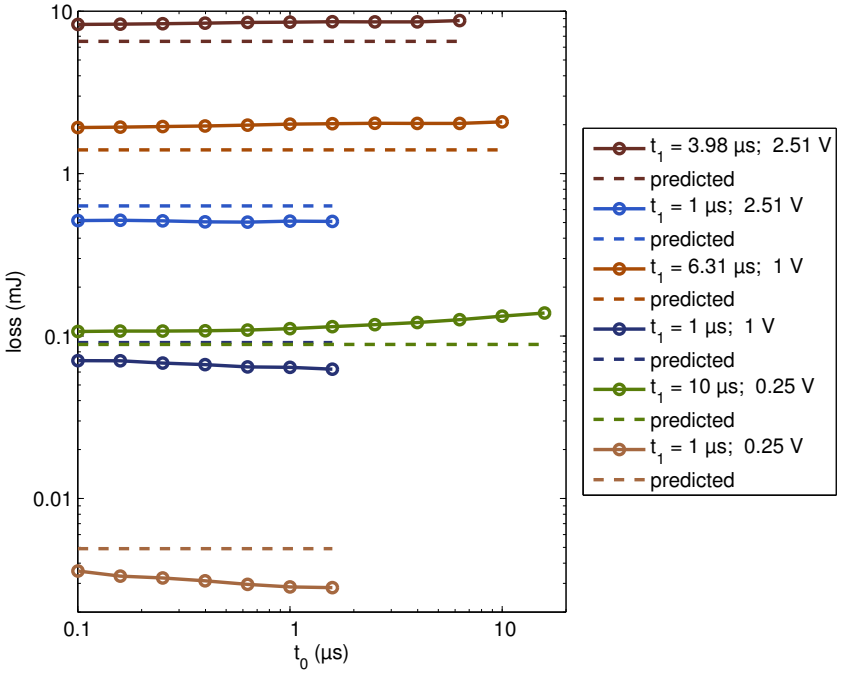

(b) Imbalanced off-times

Figure 9: Experimental data testing the extension of ferrite-core square-wave data to waveforms incorporating zero-voltage time t_0. This is done by varying the period and extending off-time t_0, or by shrinking one zero-voltage time while expanding the other to maintain a constant period. The legend gives the on-time t_1 and the per-turn pulse voltage for each curve.

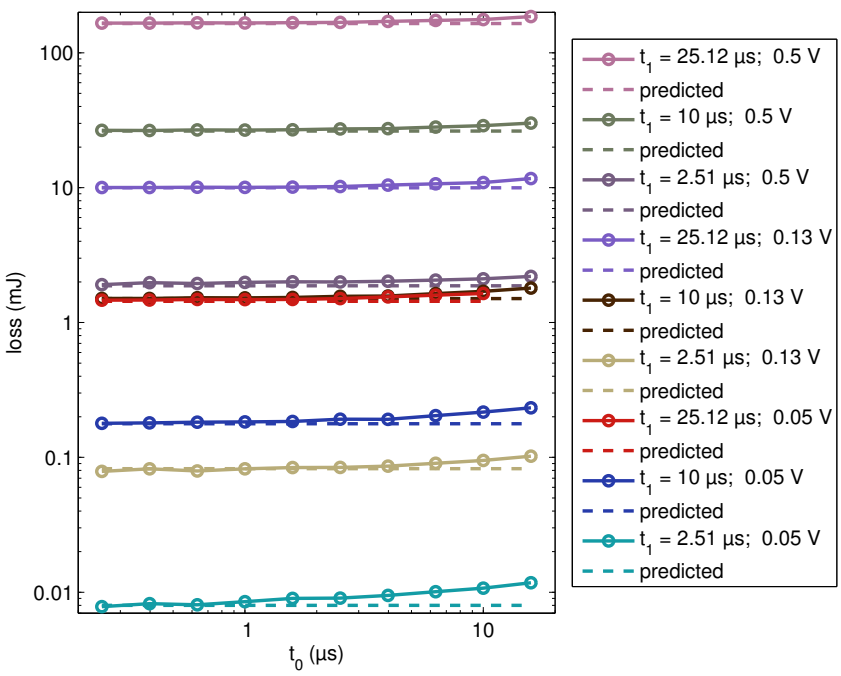

(a) Varying period

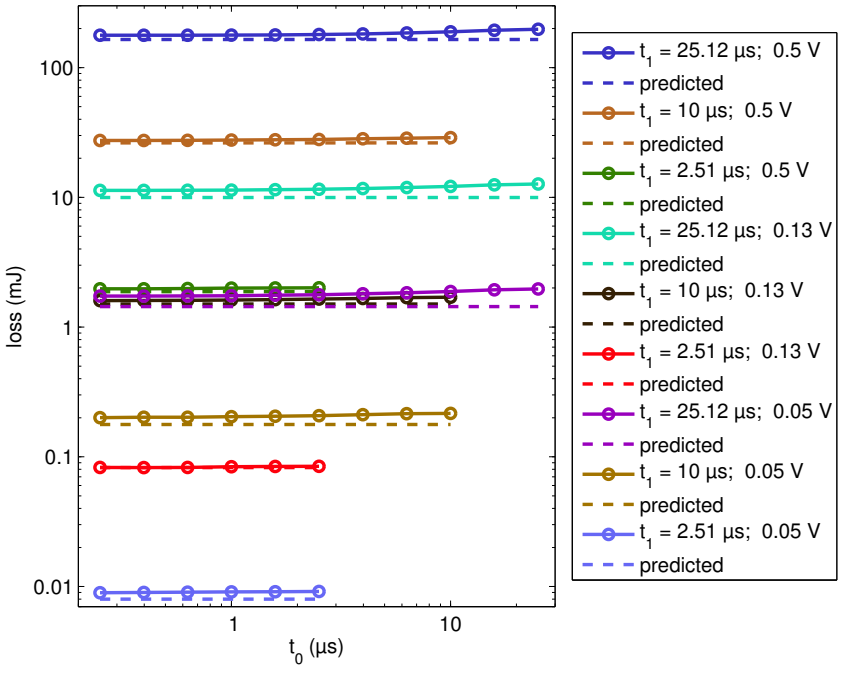

(b) Imbalanced off-times

Figure 10: Experimental data testing the extension of powdered-iron-core square-wave data to waveforms incorporating zero-voltage time t_0. This is done by varying the period and extending on-time t_1, or by shrinking one zero-voltage time while expanding the other to maintain a constant period.

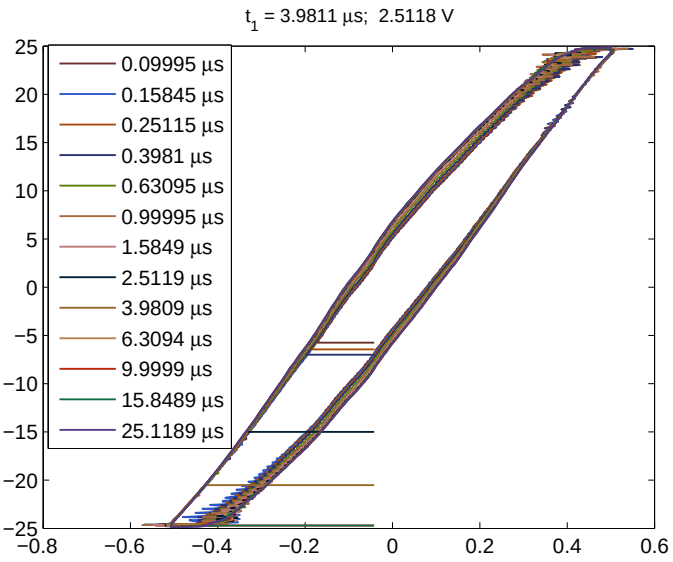

Figure 11: Hysteresis loops for one data set in Figure 9a: the top curve for $t_1 = 3.98\ \mu$s. The legend shows t_0 for each loop, corresponding to one data point on the top curve in Figure 9a.

the composite waveform hypothesis very closely, with only slight increases in loss for long off-times, which may be a result of measurement artifacts.

The results for the shifted pulse waveforms, in Figures 9b and 10b, show little variation in loss as the pulse position is shifted (increasing one off-time while decreasing another), as would be expected from the composite waveform hypothesis, but the ferrite-core loss is slightly different from that predicted from the square-wave characterization data using (2), whereas the powdered-iron core matches the predicted loss more closely. This is consistent with the results shown in Figures 9a and 10a. For the ferrite core, the relatively low variation in loss as the pulse position shifts, compared to that shown in Figures 9a and 10a, could be explained by the effects of one off-time increasing offsetting the effect of the other decreasing for a net zero effect on loss. Alternatively, if the trends shown in Figures 9a and 10a are due to measurement artifacts associated with the expanding period, this could also explain the relatively flat behavior seen in Figures 9b and 10b, because the shifted pulse experiments are immune to any errors associated with waveform period. However, the difference in behavior between the two cores seen in Figure 9a and 10a indicates that the trends seen in the data are in fact due to the true behavior of the cores, not to any unexpected measurement artifacts.

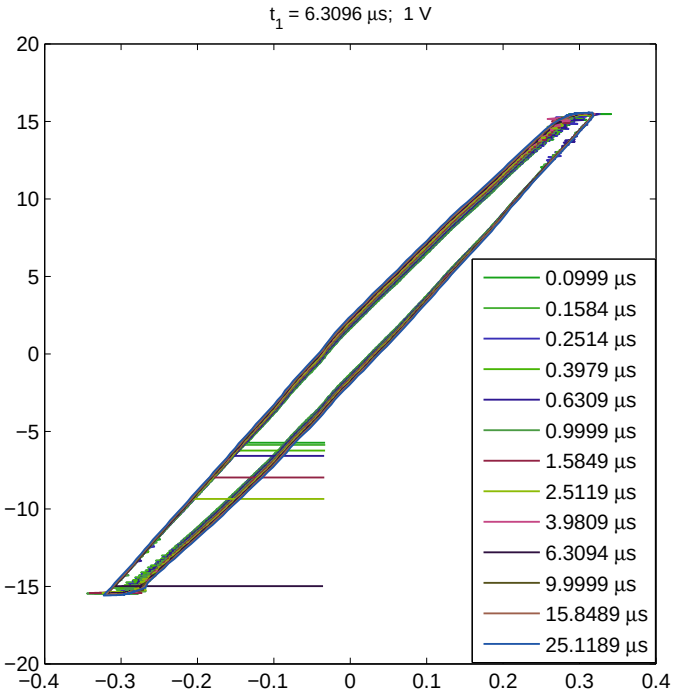

Figure 12: Hysteresis loops for one data set in Figure 9a: the second curve from the top, for $t_1 = 6.31$ μs. The legend shows t_0 for each loop, corresponding to one data point on the second curve in Figure 9a.

6 Hysteresis Loops

To further explore the phenomena causing variations in loss when the zero-voltage time between pulses, t_0, is varied, hysteresis loops for each point in several of the curves in Figure 9a are plotted in Figures 11, 12, and 13.

The scale and number of curves on these figures, together with ringing on the waveforms, makes it difficult to see a dramatic trend, particularly on the relatively narrow loops of Figure 12 and Figure 13. However, a zoomed in view of Figure 11, shown in Figure 14, provides some insight. We see that the rise to the point of maximum current and flux linkage is nearly identical on each curve, with the exception of ringing that has little effect on the area of the loop. However, the decreases diverge: those with the shortest zero-voltage time t_0 fall more directly, while those with longer zero-voltage time curve further to the left. This part of the curve immediately follows the pause at zero voltage (which is at the top right of the plot), and thus it makes sense that its shape is the most affected by the pause. An oversimplified description would be that the flux gets "stuck" near the the maximum value if it has had time to "soak" and get

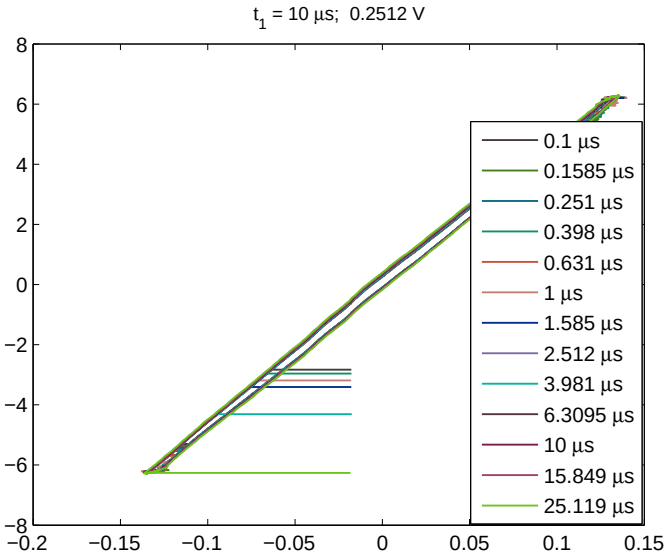

Figure 13: Hysteresis loops for one data set in Figure 9a: the fourth curve from the top, for $t_1 = 10$ μs. The legend shows t_0 for each loop, corresponding to one data point on the fourth curve in Figure 9a.

accustomed to that flux value, whereas the flux can more easily transition away from the maximum if the excitation is decreased immediately.

7 Design Techniques

The loss data derived from square-wave measurements can be provided to a magnetics designer in various forms, including tabulated data or curve-fit functions for use in software, and various types of graphical presentation. The loss data can be presented as loss per unit volume, or as total loss for a specific core, to simplify calculations for the designer. Here we discuss working from graphical data in the "Herbert curve" format of Figure 6b. These curves are parameterized by voltage per turn applied to a winding. It's also possible to provide curves like this for a specific *component* with a given number of turns, parameterized by voltage.

In general, for waveforms as shown in Figure 1a, based on (2), one can calculate loss from a Herbert plot as

$$P = \frac{1}{T}\left(P_{\mathrm{sqr}}(V_1/N, t_1)\cdot t_1 + P_{\mathrm{sqr}}(V_2/N, t_2)\cdot t_2\right) \tag{3}$$

In the case of symmetric waveforms, $P_{\mathrm{sqr}}(V_1/N, t_1) = P_{\mathrm{sqr}}(V_2/N, t_2)$, and the loss calculation reduces to

$$P = \frac{2t_1}{T} P_{\mathrm{sqr}}(V_1/N, t_1). \tag{4}$$

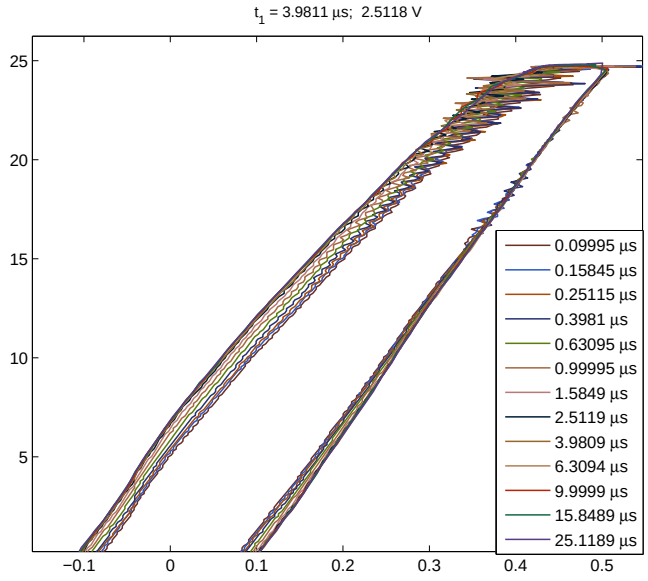

Figure 14: A zoomed-in view of the hysteresis loops in Figure 11. The legend shows t_0 for each loop, corresponding to one data point on the top curve in Figure 9a.

Consider, for example, a component operating at 50 kHz with a symmetric waveform with a duty cycle of 63%, 12 turns, and a pulse amplitude of 4.8 V. The period is 20 μs, and the positive and negative pulse widths are $t_1 = t_2 = 0.63 \cdot 10$ μs = 6.3 μs. To find the correct curve to examine in Figure 6b, we find the voltage per turn which is 4.8/12 = 0.4 V. As shown in Figure 15, we can read off the power loss for this pulse width and voltage per turn as $P_{\mathrm{sqr}} = 7.9$ mW. According to (4) we scale this result by the ratio $2t_1/T = 12.6$ μs/20 μs, to get a predicted power loss of $7.9 \cdot 0.63 = 5$ mW.

An interesting design space to explore is to maintain constant frequency and average voltage, but to vary the pulse width and period. The relevant data is along a curve of constant volt-seconds on the Herbert plot—the dashed line in Figure 16. To get power loss from these points, assuming constant frequency of 50 kHz, we then scale these points down by the ratio $2 \cdot t_1$/20 μs to get the solid line in Figure 16. This rise of this curve to the left illustrated the disadvantage of using shorter duty cycles for a given average voltage or volt-second requirement.

As an asymmetric example, consider the same 12-turn winding, with a 12 V, 10 μs pulse applied in one direction, and a 30 V, 4 μs pulse applied in the other direction, with a 20 μs overall period (50 kHz) as before (the waveform includes a total of 6 μs of zero-voltage time). $P_{\mathrm{sqr}}(V_1/N, t_1)$ and $P_{\mathrm{sqr}}(V_2/N, t_2)$ are read off Figure 15 as 244 mW and 818 mW. The overall power loss can then be found from (3) as

$$P = 50 \text{ kHz} \left(244 \text{ mW} \cdot 10 \ \mu\text{s} + 818 \text{ mW} \cdot 4 \ \mu\text{s}\right) = 286 \text{ mW}. \tag{5}$$

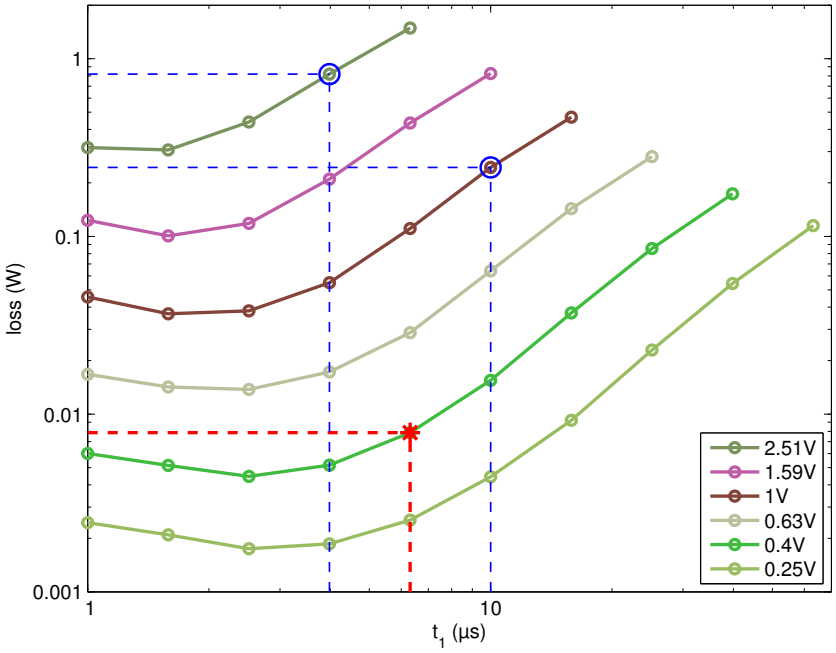

Figure 15: Reading data from a Herbert plot for the examples discussed in the text. The lower red point marked with ∗ is for the first, symmetric example. The upper blue circles are for the second, asymmetric example.

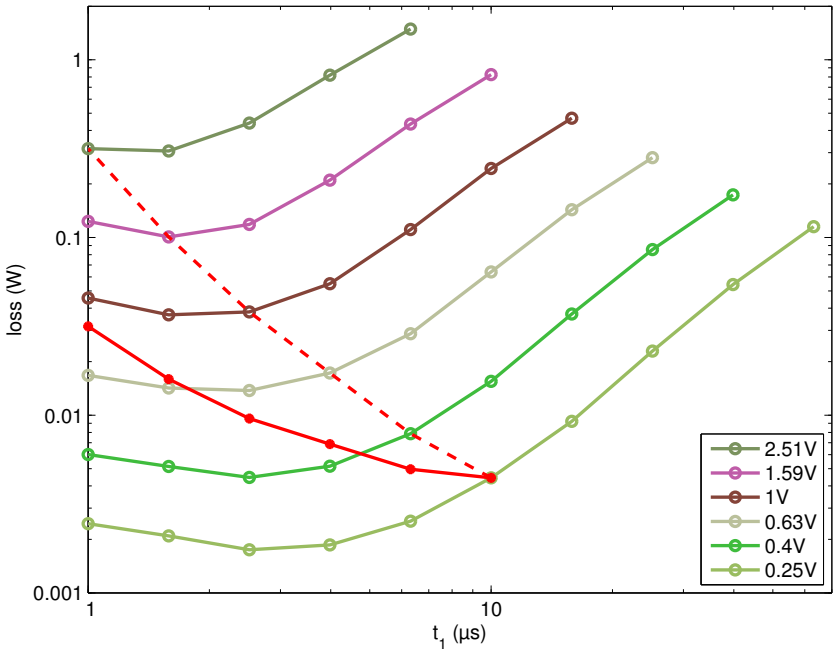

Figure 16: Example exploring different duty cycle options for a constant average voltage (constant volt-seconds). The dashed line is the raw data points used from the plot; the solid line shows the result scaled by the ratio of on-time to period to calculate actual loss, as discussed in the text.

8 Discussion

The results in Figures 8 and 8b show that the composite waveform hypothesis holds well for asymmetric waveforms, and the method provides excellent accuracy. Figure 10 shows that, for the powdered-iron core tested, it also holds very well for waveforms with zero-voltage periods, although zero voltage times can cause significant deviation in the ferrite core tested. This variation is not predicted by the composite-waveform hypothesis; nor is it predicted by any of the methods discussed in Section 2. Additional work to better characterize and model this behavior could lead to more accurate loss predictions. However, even with this error, the approach described here is expected to be more accurate than other methods which are subject to the same error, and additionally entail error due to using sinusoidal data to predict square-wave loss.

In addition to being more accurate than other methods, the new approach is also easier to use than methods like the iGSE. Thus, we believe that it would be beneficial for core manufacturers to characterize square-wave loss and provide that data graphically, electronically or both, either on a per-unit-volume basis or on a per-core basis.

As presented here, the method is only applicable to waveforms with one positive voltage pulse and one negative pulse. However, it could also be easily applied to waveforms with minor loops by separating the minor loops following the approach in [7], as long as each constituent loop comprises only one positive pulse and one negative pulse. Adapting the method to waveforms with a series of voltage pulses of the same polarity but differing amplitudes is less straightforward. The corresponding analysis in the iGSE (eq. (13) in [7]) includes a factor that depends on the total flux excursion as well as the flux change for a given pulse, and it may be necessary to introduce similar factors to accurately model losses in such cases using square-wave loss data. However, most power electronics applications use waveforms with only one positive voltage pulse and one negative pulse, such that that the analysis here applies directly.

9 Using the Data

The data generated by this works includes characterization data for two cores and verification data for the same two cores. Complete data for both is archived at the web site `http://engineering.dartmouth.edu/inductor/coredata` in files `ferrite-data.zip` and `powdered_iron-data.zip`. However, a user calculating loss for a particular waveform does not need these large ($> 20\,\mathrm{MB}$) files, but rather needs only the characterization data. This data is available in a smaller data collection, `characterization-data.zip`, on the same page. This archive contains the data plotted in Figures 6 and 7 in multiple formats, as well as the plots themselves as Portable Network Graphics (PNG) images. The data include, for each square wave tested,

- Frequency (Hz).
- Peak flux linkage (Vs).
- Volts/turn.
- Average loss (W).
- Loss per cycle (J).

The formats are:

- Microsoft Excel (`.xls`) format, with columns corresponding to each of the data listed above, and headings labeling each.
- Comma-separated value (`.csv`) format, with columns corresponding to each of the data listed above, and no text.
- Plain text (`.dat`) file, with columns corresponding to each of the data listed above, and a header row briefly identifying each column.
- Matlab `.mat` format, which, when loaded into the Matlab environment, provides the variables `f`, `dphi`, `Vturn`, `Pavg`, and `Ecycle`, corresponding to the data listed above.

These formats are explained in greater detail in the appendix.

Many users may wish to simply read values off of the graphs in Figures 6 and 7 but these files make the data available in multiple formats for use by computer software, or for analyzing, curve-fitting, or plotting the data.

10 Conclusion

The proposed measurement and loss calculation approach allows generalizing square-wave core-loss data to predict core loss with any common rectangular voltage waveform. An automated measurement system has been used to collect the required square-wave core characterization data for ferrite and powdered-iron cores, and to collect additional data to assess the accuracy of the method for other voltage waveforms. Measurements show good correlation, but also exhibit behavior not yet explained by published

models, which may lead to new insights and more accurate models. Despite the minor discrepancies, the loss prediction method yields higher accuracy, and is easier to use, than other methods for non-sinusoidal waveforms.

A Data Files and Fields

This appendix summarizes the various field names in the data files, along with their meanings. Table 3 gives a summary of all the files. In these files, we use designations to identify the four waveform types shown in Figure 1b. They are listed in Table 4.

A.1 Oscilloscope Data

The first *two* lines of the oscilloscope CSV files are heading. The first is the field identifier, the second, the units of measure. All the data are floating point numbers. The `SYNC` and `OUT` fields are the input to the waveform decoder and are only used for debugging.

x-axis Time, in seconds.

SYNC The sync signal from the arbitrary waveform generator (volts).

OUT The output signal from the arbitrary waveform generator (volts).

V The sense winding voltage, V_s, (volts).

Field	Description
set-gen.dat	The Gen-runs input data file, instructions for making a set of runs.
set-runs.dat	The output from Gen-runs and the input to the Coreloss program.
set-gen.log	A log file from Gen-runs echoing the parameters and telling which runs were skipped and why.
set-log.dat	A diagnostic file created by the Coreloss program.
set-log.csv	A diagnostic file created by the Coreloss program. It has the same informations as the `.dat` file, above, but in the CSV format.
set-run.csv	The output from the oscilloscope for a single run.
set-run.txt	A configuration log from the oscilloscope for a single run.
set-run.png	An image of a plot of the oscilloscope data for a single run, along with a plot of power and energy versus time.
output.dat	Contains the per-cycle loss data, as well as the original data.
output.csv	Contains the per-cycle loss data, as well as the original data. It has the same informations as the `.dat` file, above, but in the CSV format.
data.mat	Contains the per-cycle loss data, as well as the original data. It has the same informations as the `.dat` file, above, but as Matlab source code.

Table 3: File naming conventions for parameter and data files.

Designation	D	$t_1 = t_2$	Symmetric	Comment
`square`	$= 1$	yes	yes	
`skew`	< 1	yes	no	"shifted"
`expand`	< 1	yes	yes	varying T
`assym`	$= 1$	no	no	

Table 4: Waveform type designations

I The current (amperes).

A.2 Test Input Data

The test input file read by the Coreloss program. Each record is a white-space-delimited list of the parameters for one run. An experimental run has these parameters:

runId The run identifier. This should chosen to be be globally unique. The Gen-runs program uses the set ID, followed by a zero-padded integer, the run ID.

sample The core sample identifier.

N The number of turns on the core.

period The period, T, of the drive voltage, in seconds. (Floating point.)

t1 The pulse width of the first pulse. (Floating point.)

pinch The *pinch*, P, it the time between pulse 1 and pulse 2, t_0, expressed as a fraction of the off time for a symmetric waveform:

$$P = 1 - \frac{2t_0}{T - t_1 - t_2}$$

$0 \leq P \leq 1$ for $D < 1$. $P = 1$ for `expand` waveforms, and is undefined for $D = 1$ (indicated in the file by `-1`). (Floating point.)

D=1 A Boolean value, true (1) if $D = 1$ and 0 otherwise. This may seem redundant, but it is needed for clarity and safety because of the floating point time parameters.[1]

Vps It is the voltage requested from the power supply.

delay A delay between runs to allow for cooling. (Seconds.)

VRange Full scale voltage range setting for the oscilloscope.

IRange Full scale current range setting for the oscilloscope.

The following fields are used by the data reduction programs to group data by families:

[1] The name `D=1` was chosen for brevity and clarity. I hope the embedded math symbol is not confusing.

TSet Zero if it is not a `square` wave. Otherwise, records with the same value have the same period.

VSet Zero if it is not a `square` wave. Otherwise, records with the same value have the same V_{ps}.

expandSet Zero if it is not an `expand` waveform. Otherwise, records with the same value have the same pulse shape. (Varying t_0.)

skewSet Zero if it is not a `skew` waveform. Otherwise, records with the same value have the same pulse shape. (Varying P.)

assymSet Zero if it is not a `assym` waveform. Otherwise, records with the same value have the same pulse shape for the t_1 pulse.

A.3 Run Data Generator

The input file for Gen-runs is a white-space-delimited dictionary. The fields are:

comment This is a one-line comment that is printed at the top of the run data file.

setId The set ID is used to name the run data file and is prepended to each run ID. By convention, this is the same as the set identifier used in the source data file names.

sample The identifier for the core sample.

N The number of turns.

types A list of run types to be generated. They can be any of {`square`, `expand`, `skew`, `assym`}.

t1min Minimum pulse width for `square` wave runs.

t1max Maximum pulse width for `square` wave runs.

VpsMin Minimum power supply voltage.

VpsMax Maximum power supply voltage.

grid Spacing of the geometric series, in decilog. For five values per decade, use 2.

satLimit Saturation limit in power supply volt-seconds per turn.

delay The delay time for cooling between runs, in seconds.

expandSamples A white-space-delimited, paired list of V_{ps}/N and t_1 for the pulses used in `expand` and `skew` runs. These values will be "rounded" to the decilog preferred values (Section 4.2).

t0min The minimum off-time between pulses, t_0, to be used for `expand` and `skew` runs.

t0max For `expand` and `skew` runs, the maximum off-time. `expand` waveforms are symmetric, with the period $T = 2(t_1 + t_0)$. The off time, t_0, increases geometrically, stopping when it exceeds `t0max`.

TFactor For `skew` runs, the ratio of the period, T, to the pulse width, used to determine T, i.e., the period is `TFactor * t1`. The series starts with $t_0 = t_{0\,\mathrm{min}}$, and increases t_0 geometrically until the pulses are approximately symmetric.

For comments; both the key (`#`) and the value are ignored by the program.

B General File Formats

There a few general types of file format used in the project:

Comma separated value (CSV). This is a standard tabular format, where columns are separated by commas. Files have the `.csv` extension. It was chosen because it was the only ASCII text output file format available from the Tektronix oscilloscope. The first line or two of all the CSV files is a header.

Key-value dictionary. This is a particularly nice, human and machine readable format for configuration files. Each line has zero or more white-space-delimited key-value pairs. The *key* is a unique parameter name; the *value* is the value it is assigned. The layout and order of the pairs is unimportant. If a value is enclosed in quotation marks or braces, it may be empty or contain embedded white space.

Log. Log files are text files and usually have the extension `.log`. They give diagnostic information and are intended for human readers, and are generally not easily parsed by a computer.

White space delimited table. These are ASCII text table files that separate columns with white space—spans of one or more space or tab characters. They are easily read by a human if printed with a monospaced font, like Courier. Cells that are empty, or contain white space, must be enclosed in quotation marks or braces. Blank lines and lines beginning with # are ignored. The latter are often used for headings.

Portable network graphic (PNG). These are raster graphics files, used for the data plots.

Matlab MathWorks MATLAB source code file, which have the extension `.mat`.

Acknowledgements

Thanks to the Power Sources Manufacturers' Association and the National Institute for Standards and Technology (NIST) for support of this work.

References

[1] Edward Herbert. User-friendly data for magnetic core loss calculations. August 2008. http://fmtt.com/Coreloss2009.pdf.

[2] M. Albach, T. Durbaum, and A. Brockmeyer. Calculating core losses in transformers for arbitrary magnetizing currents a comparison of different approaches. In *27th Annual IEEE Power Electronics Specialists Conference*, volume 2, pages 1463–8, June 1996.

[3] J. Reinert, A. Brockmeyer, and R.W. De Doncker. Calculation of losses in ferro- and ferrimagnetic materials based on the modified Steinmetz equation. In *Proceedings of 34th Annual Meeting of the IEEE Industry Applications Society*, pages 2087–92 vol.3, 1999.

[4] A. Brockmeyer. *Dimensionierungswekzeug für magnetische Bauelemente in Stromrichteranwendungen*. PhD thesis, Aachen University of Technology, 1997.

[5] Jinjun Liu, T. G. Wilson, Jr., R. C. Wong, R. Wunderlich, and F. C. Lee. A method for inductor core loss estimation in power factor correction applications. In *Proceedings of APEC 2002—Applied Power Electronics Conference and Exposition*, page 439, 2002.

[6] Jieli Li, T. Abdallah, and C. R. Sullivan. Improved calculation of core loss with nonsinusoidal waveforms. In *IEEE Industry Applications Society Annual Meeting*, pages 2203–2210, 2001.

[7] K. Venkatachalam, C. R. Sullivan, T. Abdallah, and H. Tacca. Accurate prediction of ferrite core loss with nonsinusoidal waveforms using only Steinmetz parameters. In *IEEE Workshop on Computers in Power Electronics*, 2002.

[8] A.P. Van den Bossche, D.M. Van de Sype, and V.C. Valchev. Ferrite loss measurement and models in half bridge and full bridge waveforms. In *IEEE Power Electronics Specialists Conference*, pages 1535–1539, June 2005.

[9] Alex van den Bossche and Vencislav Valchev. *Inductors and Transformers for Power Electronics*. Taylor and Francis Group, 2005.

[10] S. Mulder. Power ferrite loss formulas for transformer design. *Power Conversion & Intelligent Motion*, 21(7):22–31, July 1995.

[11] E. C. Snelling. *Soft Ferrites, Properties and Applications*. Butterworths, second edition, 1988.

[12] C. P. Steinmetz. On the law of hysteresis. *AIEE Transactions*, 9:3–64, 1892. Reprinted under the title "A Steinmetz contribution to the ac power revolution", introduction by J. E. Brittain, in *Proceedings of the IEEE* 72(2) 1984, pp. 196–221.

[13] A. Brockmeyer. Experimental evaluation of the influence of dc-premagnetization on the properties of power electronic ferrites. In *APEC '96. Eleventh Annual Applied Power Electronics Conference*, pages 454–60, 1996.

[14] A. Brockmeyer and J. Paulus-Neues. Frequency dependence of the ferrite-loss increase caused by premagnetization. In *Twelfth Annual Applied Power Electronics Conference and Exposition*, pages 375–80, 1997.

[15] Wai Keung Mo, D.K.W. Cheng, and Y.S. Lee. Simple approximations of the dc flux influence on the core loss power electronic ferrites and their use in design of magnetic components. *IEEE Transactions on Industrial Electronics*, 44(6):788–99, 1997.

[16] G. Bertotti. General properties of power losses in soft ferromagnetic materials. *IEEE Transactions on Magnetics*, 24(1):621–630, 1988.

[17] G. Bertotti. *Hysteresis in magnetism: for physicists, materials scientists, and engineers*. Academic Press, 1998.

[18] K. H. Carpenter. Simple models for dynamic hysteresis which add frequency-dependent losses to static models. *IEEE Transactions on Magnetics*, 34(3):619–22, 1998.

[19] J.-T. Hsu and K. D. T. Ngo. A Hammerstein-based dynamic model for hysteresis phenomenon. *IEEE Transactions on Power Electronics*, 12(3):406–413, 1997.

[20] H. Saotome and Y. Sakaki. Iron loss analysis of Mn-Zn ferrite cores. *IEEE Transactions on Magnetics*, 33(1):728–34, 1997.

[21] W. Roshen. Ferrite core loss for power magnetic components design. *IEEE Transactions on Magnetics*, 27(6):4407–15, 1991.

[22] P. Tenant and J. J. Rousseau. Dynamic model of magnetic materials applied on soft ferrites. *IEEE Transactions on Power Electronics*, 13(2):372–9, 1998.

[23] F. Fiorillo and A. Novikov. An improved approach to power losses in magnetic laminations under nonsinusoidal induction waveform. *IEEE Transactions on Magnetics*, 26(5):2904–10, 1990.

[24] D. C. Jiles. Frequency dependence of hysteresis curves in 'non-conducting' magnetic materials. *IEEE Transactions on Magnetics*, 29(6):3490–2, 1993.

[25] Wei Shen, Fei (Fred) Wang, Dushan Boroyevich, and C. Wesley Tipton. Loss characterization and calculation of nanocrystalline cores for high-frequency magnetics applications. *IEEE Transactions on Power Electronics*, 23(1), 2008.

[26] Ray Ridley and Art Nace. Modeling ferrite core losses. *Switching Power Magazine*, 3(1):6–13, 2002.

[27] Christopher Oliver. A new core loss model. *Switching Power Magazine*, 3(2), 2002.

[28] Ferrite material selection guide, 2000. Magnetics Division of Spang & Company, Bulletin No. FC-S1.

[29] Soft ferrites and accessories, data handbook, 2009. Ferroxcube, Eindhoven, The Netherlands.

[30] Ferrites and accessories: SIFERRIT materials, 2006. EPCOS AG, Munich, Germany.

[31] K. H. Carpenter and S. Warren. A wide bandwidth, dynamic hysteresis model for magnetization in soft ferrites. *IEEE Transactions on Magnetics*, 28(5):2037–41, 1992.

[32] I. D. Mayergoyz. *Mathematical models of hysteresis*. Springer-Verlag, 1991.

[33] Ping Han, G. R. Skutt, Ju Zhang, and F. C. Lee. Finite element method for ferrite core loss calculation. In *Applied Power Electronics Conference and Exposition*, volume 1, pages 348–353, 1995.

Testing Core Loss for Rectangular Waveforms, Phase II Final Report

21 September 2011

Charles R. Sullivan
John H. Harris
Thayer School of Engineering at Dartmouth
charles.r.sullivan@dartmouth.edu
http://engineering.dartmouth.edu/inductor
8000 Cummings Hall
Hanover, NH 03755, USA

Sponsored by
The Power Sources Manufacturers Association
email: power@psma.com
http://www.psma.com/
P.O. Box 418
Mendham, NJ 07945-0418
Tel: (973) 543-9660
Fax: (973) 543-6207

Testing Core Loss for Rectangular Waveforms, Phase II Final Report

Charles R. Sullivan, John H. Harris
Thayer School of Engineering at Dartmouth
charles.r.sullivan@dartmouth.edu
http://engineering.dartmouth.edu/inductor
8000 Cummings Hall, Hanover, NH 03755, USA

21 September 2011

Summary

The Switching Power Converter Core Loss Project, Phase II is a follow-on to the Switching Power Converter Core Loss Pilot Project, conducted in 2009 [1]. In Phase II, we have accomplished these additional objectives:

- Gathered data on many more materials, particularly ferrites, and further validated the composite waveform hypothesis. More than 4000 experimental runs were performed.
- We confirmed that core losses per cycle increase when the voltage waveform includes off-time. This phenomenon was first noted in the Phase I project. Additional testing established that it is a real phenomenon, and not an artifact of the testing procedure. We also developed an alternative waveform that does not exhibit this behavior.
- Measurements were performed with a drilled core having embedding sense windings, looking for transient flux migration that might help explain off-time core loss.
- We developed a Steinmetz-like curve fit, and applied it to all the core characterization data. For the first time, a formula is available to predict loss accurately over a wide frequency range, avoiding glitches between frequency ranges that occur with other models. Furthermore, the model directly predicts loss with rectangular waveforms. It is available in different forms for different applications.
- We investigated the possibility of accidental residual magnetization biasing measurement results. We developed an automatic degaussing technique, and by comparing with previous results, we did not discover any evidence that the Phase I results were affected by such spurious magnetization.

There are four appendices to this report. In Appendix A, we illustrate that core loss of non-sinusoidal waveforms cannot be accurately predicted by separately examining the Fourier components of the waveform. In Appendix B, we provide an example of the use of the composite waveform model in a design application. In Appendix C we provide additional data plots. And in Appendix E we provide a a table with additional details of the Steinmetz-like loss modeling.

All of the data collected for this project accompany this report and are available for use by anyone. Full data from more than 4000 experimental runs are archived. For information about using the data generated in the project, see *Using the PSMA Rectangular Waveform Core Loss Data* [2].

Contents

Appendices

List of Tables

List of Figures

1 Introduction

In the design of magnetics for switching power applications, it is essential to accurately estimate core loss, but current methods based on sinusoidal data are difficult to use and inaccurate. Phase I of this project established the feasibility and value of a new method proposed by Herbert [3], in which a simplified set of square-wave measurements produces data that can be used to calculate loss for *any* alternating rectangular-voltage waveform.

The hypothesis to be tested was that, for alternating rectangular pulses and a given magnetic core material, the core loss energy per period depends only on component pulse widths and peak voltages. We call this the *composite waveform hypothesis* (CWH).

In Phase I of the program, we established that this hypothesis, while not perfect, works well enough to be a significant improvement in both accuracy and ease of use, compared with methods based on sinusoidal data. It is convenient to decompose rectangular waveforms into such pulses for analysis. Thus, it is sufficient to test cores with square voltage waveforms, and then use the data to predict losses with generalized rectangular voltage waveforms.

Phase II of the project addresses these additional objectives:

1. To gather more square wave data to characterize additional core materials and geometries, as well as validation data, to further test the CWH.
2. To investigate the dynamics of core flux distribution using embedded sense windings.
3. To provide Steinmetz or similar curve-fitting parameters, for use in numerical design techniques.
4. To investigate the anomalous results discovered in Phase I involving prolonged off-time waveforms.
5. To investigate the possibility of experimental error due to residual magnetization in sample cores.
6. To demonstrate the use to this methodology in a design application.
7. To demonstrate the shortcomings of core loss estimates obtained by summing sinusoidal Steinmetz estimates for rectangular waveform harmonics.
8. To improve data management and presentation to make the results more accessible to users.

In the sections that follow, we discuss the topics listed above in detail.

2 The Basic Experiment

In the basic experiment, a magnetic core is driven with a full bridge switching circuit (Figure 1). There is a second sense winding for measuring flux, to avoid

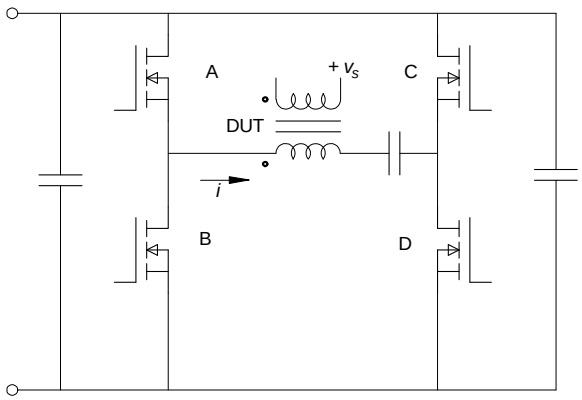

Figure 1: Full-bridge excitation circuit. The device under test (DUT) is a magnetic core.

measuring resistive loss in the drive winding. A blocking capacitor insures zero net DC current. In most tests, the capacitor voltage is negligible, and is only needed to cancel small volt-second mismatched due to timing errors. However, asymmetric waveforms are implemented by using significantly different on-times for positive and negative pulses. The capacitor voltage automatically adjusts to reduce the voltage of the longer pulse in order to have equal volt seconds between positive and negative pulses. Our apparatus is capable of taking measurements in a range of about 5 kHz to 500 kHz. The sample core is oil cooled, usually kept at 80 °C.

We take measurements with an Agilent Technologies DSO 7104A oscilloscope. Current is measured with a Tektronix P 6021 AC current probe. The switching bridge is controlled by a programmable function generator with some additional logic. This determines the frequency and pulse lengths. The bridge power supply voltage determines the voltage amplitude. All three instruments are under the control of a computer, which orchestrates sets of experiments and manages the resulting data (Figure 2). The oscilloscope sweep time is one period. It averages the information from 512 triggers, and saves voltage and current information at 1000 time-points per period.

We refer to one of these experiment as a *run*—think of a run as single captured waveform. A run takes only a few seconds, but wound cores are normally tested with a batch of runs, called a *run set*, in which frequency, amplitude, and pulse widths are varied from run to run. Run sets always include square wave runs, which characterize the coil under test. Data from more than 4000 runs have been collected and accompany this report. Other wave forms (Figure 3) are also usually included to provide validation of the CWH, or for exploring other phenomena.

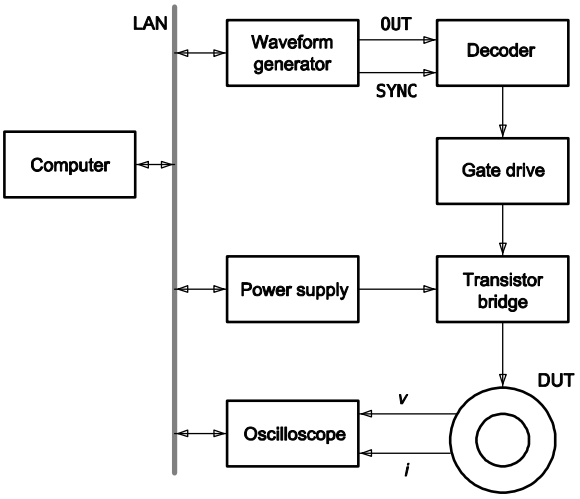

Figure 2: Block diagram of the experimental apparatus. The power supply, drive bridge, and oscilloscope are all controlled by the computer, which also gathers, and analyzes, the resulting data.

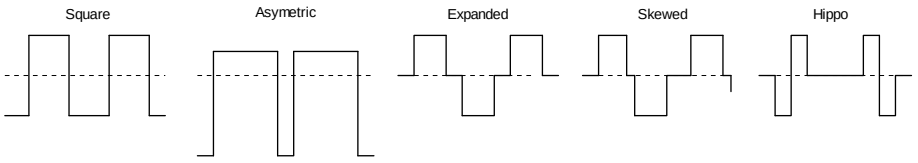

Figure 3: Excitation waveforms. The `hippo` waveform was added in Phase II, and was found to avoid the loss increase observed in the `expand` waveform.

3 Broader Data Set

We have tested and provide test data for twenty different wound samples, including eleven different materials from four different manufacturers. These are summarized in Table 1.

Most of the cores are toroidal, but to test the effect of varying cross-section area and corners, the selection includes E-cores. In another test of the effect of flux constriction, we ground a flat side on a toroidal core (Figure 4). The E cores and flattened-toroidal cores showed the same general behavior and characteristics as the toroidal cores, although the specific loss values were affected.

To search for anomalous behavior we examined over 400 files. We noted no significant qualitative difference with regard to the CWH in the results—it holds for this broader select of cores. There may be effects of the corners and constrictions that we did not discover in this evaluation, and we encourage continued examination and analysis of the data to potentially uncover additional phenomena of interest.

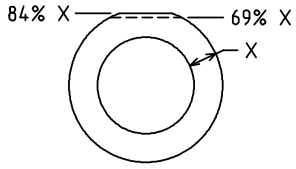

Figure 4: Toroidal core with added constriction. The same core was tested with no constriction (run set `mi01-1`), and with the cross section area reduced to 84% (`mi009`), and 69% (`mi010`) of the total, by grinding a flat section.

4 Drilled Core Experiments

We investigated core flux distribution using a ferrite core with embedded sense windings. A core was fabricated with four holes drilled through—two intersecting pairs, forming two *cross points* (Figure 5, left). One hole of a pair is radial, perpendicular to the axes of the toroid, the other is parallel to it. Each cross point divides the cross section into unequal quadrants. By threading wires through the holes, we can form a single-turn sense winding to measure the flux in any quadrant, or any adjacent pair of quadrants. By subtracting the signal from different wirings, we can infer the flux in any of the nine subsections.

4.1 Geometry

The drilled core was fabricated from a toroidal core having a square cross-section, $0.5 \times 0.5\,\mathrm{in}^2$ (a Magnetics Div., Spang & Co. Inc. 0F46113TC). The two cross points were chosen to collectively divide the core area into nine equal, square subsections. The two pairs of holes are displaced circumferentially about

Manufacturer Material	Shape	Core ID
Ceramic Magnetics Inc		
MN60	23.2,14.5,7.2T	cm01
MN8CX	23.2,15.1,7.7T	cm02
Ferroxcube		
3C81	E19/8/5	fx09
3C81	TX22/14/13	fx003
3C90	TX22/14/6.4	fx010
3F3	E19/8/5	fx05
3F3	TX22/14/13	fx004
Magnetics Inc.		
F	42206-TC	mi005
F	46113-TC	mi11-1
K	42206	mi007
L	2206	mi08
P	42206-TC	mi003
R	42206-TC	mi001
R	custom	mi009
W	42206	mi02
Payton Tech.		
amorph. Co	18x11x10	pt01

Table 1: Cores tested in the project.

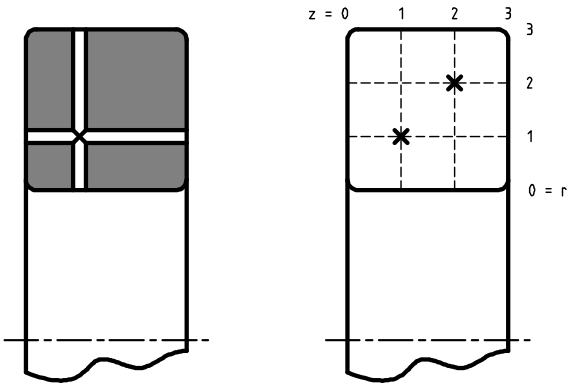

Figure 5: Section view of a drilled core showing one pair of cross-point holes (left), and the grid used to describe subsection geometry (right). Cross points are show with an $\times$.

the toroid, to avoid unnecessary constriction of the flux path due to the holes. (The drawing is to scale; a single cross-point pair consumes 15% of the core cross section area.) We take advantage of the symmetry of the toroid, and collapse the circumferential dimension, regarding the cross points as lying in one radial cross-section plane (Figure 5, right). The details of the naming of subsections, necessary for interpreting the data, are presented in the user manual [2].

4.2 Experimental Setup

For these runs, the voltage across the embedded sense winding was recorded on an additional oscilloscope channel. The core had $N = 4$ turns for the primary winding. By averaging over 512 triggers, the noise on the single-turn sense winding was typically below the resolution of the oscilloscope digitization. Unlike the routine runs, the center hole in the toroid was not blocked with a low-dielectric-constant material, in order to avoid fouling the probe holes. Measurements were made at room temperature. Automatic degaussing was used (Section 7).

The sample was driven with square wave signals, and with the `expand` validation waveform. Our objective was to detect any unusual dynamic variation of the fraction of flux passing through the subsection, under these various drive conditions. We generated plots of three values: (1) the full-core sense winding voltage, (2) the embedded winding voltage, and (3) the ratio of the two (Figure 6). To make visual comparison easier, the embedded winding voltage was scaled by NA/A_p, where N is the number of turns around the full cross-section, A is the full core cross-section area, and A_p is the "probe area," the area of the core enclosed within the sense winding. This ratio would be unity if the flux distribution were uniform.

Even under the null hypothesis that there are no new dynamic flux distribution effects discovered, and that the permeability is constant, uniform and isotropic, we would not expect the flux distribution be uniform—there is a radial gradient, with $B \propto 1/r$. The flux contained in the annulus between r_1 and r_2,

$$\Phi(r_1, r_2) = h \int_{r_2}^{r_1} B(r) dr \quad (1)$$

$$\propto \log(r_1) - \log(r_2) \quad (2)$$

and h is the height of the toroid. For our drilled core,[1] this leads us to expect (under the null hypothesis) ratios of 119%, 98.1%, and 83.4%, in that order, from inside out. The ratio in Figure 6 averages 116%.

Also, of the nine subsections, the four corner subsections have slightly less area, due to the corner radii, and will enclose less flux. The manufacturer does not specify this radius, and we did not measure it, being more interested in the dynamics of the flux distribution.

[1] Using the manufacturer's nominal dimensions.

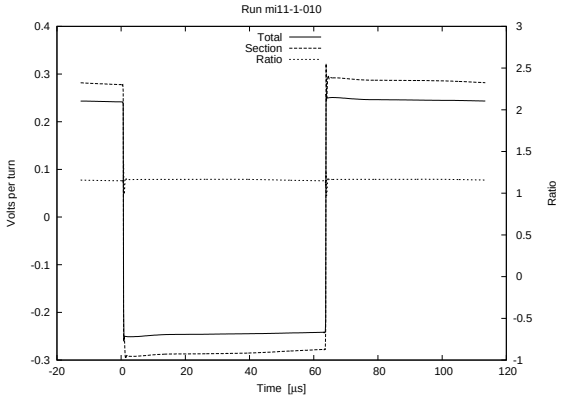

Figure 6: Flux distribution between subsections. The total flux is compared with the flux through the inner 1/3 annular section (designated 0031) of a toroidal core (the latter scaled by NA/A_p). The third plot is the ratio of the two.

4.3 Observations

We are looking for variations in the flux distribution with time, which should show up as deviations of the sense winding voltage ratios from a constant. Such deviations could be caused by changes in the flux distribution in the core, or by spurious artifacts of the measurement apparatus. Careful examination of the data can distinguish between the two.

In Figure 6 we see an interesting feature of the ratio plot—a transient at the zero crossings. Figure 7 shows this more clearly, because here the period is $8\,\mu$s, instead of $120\,\mu$s, and ringing at about 1.5 MHz is easily seen. This ringing appears in all the probe winding plots, but the outer, total-flux winding only shows the 30 MHz ringing characteristic of the drive circuitry. If the lower frequency ringing is due to flux migrating from one region to another, we expect this lower frequency ringing to sum to zero across regions, and the polarity of some regions to be reversed.

Figure 8 shows the central annulus with the same excitation voltage, and we see *inverted* low-frequency ringing. Figure 9 tells the whole story. In it, the probe winding voltages for all three annular layers of the core, and their sum,[2] are plotted together. The flux appears to move in and out of the central region from the other two regions. The lower frequency transients all cancel out in the sum of the three voltages, leaving only the high-frequency, drive circuit artifacts.

We believe the low frequency ringing is due to dimensional resonances, such as described in [4], and are evident because of the low electromagnetic propagation velocity (v) of the ferrite medium. Because v is low, resonances due

[2]This is the sum of the three probe voltages, *not* the outer sense winding voltage, scaled.

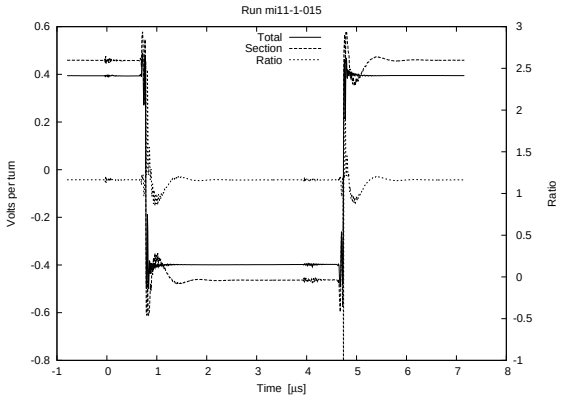

Figure 7: Flux distribution, showing a transient disturbance. This is the same subsection of the core as in Figure 6, but at a higher frequency. The disturbance could be a transient flux migration.

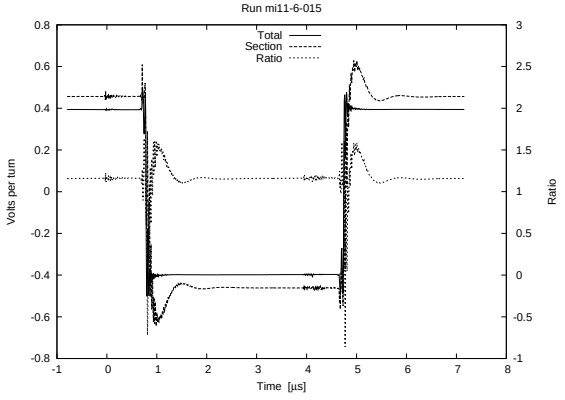

Figure 8: Central annulus flux distribution. This probe subsection is the central 1/3 annulus (designated 0132). The transient disturbance shows reversed polarity compared to Figure 7.

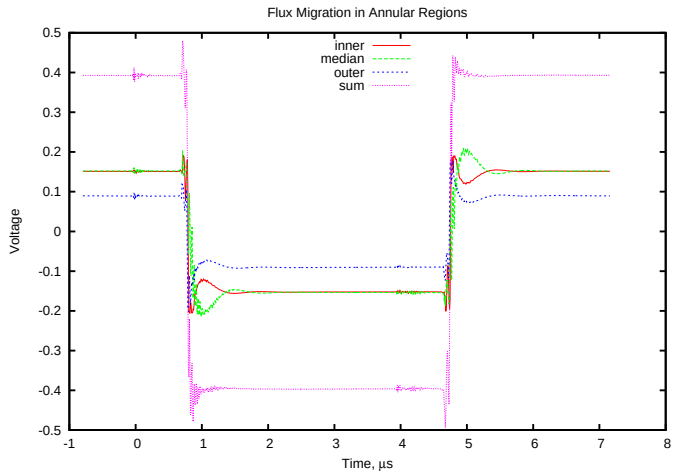

Figure 9: Flux migration is evident from probe winding voltages for the three disjoint annular regions of the drilled core. disturbance shows reversed polarity in the central region. The sum shows no low-frequency transient.

to the geometry of the core can have frequencies within the band of interest. It is perhaps counterintuitive that v could be so low that this effect would be significant for such a small device ($\sim 1\,\mathrm{cm}$) and modest bandwidth ($\sim 1\,\mathrm{MHz}$). Consider the familiar equation for propagation velocity,

$$v = \frac{c}{\sqrt{\mu_r \epsilon_r}}, \tag{3}$$

where c is the velocity of light in a vacuum, and μ_r and ϵ_r are the relative permeability and permittivity, respectively. We expect a large μ_r for a ferrite core, but ϵ_r is seldom published for ferrites, and so may be unfamiliar. Magnetics [5] gives a value of $\mu_r = 750$ for the F material used in these experiments, but does not publish a permittivity. However, Ferroxcube's catalog ([6], p.61) presents a table, for MnZn ferrites in general, of estimated ϵ as a function of f under sinusoidal excitation. It lists $\epsilon_r \approx 10^5$ at $1\,\mathrm{MHz}$.[3]

To see if dimensional resonance is a plausible explanation for the transient voltages we observe, we will try to estimate ϵ_r from our observations. Imagine an infinite cylindrical medium with a cross-section matching our toroid, driven by a step function at its boundaries. We would expect it to ring with a fundamental wavelength, λ, equal to twice its width ($2 \times 12.5\,\mathrm{mm}$). We have observed a ringing frequency, $f \approx 1.5\,\mathrm{MHz}$, so we can calculate $v = f\lambda$. Substituting this

[3] Inspecting the table, we see a strong dependence of ϵ_r on f—ferrite is a dispersive medium, and we are driving the core with square waves. We should regard this number as a rough approximation.

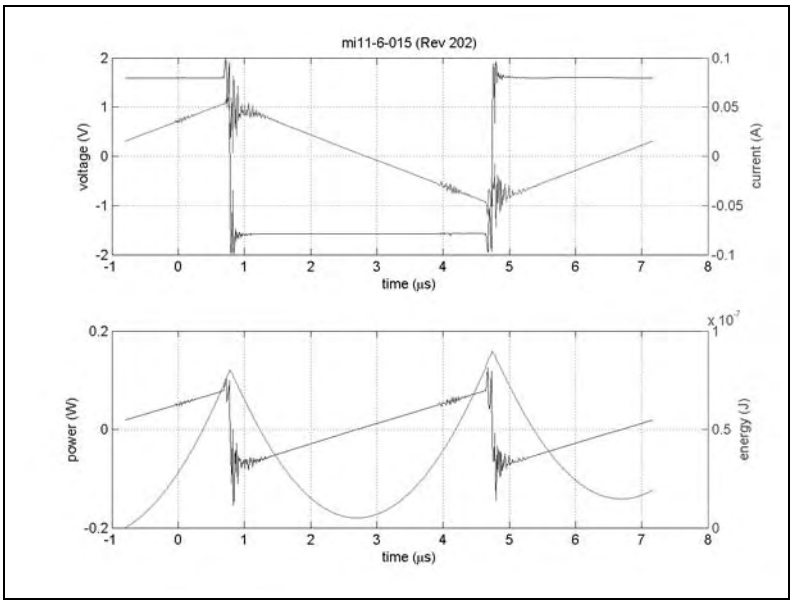

Figure 10: Raw oscilloscope data plot for the drilled core. The power and energy plots in this image could show losses due to the flux migration transient if they are significant. (The probe winding voltage does not appear in the standard oscilloscope plots.)

into (3) and solving for ϵ_r, we get

$$\epsilon_r = \frac{1}{\mu_r}\left(\frac{c}{f\lambda}\right)^2 \tag{4}$$

$$\approx \frac{1}{750}\left(\frac{3\cdot 10^8\,\mathrm{m/s}}{(1.5\,\mathrm{MHz})(25\,\mathrm{mm})}\right)^2 \tag{5}$$

$$\epsilon_r \approx 8.4\cdot 10^4. \tag{6}$$

This is close to the same order of magnitude as Ferroxcube's estimate for their similar materials, making the dimensional resonance theory look plausible, though further study is merited (Section 9.3).

One might wonder whether this flux migration causes significant loss. If so, it would appear in the oscilloscope data plot (Figure 10), and affect the current, power, and energy curves. The energy plot gives a particularly clear view, because the integration smoothes the drive circuit transient ringing. We see nothing unusual around the time of the flux migration (the first 1.5 μs of a pulse).

It is worth noting that the flux distribution transients, lasting scarcely 2 μs, are unlikely to explain the off-time loss phenomena described in Section 6.

The full data from these experiments accompanies this report, and is avail-

able for further investigation of possible flux migration phenomena.

5 Steinmetz Curve Fits

The Steinmetz[4] approximation,

$$\overline{P_v} = k f^{\alpha} \hat{B}^{\beta}, \tag{7}$$

where $\overline{P_v}$ is the average power density, f is the excitation frequency, and $\hat{B}$ is the peak flux density, is commonly used to characterize core loss data for sinusoidal excitation, but can also be applied to our square-wave data. We first describe a formulation in terms of frequency and flux density, but then also provide a formulation in terms of pulse widths and applied voltage.

To linearize the equation for curve fitting, we used base-10 logarithms (referenced to 1 V or 1 s), because the preferred values for voltage and time used in the experiment are round decilog values, and because using $\log_{10}$ makes it convenient to express the standard error in familiar units of decibels (i.e., $10 \log_{10}(P/P_{\text{ref}})$). This choice does not affect the values of the k, α, and β parameters.

In a typical case, Ferroxcube 3C81 material, fitting (7) to the entire set of square wave data gave a standard error of about 1.5 dB. Visually inspecting the plots shows a distinct increase in slope around 100 kHz. This inspired a six-parameter, two-plane curve fit,

$$\overline{P_v} = \max(k_1 f^{\alpha_1} \hat{B}^{\beta_1} + k_2 f^{\alpha_2} \hat{B}^{\beta_2}) \tag{8}$$

This fits the data to two intersecting planes that function like a single plane with a fold in it (Figure 11). It fits the 3C81 data with a standard error of 0.35 dB, much better than the single equation, and also better than simply using different parameters for different frequency ranges.

Note that while the formula we are fitting is essentially the same form as the Steinmetz equation, and we use the variable names k, α, and β, this is a *different* model, because is is based on square wave experimental data, and is intended to predict rectangular pulse core losses. In situations where this might cause confusion, we will subscript the present parameters[5] to distinguish them from the classic Steinmetz, sinusoidal, parameters.

The boundary between the two planes (the fold) projected onto the $\log_{10}(f)$-$\log_{10}(\hat{B})$ plane is a straight line,

$$\log_{10}(\hat{B}) = a_0 + a_1 \log_{10}(f) \tag{9}$$

where

$$a_0 = \frac{\log_{10}(k_1/k_2)}{\beta_2 - \beta_1}$$

[4] Named for C. P. Steinmetz's work [7], although Steinmetz did not include the frequency dependence that is now standard [8].

[5] We choose 'r', for "rectangular," thus avoiding 's' which might suggest either "square" or "sinusoidal."

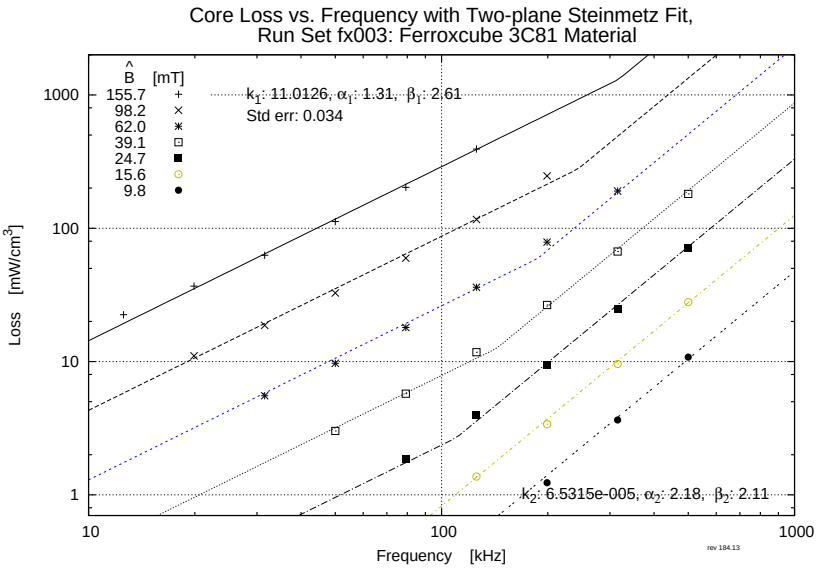

Figure 11: Two-plane Steinmetz curve fit to Ferroxcube 3C81 material, square wave loss data.

$$a_1 \quad = \quad \frac{\alpha_1 - \alpha_2}{\beta_2 - \beta_1}.$$

The parameters a_0 and a_1 might provide a useful characterization of the transition of the dominating loss mechanisms from hysteresis to eddy currents, for comparing different materials. The two-plane Steinmetz parameters from our experiments are listed in Table 2.

This method of curve fitting has advantages over the common practice of providing independent Steinmetz parameters for different frequency ranges:

1. There is no step discontinuity at frequency range boundaries.

2. There is no arbitrary choice of boundary frequency. The curve-fitting optimization chooses the best boundary line (i.e., choosing a_0 and a_1).

3. The curve fitting optimization uses *all* the data.

There is no significant computational penalty for using this model, and coding is easy; programmers can use either (8) directly, or (7), using k_1, α_1, and β_1 for $\log_{10}(\hat{B}) > a_0 + a_1 \log_{10}(f)$, and k_2, α_2, and β_2 otherwise.

The two-plane Steinmetz parameters from our experiments are listed in Table 2. The table includes two different sets of k values. The lowercase k_1 and k_2 are the values used in (8), implicitly using reference values of 1 T and 1 Hz. Also listed are uppercase K_1 and K_2 based on reference values $f_0 = 100\,\text{kHz}$

Manufacturer Material	Geom	Set	k_1	K_1	α_1	β_1	γ_1	k_2	K_2	α_2	β_2	γ_2
Ceramic Magnetics Inc												
MN60	T	cm01	6.085	86810	1.32	2.47	2.15	899.8μ	67879	2.00	2.13	1.13
MN8CX	T	cm02	63.01	182100	1.19	2.49	2.3	177.4μ	87357	2.20	2.29	1.09
Ferroxcube												
3C81	T	fx003	11.01	91200	1.31	2.61	2.3	65.32μ	41432	2.18	2.11	0.93
3C81	E	fx09	18.02	88800	1.23	2.45	2.22	350.0μ	52769	2.10	2.33	1.23
3C90	T	fx010	36.86	39570	1.19	2.94	2.75	2.895μ	18223	2.39	2.16	0.77
3F3	T	fx004	102.4	67200	1.13	2.81	2.68	11.93μ	28414	2.30	2.14	0.84
3F3	E	fx05	40.63	65950	1.14	2.50	2.36	224.8μ	38221	2.12	2.36	1.24
Magnetics Inc.												
F	T	mi005	26.41	72920	1.24	2.76	2.52	7.612μ	32369	2.37	2.22	0.85
K	T	mi007	246.2	86830	1.10	2.95	2.85	5.276μ	20750	2.41	2.48	1.07
L	T	mi08	706.8	150800	1.04	2.87	2.83	276.1m	99927	1.69	2.88	1.19
P	T	mi003	10.91	43090	1.28	2.80	2.52	75.99μ	36099	2.16	2.13	0.97
R	T	mi01-6	30.16	67220	1.25	2.90	2.65	14.55μ	30033	2.31	2.24	0.93
W	T	mi02	832.7m	131000	1.51	2.37	1.86	10.59m	123857	1.82	2.04	1.22

Table 2: Two-plane Steinmetz parameters for various magnetic materials in two general geometries, toroidal (T) and E-core (E). The k_i parameters are referenced to $f = 1\,\mathrm{Hz}$ and $\hat{B} = 1\,\mathrm{T}$; the K_i parameters are referenced to $f = 100\,\mathrm{kHz}$ and $\hat{B} = 100\,\mathrm{mT}$. All the k_i and K_i parameter have dimensions of $\mathrm{W/m^3}$. The α and β parameters for use in (8); γ is required for (11).

and $\hat{B}_0 = 100\,\mathrm{mT}$, to be used in

$$\overline{P_v} = \max\left(K_1(f/f_0)^{\alpha_1}(\hat{B}/\hat{B}_0)^{\beta_1} + K_2(f/f_0)^{\alpha_2}(\hat{B}/\hat{B}_0)^{\beta_2}\right) \tag{10}$$

Both are included because the (8) is simpler to use, but the values of K_1 and K_2 are more physically meaningful, because they are based on results near the range of values used in practice, rather than on values many orders of magnitude different.

For example, the values of K for one core shape are very similar to those for another core shape and the same material, indicating that the losses predicted by the model are very similar for the two shapes. The values of k, on the other hand, can be very different, but this is only an artifact of the use of the 1 T and 1 Hz reference points, which are distant from the actual operating point, and is not an indication that the predictions in the region of interest are significantly different.

The results tend to indicate slightly smaller losses for E cores than for toroidal cores made with the same material. This does not actually indicate of superior performance for E cores. Rather, it is a result the effective area and effective core length provided one the core datasheet, which we used in our calculations.

5.1 Model in Terms of Pulse Width and Voltage

The model (8) can be reformulated in terms of pulse width and voltage. For direct use with that composite with form hypothesis, we also reformulated it to represent the energy loss for one pulse, rather than the average power loss over a whole cycle. This results in energy loss per pulse, per unit volume, of

$$E_{v,a} = \max\left(\frac{k_1}{(NA)^{\beta_1} 2^{(\beta_1+\alpha_1)}} V_a^{\beta_1} t_a^{\gamma_1} \ , \ \frac{k_2}{(NA)^{\beta_2} 2^{(\beta_2+\alpha_2)}} V_a^{\beta_2} t_a^{\gamma_2}\right) \tag{11}$$

where V_a is the voltage applied during a pulse of duration t_a, A is the cross-section area of the core, and N is the number of turns. The parameter γ is provided in Table 2, for convenience, but can also be simply calculated from α and β:

$$\gamma = 1 + \beta - \alpha. \tag{12}$$

The application of this formula is illustrated in Appendix B.

6 Dead-Time Loss

In Phase I, we discovered a significant deviation from the CWH during periods of prolonged constant flux. This was most evident with the `expand` waveform, in which a square wave is stretched by inserting off-time between the square pulses—thus increasing the period while holding the pulse widths constant. For example, in Figure 12 we plot loss versus off time, t_0. The "predicted" value is simply the loss measured for the characterization square-wave measurement. In contrast, the CWH works well for the asymmetric waveform (Figure 13), which has no dead time

The effect is also noticeable in plots of the `skew` waveform (Figure 14). The core loss is uniformly higher than for square waves, at about the same value as seen for the `expand` waveform having the same period. Unlike the `expand` waveform, the plot is not significantly slopped—the increased loss due to greater off time in one part of the waveform is about offset by the decreased loss due to lesser off time in the other part.

In Phase II, we want to determine if the phenomenon is real, and if so, possibly characterize it.

6.1 Measurement Artifacts

In order to check for possible errors introduced by the apparatus, we repeated a representative experiment with (1) a DC current probe, and (2) increased bridge blocking capacitance. Neither precaution made a significant difference.

The magnetization current is routinely measure using a Tektronix P6021 AC current probe (set to 10 mA/mV). For this experiment we substituted a Tektronix TCP303 current probe. As an extra precaution, we did the probe degaussing procedure before each run. (Run set `mi05-5`)

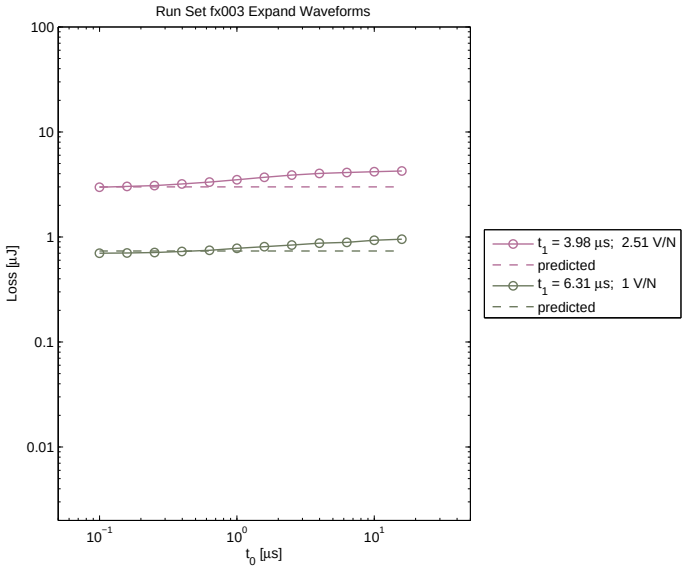

Figure 12: `expand` waveform core loss vs. off time between pulses. The "predicted" value is the loss measured for a square wave ($t_0 = 0$). Additional plots of this effect for different materials, are provided in Appendix C.

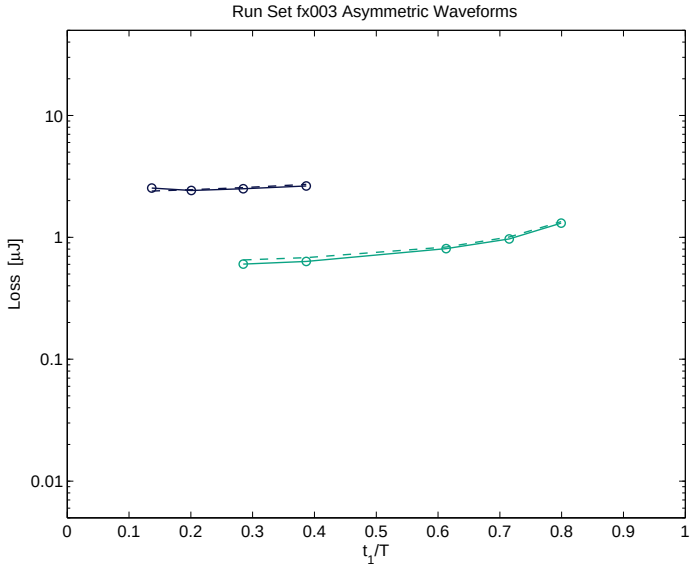

Figure 13: `asym` waveform core loss vs. asymmetry, t_1/T. The "predicted" value is the sum of the losses measured for square wave pulses of length t_1 and $T - t_1$.

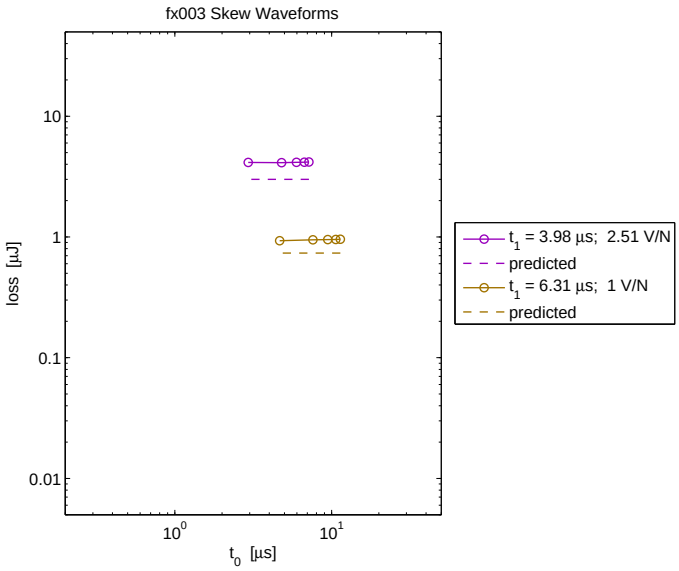

Figure 14: `skew` core loss vs. t_0, where t_0 is the off time between the first and second pulses. The other off time equals $T - 2t_1 - t_0$

.

In Phase I, the bridge was equipped with a 320 μF blocking capacitor. On very long `expand` runs, low-frequency ringing was evident. We wanted to improve this performance by increasing the blocking capacitance, while lowering the effective series resistance, so we installed 120 mF of blocking capacitance, using Epcos MKT series polyester capacitors.

6.2 Zero-Flux Off Time

In order to see if the extra loss is correlated with the presence of magnetic flux, we devised a new wave form, the *hippo* (Figure 3), named for its resemblance to hippopotamus dentition. This waveform has two pairs of pulses, with each *pair* having a width of t_1 (i.e., two opposing pulses of width $t_1/2$). Thus the flux returns to zero during the off time. Using this waveform, the measured loss matched the predicted value more closely, actually dropping somewhat (Figure 15). [6]

[6] We also note a curious hump in the plot at very low t_0. This is an artifact of the apparatus—the waveform decoder circuitry ([1], Section 4) has a delay of about 400 ns in the `OUT` signal rise time, making unable to create this short a dead time for the `hippo` waveform. The plot time scale is based on the `SYNC` signal, not the actual sense winding voltage.

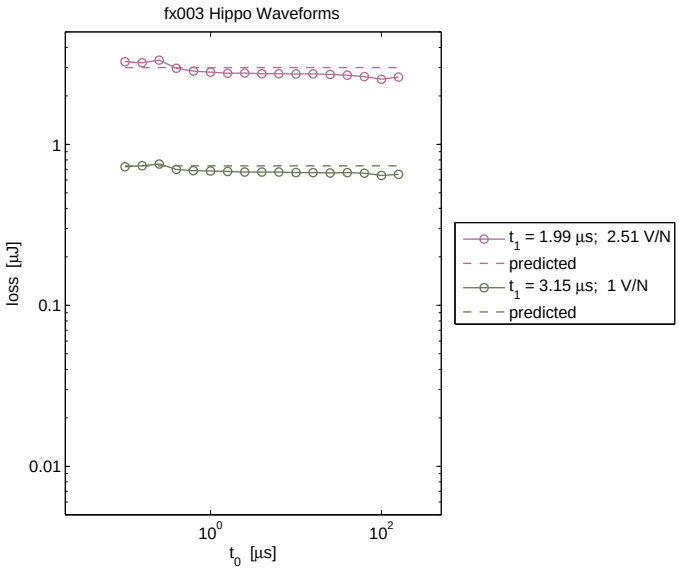

Figure 15: `hippo` waveform loss vs. off time.

6.3 An Improved "Predicted" Model

In Phase I, the "predicted" values were simply the square-wave values, taking the excitation voltage to be zero during the off time. This is not quite correct, since the power supply is merely disconnected from the device under test, instead of enforcing zero voltage across it. As a result, the iR drop across the winding causes the flux to droop during the off time—the excitation waveform has an approximately trapezoidal segment during this interval. We expect this change in flux to cause some core loss.

It is tempting to think this segment could be approximated by a square segment, and invoke the CWH, but the CWH applies only to waveforms composed of *alternating* rectangular pulses. When stepped pulses are allowed, the model becomes inconsistent; for example, it would imply that core loss is independent of frequency, as in the case of square wave pulses at frequency f, which could be considered to be composed of *pairs* of pulses of width $T/4$.

There is a piecewise linear (PWL) model presented by by Venkatachalam, et al [9], that *is* applicable. Their work is on a more general semiempirical model, but it predicts a PWL power density

$$P_D = \frac{k_i (\Delta B)^{\beta-\alpha}}{T} \sum_m \left| \frac{\Delta_m B}{\Delta_m t} \right|^{\alpha} \Delta_m t, \tag{13}$$

where ΔB is the peak-to-peak flux density for the overall waveform, and Δ_m indicates changes over the mth segment of the piecewise decomposition. The parameters α and β are the (sinusoidal) Steinmetz parameters, and k_i is their

own parameter, derived from the Steinmetz parameters.

For this application, k_i is derived from our rectangular-wave Steinmetz curve fit. We start with (13) for a square wave, i.e., $\Delta B = 2\hat{B}$ and $\Delta t = T/2$:

$$P_D = \frac{k_i (2\hat{B})^\beta}{T (2\hat{B})^\alpha} 2 \left(\frac{2\hat{B}}{T/2} \right)^\alpha \frac{T}{2}, \tag{14}$$

which reduces to

$$P_D = k_i 2^{\alpha+\beta} f^\alpha \hat{B}^\beta. \tag{15}$$

This very similar to one plane of (8), and if we equate them we find that

$$k_i = \frac{k_r}{2^{\alpha_r+\beta_r}}, \tag{16}$$

where k_r, α_r, and β_r are the rectangular-wave Steinmetz parameters.

There is still the interesting question of which plane of the two-plane curve fit to use, but in the example in the following discussion, all factors suggest the low-frequency plane is the best choice, and we will proceed with that.

This model is easy to apply to our data—after integration, the $B(t)$ data are quite clean, without evidence of ringing and switching transients. The waveform is crisp and easily decomposed into PWL segments. We will now consider a particular run, `fx003-90`, which uses a Ferroxcube 3C81 core, excited with 1.26 V/turn, 4 μs pulses, stretched to a period of 8 μs.

Model	Loss/cycle	Relative
Measured	4.243 μJ	147.4%
PWL predicted	2.918 μJ	101.4%
Simple predicted	2.879 μJ	100.0%

From this we see that the two different predictions—the simple prediction, and the corrected prediction developed in this section—differ only slightly. That means that our original conclusions are unaltered by this analysis: that is, that the off-time loss phenomenon is real. Specifically, in this case, it results in nearly a 50% increase in loss.

6.4 Conclusion

From these observations we conclude that there is indeed some loss mechanism having a long relaxation time in ferrite cores. This concurs with work recently published by Mühlethaler, et al [10]. Additional plots this effect, as in Figure 12, but for different materials, are provided in Appendix C.

7 Degaussing

In Phase I, the apparatus was designed so that if sample cores had no initial magnetization, no residual magnetization would remain as a result of a measurement process. The process control sequence was

1. Set up and run the pulse timing logic signal (before turning on the bridge power supply; the function generator is always on).
2. Upload the required voltage to the bridge power supply.
3. Enable the power supply output.
4. After a delay, initiate the oscilloscope data acquisition sequence.
5. After the oscilloscope signals that data acquisition is complete, disable the power supply output; the voltage slews to zero at about 1.5 V/s. This slew rate is not programmable—it is just a property of the particular power supply we are using.
6. Delay several seconds to allow the power supply to settle and the core to cool.

However, there was some concern that there might still be some residual magnetization, either initially, in the core as supplied by the manufacturer, or introduced inadvertently, in the handling of the wound device, or due to an undiscovered defect in the apparatus or its control algorithm.

To check for this possibility, we created a degaussing control sequence, reran some experiments and compared the results with those obtained with the original setup. The new control sequence was

1. Setup and run the pulse timing logic signal.
2. Upload the *maximum* safe voltage to the bridge power supply and enable the power supply output. The voltage slews from zero to the maximum voltage, driving the core into saturation.
3. Upload the voltage required for the experiment. The output voltage slews down to that value at about 1.5 V/s. This is the degaussing step.
4. When the power supply output voltage reaches the correct value, initiate the oscilloscope data acquisition sequence.
5. After the oscilloscope signals that data acquisition is complete, disable the power supply output.
6. Delay for power supply settling and core cooling.

With this degaussing scheme, the residual flux for a square wave is limited to about $T^2 r/2$, where T is the period and r is the slew rate. At 10 kHz, this works out to about 8 nWb per turn.

This control sequence adds significantly to the overall run time for a sample, due to the degaussing voltage decay time. To speed things up, we switched from a worst-case, fixed delay (step 4 of the old sequence), to an adaptive delay that only waits long enough for the output voltage to reach its target.

Comparing the results we saw no significant difference. This makes us more confident, but it is not a conclusive result. A better approach might be to

institute degaussing on all runs, as a precautionary measure. There is a cost in run time, however. The additional delay for the degaussing step can add about three seconds per run, and samples typically require 200 to 300 runs.

8 Using the Data

The data that has been gathered in the project has been compiled in a distributions format that is available on DVD ROM and may be offered on a web site. Its format and interpretation is detailed in *Using the PSMA Rectangular Waveform Core Loss Data* [2], found in a PDF file in the data home directory. Briefly, the distribution has this directory structure:

`/` (The home directory.) General information, including the user manual, and indexes of cores and run sets.

`/cores/` Data files describing the various magnetic cores.

`/sets/` Containing subdirectories, each containing the data for a single run set and named for the set identifier, *`setId`*.

`/sets/`*`setId`*`/` Containing various data files describing the run set, and subdirectories with raw data and plots.

`/sets/`*`setId`*`/scope/` A directory containing the raw data from the oscilloscope: one CSV file for each run (characterized by frequency, peak voltage, and wave shape). There may be several hundred runs.

`/sets/`*`setId`*`/images/` Plots for each run, showing voltage, current, power, and energy, versus time.

`/sets/`*`setId`*`/auximages/` An optional directory, with more plots for special runs, such as those for the embedded winding experiments.

`/sets/`*`setId`*`/results/` Plots summarizing the runs set, comparing runs in families of curves. Appendix C describes the characterization plots, useful for design.

`/zips/` Zip archive files of the `/sets/` subdirectories, for ease of downloading.

Users browse the indexes found in the home directory, and select runs sets of interest. They can retrieve zip archive files of those run sets from the `/zips/` directory, or browse `/sets/`*`setId`*`/`, directly.

9 Future Work

Although this project has produced scientifically interesting new results and has developed techniques that are practical and useful to practicing engineers, many scientific questions and practical problems remain to be solved. In this section we outline some possibilities for future work.

9.1 Modeling

The model developed here provides improved accuracy in modeling core loss across a wide range of practical waveforms and frequencies. However, there are three important limits on its applicability:

- It does not account for the effects of DC flux bias in the core.
- It does not account for the off-time loss phenomenon.
- It provides a method for calculation of loss from a set of excitation waveforms, but does not provide a dynamic model applicable to simulation of a component, circuit, or system in a SPICE or other computer simulation.

Although there has been work published addressing the effects of DC bias and attempting to model the off-time loss phenomenon, it is not clear that the available approaches are practical or that they will work consistently across a wide range of excitation parameters, such as the data collected here. There is also a range of simulation models available for hysteretic behavior. However, most of these models address only static (rate-independent) hysteresis, and do not begin to capture the frequency and waveform dependence captured in the models and data we have developed. Work is needed on all three issues. The data collected in Phase II provides a rich resource for such work. For example, one would want to ensure that models developed provided results for the `hippo` waveform consistent with the data.

9.2 Hardware

Further hardware development may be considered for the purposes of developing capabilities beyond those of the equipment used in this work, and for developing equipment that is practical for routine square-wave core-loss measurement by core manufacturers and by core users.

The maximum frequency used in our testing was 500 kHz. Although applications at higher frequency are limited, rapid progress in wide-bandgap semiconductors is generating increased interest in switching frequencies in the MHz range. In addition, testing at higher frequencies could help ensure that the modeling provides accurate results for any waveform. Improvements in switching speed and stray impedances that would be needed to increase the frequency of operation would simultaneously increase the fidelity of waveforms and provide more accurate results near 500 kHz.

Now that the applicability of square-wave testing has been demonstrated, core manufacturers and by core users may wish to develop their own capability for this type of measurement. This calls for an easily replicable test setup using commercially available components, perhaps with some custom-made components.

9.3 Flux Spatial Dynamics

A small set of drilled-core measurements has shown that the flux distribution is not uniform across a core throughout a switching cycle. We hypothesize that the flux migration we see is consistent with the dimensional resonance effects analyzed in detail in [4]. In order to verify this, the dielectric constant of the material used needs to be measured. With this parameter, it would be possible to develop a simulation of expected behavior in the scenario we tested, to verify that what we observed can be attributed to this phenomenon. Another verification approach would be to repeat the drilled-core tests with sinusoidal excitation for which modeling is easier. If the behaviors do not agree, additional theoretical and experimental investigations would be called for.

Although [4] provides guidelines for determining when dimensional resonance effects become important, and approaches for calculating the effects when they are important, the analysis assumes sine-wave excitation. More work is needed to fully understand the implications of dimensional resonance effects with square-wave and other non-sinusoidal waveforms.

9.4 Design Implications

The most important implication of the data collection and modeling we performed for design work is that it is now possible to design a magnetic component and have fewer surprises about its loss behavior in a power electronics application. Having accurate models also allows employing computer optimization of designs.

Some of the design implications of the square wave loss data can be understood when the data is plotted in a Herbert plot as discussed in [11]. However, that discussion does not take into account the off-time loss phenomenon, or the different loss results obtained with the hippo waveform. Further work is needed to fully explore the design implications of these effects.

10 Conclusion

Together with the work in Phase I of this project, this work has greatly improved our understanding of core loss with non-sinusoidal waveforms. A key result is a simple approach to predict losses for various rectangular voltage waveforms. These calculations can be performed based on parameters we provide for materials we have measured, or can be based on simple square-wave measurements of other materials. An additional outcome of this work is a large data set of loss measurements for a wide variety of materials and waveforms that can be used for future study in this area.

A key component of this work was the evaluation of the composite waveform hypothesis, which allows analyzing the loss for various rectangular waveforms based on data taken for only square-wave excitation. This approach has been shown to be effective, and can be expected to give more accurate results than previous approaches.

Our detailed investigation of the composite waveform hypothesis uncovered a phenomenon in which the per-cycle losses increase with increasing "dead time" during which the core sits with a constant, elevated flux level. Further investigation of this has confirmed that it is a real effect, and it has generated international attention, with experiments by another group confirming the phenomenon we discovered. An approach to predicting loss including this effect has been proposed in [10]. Future work could develop better understanding of the phenomenon and easier approaches to predicting behavior considering it.

We also investigated the time dependence of the flux distribution through different regions of the core, both vertically and horizontally. We see transient oscillations of flux distribution that probably indicates the existence of standing waves due to low electromagnetic propagation velocity due to the high permeability and permittivity of the ferrite material. There is no indication that this is a significant loss mechanism for the experimental configuration, nor that it has any relevance for the dead-time loss anomalies.

This does not exclude the possibility that there are dynamic flux distribution effects at the micro or nano scale, but only shows that those we can detect on the scale of these experiments are not involved in a significant loss mechanism.

Three results of this work can readily be applied in practice. The first is predicting loss for any rectangular waveform using data from square-wave measurements. The second is using a two-plane Steinmetz model to fit this data over a wide frequency range. The third is the set of parameters for this model that we provide in Table 2 for the particular materials that we measured. An example and tutorial for using these parameters to predict loss with rectangular waveforms is provided in Appendix B.

Appendix

A Steinmetz Harmonic Analysis

In this appendix, we will examine core loss due to a square wave excitation voltage, as estimated by summing loss terms for the harmonics of the waveform, using the (sinusoidal) Steinmetz equation. Before beginning this analysis, it is useful to note that because of the nonlinear nature of the loss phenomena, one should not expect the Fourier approach to work well. We proceed with this analysis anyway to confirm the expectation that it will not work well. More discussion follows the analysis.

To examine calculate loss on the basis of the Fourier approach, we simply sum (7) over the harmonics, n:

$$\begin{aligned} \overline{P_v} &= \sum^{n} k f_n^{\alpha} \hat{B}_n^{\beta} \\ &= \sum^{n} k (nf)^{\alpha} \hat{B}_n^{\beta}. \end{aligned} \tag{17}$$

It is tempting to factor out k, α, and β, but they are somewhat dependant on frequency.

In our example, the Fourier series for our flux density, a triangle wave, is

$$B(t) = \frac{8\hat{B}}{\pi^2} \sum_{\text{odd}}^{n} \frac{(-1)^{(n-1/2)}}{n^2} \sin(2n\pi f t).$$

Using the Steinmetz model, we are only interested in the peak flux amplitude of each term, so we can simplify this to get

$$\hat{B}_n = \frac{8\hat{B}}{\pi^2 n^2}. \tag{18}$$

We then substitute this into (17),

$$\overline{P_v} = \sum_{\text{odd}}^{n} k (nf)^{\alpha} \left(\frac{8\hat{B}}{\pi^2 n^2} \right)^{\beta} \tag{19}$$

For a quantitative example, we will look at run `mi01-6-028`, which tests a Magnetics, div, Spang & Co. Inc. F material core (Table 3) at 125 kHz and $\hat{B} = 76$ mT. The measured value of the core loss power density was 39 mW/cm^3. Using the Steinmetz harmonic analysis, we estimate the value at 28 mW/cm^3, low by 28%.

Parameter	Value for f above		
	0 kHz	100 kHz	500 kHz
k	0.074	0.036	0.014
α	1.43	1.64	1.84
β	2.85	2.68	2.28

Table 3: Published Steinmetz parameters for Magnetics Div., Spang & Co. R material [12]. Frequencies are referenced to 1 kHz, flux density to 1 kG, and $\overline{P_v}$ [=] mW/cm^2.

The failure of the harmonic analysis based on Fourier series to predict the loss accurately may be understood based on the nonlinear nature of the core loss. For linear phenomena such as resistive losses in windings or other conductors, in which loss is proportional to the square of the excitation amplitude, the loss calculated based on the Fourier decomposition can be mathematically proven to be identical to the loss calculated directly from the original waveform. However, this does not hold for a nonlinear system. Particularly in the lower end of the frequency range of interest, the Steinmetz parameters in Table 11 show that the power loss is proportional to the flux density to a power significantly greater than two, typically in the range of 2.4 to 3. On this basis, one can expect that when the full flux is considered together the loss will be higher than that that would be predicted based on the individual components considered separately. That is what we see in the results above.

Another experiment that illustrates the futility of using a Fourier decomposition to accurately predict core loss is described in [13]. A waveform consisting of a fundamental and a third harmonic is synthesized, and applied to a core under test. Varying the phase of the third harmonic has a significant effect on the loss. A Fourier decomposition could not capture this effect.

B Example Application

This section will demonstrate an example of using the two-plane Steinmetz fit parameters in Table 2 to calculate loss for an unusual waveform. The loss will be calculated using the conventional Steinmetz parameters of frequency and flux amplitude, and then the example will be repeated using voltage and pulse width as parameters. The design parameters for the example are shown in Table 4, and the waveform in Figure 16. The calculation of core loss would be identical whether this were an inductor or a transformer, and so we do not specify which. In the case of a transformer, there might be different numbers of turns and voltages on different windings, but the number of turns and corresponding voltage on any one winding would be adequate information.

B.1 Conventional Parameters

For the calculation based on frequency in flux density, we first calculate the amplitude of the flux density,

$$B_{\text{peak-to-peak}} = \frac{\int v dt}{NA} = \frac{5 \cdot 75 \text{ V}\mu\text{s}}{20 \cdot 154.8 \times 10^{-6} \text{ m}^2} = 0.12112 \text{ T} \tag{20}$$

$$\hat{B} = \frac{B_{peak-to-peak}}{2} = 0.06056 \text{ T} \tag{21}$$

Next, we need the square-wave loss for that flux amplitude, and for each of the pulse widths in the waveform: 5 μs and 7.5 μs. A square wave with a pulse width of 5 μs would have a period of 10 μs, and thus a frequency of 100 kHz. A square wave with a pulse width of 7.5 μs would have a period of 15 μs, and a frequency of 66.7 kHz. Based on the parameters in Table 2 for 3C90 material, we can calculate the square wave loss from (8). To do that, we calculate first with k_1, α_1, and β_1, and then again with k_2, α_2, and β_2, and we select the larger of the two calculated values. For example, at 100 kHz, for k_1, α_1, and β_1,

$$P_{v,1} = 36.86 \cdot (100 \times 10^3)^{1.19} \cdot (0.061)^{2.94} = 8819 \text{ W/m}^3 \tag{22}$$

The results for these calculations for each of the two frequencies and for each of the two parameter sets are shown in Table 5.

Parameter	Value
Core shape	PQ32/30
Core material	Ferroxcube 3C90
Effective core area, A	154.8 mm^2
Effective core volume	10.44 cm^3
Number of turns, N	20

Table 4: Example design parameters.

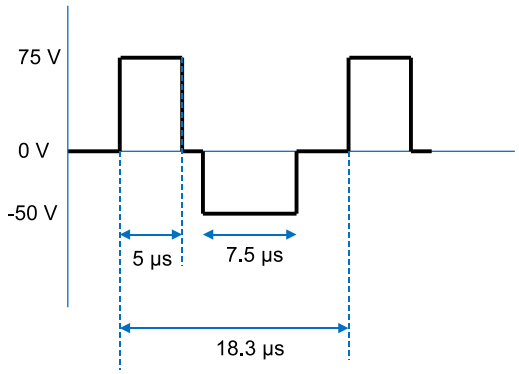

Figure 16: Example design voltage waveform applied across the winding of the device.

Plane	100 kHz	66.7 kHz
k_1, α_1, β_1	8.63 kW/m^3	5.33 kW/m^3
k_2, α_2, β_2	6.04 kW/m^3	2.29 kW/m^3

Table 5: Calculated square-wave loss.

From Table 5, we choose the maximum value in each column, to implement the maximum function in (8). In this case, the values in the first row of the table are the maxima for both frequencies.

We now have the square-wave power loss values, and in preparation for using the composite waveform hypothesis, we convert the form of these values to obtain the energy lost in each pulse. For the positive, 5 μs pulse, the energy loss is simply the pulse width multiplied by the corresponding power per unit volume: $E_a = 5\ \mu\text{s} \cdot 8.63\ \text{kW/m}^3 = 43.2\ \text{mJ/m}^3$ per pulse. Similarly, for the negative pulse, $E_b = 7.5\ \mu\text{s} \cdot 5.33\ \text{kW/m}^3 = 40.0\ \text{mJ/m}^3$. The total loss for cycle is the sum of the loss for each of these pulses, or 83.2 mJ/m^3. We can now convert that back to a power loss number by dividing by the total period, 18.3 μs, which results in a power per unit volume $P_v = 4.54$ kW/m^3. Based on the fact that kW/m^3 are the same as mW/cm^3, we can multiply that loss number by the volume in cm^3 to obtain the final power loss in milliwatts:

$$P = 4.64 \cdot 10.44 = 47.4\ \text{mW} \tag{23}$$

One can easily automate this calculation using Excel, Matlab, or any programming language, but it has been presented here in terms of the manual process in order to ensure that all the steps are clear without reference to any particular programming language.

B.2 Pulse width and Voltage as Parameters

In this case, we directly apply (11), repeated here for convenience:

$$E_{v,a} = \max\left(\frac{k_1}{(NA)^{\beta_1}2^{(\beta_1+\alpha_1)}}V_a^{\beta_1}t_a^{\gamma_1}\ ,\ \frac{k_2}{(NA)^{\beta_2}2^{(\beta_2+\alpha_2)}}V_a^{\beta_2}t_a^{\gamma_2}\right) \tag{24}$$

We substitute in values from Table 4 and values of parameters $k_1 = 36.86$, $\alpha_1 = 1.19$, $beta_1 = 2.94$ and $\gamma_1 = 2.75$ for the first set and $k_2 = 2.895$, $\alpha_2 = 2.39$, $beta_2 = 2.16$ and $\gamma_2 = 2.77$ for the second. We obtain, for 5 μs and 75 V, $E_{v,a} = 43.2$ mJ/m^3, and, for 7.5 μs and 50 V, $E_{v,b} = 40.0$ mJ/m^3, exactly the same as was found with the other approach. Any difference would only occur as a result of roundoff errors tracking through the calculation.

As before, the total loss for cycle is the sum of the loss for each of these pulses, or 83.2 mJ/m^3. We can now convert that back to a power loss number by dividing by the total period, 18.3 μs, which results in a power per unit volume $P_v = 4.54$ kW/m^3, and an average power loss of 47.4 mW.

C Characterization Plots

Various plots have been provided with the data (Section 8) for visualizing the characterization (square wave) data. We present example plots in this appendix. For a more detailed explanation, see the user manual [2]. Image file names have the form *type*`conven-`*setId*`.`*ext*, where *type* is the type of plot, *setId* is the run set identifier, and `.`*ext* is the graphics file extension.

C.1 Conventional Core Loss Plots

Conventional plots of core loss versus $\hat{B}$ are provided. These are similar to the loss plots provided by manufacturers for sinusoidal excitation, but are for our square wave data.

Image file names have the form `conven-`*setId*`.`*ext*.

C.2 Herbert Curves

Herbert plots (Figure 17) show core loss versus pulse width, t_1, parameterized by $\hat{B}$. Herbert [3] describes their use in design.

Image file names have the form `conven-`*`setId.ext`*.

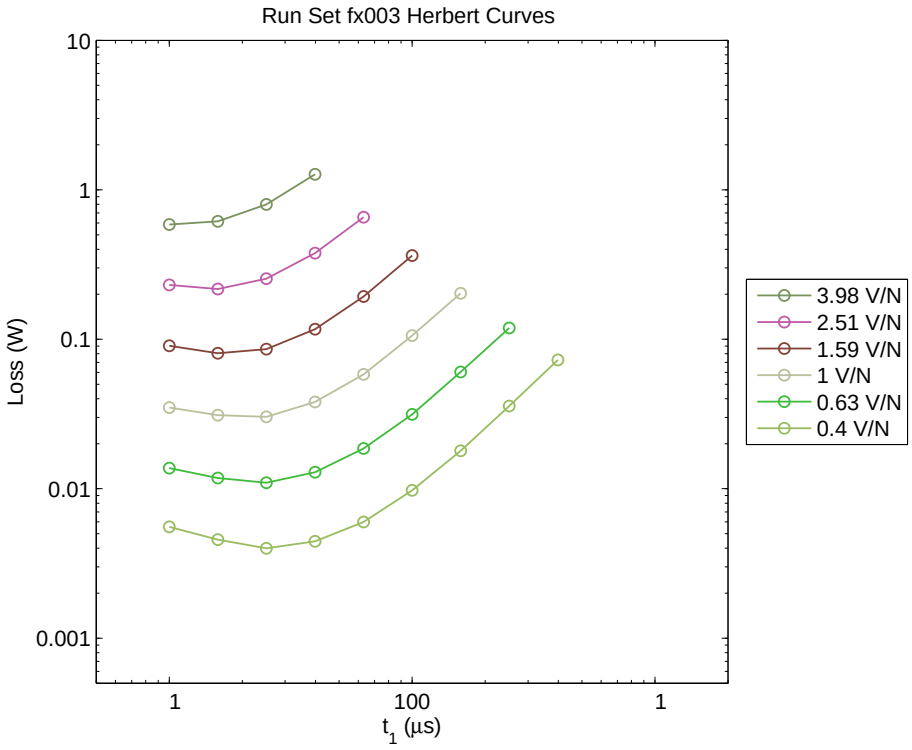

Figure 17: Herbert plot for Ferroxcube 3C81 material.

C.3 Hysteresis Plots

Hysteresis plots are provided for the characterisation square-wave data (Figure 18). The plots are presented in families of constant pulse width, varying $\hat{B}$. Because of ringing in the sense voltage signal due to limitation in the apparatus, simply plotting B versus H gives a messy plot, with the hysteresis loop shape obscured by the ringing. We use boxcar averaging, tuned to the ringing frequency (with a 85.3 μs window) to drop out the ringing. These plots do not have long saturation tails, partly because of this filtering, but also because the experiments did not generally drive the cores deep into saturation.

Image file names have the form `hyst-`*`setId`*`-`*`Tset`*`.`*`ext`*, where *`Tset`* is the pulse width family identifier.

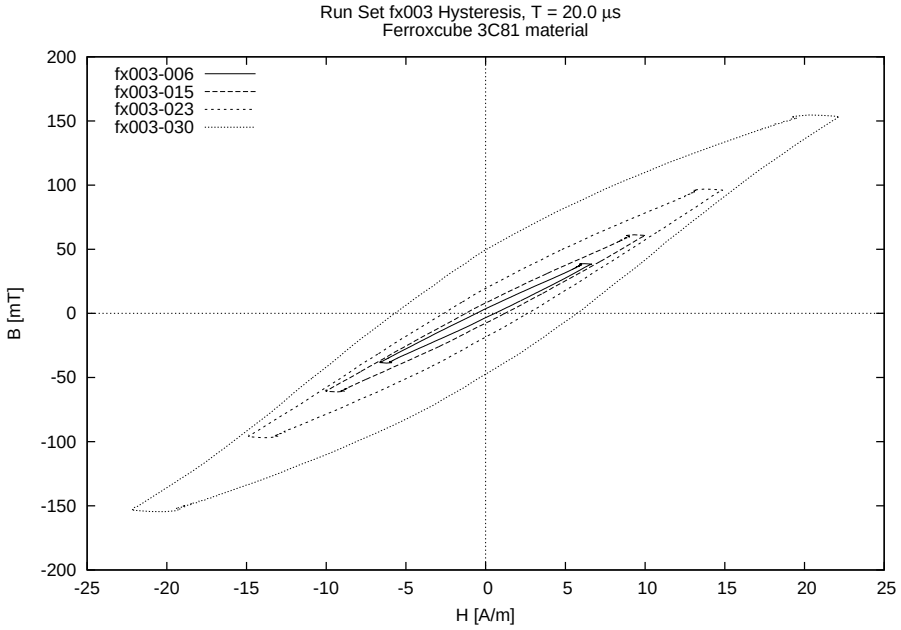

Figure 18: Hysteresis plot for Ferroxcube 3C81 material square wave data, 10 μs pulses. The legend gives the run identifiers, but these are not needed, as the only difference between the loops shown is the amplitude of excitation, and the value of $\hat{B}$ can be read from the plot.

D Expand Plots

In this appendix we present the `expand` waveform loss versus off-time plots for all the core materials tested.

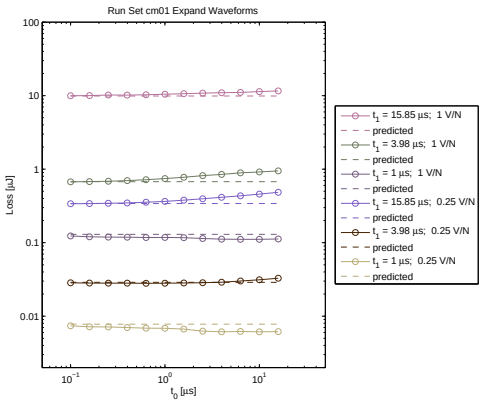

Figure 19: `expand` core loss vs. off-time for Ceramic Magnetics MN60.

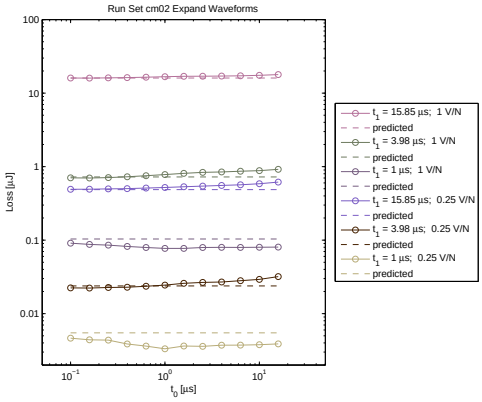

Figure 20: `expand` core loss vs. off-time for Ceramic Magnetics MN8CX.

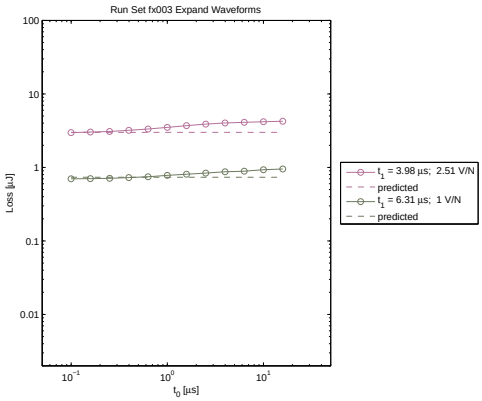

Figure 21: `expand` core loss vs. off-time for Ferroxcube 3C81.

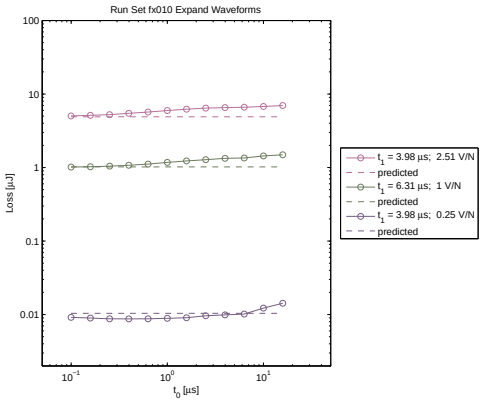

Figure 22: `expand` core loss vs. off-time for Ferroxcube 3C90.

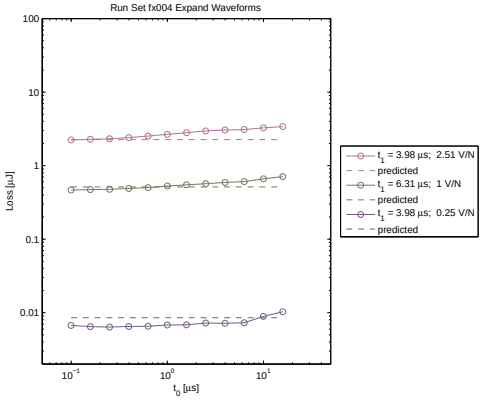

Figure 23: `expand` core loss vs. off-time for Ferroxcube 3F3.

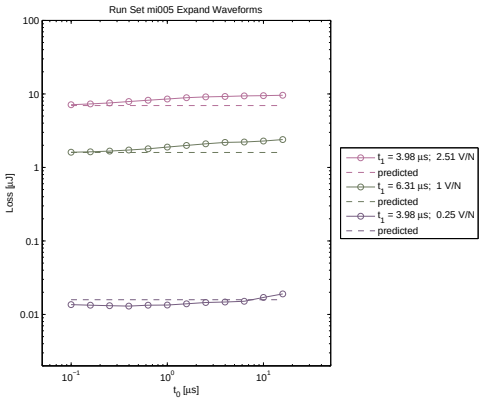

Figure 24: `expand` core loss vs. off-time for Magnetics F.

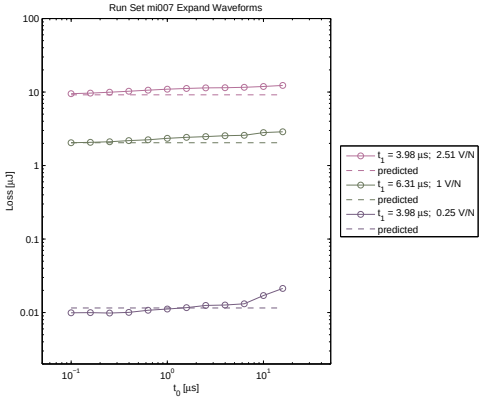

Figure 25: `expand` core loss vs. off-time for Magnetics K.

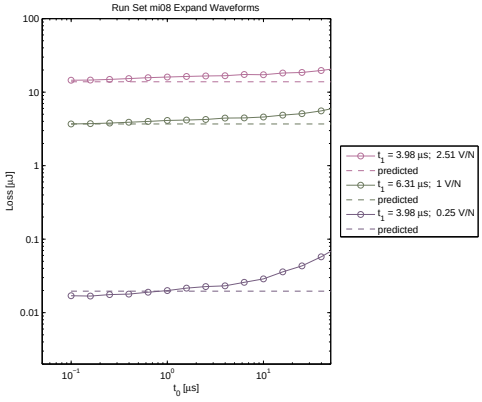

Figure 26: `expand` core loss vs. off-time for Magnetics L.

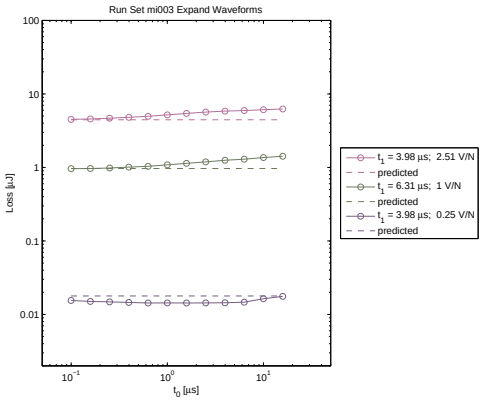

Figure 27: `expand` core loss vs. off-time for Magnetics P.

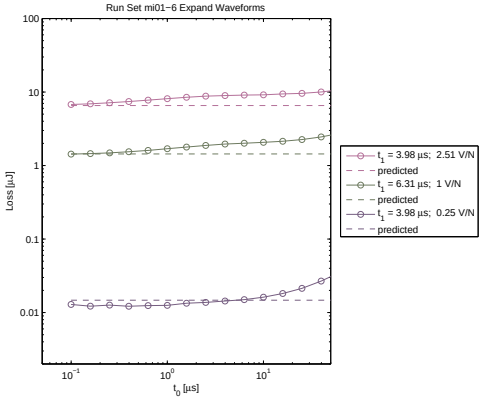

Figure 28: `expand` core loss vs. off-time for Magnetics R.

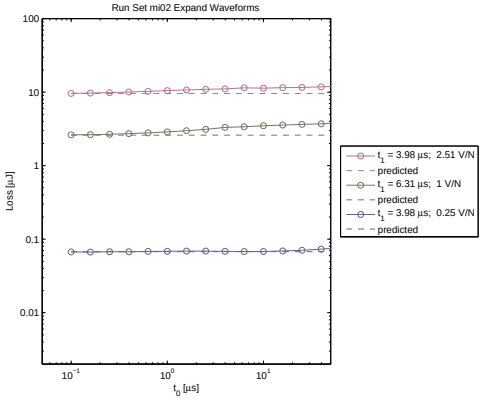

Figure 29: `expand` core loss vs. off-time for Magnetics W.

E Extended Steinmetz Table

In this appendix, we present Table 6, which is like Table 2, with the addition of the standard error of fit, in decibels, plus the parameters for additional run sets, including custom cores and nonstandard experiments for validating the apparatus.

Note:

1. The constriction experiment (Figure 4) comprised three run sets, starting with a Magnetics Inc. F42206-TC core, which was then modified by removing material to create a flux constriction.

2. Various other run sets used nonstandard procedures aimed at detecting problems with the apparatus that might explain the dead-time loss phenomenon (Section 6).

3. Run set `mi11-1` is the first of the drilled core experiments (Section 4), which all use the same core, `mi11`. Its effective area is somewhat less than the Magnetics Inc. 0F46113-TC core from which it was fabricated, due to the probe winding holes.

Manufacturer Material, shape (run set)	k_1 k_2	K_1 K_2	α_1 α_2	β_1 β_2	Std err Note
Ceramic Magnetics Inc					
MN60, 23.2,14.5,7.2T (cm01)	6.085	86810	1.32	2.47	0.33 dB
	899.8μ	67879	2.00	2.13	
MN8CX, 23.2,15.1,7.7T (cm02)	63.01	182100	1.19	2.49	0.32 dB
	177.4μ	87357	2.20	2.29	
Ferroxcube					
3C81, TX22/14/13 (fx003)	11.01	91200	1.31	2.61	0.34 dB
	65.32μ	41432	2.18	2.11	
3C81, E19/8/5 (fx09)	18.02	88800	1.23	2.45	0.46 dB
	350.0μ	52769	2.10	2.33	
3C90, TX22/14/6.4 (fx010)	36.86	39570	1.19	2.94	0.44 dB
	2.895μ	18223	2.39	2.16	
3F3, TX22/14/13 (fx004)	102.4	67200	1.13	2.81	0.48 dB
	11.93μ	28414	2.30	2.14	
3F3, E19/8/5 (fx05)	40.63	65950	1.14	2.50	0.44 dB
	224.8μ	38221	2.12	2.36	
Magnetics Inc.					
F, 42206-TC (mi005)	26.41	72920	1.24	2.76	0.40 dB
	7.612μ	32369	2.37	2.22	note 2
F, 46113-TC (mi11-1)	142.9	63340	1.02	2.43	0.49 dB
	6.299μ	28835	2.35	2.11	note 3
K, 42206-TC (mi007)	246.2	86830	1.10	2.95	0.55 dB
	5.276μ	20750	2.41	2.48	
L, 2206 (mi08)	706.8	150800	1.04	2.87	0.96 dB
	276.1m	99927	1.69	2.88	
P, 42206-TC (mi003)	10.91	43090	1.28	2.80	0.37 dB
	75.99μ	36099	2.16	2.13	
R, 42206-TC (mi01-2)	12.39k	36760	0.83	3.65	1.84 dB
	18.21m	68202	1.75	2.15	
R, custom (mi009)	148.9k	6237	0.71	4.90	1.48 dB
	1.796	100162	1.39	2.18	note 1
R, 42206-TC (mi01-1)	29.19k	38530	0.69	3.34	1.61 dB
	124.2m	77954	1.59	2.16	note 1
R, custom (mi010)	68.73k	28710	0.71	3.92	1.14 dB
	423.7m	90425	1.50	2.17	note 1
R, 42206-TC (mi01-3)	38.01	65250	1.24	2.99	0.40 dB
	40.00μ	31023	2.21	2.16	note 2
R, 42206-TC (mi01-4)	38.72	121900	1.19	2.44	0.34 dB
	8.618m	65931	1.84	2.31	note 2
R, 42206-TC (mi01-5)	44.61	68680	1.22	2.92	0.40 dB
	18.93μ	27996	2.28	2.21	note 2
R, 42206-TC (mi01-6)	30.16	67220	1.25	2.90	0.36 dB
	14.55μ	30033	2.31	2.24	note 2
W, 42206-TC (mi02)	832.7m	131000	1.51	2.37	0.19 dB
	10.59m	123857	1.82	2.04	

Table 6: More two-plane Steinmetz parameters including custom cores and nonstandard experiments. The k_i parameters are referenced to $f = 1\,\mathrm{Hz}$ and $\hat{B} = 1\,\mathrm{T}$; the K_i parameters are referenced to $f = 100\,\mathrm{kHz}$ and $\hat{B} = 100\,\mathrm{mT}$. All the k_i and K_i parameter have dimensions of $\mathrm{W/m^2}$. The notes are explained in the text.

Acknowledgements

We thank the Power Sources Manufacturers Association and the National Institute for Standards and Technology (NIST) for support of this work.

References

[1] Charles R. Sullivan and John H. Harris. Testing core loss for rectangular waveforms, phase I final report. Technical report, Power Sources Manfacturers Association, 2010. Available at `http://www.psma.com/sites/default/files/Sullivan\%20Core\%20Loss\%20Report\%200207101.pdf`.

[2] Charles R. Sullivan and John H. Harris. *Using the PSMA Rectangular Waveform Core Loss Data*. Power Sources Manfacturers Association, 2011.

[3] Edward Herbert. User-friendly data for magnetic core loss calculations. Unpublished., August 2008.

[4] Glen R. Skutt. *High-Frequency Dimensional Effects in Ferrite-Core Magnetic Devices*. PhD thesis, Virginia Polytechnic Institute and State University, 1996.

[5] Ferrite material selection guide, 2000. Magnetics Division of Spang & Company, Bulletin No. FC-S1.

[6] Soft ferrites and accessories, data handbook, 2009. Ferroxcube, Eindhoven, The Netherlands.

[7] C. P. Steinmetz. On the law of hysteresis. *AIEE Transactions*, 9:3–64, 1892. Reprinted under the title "A Steinmetz contribution to the ac power revolution", introduction by J. E. Brittain, in *Proceedings of the IEEE* 72(2) 1984, pp. 196–221.

[8] E. C. Snelling. *Soft Ferrites, Properties and Applications*. Butterworths, second edition, 1988.

[9] K. Venkatachalam, C. R. Sullivan, T. Abdallah, and H. Tacca. Accurate prediction of ferrite core loss with nonsinusoidal waveforms using only Steinmetz parameters. In *IEEE Workshop on Computers in Power Electronics*, 2002.

[10] J. Mühlethaler, J. Biela, J. W. Kolar, and A. Ecklebe. Improved core loss calculation for magnetic components employed in power electronic systems. In *Proceedings of APEC 2011—Applied Power Electronics Conference and Exposition*, pages 1729–36, 2011.

Testing Core Loss for Rectangular Waveforms

February 7, 2010

Charles R. Sullivan
John H. Harris
Thayer School of Engineering at Dartmouth
charles.r.sullivan@dartmouth.edu
http://engineering.dartmouth.edu/inductor
8000 Cummings Hall
Hanover, NH 03755, USA

Edward Herbert
closs@eherbert.com
http://fmtt.com/
1 Dyer Cemetery Road
Canton, CT 06019, USA

Sponsored by
The Power Sources Manufacturers Association
email: power@psma.com
http://www.psma.com/
P.O. Box 418
Mendham, NJ 07945-0418
Tel: (973) 543-9660
Fax: (973) 543-6207

[11] Charles R. Sullivan, John H. Harris, and Edward Herbert. Core loss predictions for general PWM waveforms from a simplified set of measured data. In *Applied Power Electronics Conference and Exposition (APEC), 2010 25th Annual IEEE*, pages 1048–1055, February 2010.

[12] Curve fit equations for ferrite materials, 1999. Magnetics Division of Spang & Company, Bulletin No. FC-S7.

[13] Jieli Li, T. Abdallah, and C. R. Sullivan. Improved calculation of core loss with nonsinusoidal waveforms. In *IEEE Industry Applications Society Annual Meeting*, pages 2203–2210, 2001.

Appendix B–The Data

In general, the data is provided both as zip files, for convenient download and as expanded files, for convenient browsing.

Using the data

For those who are familiar with SQLite, the database files may be useful (Phase II Project only). There is a good extension to the Firefox browser that I used to view the files. The coreloss.db file contains all of the data from the run sets .csv files, plus a number of calculated values determined using MatLab.

I preferred using the .csv files, partly because it is necessary for the Pilot Project data but mostly because I wanted to process the data to export to SPICE, and it is necessary to convert the negative times. It is easy to do that and to do other calculations in spreadsheets. See Appendix C, The Excel Tool–Viewing the Data

In addition to the data provided by Dartmouth, I have converted some of the data into Excel files. In addition, I have resorted some of the data in Excel files. These add nothing new, but may be convenient to the user and ar available for download at http://www.psma.com/coreloss/tools

The added files are summarized at the end of this Appendix.

Pilot Project Data

The data for the Pilot Project can be downloaded at
http://www.psma.com/coreloss/pilot

The are three sub-directories,

1. Characterization-data
2. Ferrite-data
3. Powdered-iron-data

Characterization-data sub-directory

The characterization data summarizes the square-wave results from the various tests, with headers of Frequency, Peak flux linkage, Volts/turn, Average loss and Loss per cycle.

The characterization data is provided in several formats: MicroSoft Excel (.xls), Comma-separated value (.csv), plain text (.dat). There are shortcuts to MicroSoft Access files, but there seem to be no corresponding files. The report says that there are Matlab (.mat) files, but they seem to be missing.

There are several additional files in portable network graphic (.png) format, which are illustrations from the report.

The Excell (.xls) files seem to be the best format for browsing. Unfortunately, there seems to be no index to locate the test runs from which the data is taken.

The white space delimited tables (.dat) do not seem to have consistent spacing. I was unable to import them into Excel and have them align properly. They are the same data as the .xls and .csv files, so that is unimportant and I made no effort to fix the problem.

Ferrite-data and *Powdered-iron-data* sub-directories

The file formats and data in general are the same format for both the ferrite-data and the powdered-iron-data sub-directories.

For viewing test results graphically, the portable network graphic (.png) files seem best. There are several .png files which are illustrations from the report. In addition, for each test run, there are two .png files, one of the format xxx-xxx.png (for example, f10-010.png) showing two graphs vs time for one cycle: Voltage and current vs. time are shown in the first graph and power and energy vs. time are shown in the second graph.

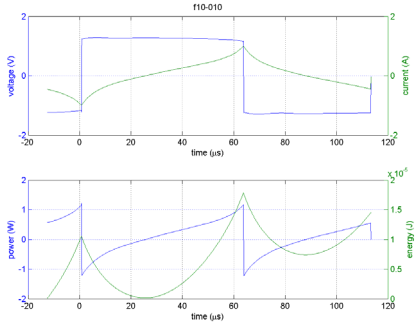

The other .png file has the format xxx-xxx-hyst.png (for example, f10-001-hyst.png) and shows the hysteresis loop for the same test. The .fig files probably duplicate these graphics.

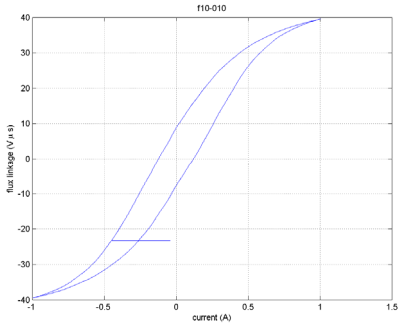

Outfile.dat has an index of the test runs. I cannot identify the data in outfile.csv; it is not the same.

In the powdered-iron-data directory, there are additional indexes of the runs with self-explanatory names: i02-all-runs.dat and i02-good-runs.dat.

For accessing the raw data, the comma-separated-value (.csv) files are used. The formats for the Pilot Project data and the Phase II data is similar, and they are described below.

There are several miscellaneous files that I did not explore. Some seem to be duplicate graphics in other formats. Some seem to be used by the test equipment.

Phase II Project Data

The data for the Phase II Project can be downloaded at
http://www.psma.com/coreloss/phase2

There is an exhaustive description of using the data in the Users Manual (user.pdf), and those who want to make maximum use of the data should refer to that manual. Following is a summary:

- cores/ directory.
  The `cores/` directory contain files with data, other than the experimental results, such as manufacturer's specifications, describing the magnetic cores under test.

- sets/ directory.
  The `sets/` directory contains various subdirectories, each containing the data for one run set, including data files describing the run set, and subdirectories with raw data and plots. A run set subdirectory has the run set identifier for its name, and typically contains about 50 MB of data, for several hundred runs, each characterized by frequency, peak voltage, and wave shape.

The contents of the sets/ directory are described in more detail below.

- zips/ directory.
  The `zips/` directory contains zip archive files of the run set directories, for convenient downloading and distribution. The zip files have names like `runs-`*`setId`*`.zip`. Each zip file is self-contained, containing supporting information for the user. There is also an archive, `cores.zip`, of the contents of the `/cores/` directory.

- `steinmetz.dat` is a table of two-plane, square-wave Steinmetz parameters for the various materials tested in the project.

- `setsrept.txt` is a summary of run set parameters to help in locating run set directories of interest.

- `corerept.txt` contains a summary of the information contained in the `cores/` directory data files.

- `corerept.csv` is a comma-separated-value text file table of parameter for the various cores tested in the project. Like `corerept.dat` it summarizes the information contained in the `cores/` directory, but in a machine-readable format.

- coreloss.db is an SQLite database file. The information it contains duplicates that found in the other files of the data set, and is only provided for the convenience of experienced SQLite users.

- readme.txt is the readme file for this directory. It is for the benefit of someone browsing the directory, and mostly directs the user to the user manual.

(The .txt and .dat files can be viewed with an ordinary ASCII text editor such as Notepad or Wordpad.)

The sets/ directory

The sets/ directory contains 30 sub-directories, each containing files associated with a set of tests. Most are for individual cores, but some represent multiple sets on one core or core type, identified by a common prefix. As an example, set fx003 are tests on one core, Ferroxcube, TX22/14/13 shape, 3C81 material. The sets mi01-1 through mi01-6 are tests run on three cores Magnetics Inc., 42206-TC shape, R material. The sets mi11-1 through mi11-8 are sets run on the drilled core, with various different test windings. See setsreport.txt in the main directory for a description of each set.

Readme.txt file of sets/ directory:

The readme.txt file contains a comprehensive explanation of the files in the sets/ sub-directories and is copied here, with edits.

```
[Read-me File for PSMA Core Loss Run-set Directories. readme.txt
(from Coreloss rev 212)]

This directory contains data generated by the PSMA Coreloss
testing system. In this generic readme file, we use <setId> to
refer to the run-set identifier of this particular run set. See
the gen-<setId>.dat file for the details of this run set. See
user.pdf for a detailed explanation of the data.

The following files (and perhaps others) are contained in this
directory:

user.pdf:  This is the user's manual for the PSMA Core Loss data
set.

gen-<setId>.dat:  This file is the input to the run-set generator
program and also contains additional information in the note and
comment fields.

runs-<setId>.dat:  This is the output file created by the run set
generator. It is the input file for the coreloss test apparatus.

data-<setId>.dat:  This file is generated by the Matlab code and
is quite similar to the runs-<setId>.dat file, but with
```

additional computed fields on the right, including energy per period, and power.

core-<coreId>.dat The core data for the core used in the run set. A core ID uniquely identifies a manufacturer and part number, but does not distinguish between different instances of the manufacturer's SKU. This file is a copy of the core data file mentioned in the gen-<setId>.dat file, made at the time the directory was zipped.

readme.txt: This file.

<setId.db: This is a SQLite relational database file containing all the scope data. It can be joined with the main database file, coreloss.db, found in the data/ directory. The data differ from that in the scope/*.csv files in that DC offsets have been removed, and a volt-seconds column has been added. See the user manual user.pdf for more details.

Note: The times start with negative values, a problem for some uses of the data.

scope-ddl.sql: This is the SQL data description for the SQLite database file, <setId>.db, above.

These subdirectories contain the experimental data and results:

scope/: This directory contains the output files written by the oscilloscope during the coreloss run set. The CSV files are the raw data. The text files give the oscilloscope configuration.

For using the data, the comma-separated-value (.csv) files are used. The formats for the Pilot Project data and the Phase II data is similar, and they are described below.

Note: The times start with negative values, a problem for some uses of the data. Also, the voltage and current data have zero offsets that must be removed.

images/: This directory contains waveform plot images generated by the Matlab code from the files in the scope/ directory. There are three formats. Each image has four plots: Voltage vs time, current vs. time, power vs time, and energy vs. time, all for one particular waveform.

results/: This directory contains images of various plots comparing the core loss for similar pulse shapes in different waveform contexts.

auximages/: The embedded probe winding experiments have an additional image directory.

Added files

I have added several file for the convenience of the user. These can be downloaded at http://www.psma.com/coreloss/tools

The following is a pdf, an edited copy of "setsrept.txt." The physical and magnetic sized of the cores have been added where known.

modsetsrept.pdf

The following are the Excel Tool. The first is written in Office 2003 Excel and is the one that I use. The second is converted to Office 2007 and is untested.

extool.xls, 1.8 M

extoolm.xlsm 1 M

The following is the Pilot Project ferrite data outfile.dat, converted ot .xls.

outfile.xls 121 k

The following files are the data table from coreloss.db, opened in FirefoxSQLite, exported as .csv with headers added. The second was that file, opened in Excel 2003, saved as an .xls file.

data.csv 663 k

data.xls 1.45 M

The files following are derived from data.xls. They have been sorted and some rows and columns deleted. The names are descriptive.

purged_data.xls 636 k

drilled_data.xls 367 k

purged_expand_data.xls 250 k

purged_hippo_data.xls 251 k

purged_sqare_data.xls 211 k

Appendix C
The Excel Tool–Viewing the Data

To make it easier to use the data, I created an Excel Tool. It is generated using Excel in MSOffice 2003, and uses VBA macros. Excel macros are notoriously buggy, particularly if used in different versions of Excel or on different computers with different operating systems. The Excel Tool was written as an aid in writing this report. It is a bonus if others can use it. It can be downloaded at http://www.psma.com/coreloss/tools/extool.xls

Using the data

For those who are familiar with SQLite, the database files may be useful (Phase II Project only). There is a good extension for the Firefox browser that I used to view the files. The coreloss.db file contains all of the data from the run sets .csv files, plus a number of calculated values determined using MatLab.

I preferred using the .csv files, partly because it is necessary for the Pilot Project data regardless, but mostly because I wanted to process the data to export to SPICE, and it is necessary to convert the negative times. It is easy to do that and to do other calculations in spreadsheets.

Source data files, .csv data

The comma-separated-value (.csv) files are the same format for the Pilot Project and the Phase II Project. They are easily imported into MicroSoft Excel spreadsheets.

The first two lines are headers:

x-axis	**SYNC**	**OUT**	**V**	**I**
second	**Volt**	**Volt**	**Volt**	**Ampere**

The first column **A** "x-axis/second" is the time, in seconds. Unfortunately, the time starts with a negative value, which cannot be used by some programs, like SPICE. Time = 0 is a trigger event.

The second column **B** "SYNC/Volt" is a signal from the waveform generator. Detecting rise and fall times may be useful for synchronizing data from other test runs.

The third column **D** "OUT/Volt" is another output of the waveform generator for most test runs, but it is used for the sense winding voltage for the drilled core tests.

The fourth column **E** "V/Volt" is the voltage of the voltage sense winding. This data may have a voltage offset that must be removed if the data is used for calculations.

The fifth column **F** "I/Ampere" is the current probe. This data may have a current offset that must be removed if the data is used for calculations.

In general, I found that the last row of data is unreliable, so I did not use it for further calculations nor did I export it to SPICE.

Using The Excel Tool

There are four functions of the Excel Tool for handling data:

1. Import the data from the selected source file.
2. Calculate needed parameters
3. Export the data as files that can be used by SPICE and other programs
4. Display selected calculated data as graphs and parameters.

The Excel Tool can be downloaded from http://www.psma.com/coreloss/tools/extool.xls

The **Cmd!** sheet of the Excel Tool workbook is shown on the next page. Various parts of the worksheet, and how to use them, are explained in the text following.

Macros

The Excel Tool uses macros. Macros can contain viruses, so many company servers block macros, and the settings on personal computers may have to be changed to run the macros. I suggest not running macros using any files that have been obtained from a third party. The user should download the Excel Tool himself self from the web site indicated above, to ensure that the macros have not been compromised.

Import and Export tool

The first sheet of the Excel workbook (Cmd!) is for control and display. An input file from the *Pilot Project* or the *Phase II Project* is selected.

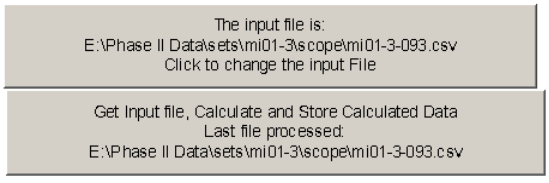

Click the top right button to select the input file, and confirm it by clicking the dialog box. Next, the processing is initiated by clicking the bottom right button, which imports the data, executes a number of calculations, exports the calculated data and displays the results as graphs and parameters.

The Vi output file is:
C:\TestVi.txt
Click to change the Vi output file

The Ii output file is:
C:\TestIi.txt
Click to change the Ii output file

The input file is:
E:\Phase II Data\sets\mi01-3\scope\mi01-3-093.csv
Click to change the Input File

The Flux output file is:
C:\TestFlux.txt
Click to change the Flux output file

The Probe output file is:
C:\TestPr.txt
Click to change the Probe output file

Get Input file, Calculate and Store Calculated Data
Last file processed:
E:\Phase II Data\sets\mi01-3\scope\mi01-3-093.csv

To show the hysteresis loop below with magnetic material parameters, enter the values below: These values are not imported automatically.

Ae	2.62E-05	m
Le	5.41E-02	m
n	5	turns

Note:
Disregard theProbe Voltge
Unless the core has an embedded
Sense winding.

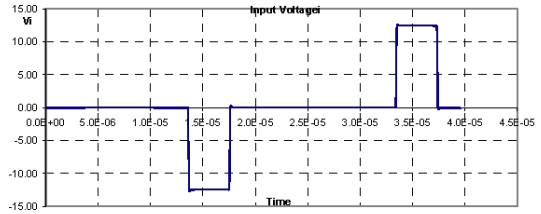

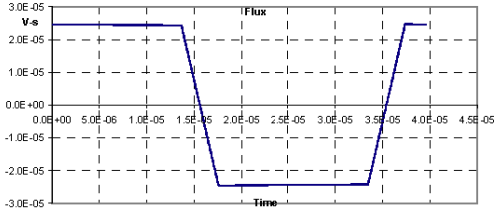

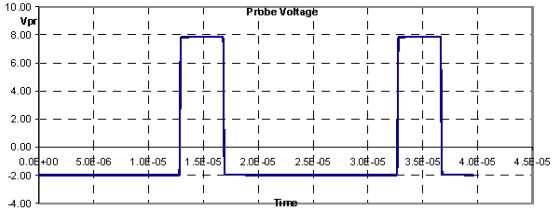

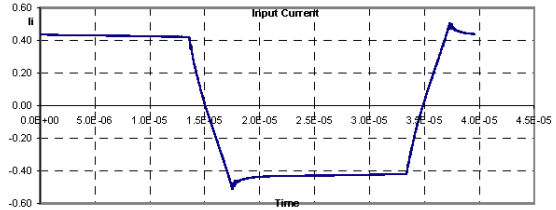

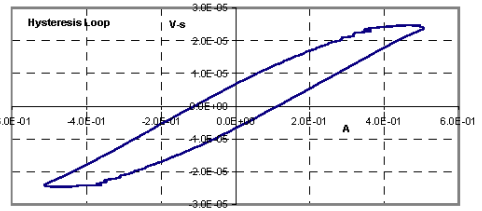

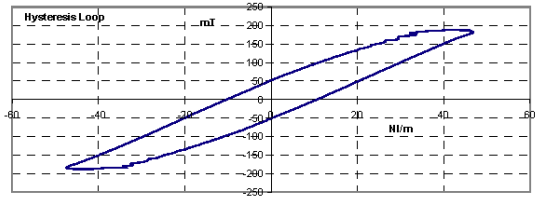

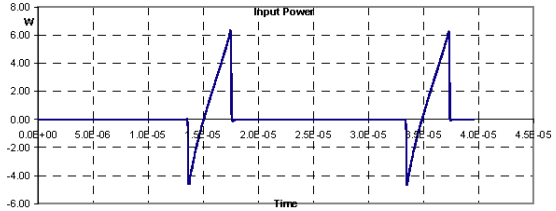

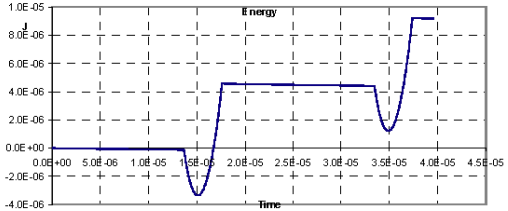

File	E:\Phase II Data\sets\mi01-3\scope\mi01-3-093.csv		
Power, method 1	2.316602E-01 W	Δ Flux, pos	4.87615E-05 V-s
Power, method 2	2.318954E-01 W	Δ Flux, neg	-4.87551E-05 V-s
Energy, method 1	9.178579E-06 J	T, pos (total)	3.92634E-06 s
Energy, method 2	9.150891E-06 J	T, neg (total)	3.92634E-06 s
Avg. V, pos	1.241908E+01 V	Duty-ratio, pos	0.09939759
Avg. V, neg	-1.241745E+01 V	Duty-ratio, neg	0.09939759
Flux, max	2.469139E-05	Period	3.9501E-05 s
Flux, min	-2.463122E-05	Frequency	2.531558E+04 Hz

The import data

The input data is stored in the second worksheet, "**Data!**," and is not altered.

The export data

Files for exporting data to be used in SPICE or other programs can be selected or created by clicking the four left buttons on the **Cmd!** sheet, as indicated by the text on the buttons. Usually, the export files are set once, then left alone. They are updated with new data each time new data is processed. When new data is imported into **Data!**, the four export files are generated and written automatically. If not changed, the same files are updated when new data is imported and processed.

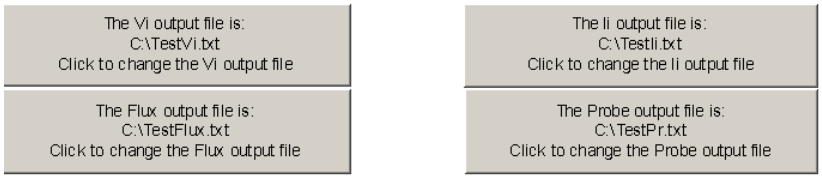

The equations for the export data are on the second sheet "**Calc!**". When a new data file is imported, the calculations are done immediately, to avoid any chance of unprocessed data being associated with the previous calculation.

Additional workbook sheets, **Vi!**, **Ii**, **Flux!**, **Emb!**, **Power!** and **Energy!** also contain the export data. To facilitate the macros, the data to be exported is always in columns **A** and **B**. The **Power!** and **Energy!** data is available, but no export is set up because no need for these data were identified in SPICE. At first, this was the only data on these sheets, but then some additional columns were added to **Vi!** and **Ii!** for additional calculations for the graphs and parameters displayed on the **Cmd!** sheet.

Calculated data table display

File	E:\Phase II Data\sets\mi01-3\scope\mi01-3-093.csv		
Power, method 1	2.316602E-01 W	Δ Flux, pos	4.87615E-05 V-s
Power, method 2	2.318954E-01 W	Δ Flux, neg	-4.87551E-05 V-s
Energy, method 1	9.178579E-06 J	T, pos (total)	3.92634E-06 s
Energy, method 2	9.150891E-06 J	T, neg (total)	3.92634E-06 s
Avg. V, pos	1.241908E+01 V	Duty-ratio, pos	0.09939759
Avg. V, neg	-1.241745E+01 V	Duty-ratio, neg	0.09939759
Flux, max	2.469139E-05	Period	3.9501E-05 s
Flux, min	-2.463122E-05	Frequency	2.531558E+04 Hz

A short table of calculated data is displayed in the lower right corner, with the input file name as the first line. Some parameters are calculated two ways, as an error check.

The data table can be copied and pasted.

Graphs

Six graphs are displayed on the left side of the **Cmd!** worksheet. These are generated using the Excel Chart function, but use the same data as is generated for export.

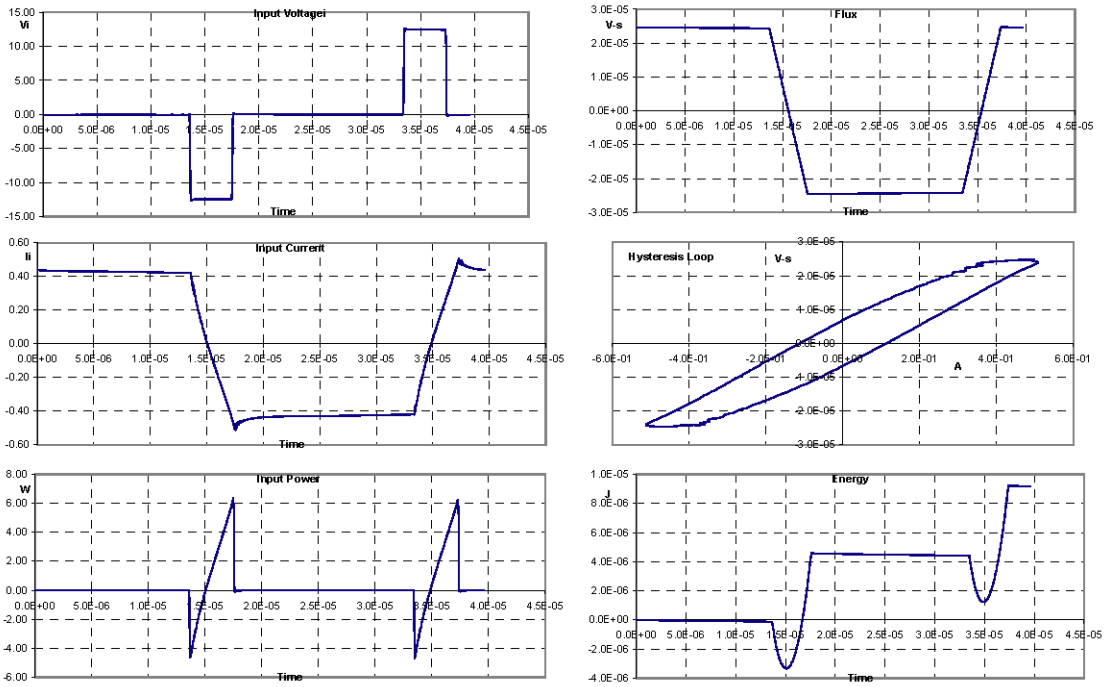

The hysteresis loop uses the Flux and the input current Ii as its axes, so it displays Volt-seconds vs Amperes. This is a device hysteresis loop, so it is not corrected for turns, nor does it have any dimensional factors.

These graphs can be copied and pasted into Word, but I was unable to paste them directly into email. Once copied into Word, they can then be copied and pasted to email.

The power and energy data are generated but not exported. The files are available for manual export, or the macro could be edited to add export files for them.

The graphs can be copied and pasted into MSWord. I was unable to paste them into email, but if copied to MSWord first, the MSWord copy can then be copied and pasted into email.

Hidden data on the Cmd! worksheet

Underlying the buttons and graphs are a number of columns of data from the other worksheets. These data are not visible because they are covered by the other features and because the text color is white. This was done so that the export data were on the same worksheet as the buttons that controlled the export files. This would be done differently if done over, but it is not worth the effort to change it.

Embedded windings graph

The mi11-X-xxx sets contain data for drilled cores with an extra sense winding, "Probe Voltage." The data is imported to the **Data!** worksheet and is in the third column **D** "OUT/Volt." This column is used for an output of the waveform generator for most test runs, but it is used for the sense winding voltage for the drilled core tests. The picture below shows the graph for the mi11-2-131 run. The data is also sent to an external file for use in SPICE or other programs.

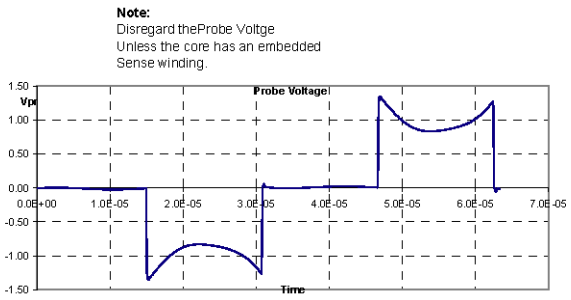

Magnetic data and graph

The dimensional data for the cores and the number of turns are not in the .csv files, so that data must be entered manually

To show the hysteresis loop below with magnetic material parameters, enter the values below: These values are not imported automatically.

Ae	2.62E-05	m
Le	5.41E-02	m
n	5	turns

A graph is generated to display the hysteresis loop in magnetic parameters, but it will be correct ONLY IF the magnetic data has been entered manually.

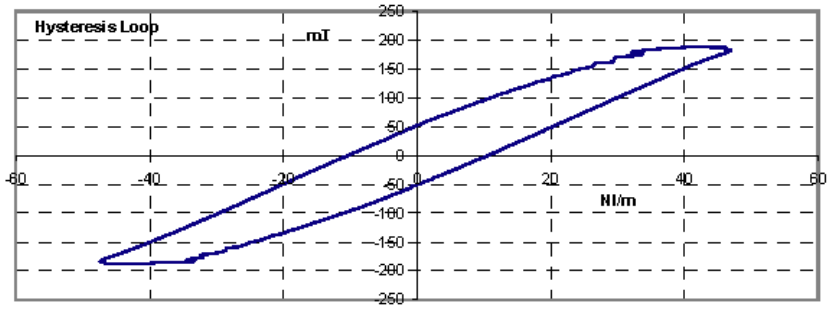

Data files on the Calc! sheet:

Note: The data in the last row of the imported files seems to be unreliable, so it is not used. The input data has 1000 rows, and the calculated data has 999 rows.

Calc A: "Time, all positive". SPICE cannot use negative times, and the imported data starts at a negative time, with 0 being a "trigger point." This is the time from **Data!A** modified so that it starts at 0.

Calc C: "Out, offset removed". This is the voltage of column **Data!C** with the offset removed. This data is not used except for the drilled core tests in Phase II.: "V, offset removed". This is the voltage of column **D** with the offset removed.

Calc D: "V, offset removed". This is the voltage of column **Data!D** with the offset removed.

Calc E: "I, offset removed" This is the current of column **Data!E** with the offset removed.

Calc F:: "Flux cumulative". This is the cumulative flux from time = 0 (column **Calc!A**, the sum of the product of the voltage in column **Calc!D** and the incremental time. Effectively, it is a piece-wise integration of the voltage

$$\int v \; dt.$$

Calc G: "Flux, offset removed". This is the flux of column **Calc!F** with the offset removed.

Calc H: "Power". This is the instantaneous power, the product of the voltage in column **Calc!D** and the current in column **Calc!E**.

Calc I: "Energy". This is the cummulative sum of the product of the power of column **Calc!H** and the incremental time. Effectively, it is a piece-wise integration of the power

$$\int p \; dt.$$

Calc B: "Time, new zero". This function allows the user to select a different point as time 0. I do not use this data, and if it is used, additional processing is needed to sort on this column or to discard rows having negative time. This is the time of column **Data!A** with 0 pinned to a trigger time of the user's choice. Before sorting, the chosen time becomes 0 in column Calc!**B**, and in rows following, the time increments from 0. Earlier times increment from the last value in column**.**

If this function is used, and after calculation, if the data is sorted on this column, time increments from 0 and all data points follow in order so that a graph can be made using the chosen trigger time as the origin. Again, I did not identify any need for this function, and no export is done for these data.

Data on the Vi!, Ii!, Flux!, Emb!, Power! and Energy! worksheets

There are six additional worksheets, **Vi!**, **Ii!**, **Flux!**, **Emb!**, **Power!** and **Energy!**.

Mostly, this is data rearranged in convenient columns for export, with the headings removed. To be used in SPICE as PWL inputs, the data must be in two columns, time and the parameter being simulated. (It is supposed to be possible to add comment lines in the PWL data with a leading apostrophe so that the line is ignored, but instead it generated errors, so the headers were removed.)

Equations for the export data:

Removing the negative times

To convert the time column so that the time is always positive, add a new column **Calc A**. For each cell, starting with **Calc!A3**, I subtracted the value of the first time data cell **Data!$A$3** from the times in column **Data!A** using the expression **=Data!$A3-Data!$A$3**. When extended down the column, the subsequent cells become **=Data!$A4-Data!$A$3**, **=Data!$A5-Data!$A$3**, etc., for example
Calc!A3: =Data!$A3-Data!$A$3
Calc!A4: =Data!$A4-Data!$A$3
Calc!A5: =Data!$A5-Data!$A$3

Etc.

Removing the zero offset voltages and current.

Use new columns **Calc!C, Calc!D** and **Calc!E**. In the second cell of the new columns, insert the average value of the respective voltages or current for columns **Data!C, Data!D** or **Data!E**. For example, to remove the off set from the output current in column **Data!E**, and put the result in the new column **Calc!E**, calculate the average of column **Data!E** and put it in **Calc!E2**: **=AVERAGE(Data$E3:$E1002)**. Then subtract this value from each cell in column **E**, for example:

Calc!E2: =AVERAGE(Data!$E:Data!$E1002)

Calc!E3: =Data!$E3-$E$2.

Calc!E4: =Data!$E4-$J$2.

Etc.

Calculating the flux

To display a hysteresis loop, the flux is needed for the Y-axis. From the data, it is not possible to know the true value of the flux but the incremental flux is calculated as the product of the voltage in column **Calc!D** and the incremental time, and that is summed to

get the cumulative flux from time = 0, with reference to column **Calc!A**. Add a new column **Calc!F**.

Calc!F3: =($A4-$A3)*$D3
Calc!F4: =$F3+($A4-$A3)*$D3
Calc!F5: =$F4+($A5-$A4)*$D4

etc.

The offset is then removed in the same manner as it is for the voltages and current with the result put in column **Calc!G**.

Calc!G2: =AVERAGE($F4:$F1002)
Calc!G3: =$F3-$FG2
Calc!G4: =$F4-$FG2

etc.

Calculating the power and energy

Power and energy are more easily calculated in SPICE, but if desired, they can be calculated in the worksheet. Use column **Calc!H** for the power and column **Calc!I** for the energy.

Power is the product of the voltage in column **Calc!D** and the current in column **Calc!E**, for example:

Calc!H3: =$D3*$E3
Calc!H4: =$D4*$E4
Calc!H5: =$D5*$E5

Etc.

The energy input during one cycle is the cumulative sum of the product of the power in column **Calc!H** and the incremental time from column **Calc!A**, for example:

Calc!I3: =($A4-$A3)*$H3
Calc!I4: =$I3+($A4-$A3)*$H3
Calc!I5: =$I4+($A5-$A4)*$H4

Etc.

Changing the zero time reference (Alternative)

To use an event as the zero time reference point, further convert the time data using a new column **Calc!B**. Find the time in column **Calc!A** that corresponds to the desired zero reference, and put that value in **Cald!B2**. Subtract that value from each cell in column **Calc!A**, for example, $**A3-$B$2**. If the result is negative, then add the difference between the final value in column **Data!A**, for example, **(Data!$A$1001)** to the next cell in column **F**. For example, to set the new 0 at time = 1.26880000E-05, put that value in **Calc!B2.** Alternatively, put in a cell containing that value, for example **Calc!A613**. For example:

Calc!B2: 1.26880000E-04 Or:

Alternatively, **Calc!B2: =$A$613**
Calc!B3: =IF((Data!$A3-$B$2)<0,
Data!$A4+Data!$A$1001-$B$2,
$A3-$B$2))
Calc!B4: =IF((Data!$A4-$B$2)<0,
Data!$A5+Data!$A$1001-$B$2,
$A4-$B$2))
Calc!B5: =IF((Data!$A5-$B$2)<0,
Data!$A6+Data!$A$1001-$B$2,
$A5-$B$2)))
Etc.
Then sort the data ascending, using column **Calc!B**.

Miscellaneous equations on other worksheets

On the **Vi!** worksheet, four additional columns are generated.

In column **G**, the voltage in column **B** is tested to see if it is above a threshold equal to 1/3 of the maximum voltage in column **B**. If it is, the time increment is put in the cell, otherwise 0. The sum is the total time that the voltage is positive (above the threshold), and that is displayed the positive time (T-pos) on the **Cmd!** sheet.

In column **H**, the voltage in column **B** is tested to see if it is below a threshold equal to 1/3 of the minimum voltage in column **B**. If it is, the time increment is put in the cell, otherwise 0. The sum is the total time that the voltage is negative (below the threshold), and that is displayed as the negative time (T-neg) on the **Cmd!** sheet.

In column **J**, the data in column **B** (the input voltage) is multiplied by the data in column **G** to generate the incremental positive flux. The sum is displayed as the Δ positive flux on the **CMD!** sheet.

In column **K**, the data in column **B** (the input voltage) is multiplied by the data in column **H** to generate the incremental negative flux. The sum is displayed as the Δ negative flux on the **CMD!** sheet.

On the **Ii!** worksheet, there are three extra columns. (Columns **A** and **B** are the data for the Ii export file).

Column **C** contains the flux, so that columns **B** and **C** are the data source to generate the hysteresis graph on the **CMD!** sheet.

Columns **E** and **F** are the data in columns **B** and **C**, factored by the magnetic parameters (core area, core length, turns) as the source data to generate the hysteresis loop in magnetic parameters on the **Cmd!** sheet.

Miscellaneous calculations on the Cmd! worksheet

The following calculate parameters of the data table on the **Cmd!** worksheet.

Power, method 1 is calculated as **=AVERAGE(Power!B1:B999)**.

Power, method 2 is calculated as **=Energy!B999/Energy!A999**. **Energy!B999** is the final value of the energy column **B** on the worksheet **Energy!**. **Energy!A999** is the period.

Energy, method 1 is **=Energy!B999**, the final value of the energy column **B** on the worksheet **Energy!**.

Energy, method 2 is calculated as **=AVERAGE(Q42,Q43)*Calc!A999**, where **Q42** is the power, method 1, **Q43** is Power, method 2 and **Calc!A999** is the period.

The following six calculations are based upon calculations on the worksheets **Vi!** and **Flux!** as explained above.

Δ Flux, Pos is calculated as **=SUM(Vi!J1:J999)**.

Δ Flux, Neg is calculated as **=SUM(Vi!K1:K999)**.

T Pos (total) is calculated as **=SUM(Vi!K1:K999**)

T Neg (total) is calculated as **=SUM(Vi!$H1:$H999)**

Flux, max is calculated as **=MAX(Flux!B1:B999)**.

Flux, min is calculated as **=MIN(Flux!B1:B999)**

Calc!A999 contains the last time of data, with negative values of time converted.

Period is =**Calc!A99**9.

Frequency is calculated as =1/**Calc!A99**9.

Exporting voltages, current and flux into SPICE

SPICE voltage and current sources include a Piecewise Linear Source (PWL) function. Starting at time = 0, a voltage or current is specified, then a table is built, line by line, each line specifying a new time and a new voltage or current. In this manner, any arbitrary waveform can be constructed.

With 999 points, the calculated data cannot be entered by typing each line, but the calculated data is formatted correctly so that it can be entered manually by "copy and paste" or by automatic file export.

Manual export:

Data can be imported into SPICE using the PWL function of a voltage or current source. In the PWL function, the first column is time, and the second column is the parameter list.

To import the data manually, a column with the time and a column with parameters are selected, copied and pasted into the PWL function. For example, to import the output voltage Vi, select column **Calc!A**, the time, then pressing <Ctrl> select column **Calc!D**, the voltage. These columns then can be copied and pasted into the PWL function of the voltage source.

This is repeated for the current and flux. It can also be used for the power and energy, but since the time, voltage and current are available to SPICE once imported, power and energy can be generated in SPICE, saving the effort of two copy and paste steps.

This is explained in more detail with examples in Appendix D.

Automated file export:

When new data is imported into **Data!**, four files are generated and written automatically. These files are selected or created on the **Cmd!** sheet. The export file paths and names can be chosen once, then left alone. In this case, the same files are updated when new data is imported and processed.

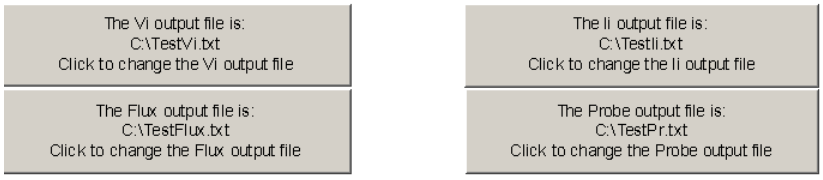

One of the choices for importing PWL data into SPICE is "File." A text file is designated, and each time the SPICE model is run, the PWL data is read from that file. If the file is updated before the run, the new data is used.

In this way, once a new source file is imported into the spreadsheet, the data is also exported to the SPICE file and is immediately available for use.

Appendix D-The SPICE Tool–Using SPICE to examine data

These directions show how I went through the steps. The Excel Tool is available at http://www.psma.com/coreloss/tools/extool.xls It is written in Excel from MSOffice 2003 on a Win7 Home Premium operating system. Excel is notoriously quirky if used in different versions of MSOffice, on different operating systems or on different computers. If it works for you, that is a bonus.

I use IntuSoft ICAP/4 Windows as my SPICE program. It has not been updated for several years, and I have never successfully exported a SPICE model for others to run, so I won't even try. I have included the steps in making a SPICE circuit for viewing the data, so the reader can reconstruct a similar model in his own flavor of SPICE.

Macros

The Excel Tool uses macros. Macros can contain viruses, so many company servers block macros, and you may have to change the settings on personal computers to run the macros. I suggest not running macros using any files that have been given to you by others. Download the Excel Tool yourself from the web site indicated above, to ensure that they have not been hacked.

Import and process the data

Open the Excel Tool, select the core .csv file, and import the data. A number of calculations will be made, and selected results are displayed on the first page (Cmd!, sheet7). If you are using the automatically exported file, be sure to select their paths and names before processing.

Import selected data to SPICE

Open a model in SPICE, and create three voltage sources with grounds and terminals. I chose the terminal names "Vi", "Ii" and "Flux." The run set being viewed may be entered and displayed using a text box.

```
mi01-3-093
```

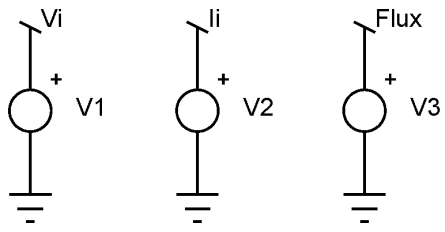

Open the voltage sources, each in turn, select Trans, then File and select the file to which the data has been saved. (Alternatively, open PWL and copy and paste the data from the Excel Tool, columns 1 and 2 of the Vi! worksheet, the Ii! worksheet and the Flux! worksheet.)

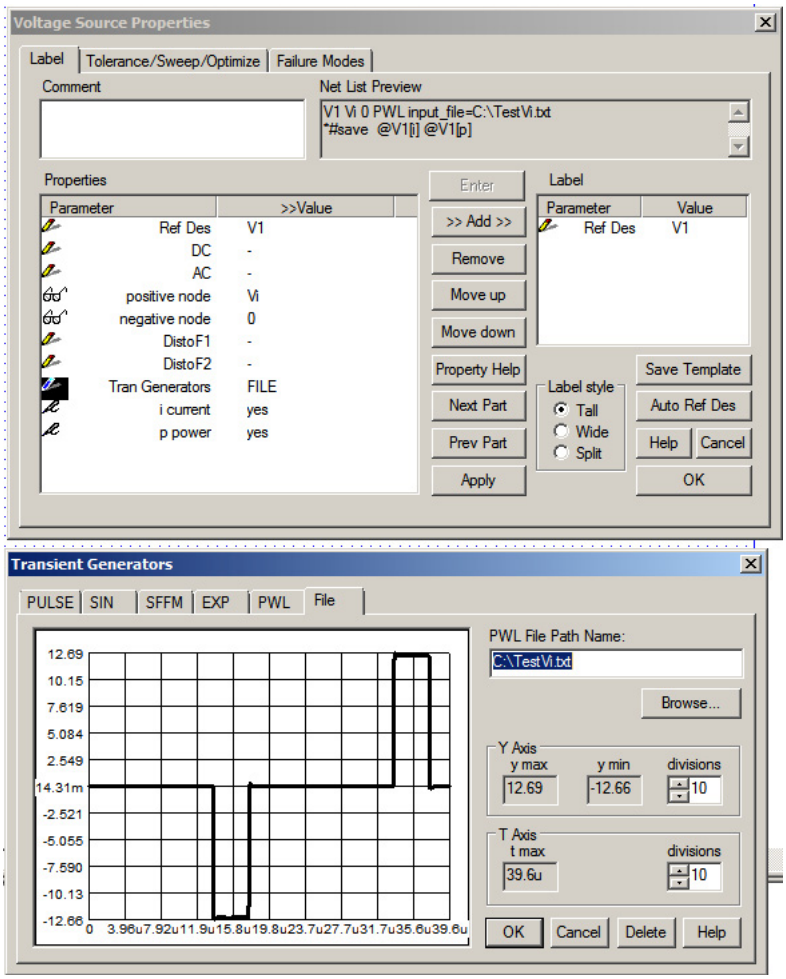

Once the file is selected, its wave shape is shown. Do the same for the current and flux files. Name and save the model file.

Set up the Simulation

Set the transient run time in the Simulation Setup. In the example, the selected cycle time is 39.5 us, so I chose 40u. Also tick the Use Initial Conditions box, as they will be needed later.

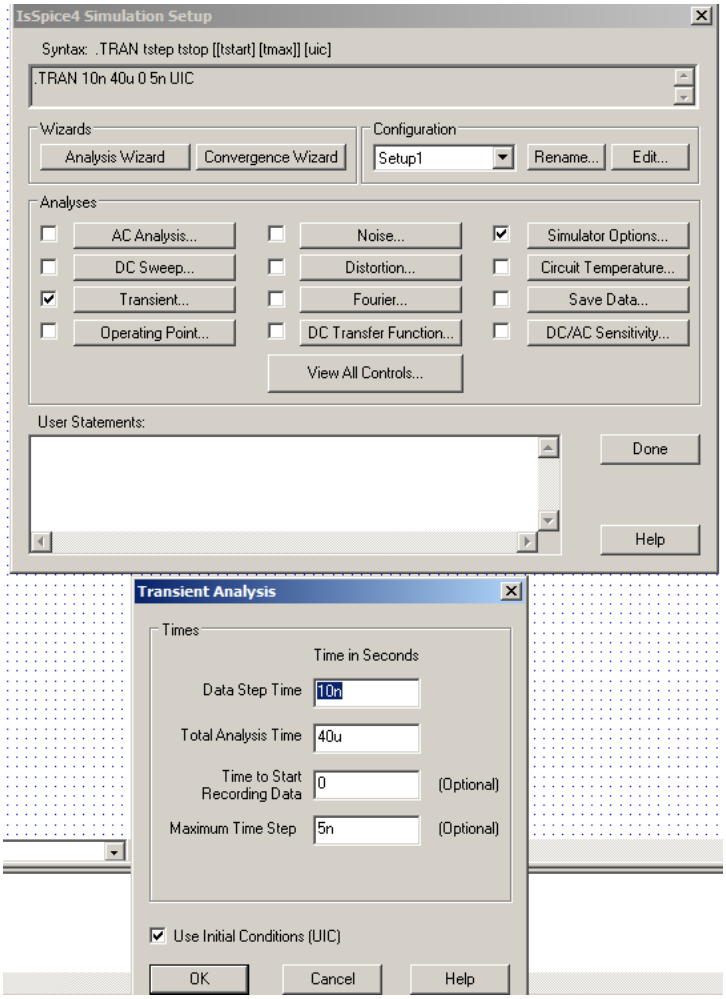

You can now run the model and display the wave shapes in the oscilloscope function. Below is the hysteresis loop, Flux vs Ii.

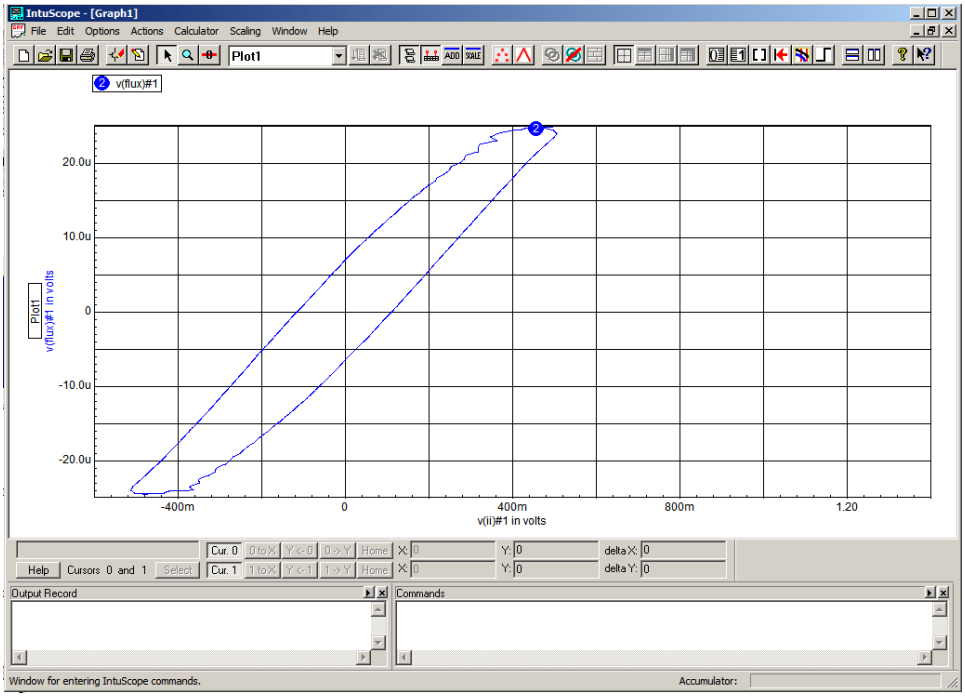

If desired, the oscillograph can be rescaled, the color can be changed, nomenclature can be added, the axes can be labeled, etc. I prefer to do that in CAD.

Appendix E
The CAD Tool

Export to CAD

The following examples use DesighCad 3D Max 18. I expect that the steps will work in other CAD programs, but I do not know.

To copy SPICE oscillograph to CAD (See Appendix D, The SPICE Tool), use the oscilloscope PRINT, then Copy to Clipboard. Open CAD and paste.

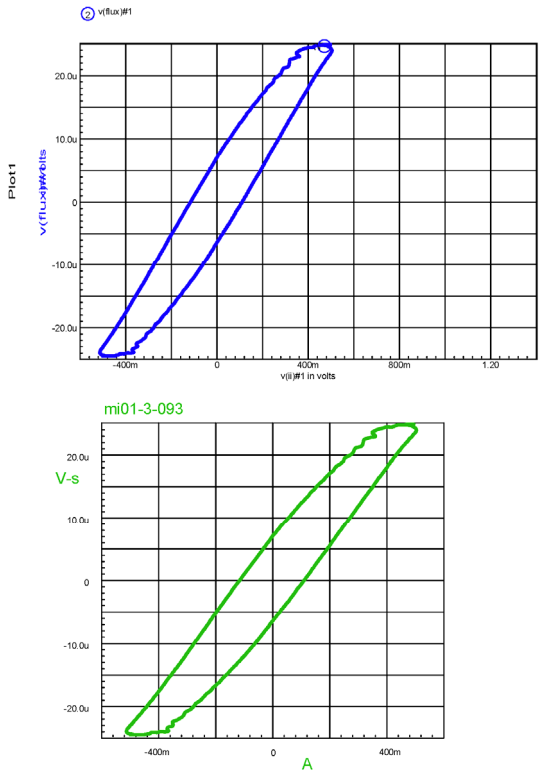

The first graph is "as imported". In the second graph, the legend has been added, extra grid has been deleted, the horizontal scale (but not the values) has been changed, the color has been changed and some artifacts have been cleaned up.

Print to graphics program

The CAD drawing may be copied and pasted into Word, maybe. Much better control of the appearance is possible "printing" the CAD drawing to a graphics program. I print to Adobe Acrobat, then crop the picture as desired and save it as a .tif file.

Rescale, add lines and nomenclature

Although I prefer to view waveforms at expanded scale using the SPICE oscilloscope zoom function, grapsh can also be rescaled in CAD.

Adding reference lines, identifiers and captions is easy, too.

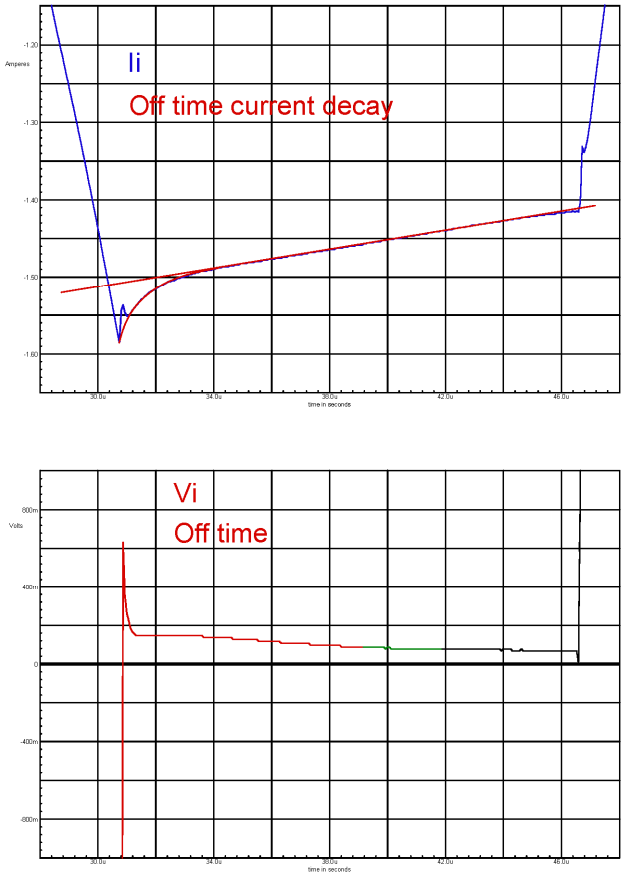

Of course, line drawings can be imported from CAD as well.

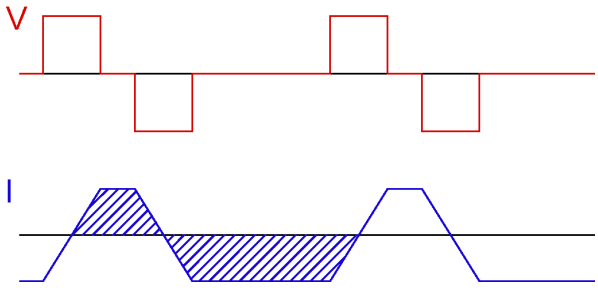

Comparing traces,

Traces can be plotted on the same graph in the SPICE oscilloscope, but only if the x-axis is the same. This makes it very difficult or impossible to compare some traces, such as hysteresis loops with different current reference or waveforms where the time axis is different. Comparing oscillographs from different simulations is quite tricky in SPICE, but easy in CAD, as long as one is careful of the scaling. Just copy and paste as required to superpose traces.

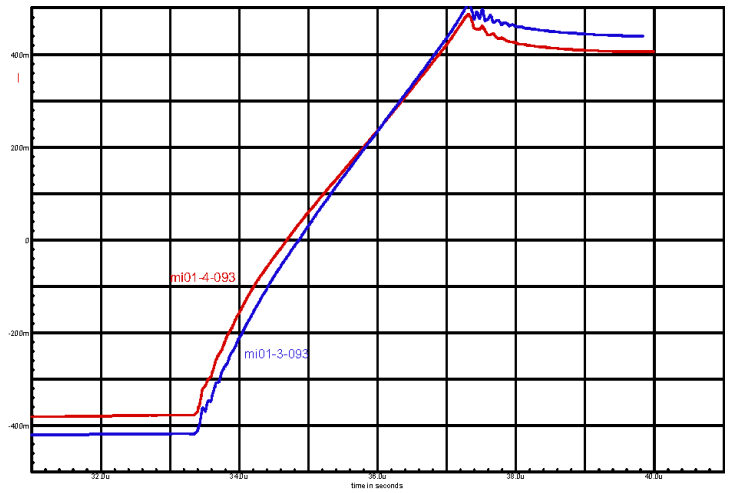

The color assignment in the SPICE oscilloscope is limited and somewhat random. It is much easier to change the color in CAD, and the width and type of line can be changed, for example, making a line heavier or dashed.

Comparing areas to estimate relative losses:

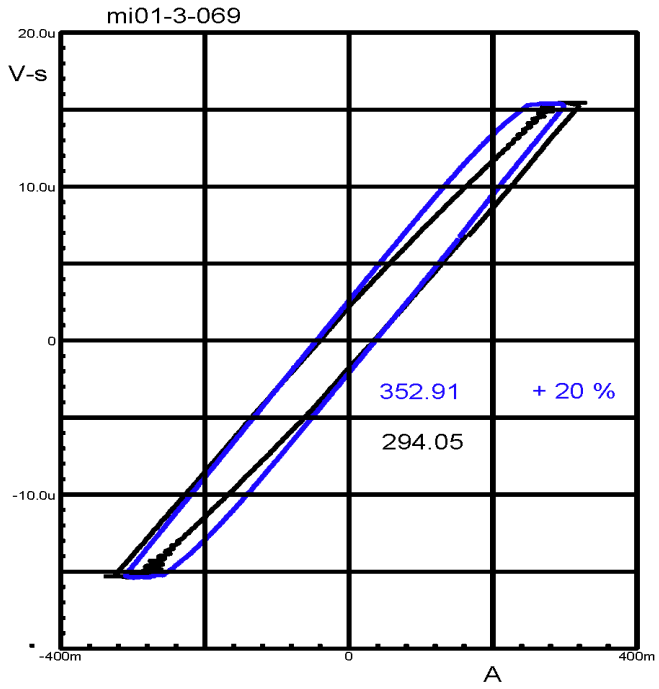

The area inside a hysteresis loop is the loss per cycle. This may or may not be straightforward, depending on the units used. If the hysteresis loop is in conventional magnetic units, then both unit conversion and dimensional conversion are necessary. If the hysteresis loop coordinates are V-s and A (with both the drive coil and the sense winding having the same number of turns, n), then the area correlates directly to watts.

CAD has a function allowing the determination of an area within a selected line. In DesignCad, the procedure is to selecte the line enclosing an area. Then choose Dimensions>Info>Area, then check the box that indicates that you want to calculate the area inside the selected line.

DesignCAD calculates the area as square units, a non-sense number, usually. That is sufficient, however, for comparing areas or calculating their ratios. It is straightforward to convert to Watts, however, if the number of units per ampere are noted for the x axis and the number of units per V-s are noted for the y axis. Divide by those conversion factors to get the answer in Watts.

Alternative graphics

While very useful, CAD is not the only way to import graphics.

Excel graphs can be copied, pasted, resized and rescaled. In Excel, select the drawing, then copy it. Paste it into Word. If it is the wrong size, select it, right click, and choose Format Picture. By default, size changes are proportional, but the height and width can be scaled differently.

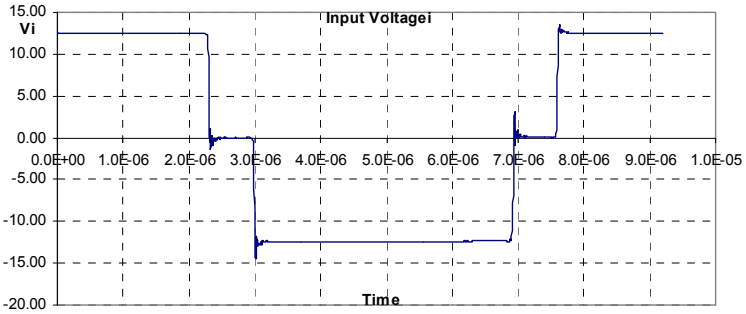

Screenshots, made using the PrtSc key and opened (paste clipboard) in a photo program such as PhotoShop Elements. The figures can be cropped and saved as graphic files and imported.

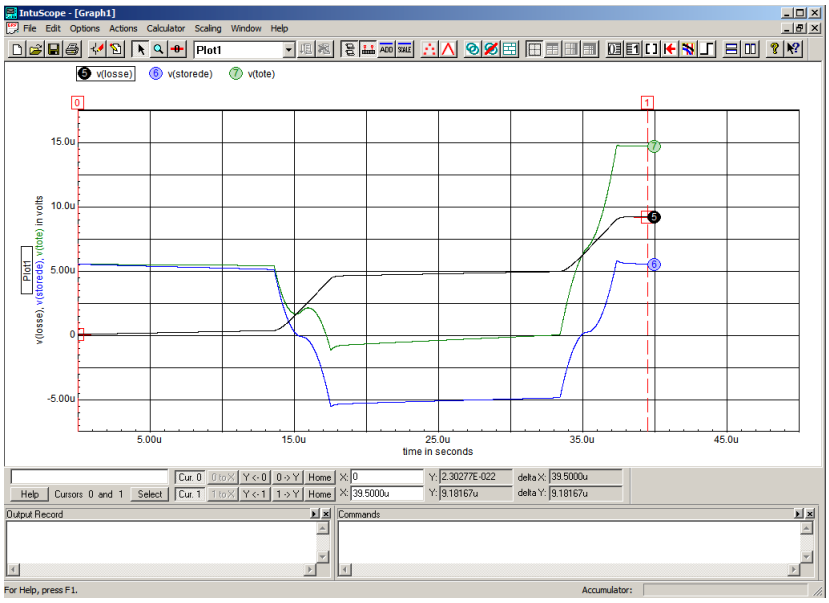

This picture shows the SPICE oscilloscope, but the graph alone could be imported by cropping the PrtSc image to the graph only. This is faster but any editing has to be done in SPICE. The SPICE oscilloscope has some editing features, though I found them more cumbersome and limited.

Appendix E
Off-time core loss phenomenon

Ferrite cores

An unexpected finding of the Pilot Project was that for excitation pulses of fixed voltage and pulse width, the core loss per cycle increased as the off-time between pulses increases. This is because energy is stored in the core as ½ I^2 L, and to the extent that the energy is recovered, the loss in the next pulse is reduced. With off-time, some energy is lost, so more input energy is required at the next pulse.

Hippo and square waveforms

To better understand this, we can examine the "Hippo" waveform. A pulse of one polarity is immediately followed by a pulse of the opposite polarity. The current ramps up, then ramps down, ideally an equal amount so that the current is zero between pulses. With zero current, there is no stored energy, so the next pulse gets all of its energy from the input power. In practice, the current is not zero, but close as can be seen in the upper right graph below.

mi01-3-156

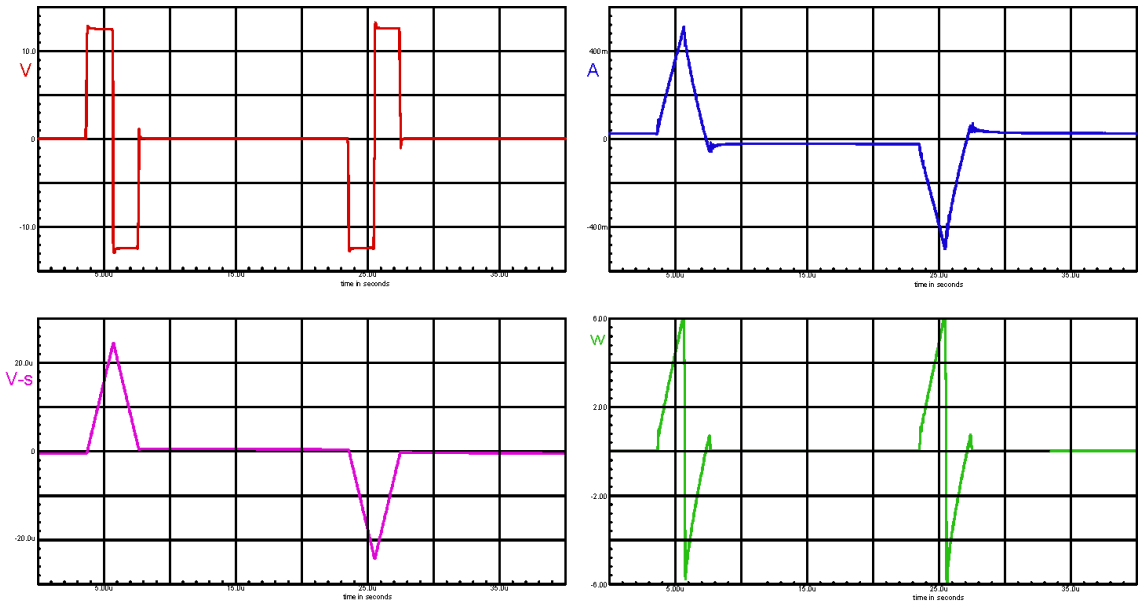

The graphs above show a full cycle for a hippo excitation, mi01-3-156, showing the sense voltage, the input current, the flux and the input power.

The mi01-3 sets are data from the Phase II project, but it uses the same core and winding as the Pilot project.

Following are graphs made using the SPICE scope function, zoomed in to the width of the excitation pulse, then copied and pasted into CAD.

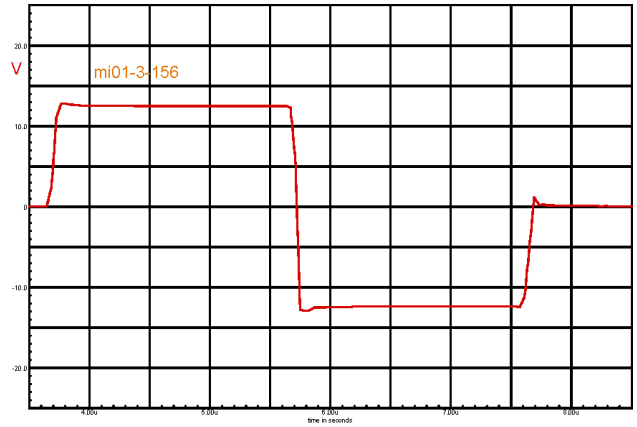

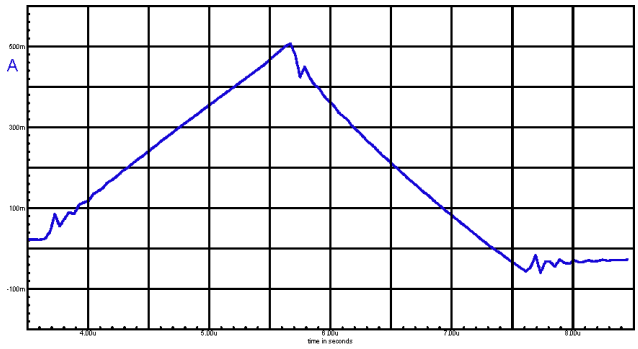

Note that initially the input current is nearly zero, so there is no stored energy. After the positive voltage source, the current is maximum, and so is the stored energy. When the voltage goes negative, it takes nearly the entire pulse width for the current to reach zero, and during this time, the power is negative, that is, energy is returned to the voltage source. There is only a very short interval of positive power, right at the end.

Thus with the hippo excitation, we see an excitation pulse that requires the maximum power with no stored energy, followed by a pulse with maximum stored energy that

requires minimum power from the source. The current in the hippo waveform goes from near zero to a peak value of about 0.5 A, then back to zero.

By contrast, the current in the square wave goes from about – 0.25 A to + 0.25 A then back to – 0.25 A. There no square wave data that is comparable to the Hippo excitation, so a square wave of slightly longer pulse width (5 µs vs. 4 µs) is used, mi01-3-038.

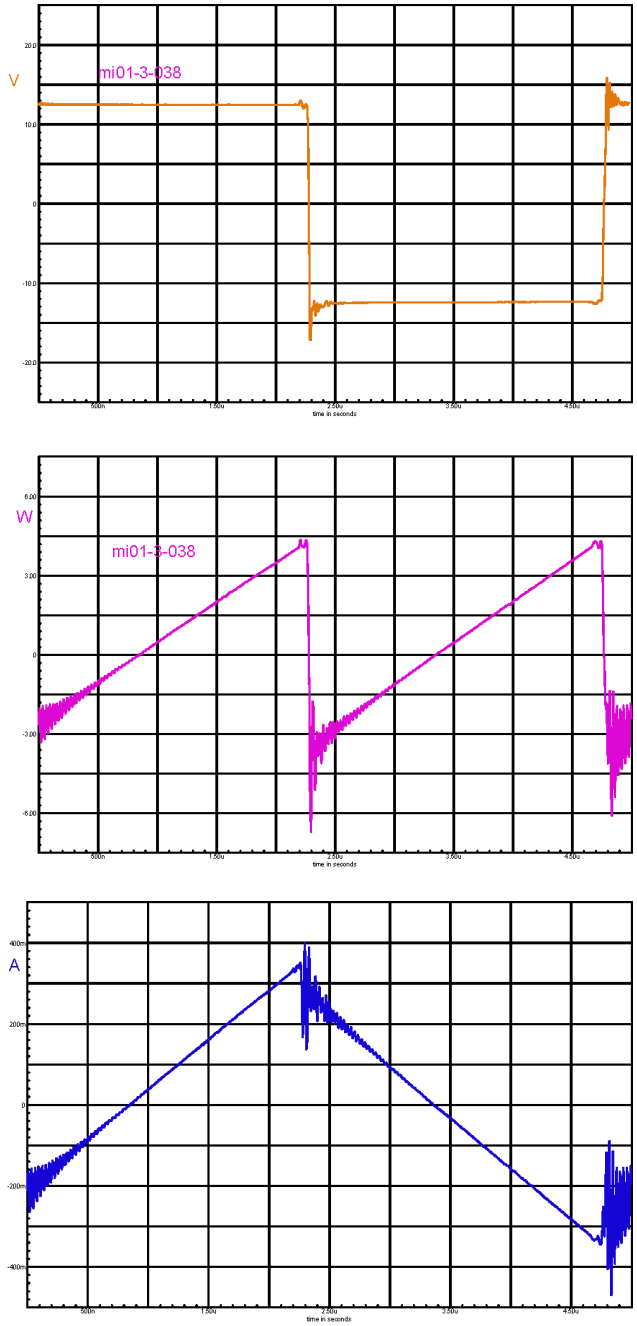

By contrast, with a square wave, equilibrium has been reached so that the power of each half cycle is equal. There is less stored energy at the beginning of the excitation pulse, so the period of negative power is less.

Energy is the integral of power with respect to time,

$$E = \int P dt$$

The power curves can be copied and pasted into CAD, and the CAD area function can be used to find the area under the curves. Because the coordinates in CAD do not relate to Watts and time linearly, the area function does not derive Joules, but it can be converted to joules with appropriate scaling. In this example, we are using the area function for comparison only, so they need not be scaled. As long as the scale of the y and x axes are the same for the graphs being compared, the ratio is valid.

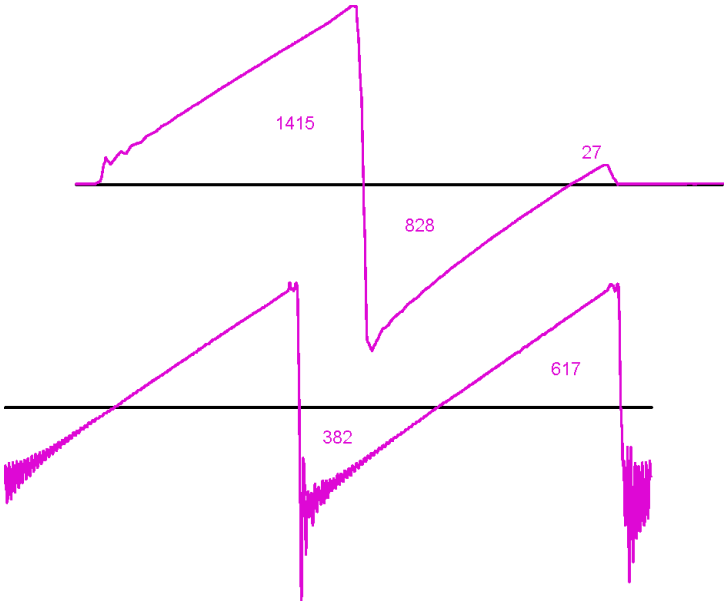

With an ideal inductor, all of the applied power would be stored as energy, and it would be returned during the reverse excitation pulse. In actuality, some of the applied power is stored as energy and some is dissipated. I do not know how to separate them, but qualitatively, 1415 units of energy went into the core, 828 units came back out, then 27 units more went in, for a net of 1415 -828 + 27 = 614 units for the cycle.

In the square wave excitation, equilibrium was established so that the power if each half cycle is equal. 382 units of power are returned, then 617 goes in, for a net of 617 – 382 = 235 units. That is for half a cycle, so 235 * 2 = 470 units for the cycle.

Even though the square wave cycle is significantly longer than the positive-negative pulses of the hippo waveform (5 µs vs. 4 µs), its net energy is less. The ratio is 470/614 = 0.765.

Expanded waveform

The graphs below show the excitation voltage, current, flux and the hysteresis loop for mi11-X-131 test runs. The graphs use component electrical engineering terms, volts, current and volt-seconds.

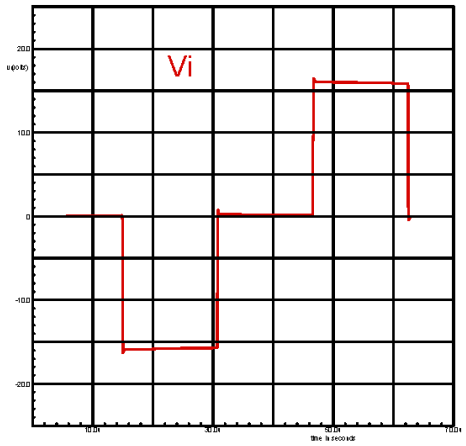

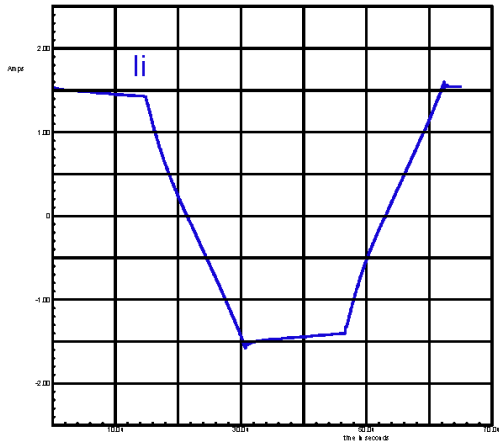

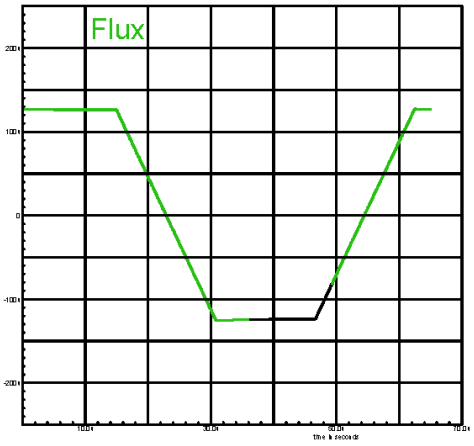

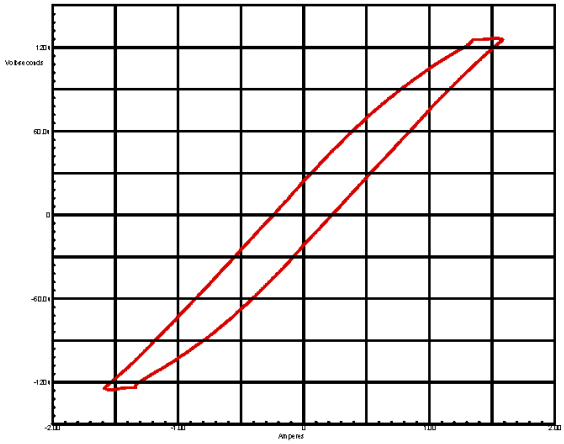

The current and voltage during the off time are shown below with expanded scale. As can be seen in the graphs on the previous page, the current ramp is quite small and the voltage is very low. The small voltage is positive and the current is negative, so that is power out of the core, but the amount of power is too small to account for the off time loss phenomena.

Two loss components are visible during the off-time. A short exponential reduction in current is followed by a long linear ramp. The latter is the very small IR drop of the circuit resistance and the circulating current. The initial exponential current drop probably accounts for most of the lost energy as a reduction of stored energy, $E = \frac{1}{2} I^2 L$. The red reference lines were added in CAD.

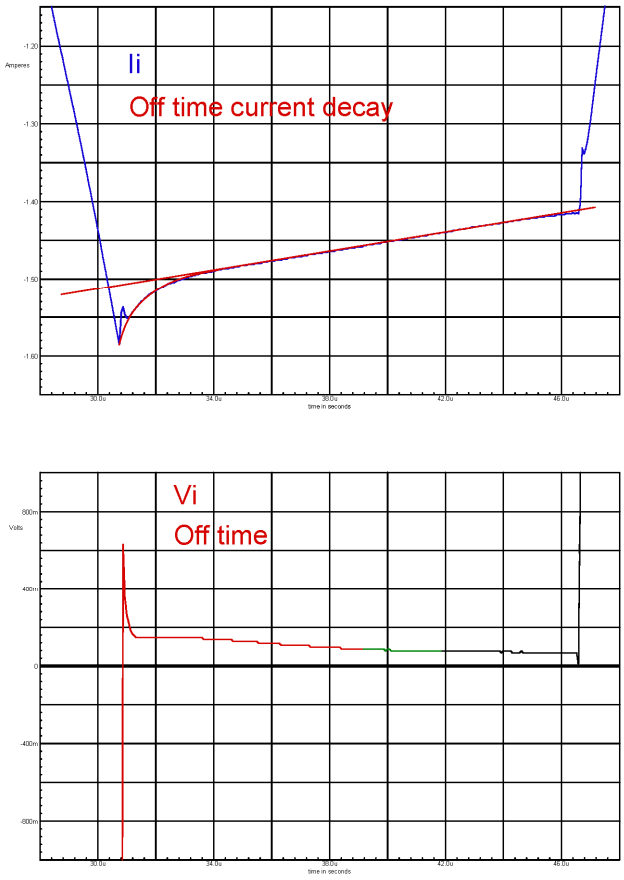

The flux changes revealed by the embedded windings do not appear to be a significant factor in explaining the off time loss phenomena. They are small, and the timing is not consistent.

Note the leading edge spike on the sense voltage winding.

Powdered iron core

The powdered iron core tested in the Pilot project exhibits the same off-time loss behavior, at least at higher currents, but the effect is much smaller.

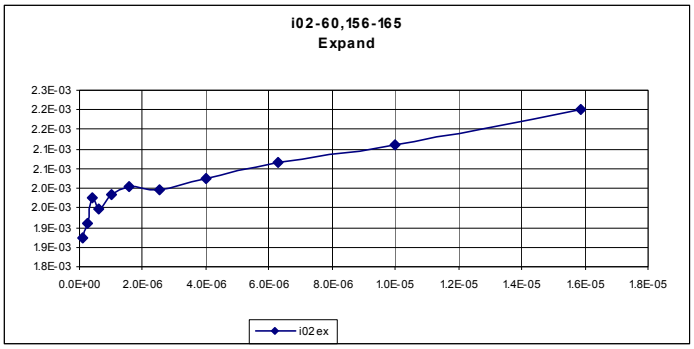

Compared to ferrite, the exponential drop immediately following the on-time pulse is much less pronounced. There is a gentle down-slope in the current during the off-time

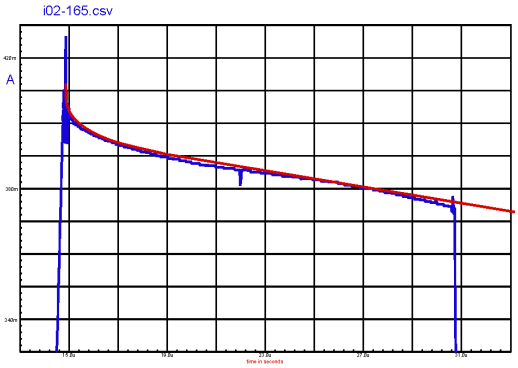

At expanded scale, exponential drop and the current down-slope is more visible. The red curve and line were added in CAD.

Skew and symmetrical wave shapes

Skewed and symmetric wave shapes

A lot of data was taken with skewed and asymmetrical excitation. A blocking capacitor was used, and that makes these data difficult to interpret. The excitation of a magnetic core must have balanced volt-seconds, to avoid flux walking and saturation effects, and a blocking capacitor can ensure balanced excitation. Unfortunately, the blocking capacitor also forces balanced ampere-seconds (equal coulombs), and some wave shapes do not naturally have balanced currents.

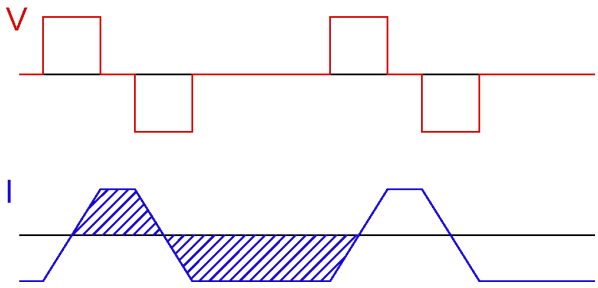

The graph above shows a generic skewed excitation and the expected current for an ideal inductor. It is obvious by inspection that the ampere-seconds are not equal, so no skewed data was used for this report. It is not as obvious whether the ampere-seconds for an asymmetric waveform are not equal. Nonetheless, I regard asymmetric test data as suspect and did not use asymmetric data either.

The hysteresis loops for the skew data are distorted, the hysteresis loop below being an extreme example.

f10-133.csv

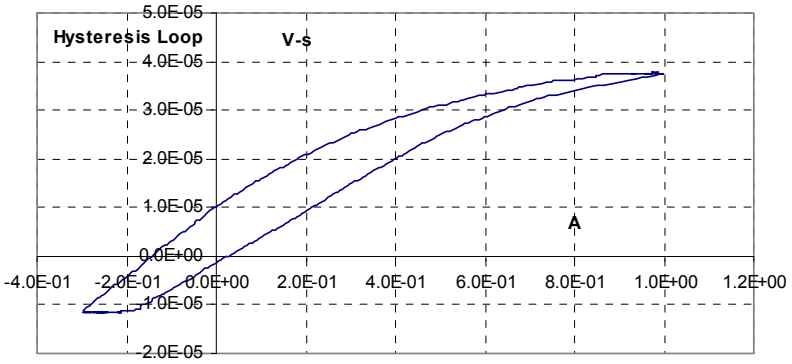

A possible explanation is that the blocking capacitor forces the ampere-seconds (coulombs) to be equal. Because the current is positive for a much shorter time, its magnitude is forced to be much higher so that its average is zero. This can be seen both by the high positive currents in the hysteresis loop and in the current graph below.

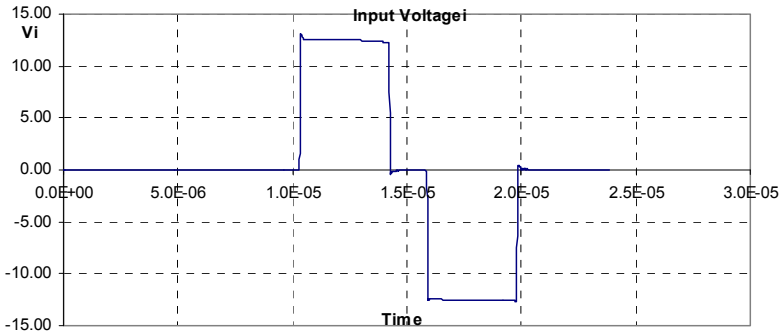

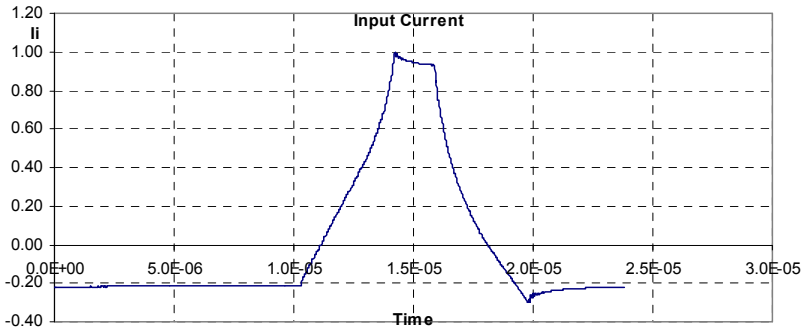

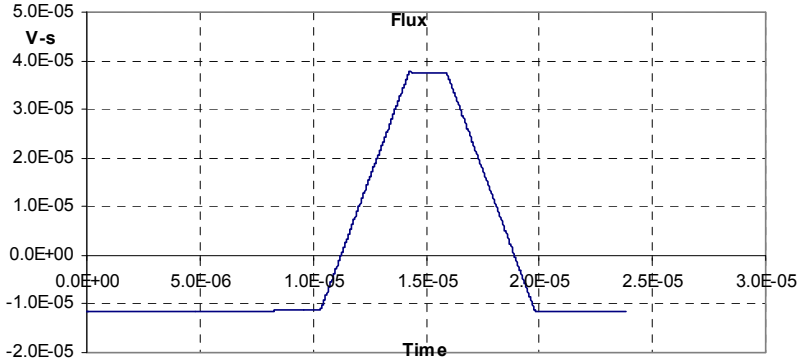

File E:\Pilot data\ferrite-data\f10-133.csv

Power, method 1	3.604167E-01	W	Δ Flux, pos	4.88584E-05	V-s
Power, method 2	3.607778E-01	W	Δ Flux, neg	-4.9085E-05	V-s
Energy, method 1	8.601744E-06	J	T, pos (total)	3.91796E-06	s
Energy, method 2	8.575913E-06	J	T, neg (total)	3.91796E-06	s
Avg. V, pos	1.247037E+01	V	Duty-ratio, pos	0.164658635	
Avg. V, neg	-1.252820E+01	V	Duty-ratio, neg	0.164658635	
Flux, max	3.767770E-05		Period	2.3794E-05	s
Flux, min	-1.169684E-05		Frequency	4.202662E+04	Hz

As part of the processing, the zero offsets are removed from the data by finding the average of the raw data and subtracting it to reset the data so that its average is zero. This

also forces the ampere-seconds (coulombs) to be equal, and it may accurately represent what is happening with the current in view of the blocking capacitor.

From the graph and the data above, it can be seen that the positive and negative voltage pulses are very close to being equal, so the flux excursions should be equal, and the data table shows that they are. Yet the core spends much less time at positive flux than it does at negative flux, so the average weight of the positive flux is much less and it shifts the zero. From the shape of the hysteresis loop, it seems that flux walking has pushed the flux to near saturation in one direction.

The core would not exhibit this behavior without the blocking capacitor. It is my view that skew and asymmetric data should be taken without a blocking capacitor. In fact, probably all data in the future should be taken without a blocking capacitor, just to be sure that it does not influence the data. This may require some other provisions to ensure that flux walking is not a problem. Current mode control is one method, and surely there are others.

Blocking capacitor investigation

There was some concern that the blocking capacitor may be affecting the test results. Accordingly, some tests were run with a larger blocking capacitor.

In the Phase II Project report: "In Phase I, the bridge was equipped with a 320 μ F blocking capacitor. On very long expand runs, low-frequency ringing was evident. We wanted to improve this performance by increasing the blocking capacitance, while lowering the effective series resistance, so we installed 120mF of blocking capacitance, using Epcos MKT series polyester capacitors."

From this rather neutral statement, I assumed that there was no significant difference. However, a review of the expanded loss curves shows a substantial difference.

It took a while to determine the cause of the difference, but a line in the setsreport.txt file provided the answer; the tests with the big capacitor were done a "room temperature," whereas the other tests were done in oil at 80 º. From the manufacturer's specification for the core (Magnetics Inc. R material), the difference actually should be greater, so there was probably significant self-heating of the core.

The following exploration was done to try to identify the reason for the difference before the cause was known. I am leaving it unedited as an example of how to explore differences using the data. Trying to solve this riddle resulted in a much closer study of the waveforms and their comparison, and led to much speculation and many ideas. This proved to be pivotal to finding a new hypothesis.

The graphs of the energy per cycle for the comparable test runs with the larger 120 mF capacitor (mi01-4-xxx) and with the Pilot Project baseline 320 µF capacitor (mi01-3-xxx) are shown below. A third run, with a 1.8 mf capacitor (mi01-6-xxx) is also included.

In the first set, the on-time is 3.9 µs and the voltage is 1.24 V. In the second set, the on-time is 6.2 µs and the voltage is 4.9 V. In the last set, the on-time is 3.9 µs and the voltage is 12.4 V. The vertical axis is joules and the horizontal axis is increasing off-time in seconds.

mi01-3, mi01-4 and mi01-6 (-040 to -051)

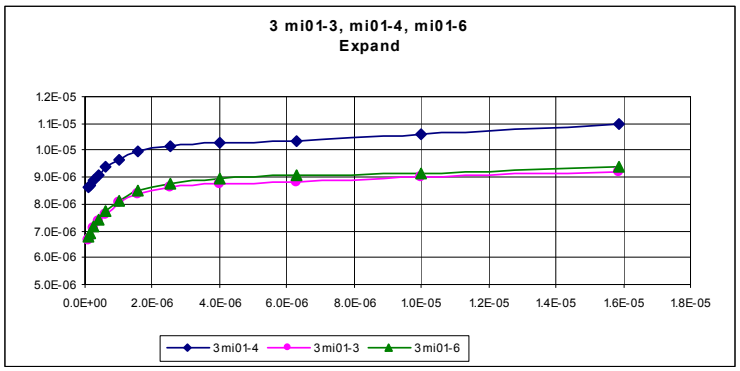

-061 to -072

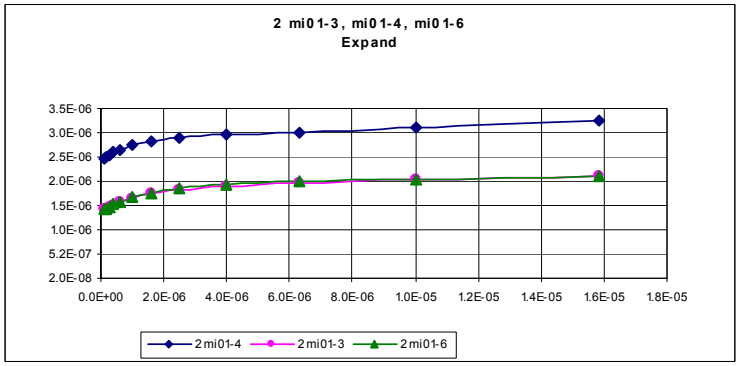

-082 to -093

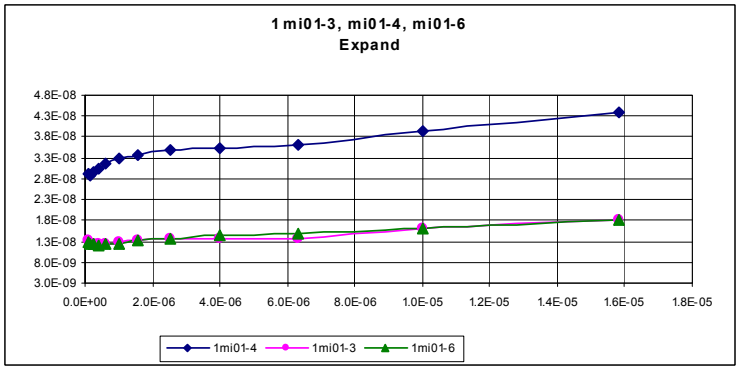

Below are the input current, the hysteresis loop and the input power is shown for the mil-3-093 run. Following that are the same graphs for the mil-4-093 run.

mi01-3-093.csv

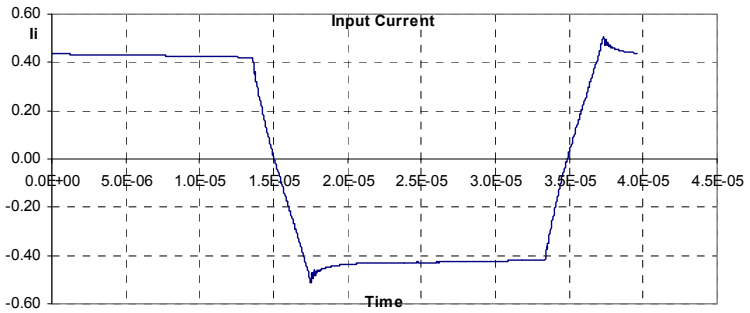

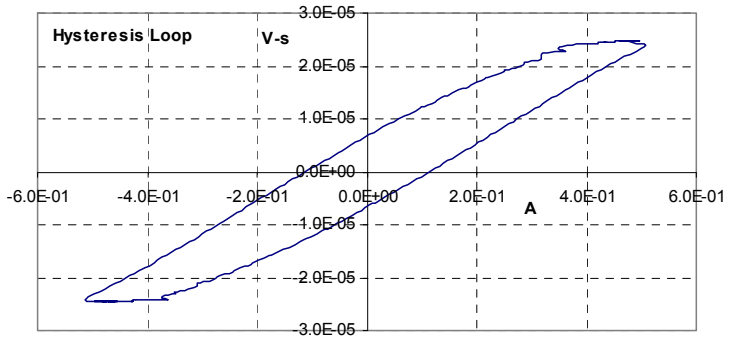

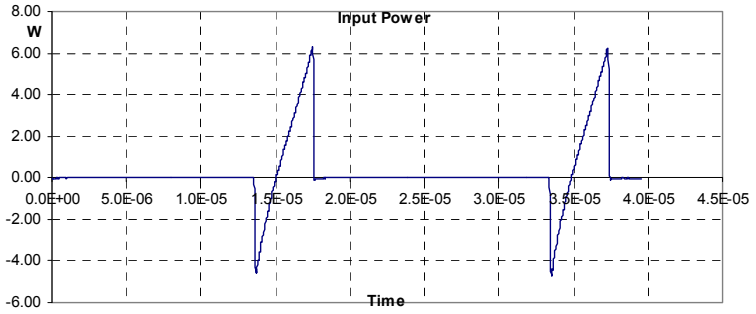

mi01-4-093.csv

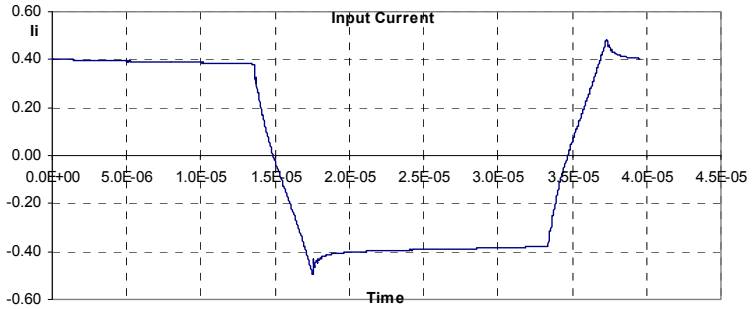

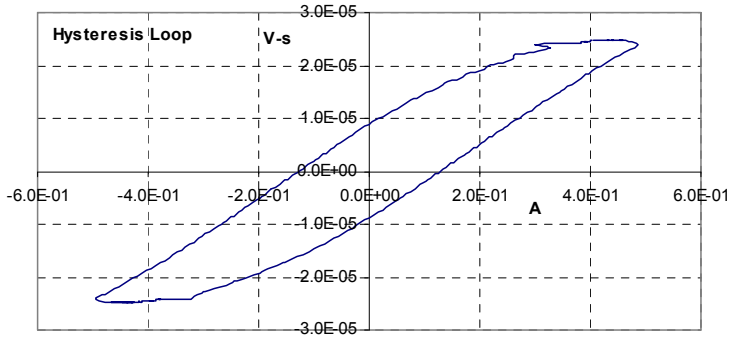

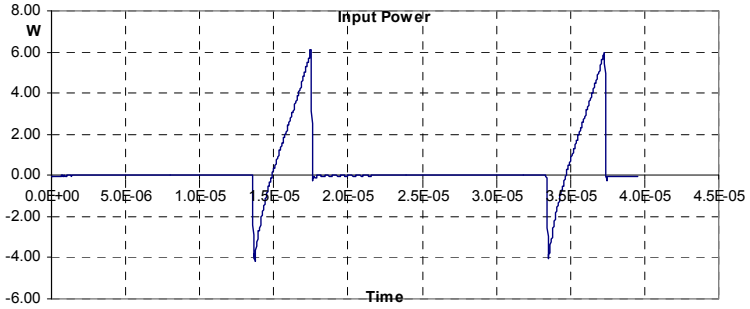

To investigate further, I imported various parameters for the two runs into SPICE voltage sources using the PWL function. This allowed displaying them using the SPICE scope utility. Selected scope traces were copied into CAD and superposed for comparison. Those graphs follow the other graphs below.

The graph below shows the sense voltages for the two runs, mi01-3-093 and mil01-4-093, imported into SPICE voltage sources using the PWL function. A possible source of energy difference would be a voltage difference, but they are so close as to be almost indistinguishable. The scope function traces were zoomed to the positive excitation pulse.

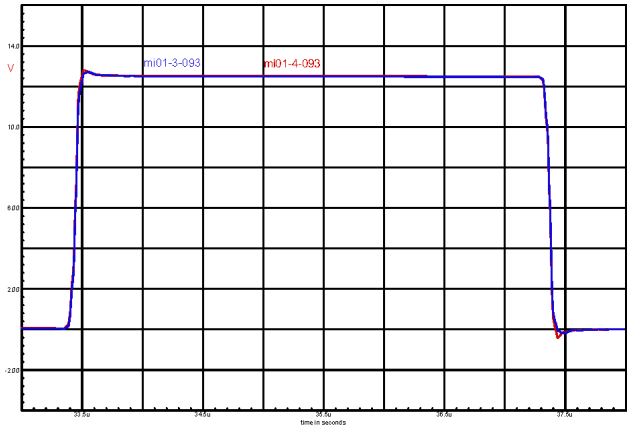

The input current waveforms were also imported and superposed. The first graph shows the entire cycle; the second is zoomed to the positive excitation pulse. It is very hard to see a significant difference, but the current trace in mil-3-093 shows a greater magnitude, seemingly anomalous with the fatter hysteresis loop of mil-4-093. However, what is seen most easily is the off-time current, and its relationship to the energy per cycle is more complicated.

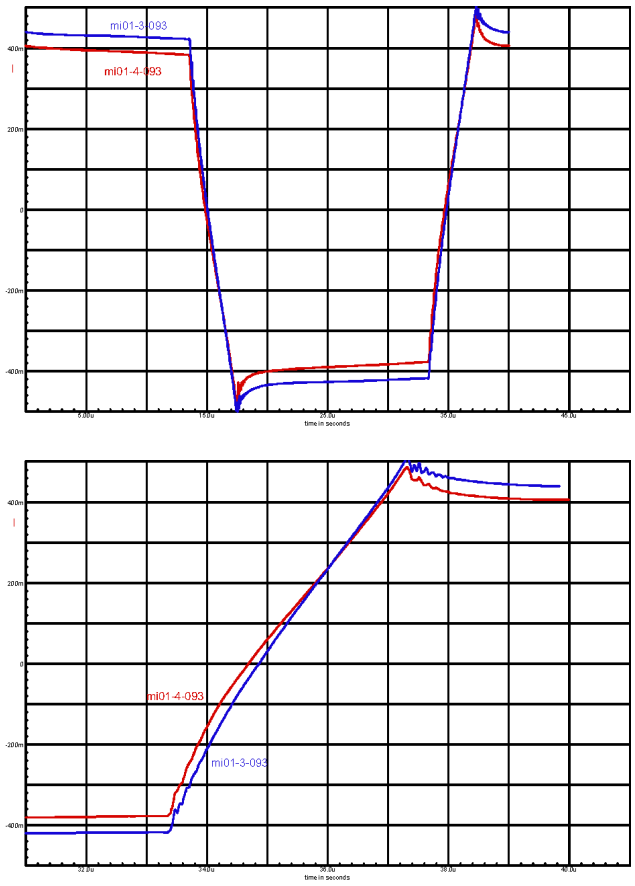

Note that the mil-3-093 current is higher during the off-time, with the difference increasing at the start of the on-time. The voltage is positive and the current is negative, so initially the power is negative, out of the core, reducing the energy. It is more negative for a longer period of time than it is for the mil-4-093 run, so more energy is recovered at the start of the excitation time. This is shown more clearly in the power traces, below.

The first graph below shows the power into the core for the entire cycle; the second is zoomed to the positive excitation pulse width.

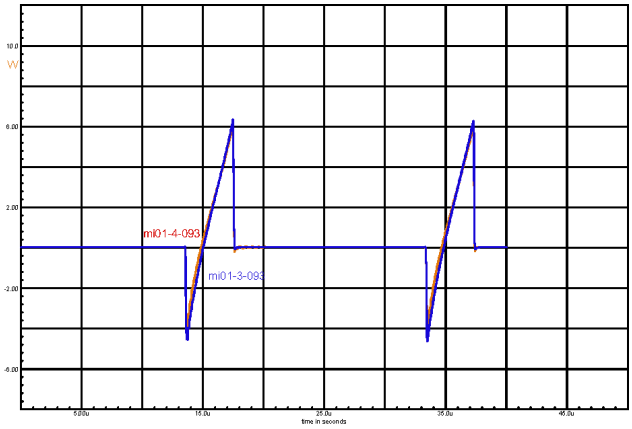

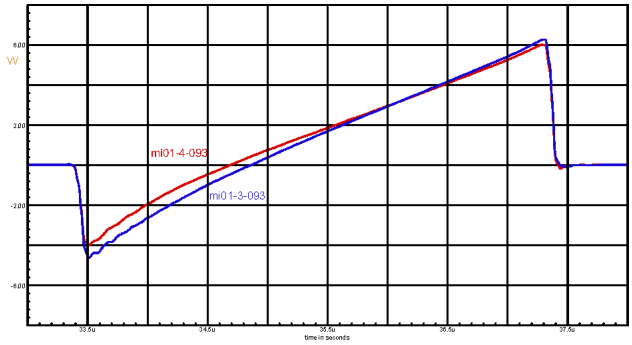

Note that at the beginning of the excitation pulse, the power is negative. It is more negative and it is negative longer for the mi01-3-093 pulse, so much more energy is carried forward. At the trailing edge, where the input energy is positive, the difference is smaller.

The following graph shows the energy into the core for the entire cycle.

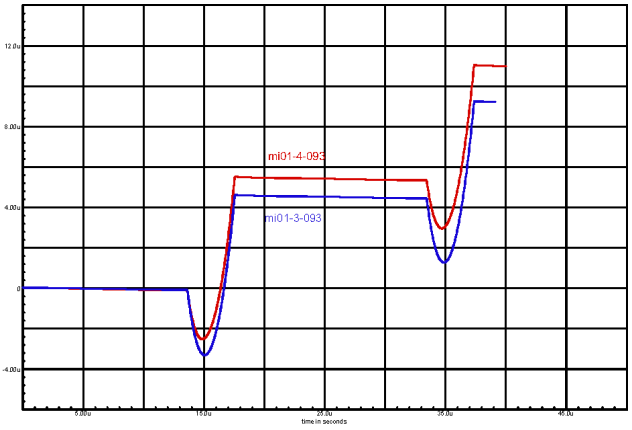

In the scope trace below, the hysteresis loops for the mi01-3-093 and mi01-4-093 are superposed.

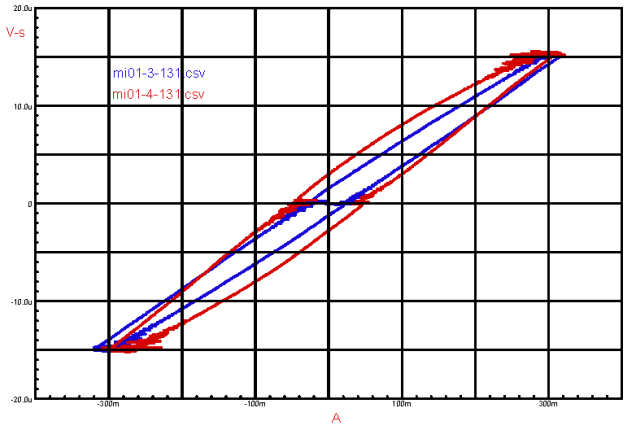

This reinforces the hypothesis that the energy stored and recovered is significant to the energy consumed per cycle. It did not explain, however, why the data using the 120 mF blocking capacitor makes so much difference.

One possible explanation for the data is that the wrong core was used in the test. However, the data does not match data for any of the other cores using the same test protocol. After writing the above, I discovered that the tests were the same core, but the mi01-4-xxx data was taken "at room temperature," whereas the other tests were in oil, controlled to be 80 º C. From the Magnetics Inc. data for R material, the difference should be greater, so there was probably significant self heating.

Another possibility considered was that the much larger blocking capacitor might allow a degree of flux walking, and the hysteresis loops of interest might be a more lossy minor loop. However, a comparison of the mi01-3 and mi01-4 hysteresis loops from the sets images directory shows that both resemble the square wave hysteresis loops, they reasonably well centered, and they approaching but not into saturation. The -039 curves are the reference square waves for the data of interest. The lower voltage loops appear to be fatter as well.

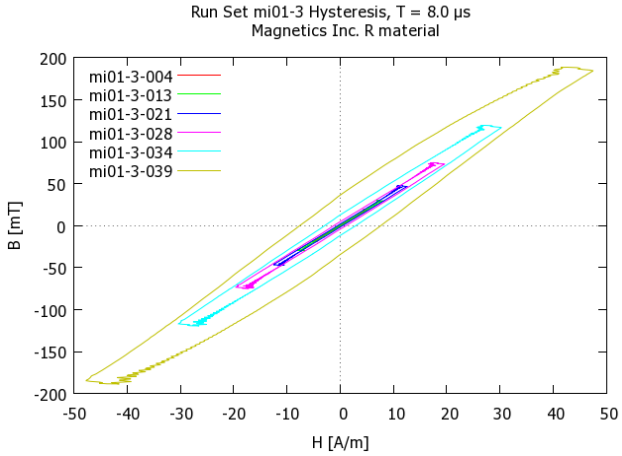

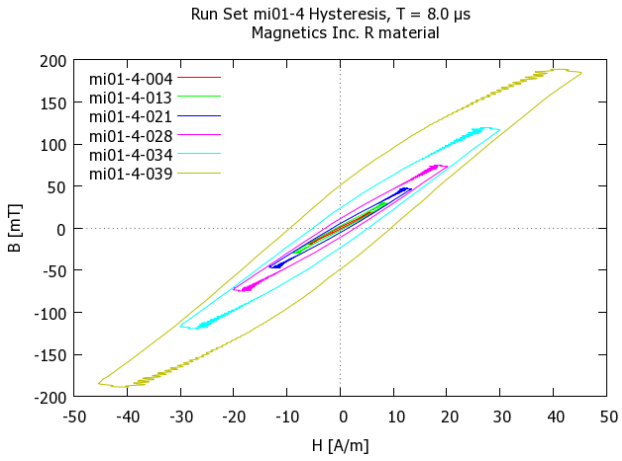

The comparable square wave data from the Pilot Project was checked.

File	E:\Pilot data\ferrite-data\f10-049.csv				
Power, method 1	8.170167E-01	W	Δ Flux, pos	4.974934E-05	V-s
Power, method 2	8.178835E-01	W	Δ Flux, neg	-4.977878E-05	V-s
Energy, method 1	6.499372E-06	J	T, pos (total)	3.949400E-06	s
Energy, method 2	6.479474E-06	J	T, neg (total)	3.989213E-06	s
Avg. V, pos	1.259668E+01	V	Duty-ratio, pos	4.979920E-01	
Avg. V, neg	-1.247835E+01	V	Duty-ratio, neg	5.030121E-01	
Flux, max	2.488376E-05		Period	7.930650E-06	s
Flux, min	-2.490285E-05		Frequency	1.260931E+05	Hz

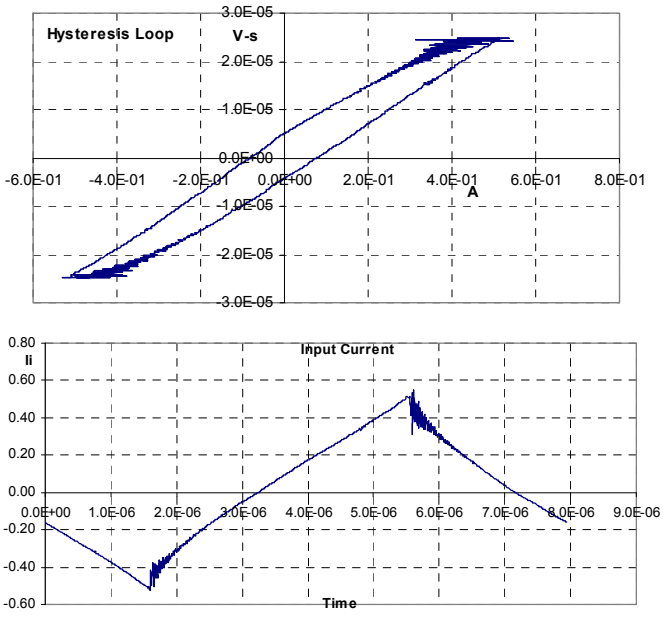

The square wave Pilot Project data compares closely to the Phase II mi01-3-039 data:

File	E:\Phase II Data\sets\mi01-3\scope\mi01-3-039.csv				
Power, method 1	8.380325E-01	W	Δ Flux, pos	4.943937E-05	V-s
Power, method 2	8.388997E-01	W	Δ Flux, neg	-4.939588E-05	V-s
Energy, method 1	6.666379E-06	J	T, pos (total)	3.989213E-06	s
Energy, method 2	6.646142E-06	J	T, neg (total)	3.949400E-06	s
Avg. V, pos	1.239326E+01	V	Duty-ratio, pos	5.030121E-01	
Avg. V, neg	-1.250719E+01	V	Duty-ratio, neg	4.979920E-01	
Flux, max	2.472378E-05		Period	7.930650E-06	s
Flux, min	-2.471559E-05		Frequency	1.260931E+05	Hz

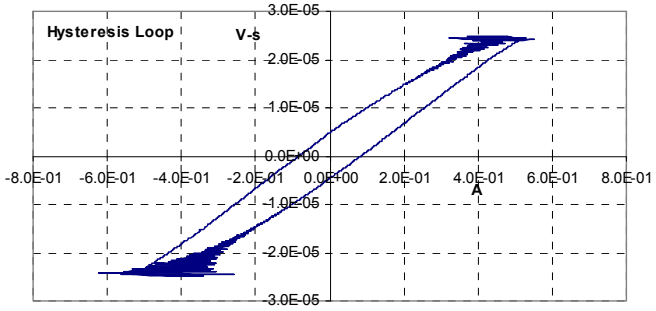

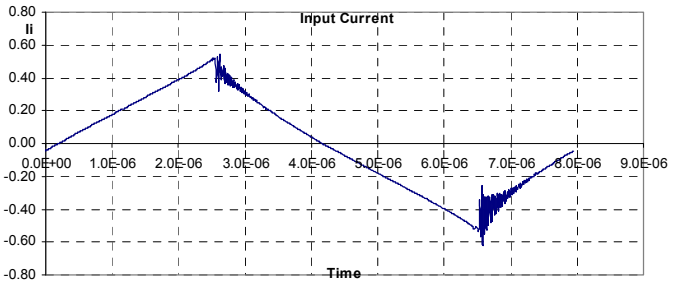

For comparison, see the mi01-4-039 square wave data below.

File	E:\Phase II Data\sets\mi01-4\scope\mi01-4-039.csv				
Power, method 1	1.058415E+00	W	Δ Flux, pos	4.955600E-05	V-s
Power, method 2	1.059509E+00	W	Δ Flux, neg	-4.952144E-05	V-s
Energy, method 1	8.419470E-06	J	T, pos (total)	3.981250E-06	s
Energy, method 2	8.393918E-06	J	T, neg (total)	3.957362E-06	s
Avg. V, pos	1.244735E+01	V	Duty-ratio, pos	5.020080E-01	
Avg. V, neg	-1.251375E+01	V	Duty-ratio, neg	4.989959E-01	
Flux, max	2.477251E-05		Period	7.930650E-06	s
Flux, min	-2.474893E-05		Frequency	1.260931E+05	Hz

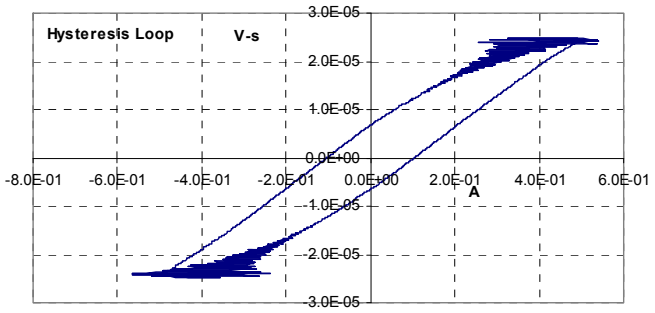

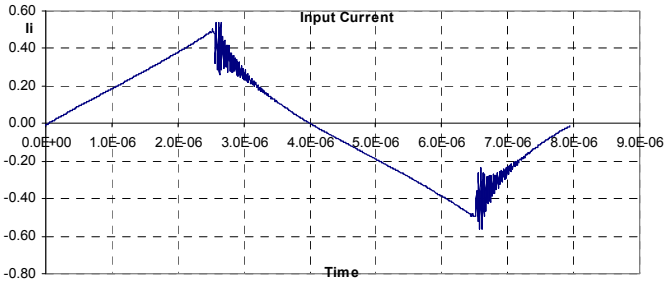

Comparisons to a SPICE model

I created a SPICE model, below, as explained in Appendix J, Simple SPICE model. I ran the mi01-3-093.csv file in the Excel Tool, which exports the Vi, Ii and Flux data to files accessible by SPICE. These become the PWL function for the three voltage sources with terminals having the same names. When run, the model makes the mi01-3-093 parameters available on the terminals.

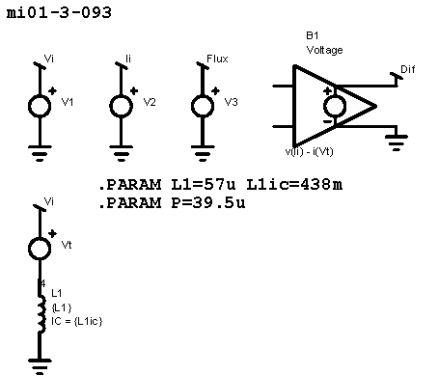

I added an inductor L1 and a voltage source Vt set to 0 V. This is the SPICE recommended way to measure current as i(Vt). The inductor and its ammeter are connected to Vi through a terminal, so the model has the same excitation voltage as mi01-3-093.

The purpose of this exercise is to compare the model currents and hysteresis loops to the mi01-3-093 run. To make the difference current easier to see, a behavioral voltage source B1 generates the difference term, v(Ii) –i(Vt). SPICE does not care that I am subtracting a current from a voltage, it just yields the numeric difference.

The first graph below shows the currents Ii and i(Vt) with the difference.

The graphs below show the mi01-3-093 current, red, and the model current i(Vt), blue. The green line is the difference. The difference current is green. It is very hard to visualize he the vertical separation of the Ii and i(Vt) lines, so the difference function is important.

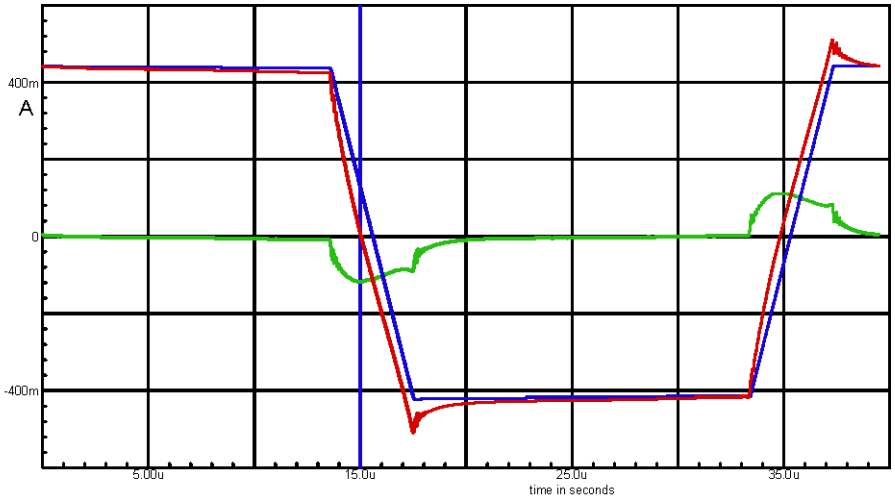

The hysteresis loops for Ii vs Flux (red) and i(Vt) vs Flux, blue, are superposed. With only an inductor, the model hysteresis is a straight line.

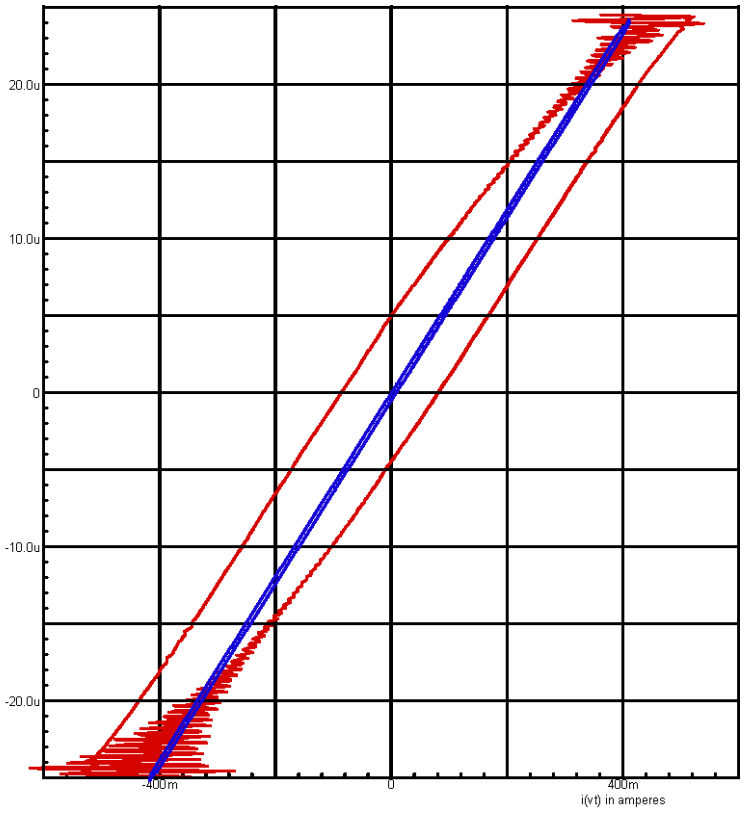

We now add some resistors to the model. The small series resistor R1, 0.12 Ω, models the shallow down-slope seen in the mi01-3-093 current Ii. There is a substantial difference current component seen only during the on-time. This suggests the parallel resistor R1.

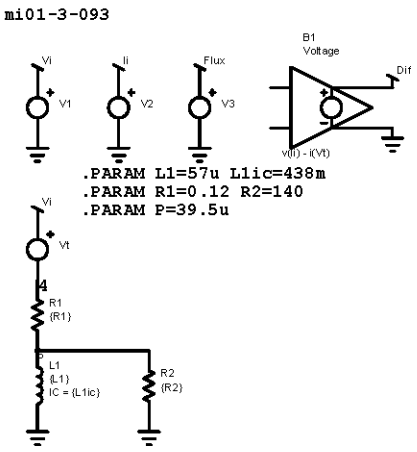

The addition of the resistors makes the currents match much more closely. The difference in the sloped portions of the curve is very difficult to see, but is quite evident in the difference current display. Note that the difference currents have about the same time constant when the excitation is applied and when it is removed.

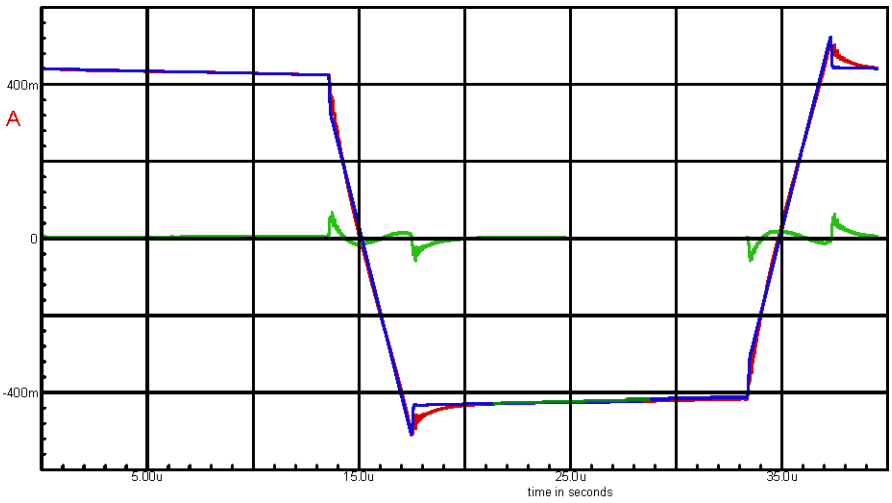

Note that the current step is approximately correct, but the time constant is way off. The error is fairly easy to spot in the relatively flat curve at the off-time. It is about the same when the voltage is applied, but that is very difficult to see without the difference current display.

The hysteresis loop of a resistor alone is a rectangle centered on the vertical axis. In parallel with the inductor, it fattens the hysteresis loop so that the area equals the losses. The very straight sides are a little too fat, but in this demonstration, I am building incrementally a circuit that has already been optimized, so that will be moderated.

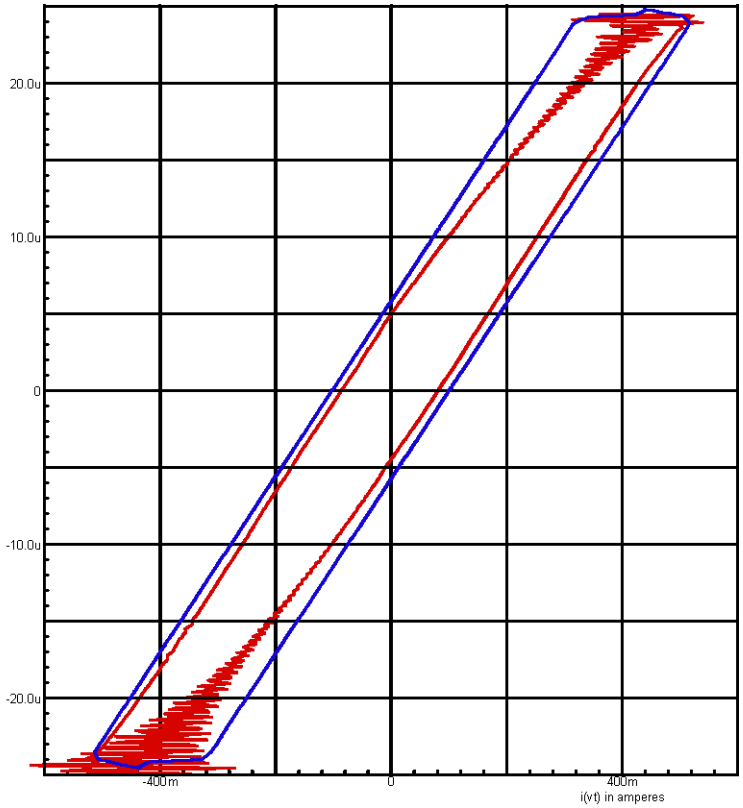

An inductor L2 is added to the model. This is to slow down the transition current in the resistor. There is no illusion that this indicates what is happening in the core, it is a curve fitting exercise.

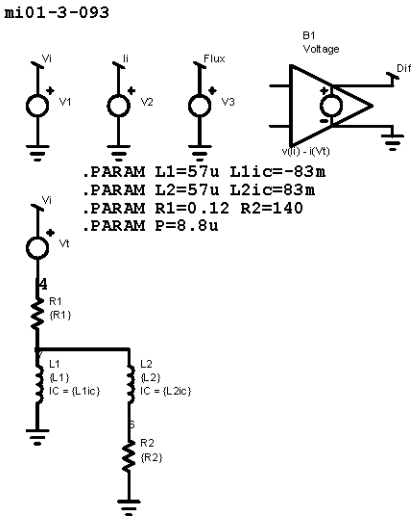

The graph below has added the excitation voltage as reduced scale. The current traces now fit quite closely.

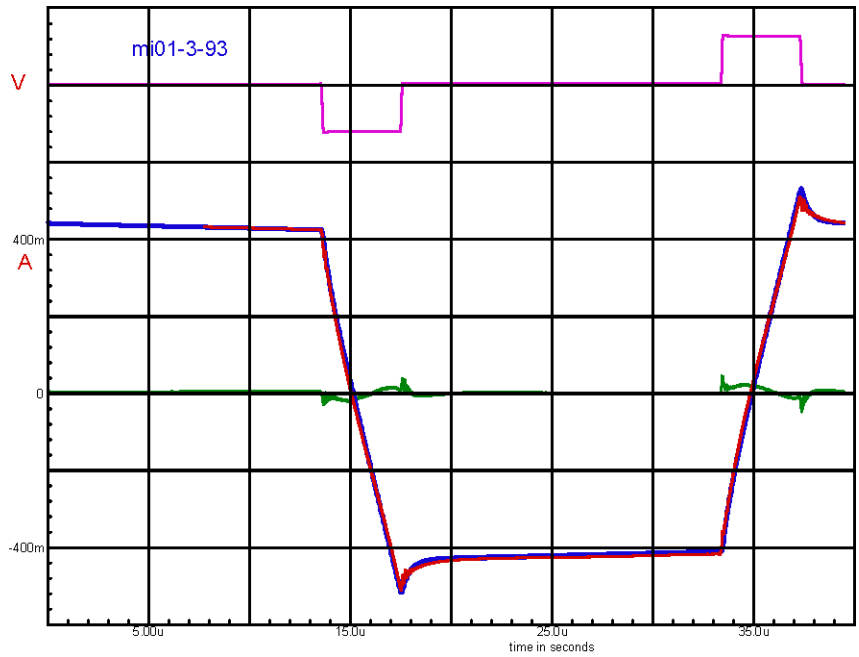

The graph below is the same curves, but it is zoomed in to highlight the time of the negative excitation pulse. The difference between the current traces is somewhat easier to see, but the difference current display is useful nonetheless.

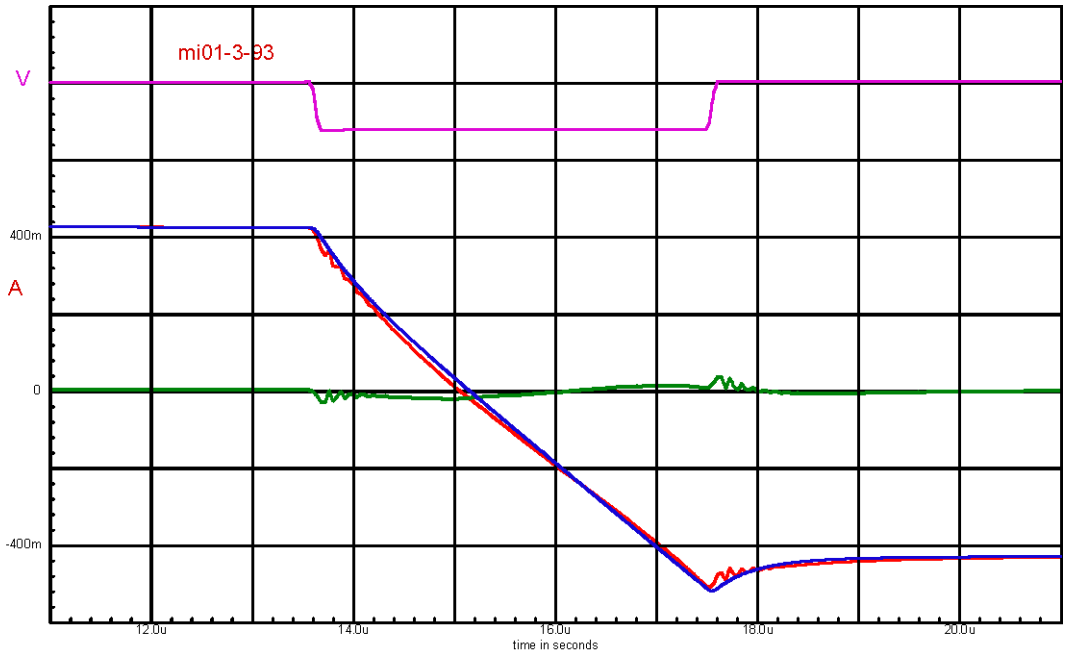

The difference current display is particularly valuable in showing that the error (the difference current) is about the same when excitation is applied as when it is removed. This suggests that the off-time phenomenon is mis-named. It is there throughout.

The hysteresis loops now are quite close as well. The model has slightly higher current in the corners, and that can be seen in the current traces as well, but it is much more conspicuous in the hysteresis loop. For core loss estimates, the important parameter is the respective areas, and they look to be quite similar.

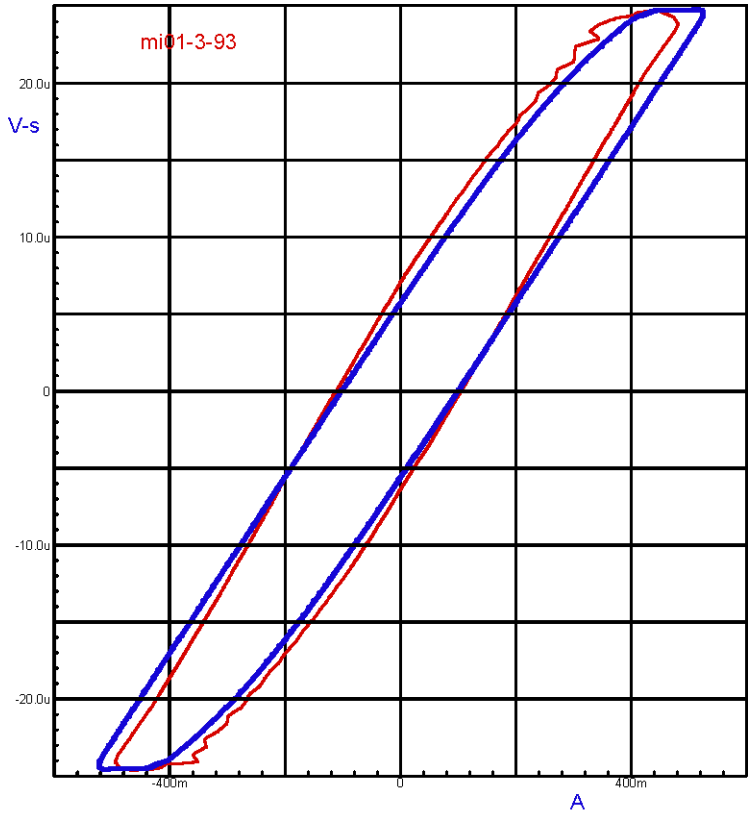

We can now see how the model performs with a different waveform. The file mi01-3-88 is loaded into the Excel Tool and calculated. This exports new data to the PWL files that the SPICE program access when run. Because the period is much shorter, the run time is reset. Also, the initial conditions on the inductors must be reset.

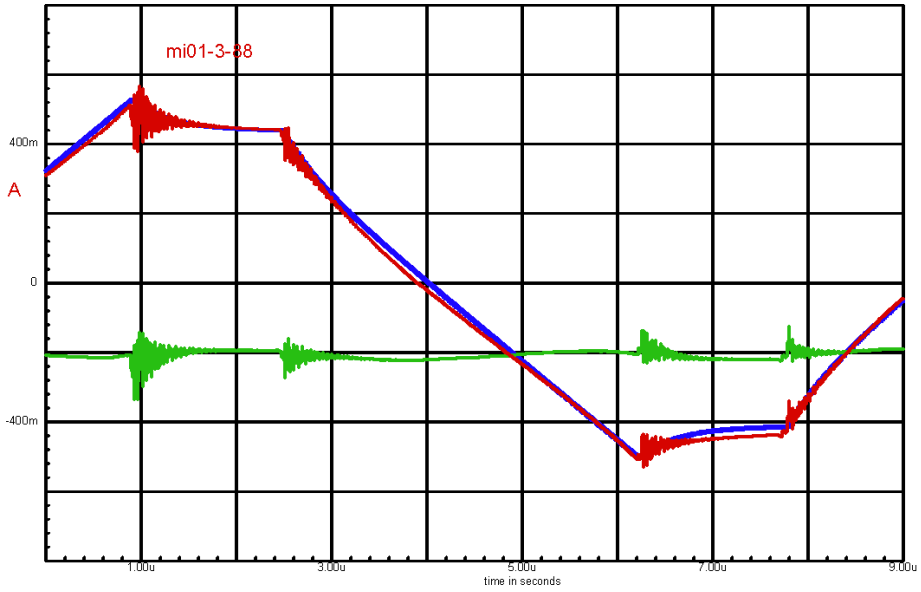

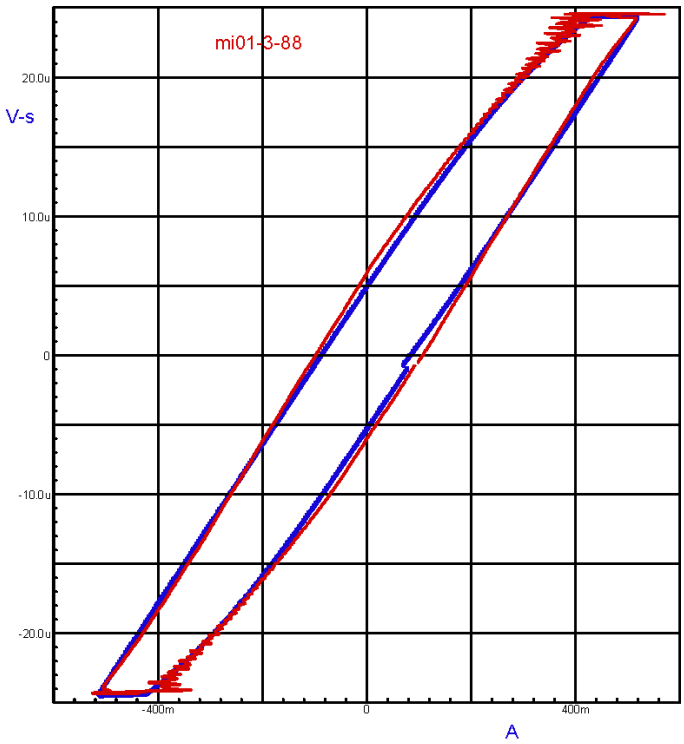

The slight mismatch at in the hysteresis loop of the model (blue) is because one of the initial condition currents is slightly off. That is the starting point of the loop.

We now repeat the procedure for the mi01-3-85 run. This one is interesting because the off-time is very short, of the order of the time constant of the current transient. Note that there are two very similar transients, at the start and at the end of the off-time, repeating at the next off-time.

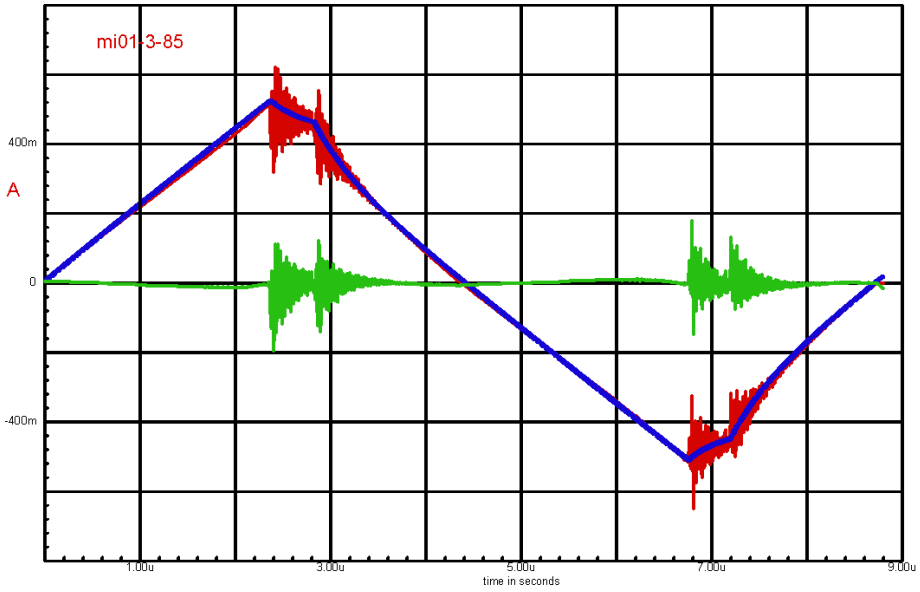

The hysteresis loops match reasonably well, though it is somewhat obscured by the noise in the current waveform.

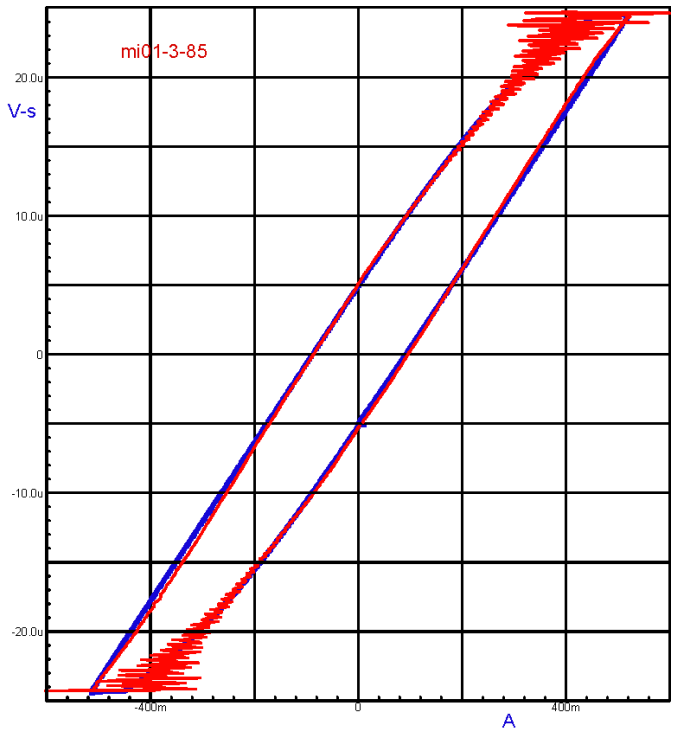

Finally, we use the model with the square-wave, mi01-039. Note that the same transients are present at the transitions, but the magnitude is twice as large. This is reasonable, as the change in voltage going directly from +V to –V is twice what it is goind from +V to 0, then 0 to –V.

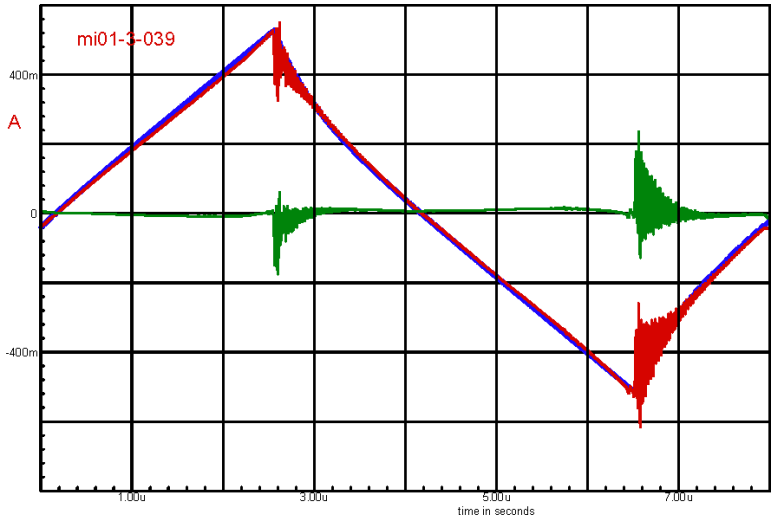

The hysteresis loop is still a reasonably good fit.

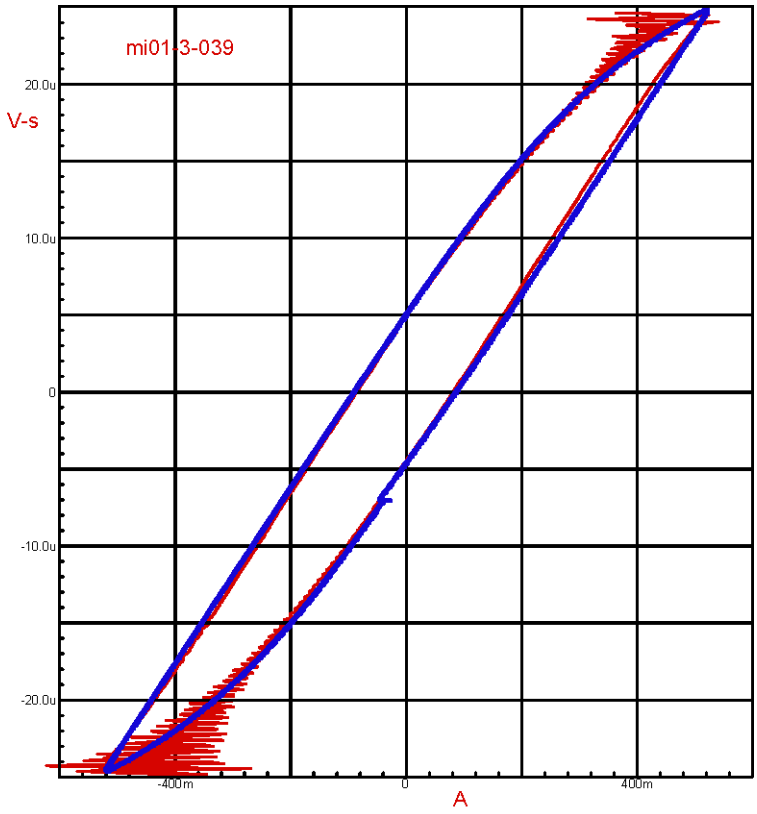

Before becoming too pleased with the model, it is worth stating that it performs less well with the hippo curve. With experience and rigor, I believe that a voltage waveform test protocol can be developed that will reveal the model component parameters in a fairly straightforward manner. Until that expertise is developed, perfecting the model is somewhat like playing "Whac-a-mole."

While not conclusive, this exercise is suggestive that an impedance model can model core losses quite well. The model of this example is quite simple, yet would be useful for hysteretic waveforms of varying off-time.

Test rig influences

A possible cause of the off-time phenomena is "test rig artifacts."

A close look at the data suggests that the test rig does influence core losses, but dismissing them as "test rig artifacts" misses the point that they may be present in practical circuits. Identifying the losses, understanding them and quantifying them may be important.

During the off-time and in part of the following excitation pulse, the current is flowing "backwards" and the core inductance is the power source. Anything that loads the core will reduce the current, and that is hypothesized to increase core losses in the following excitation pulse. This effect may be there whether there is an off-time or not.

One mode is identified both in Jonas Mühlethaler's paper [2] and in the Phase II report, impedance in the off-time current loop.

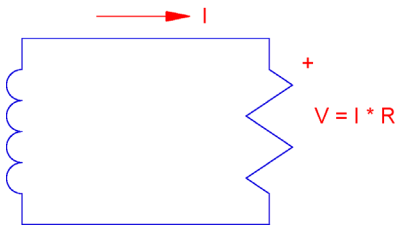

The voltage drop in the load resistance applies a voltage to the core and the resulting flux change and loss of energy is no surprise, though it may not have been given any attention.

If a component of that current I is reflected load current in a transformer, the effect may be greater, leading to increased core loss. Most regard load current as having an effect only on winding losses.

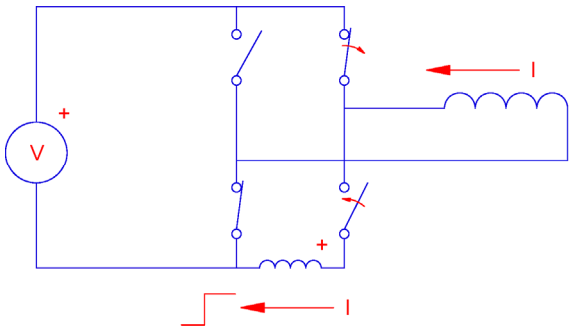

When the bridge switches, some branches of the circuit will see a step increase in current. If there is significant stray inductance, that inductor will be charged as a step function, and the energy to do so will come from the core, with losses.

If this happens, a voltage spike should be seen at the core. There is some suggestion of such a spike, but it is difficult to be sure that it is not noise.

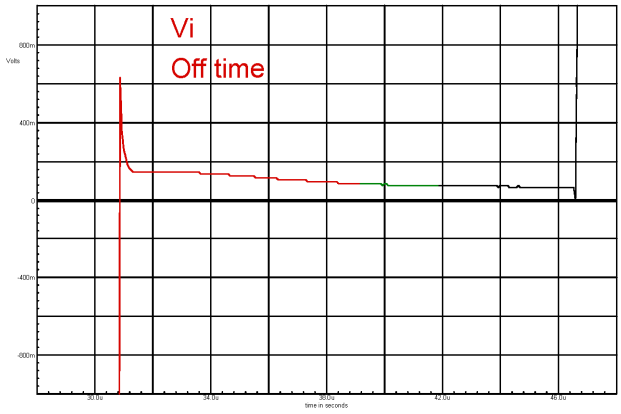

The gentle down-slope is probably decreasing I*R drop in the load resistance as the current decays.

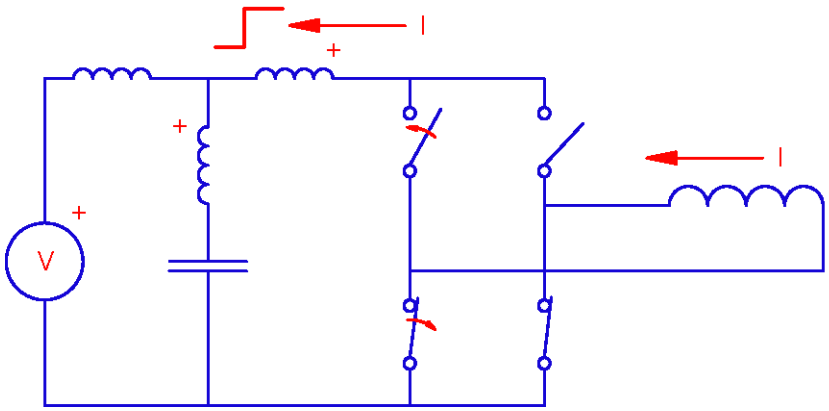

The same situation occurs when the bridge switches again to connect to the power source for the next excitation pulse. The stray inductance to the power source and the power source characteristics probably mean that it is effectively disconnected from the circuit at the first instant, but there will be a step change in current in any stray inductance in the circuitry that is switched in. The stray inductance of the decoupling capacitor and its leads may be particularly significant.

This is not an "off-time" loss, but it will occur on the leading edge of the excitation pulse, and the loss of energy may be significant.

Often when a bridge circuit is switched, dead-time is used to ensure that there is no punch-through current.

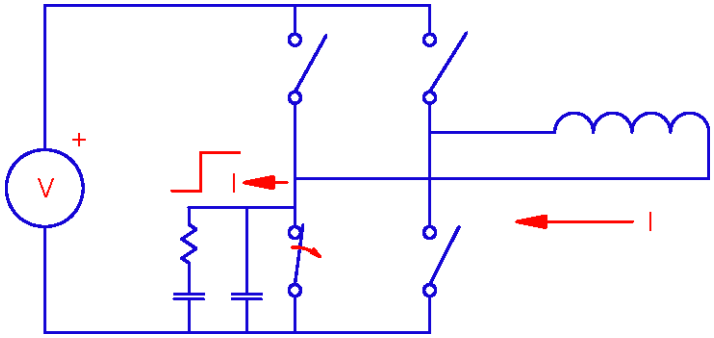

If the dead-time is excessive, the circuit is open momentarily. It's not really open, the winding is connected to the MOSFET that is turning off, a complicated scenario. It will be the source of the energy that charges the drain source capacitor. If there are snubbers, it is worse, as they are designed to absorb energy when the switch opens.

The effects may combine to explain much of the off-time loss phenomenon. A question would be the time constant, which is much longer than would be expected from switching effects.

These losses could be much more significant in a poorly designed power converter, particularly as frequencies increase, so they should be understood and quantified.

Appendix F–Expand data

When a sequence of energy per cycle is plotted for expanded waveforms having increasing off time, in many cases the energy per cycle increases as the off-time increases. Although the Phase II Report states that run sets always include a square wave, in the sequences as logged in the expanded waveform data, the comparable square wave base line is missing. That data has to be found elsewhere and appended at the top of the column to make the graph in Excel.

The figure below shows the expand on-time and voltages to scale as the x axis and y axis, respectively. The flux in µV-s is shown.

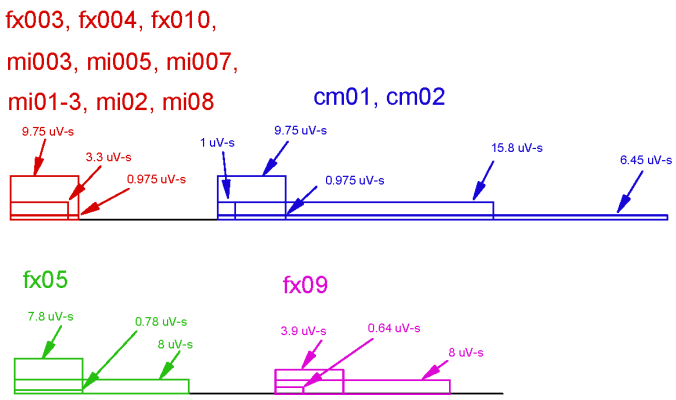

There are no sequences that allow exploring waveforms of varying voltage and time with constant flux, as in a buck converter. Only one is close, 7.8 µV-s and 8 µV-s for the fx05 E-core.

There is no expand data for the amorphous iron core, pt01.

The graphs below show run sets, the first being identified as "3" in the data table. Care must be used in identifying the run sets. Although it is stated that expand runs with the same numeric designator are the same, significant differences were found and they had to be segregated. The graph below shows the run sets that have consistent voltage and timing.

Most of the cores have 5 turns. The fx003 core has 3 turns and the fx004 core has 4 turns.

3.9 us on time, 2.5 V/turn.

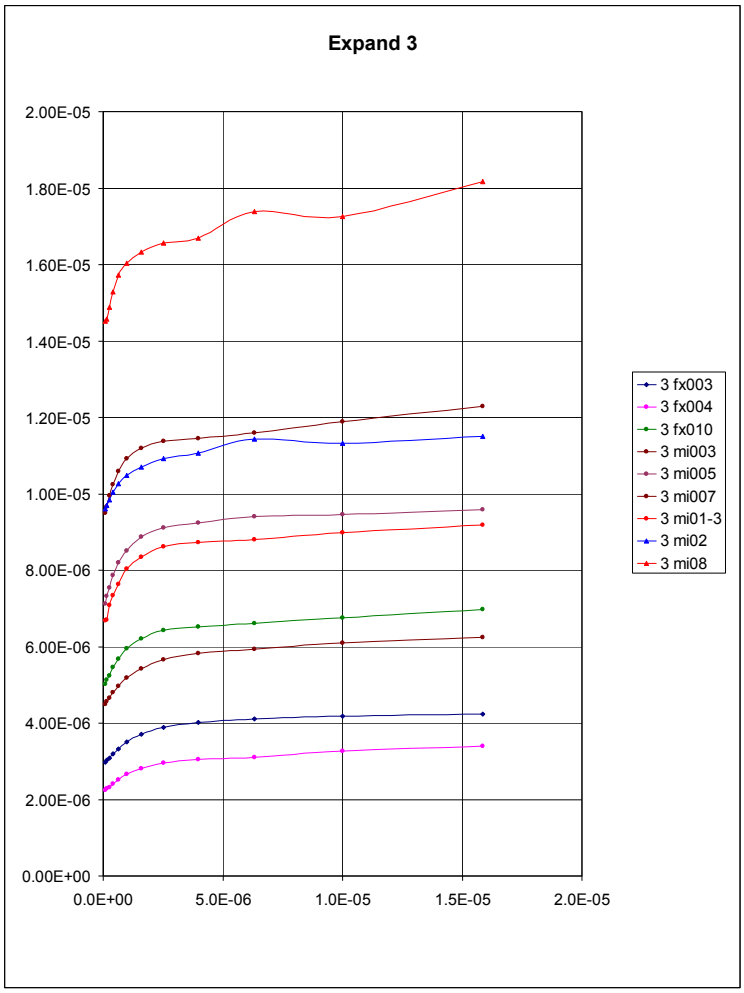

3.3 us on time, 1 V/turn

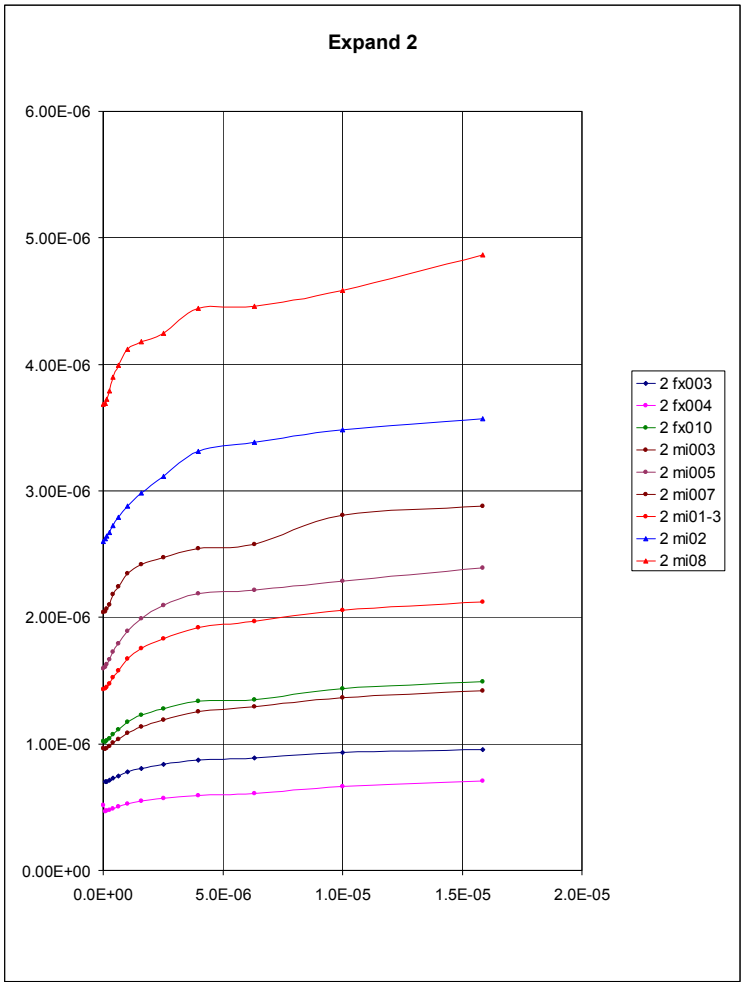

3.9 us on time, 0.25 V/turn.

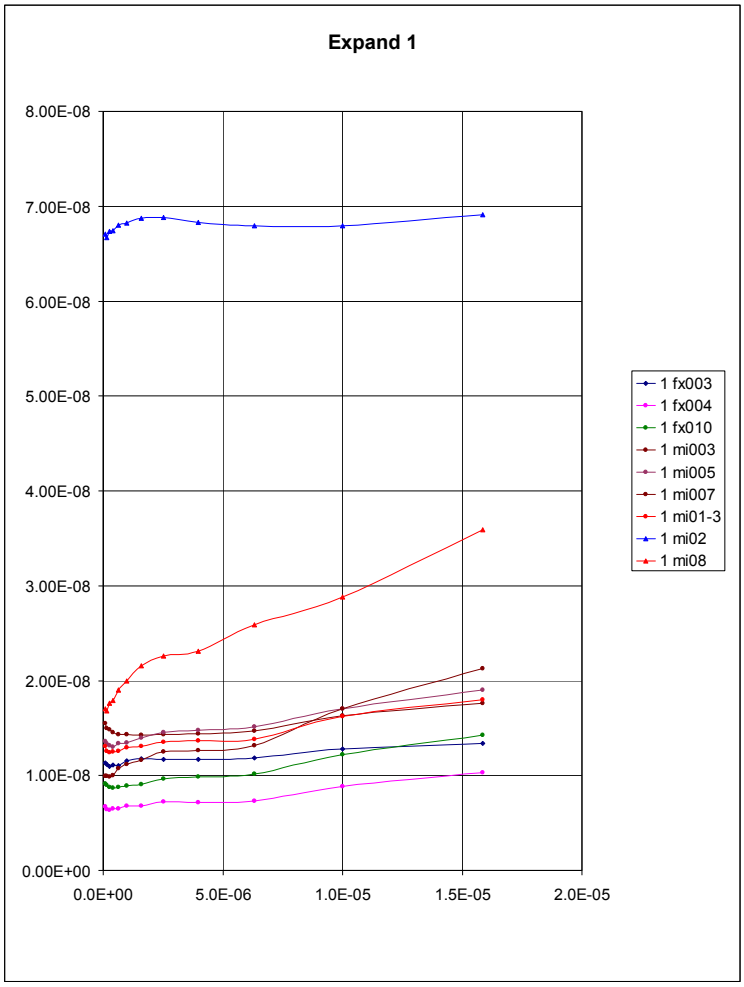

There is no explanation for the mi02 curve having higher losses. It is possible thtat it was at a lower temperature.

The data for the Ceramic Magnetics cores Cm01 and Cm02 have different protocols, and were tested with a greater variety of waveforms. The linear plots are shown separately, as an attempt to plot them on one graph had five pairs so much smaller that they hugged the bottom of the graph.

15.8 us on time, 1 V/turn. The cm01 core has 4 turns, the cm02 core has 5 turns.

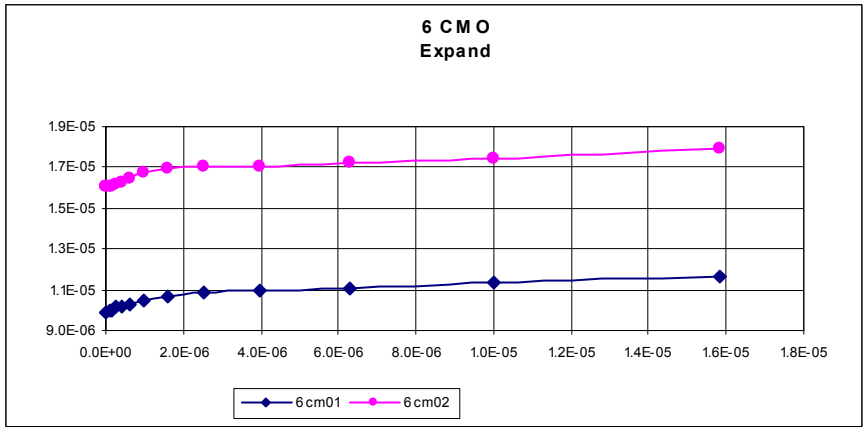

3.9 us on time, 2.5 V/turn.

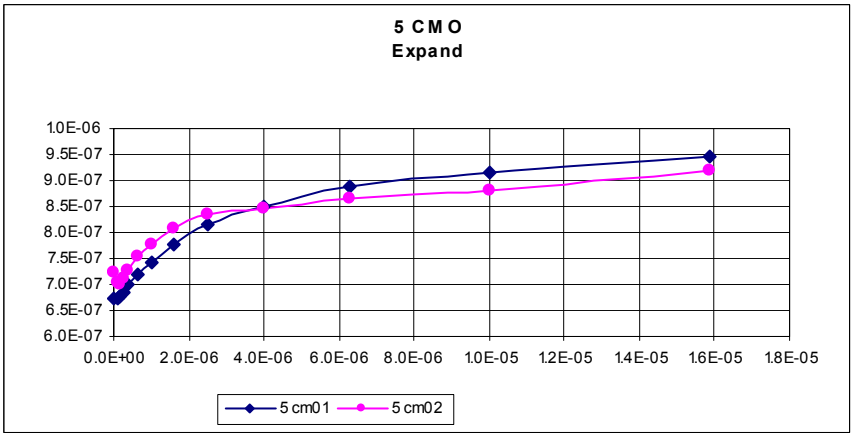

1 us on time, 1 V/turn

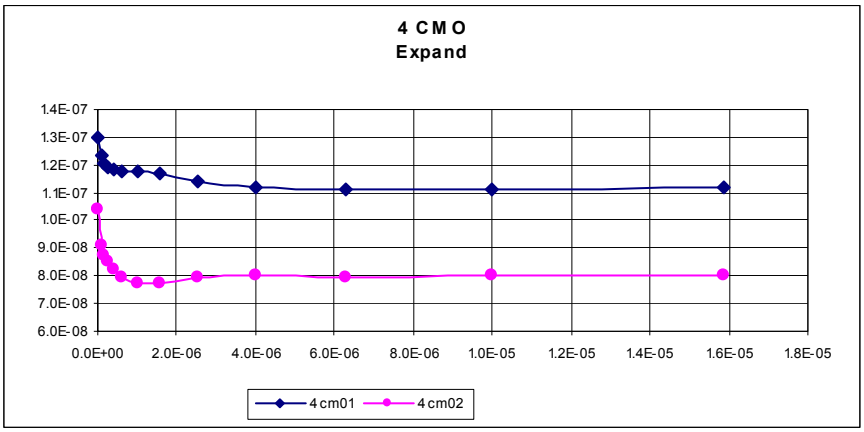

25.8 us on time, 0.25 V/turn

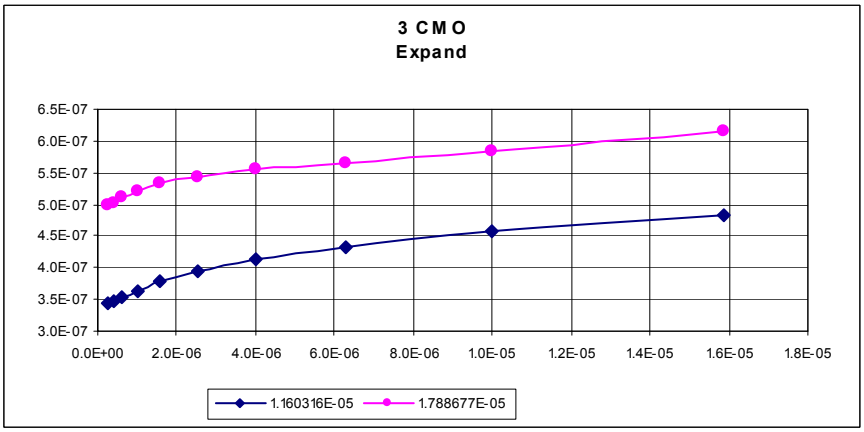

3.9 us on time, 0.25 V/turn

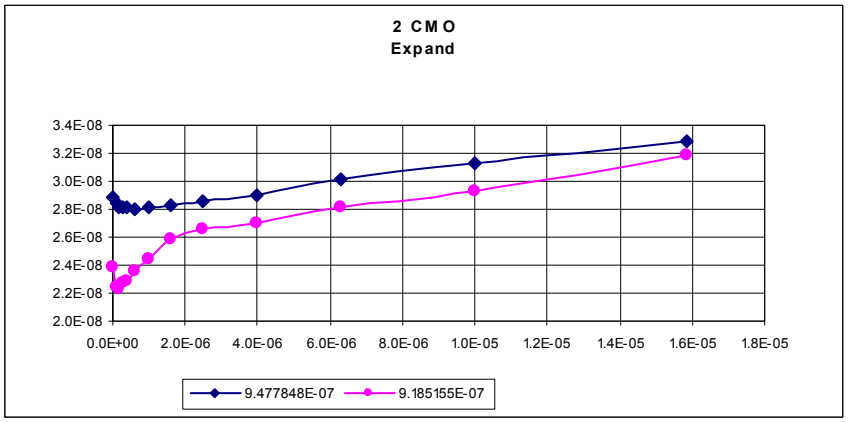

1 us on time, 0.25 V/turn.

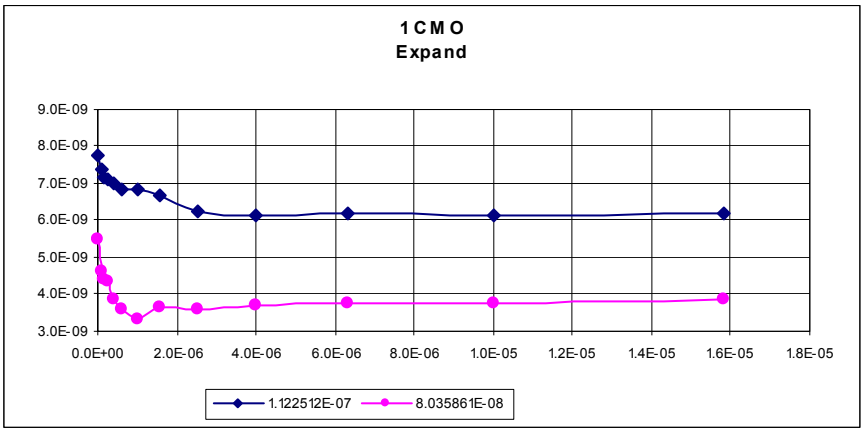

The six pairs can be shown on one log-log plot. Note that only the higher power curves show increased loss with increased off-time. Because 0 does not have a valid log function, the off-time of the square wave baseline was set to 10^{-7}.

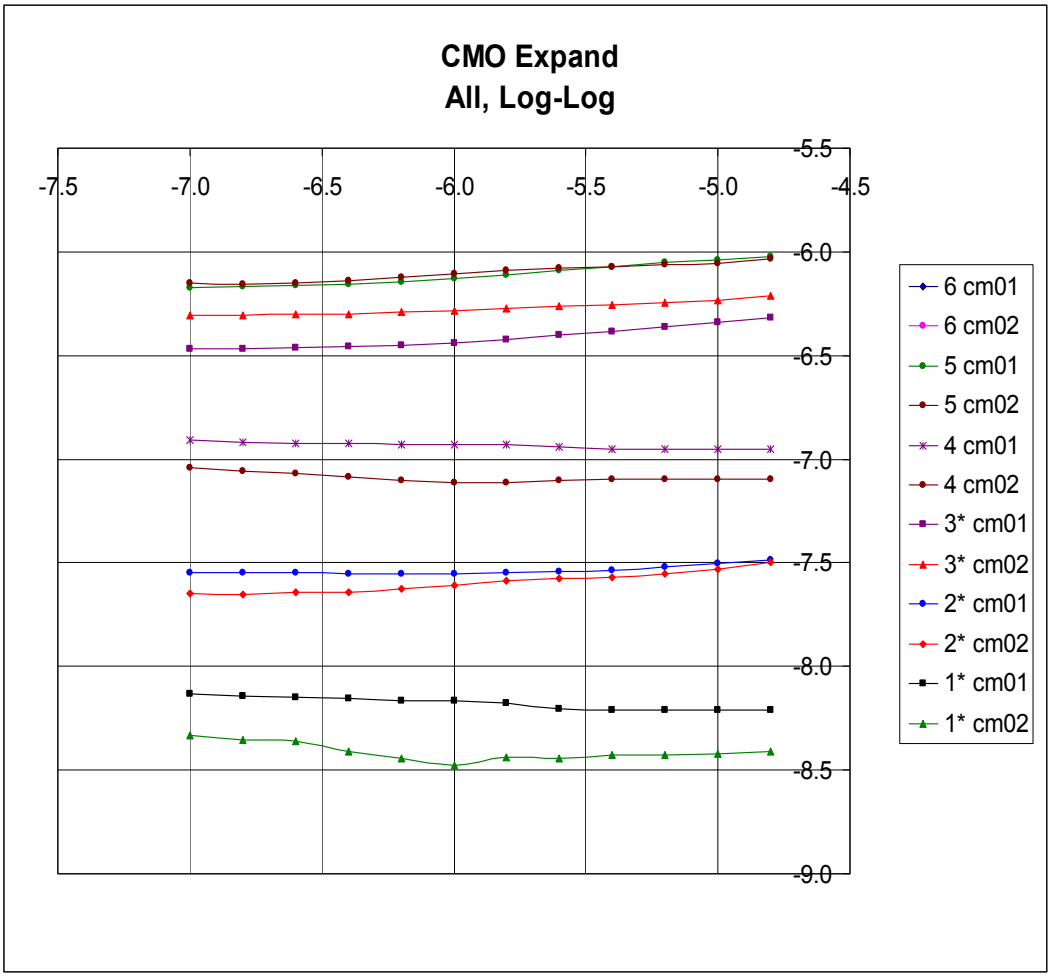

The on times and voltages can be found by reference to the headings of the previous graphs, matching numeric prefixes.

Expand data for the drilled core, mi11-1-xxx.

15 us on time, 4 V/turn (4 turns)

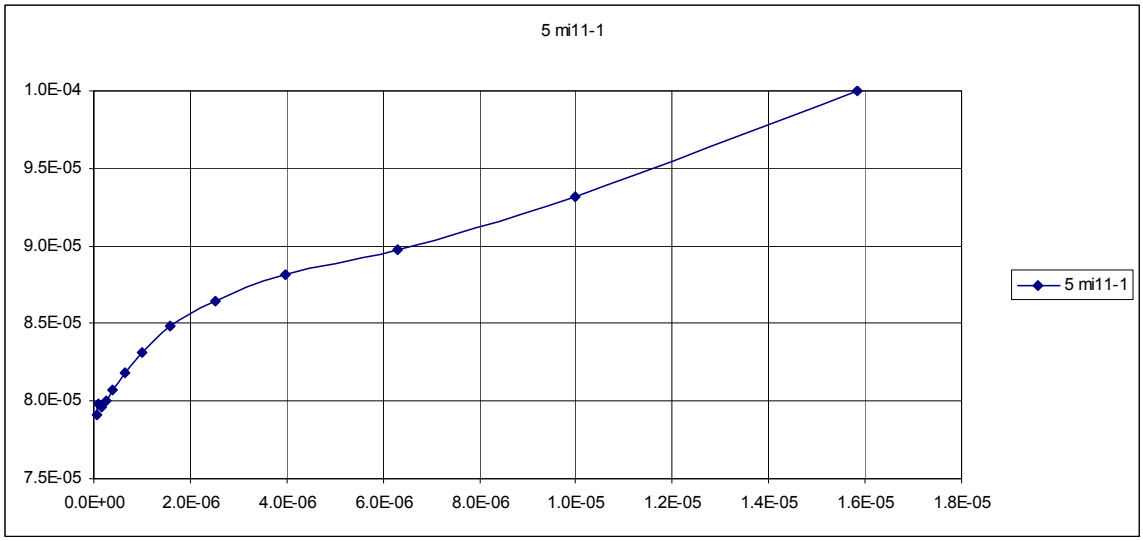

39.9 us on time, 1 V/turn.

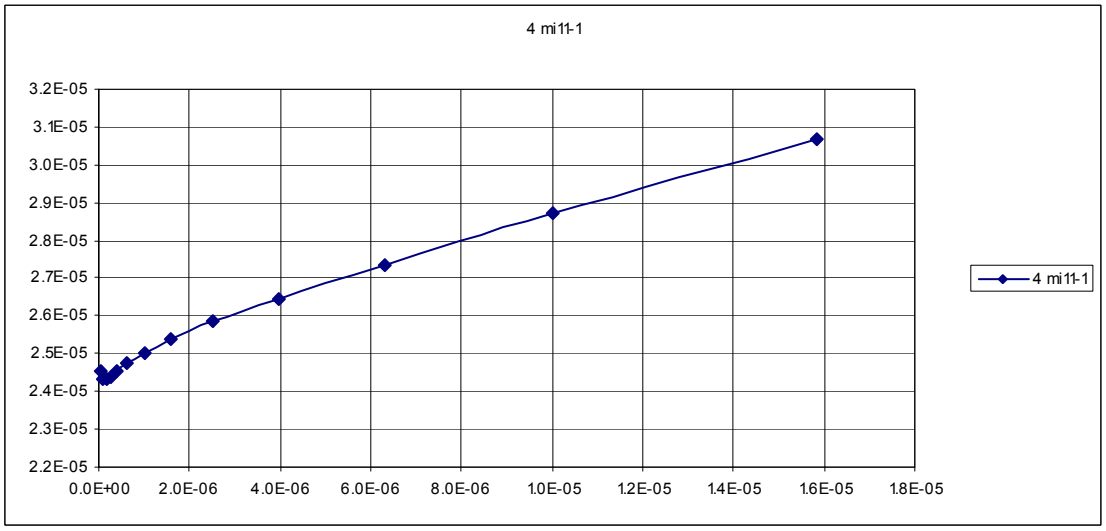

Only the two highest power curves for the drilled cores are shown with linear plots above, but all 5 run sets are shown on the log-log plot below.

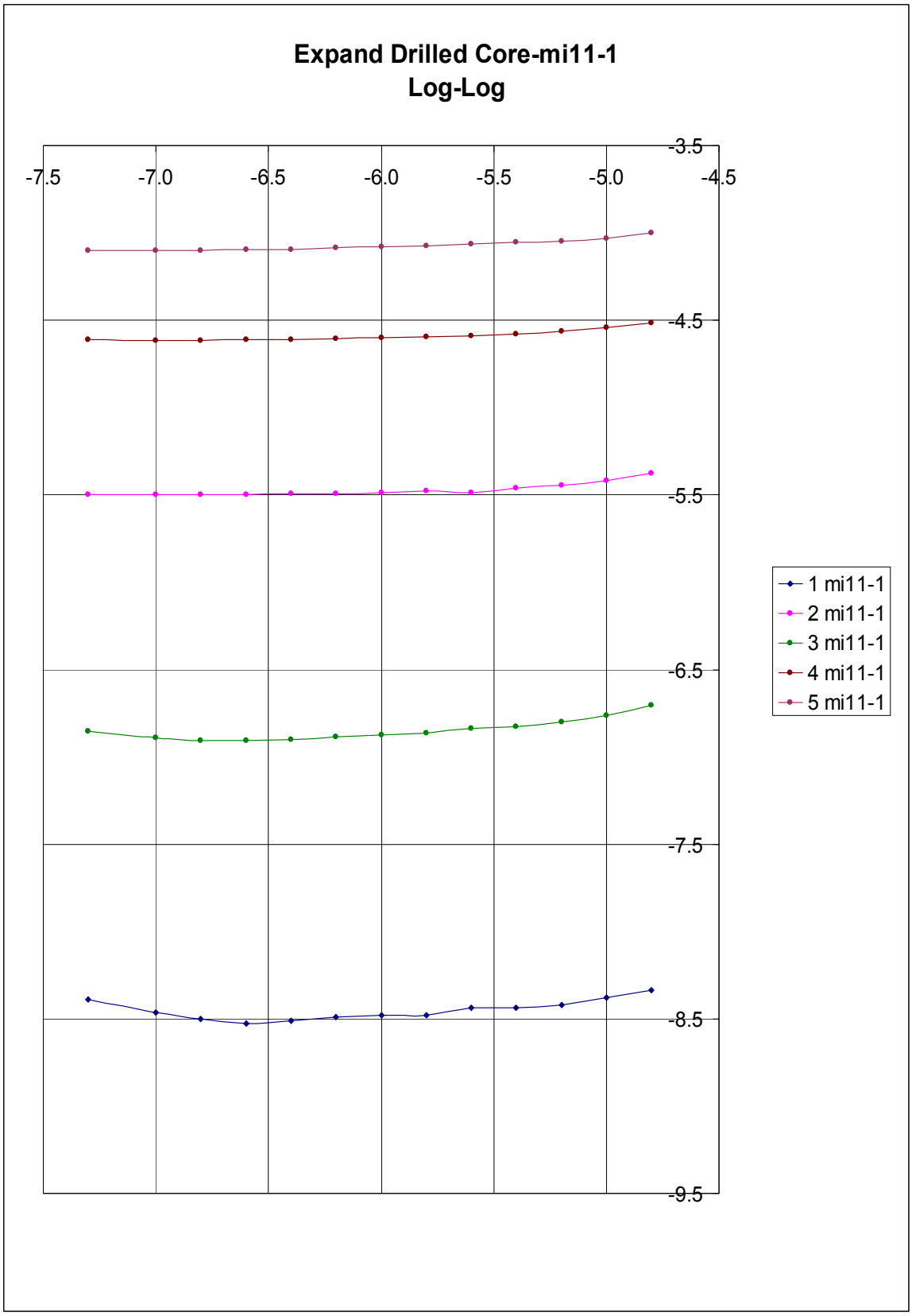
Expand Drilled Core-mi11-1
Log-Log
-7.5
-7.0
-6.5
-6.0
-5.5
-5.0
-4.5
-3.5
-4.5
-5.5
-6.5
-7.5
-8.5
-9.5
1 mi11-1
2 mi11-1
3 mi11-1
4 mi11-1
5 mi11-1

Expand data for the E core, fx05

The data for this E-core is shown separately, as the excitation is different. The fx05 E-core has 6 turns.

The excitations are:

3 fx05, 3.9 us on time, 2 V/turn
2 fx05, 10 us on time, 0.8 V/turn
1 fx05, 3.9 us on time, 0.2 V/turn

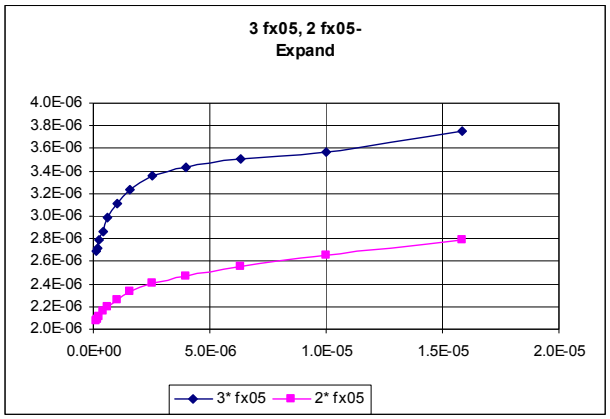

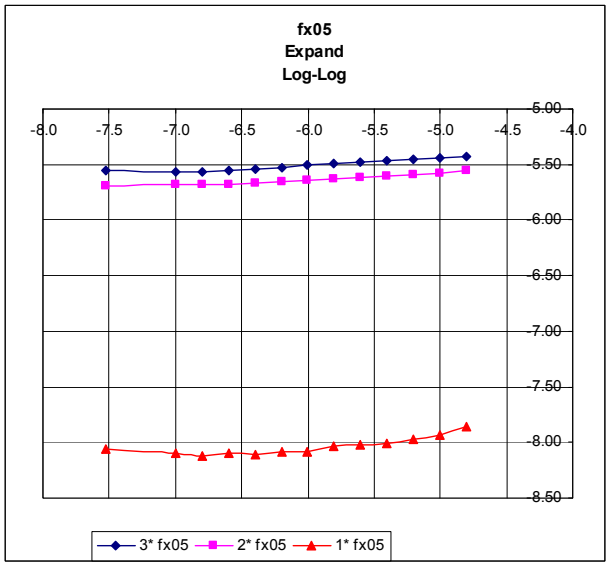

Expanded data for E-core, fx09

The data for this E-core is shown separately, as the excitation is different. The fx09 E-core has 5 turns.

The excitations are:

3 fx09, 1.6 us on time, 0.4 V/turn
2 fx09, 10 us on time, 0.8 V/turn
1 fx05, 3.9 us on time, 1.4 V/turn

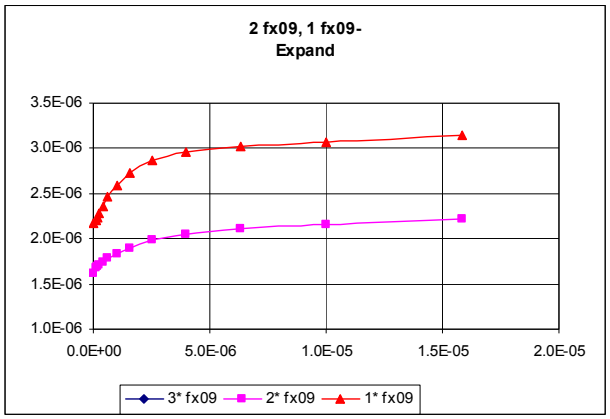

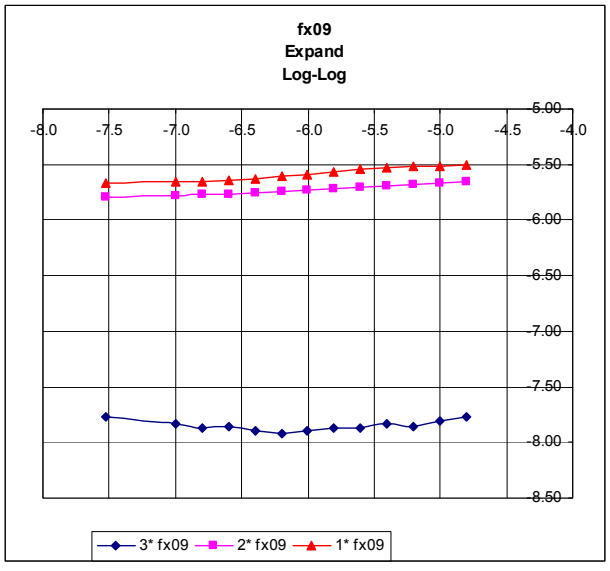

Unlike the other expand series, run 3 has the lowest power.

Powdered iron core

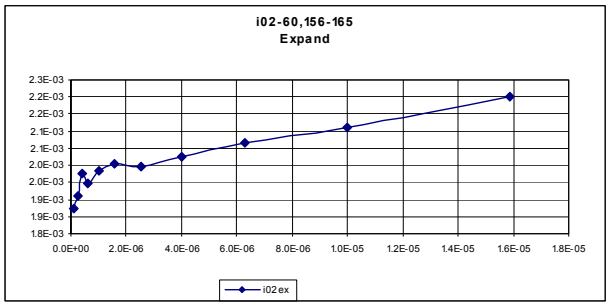

The off-tine loss effect is lower in powdered iron cores, but still significant at higher excitation levels.

Appendix G–Hippo data

The Hippo waveform is characterized by a pulse of one polarity immediately followed by an equal pulse of the opposite polarity.

mi01-3-110

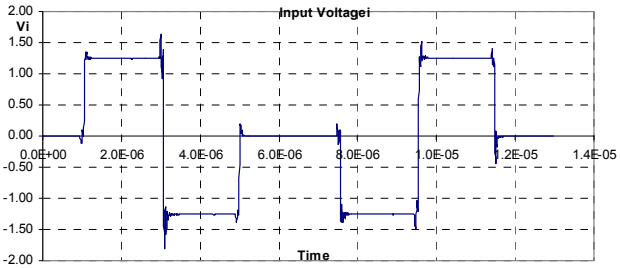

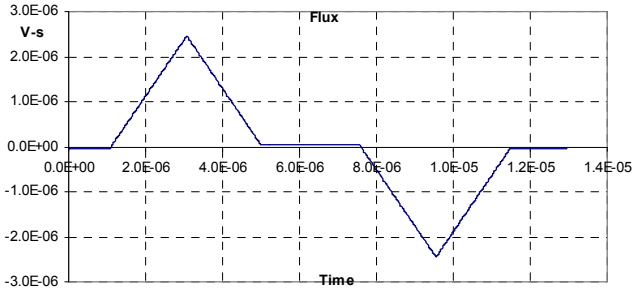

The concept is to reduce the input current to 0, so that there is no energy carried forward as $E = \frac{1}{2} I^2 L$.

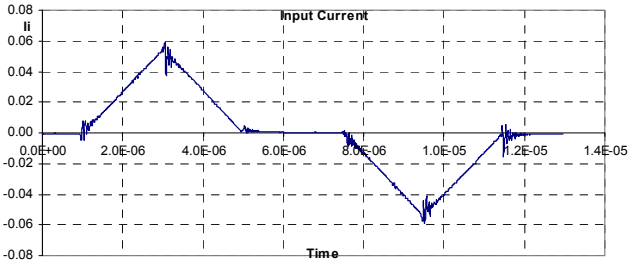

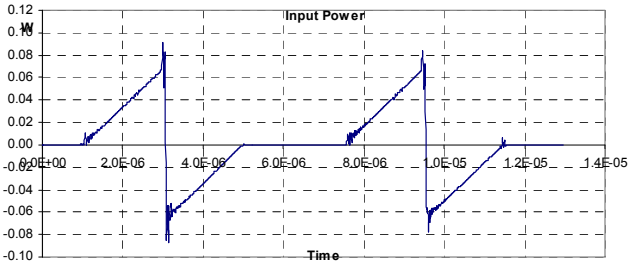

When a sequence of energy per cycle is plotted for hippo waveforms having increasing off time, it appears as if the energy per cycle decreases as the off-time increases. Although the Phase II Report states that run sets always include a square wave, in the sequences as logged in the hippo waveform data, the comparable square wave base line is missing. That data has to be found elsewhere and appended at the top of the column to make the graph in Excel.

The graphs below show run sets, the first being identified as "3" in the data table. Care must be used in identifying the run sets. Although it is stated that hippo runs sets with the same numeric designator are the same, significant differences were found and they hav to be segregated. The graph below shows the run sets that have consistent voltage and timing.

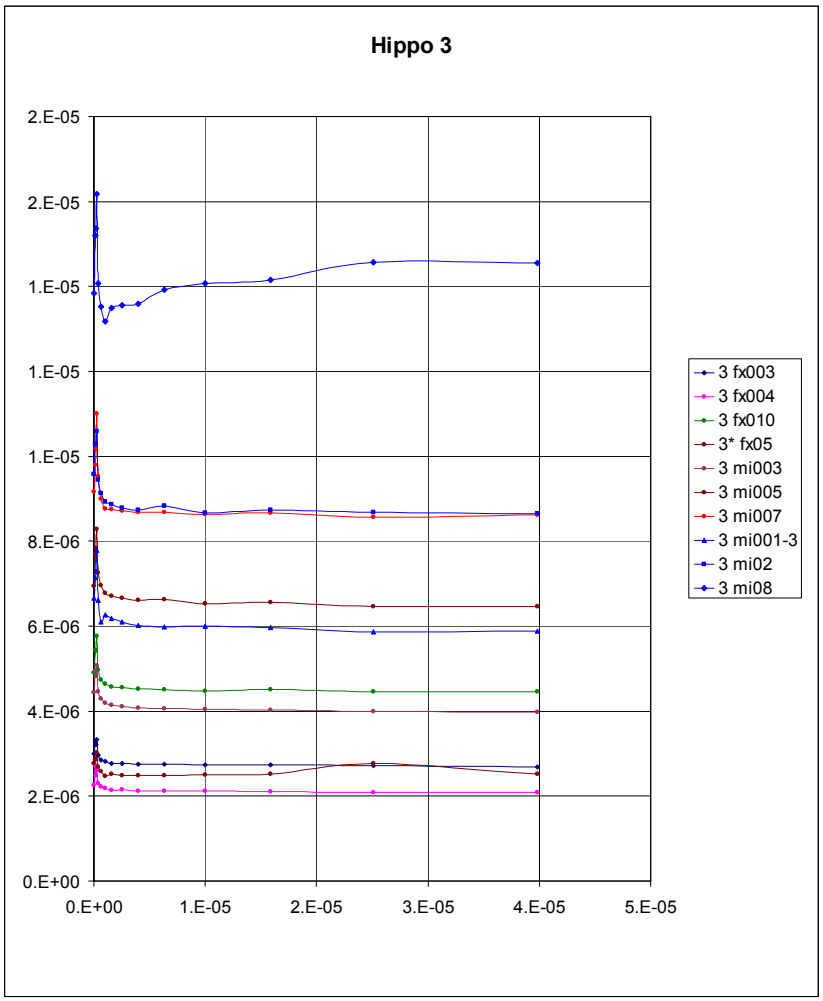

However, if the x axis is expanded, it can be seen that the energy per cycle starts low, then increases in the next few pulses before settling out at about the same value as the baseline square wave energy per cycle.

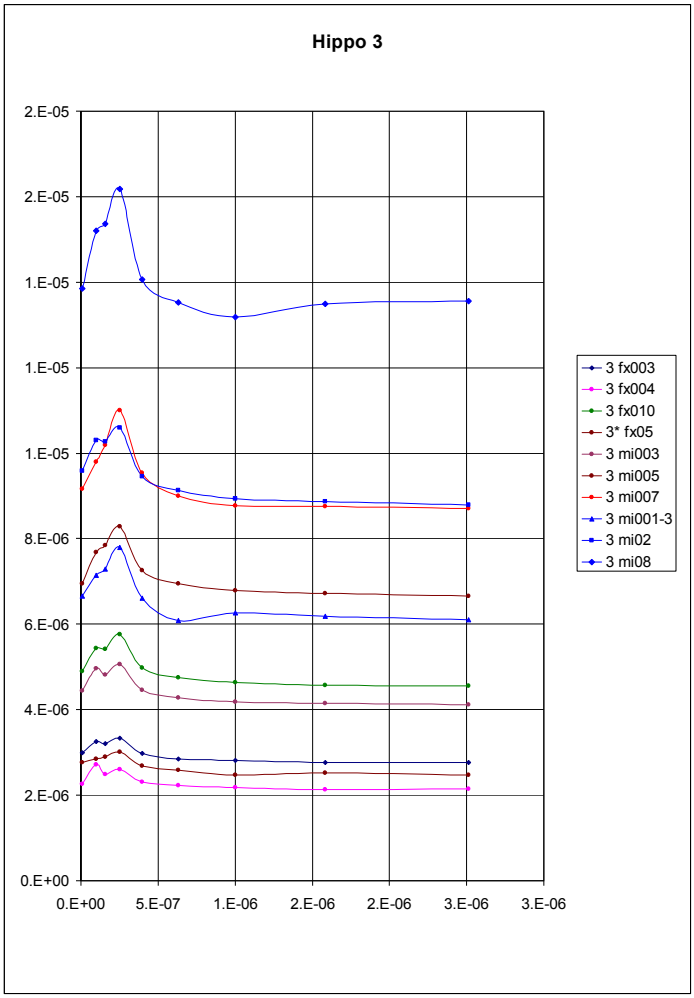

Inspection of the square wave baseline and the first four hippo pulses shows why this is so. The first three hippo pulses lack an off-time, so they are actually increasingly fat square-waves. It is only on the fourth pulse that a true hippo waveform is evident.

Below are the data blocks for the square wave base line and the first four hippo pulses as well as the corresponding voltage waveform graphs from the Excel Tool.

fx004 Square wave baseline

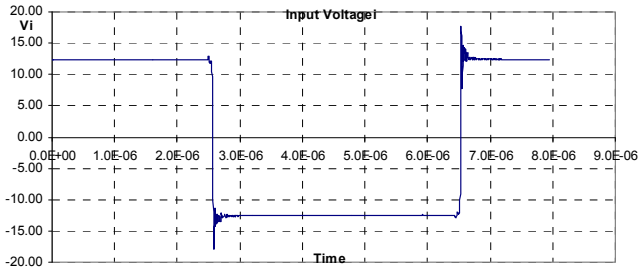

3 fx004 Hippo #1

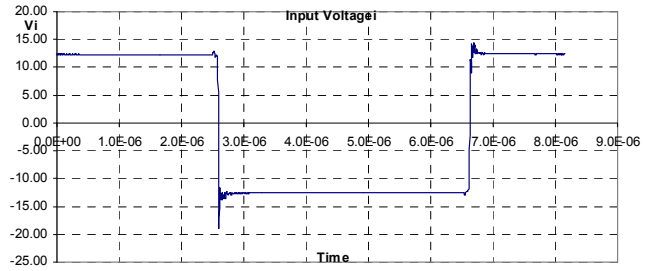

3 fx004 Hippo #2

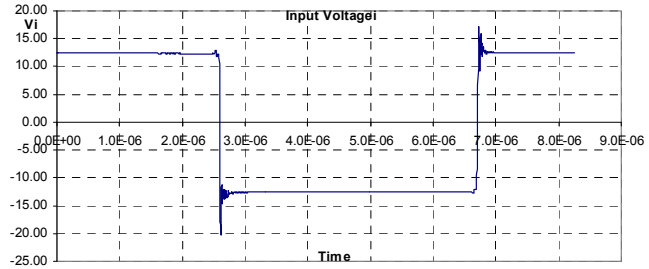

3 fx004 Hippo #3

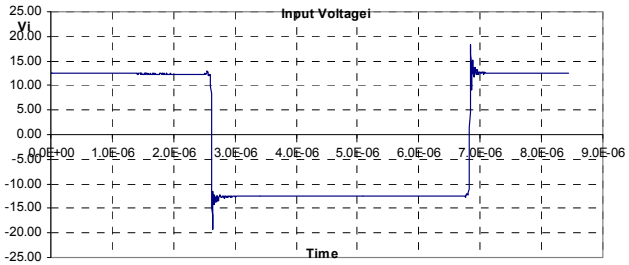

3 fx004 Hippo #4

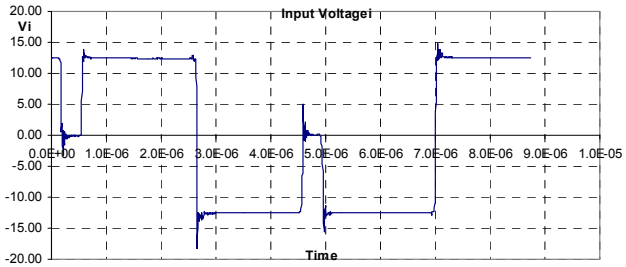

This anomaly is noted is noted in the Phase II Report, but the above presentation notes it more clearly.

In the hippo sequences that follow, the first three pulses of the hippo sequence are deleted. The first pulse is the square wave baseline.

If there is any energy reduction, it is slight and inconsistent. The conclusion is that for the hippo waveforms, the length of the off time does not affect the core loss per cycle, as expected.

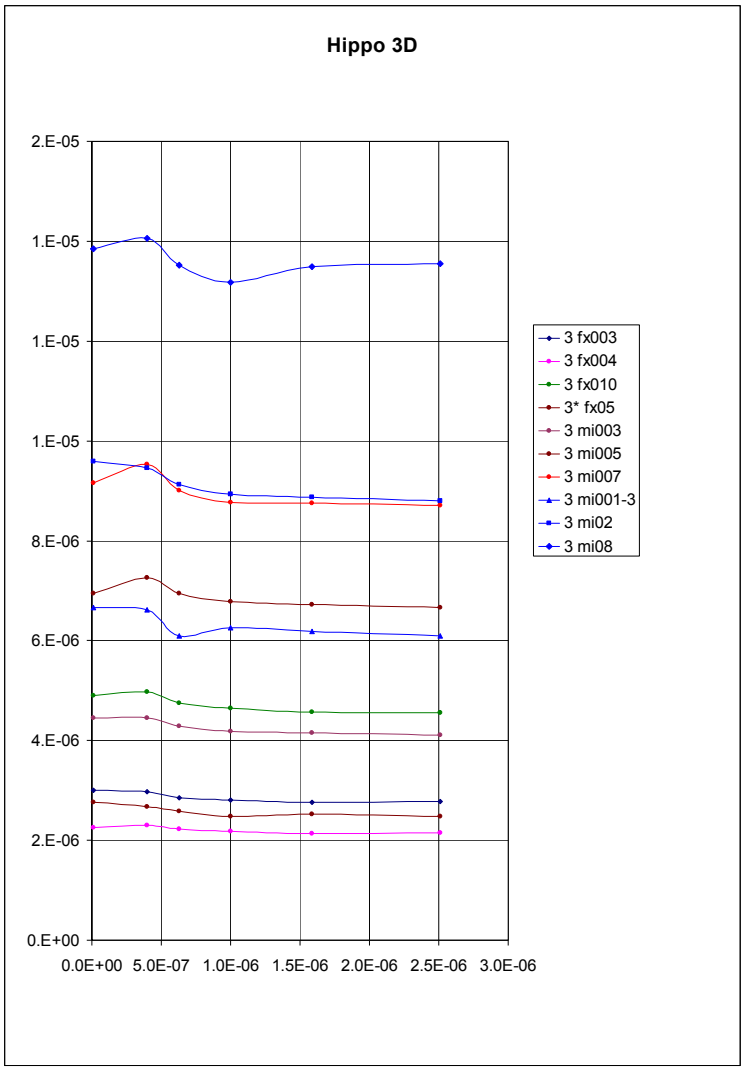

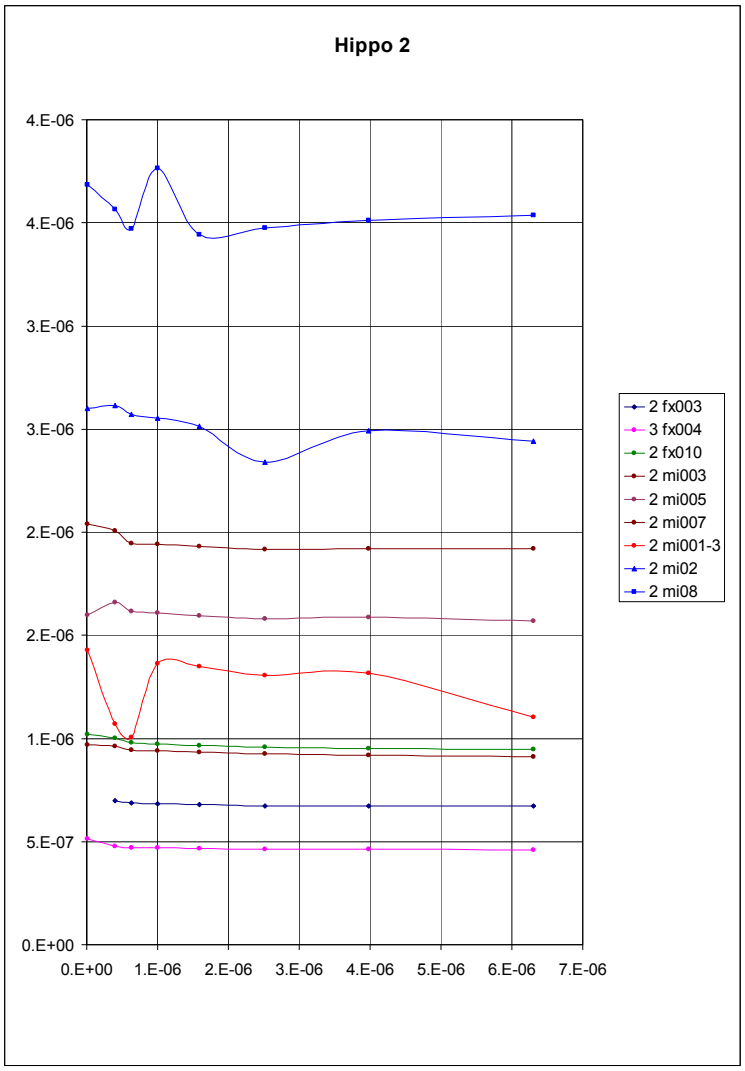
Hippo 2
4.E-06
4.E-06
3.E-06
3.E-06
2.E-06
2.E-06
1.E-06
5.E-07
0.E+00
0.E+00
1.E-06
2.E-06
3.E-06
4.E-06
5.E-06
6.E-06
7.E-06
2 fx003
3 fx004
2 fx010
2 mi003
2 mi005
2 mi007
2 mi001-3
2 mi02
2 mi08

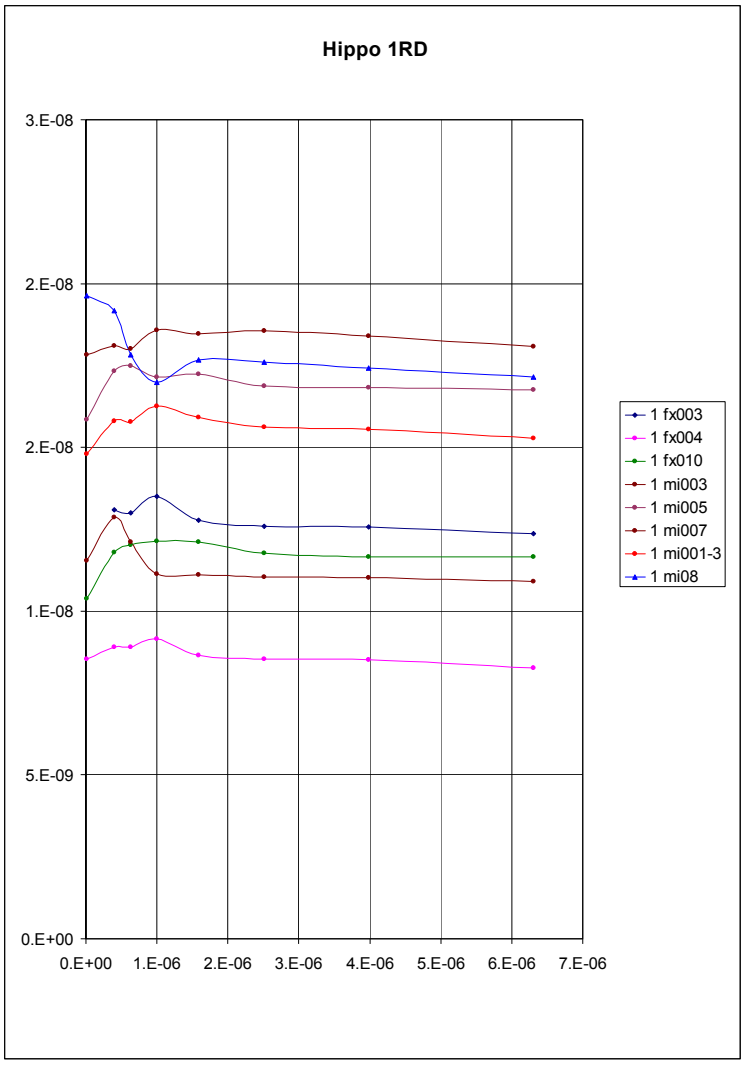
Hippo 1RD
3.E-08
2.E-08
2.E-08
1.E-08
5.E-09
0.E+00
0.E+00
1.E-06
2.E-06
3.E-06
4.E-06
5.E-06
6.E-06
7.E-06
1 fx003
1 fx004
1 fx010
1 mi003
1 mi005
1 mi007
1 mi001-3
1 mi08

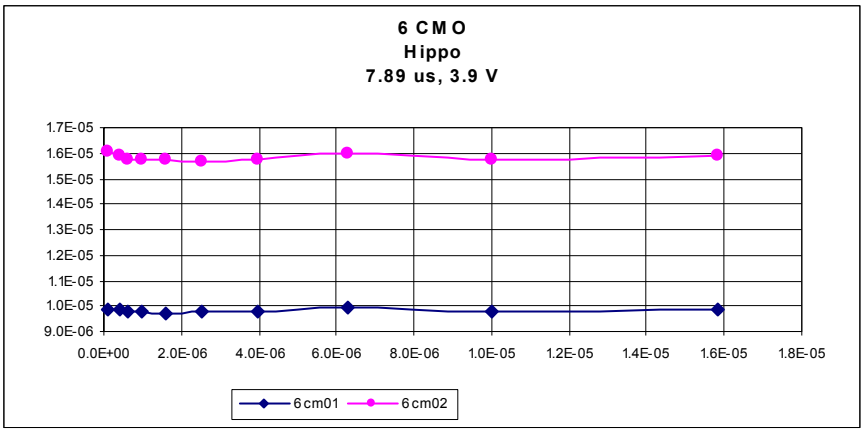
6 CMO
Hippo
7.89 us, 3.9 V
1.7E-05
1.6E-05
1.5E-05
1.4E-05
1.3E-05
1.2E-05
1.1E-05
1.0E-05
9.0E-06
0.0E+00
2.0E-06
4.0E-06
6.0E-06
8.0E-06
1.0E-05
1.2E-05
1.4E-05
1.6E-05
1.8E-05
6 cm01
6 cm02

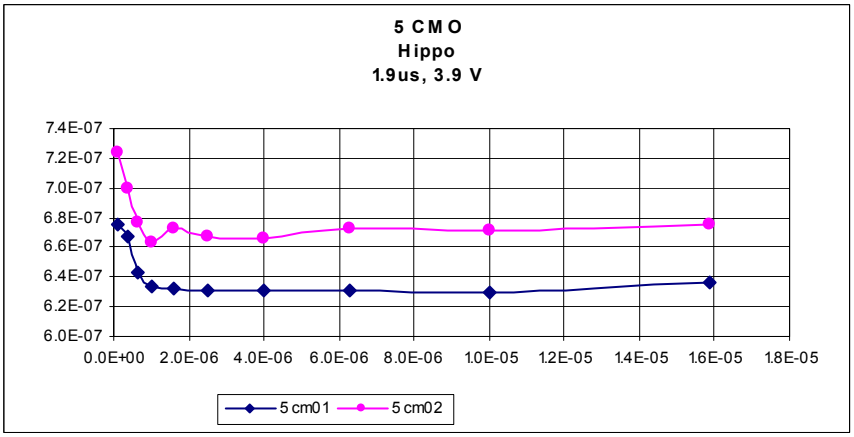
5 CMO
Hippo
1.9us, 3.9 V
7.4E-07
7.2E-07
7.0E-07
6.8E-07
6.6E-07
6.4E-07
6.2E-07
6.0E-07
0.0E+00
2.0E-06
4.0E-06
6.0E-06
8.0E-06
1.0E-05
1.2E-05
1.4E-05
1.6E-05
1.8E-05
5 cm01
5 cm02

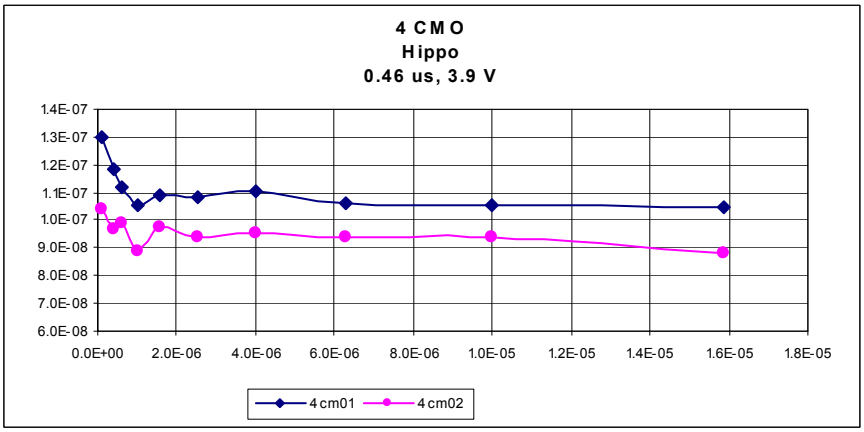
4 CMO
Hippo
0.46 us, 3.9 V
1.4E-07
1.3E-07
1.2E-07
1.1E-07
1.0E-07
9.0E-08
8.0E-08
7.0E-08
6.0E-08
0.0E+00
2.0E-06
4.0E-06
6.0E-06
8.0E-06
1.0E-05
1.2E-05
1.4E-05
1.6E-05
1.8E-05
4 cm01
4 cm02

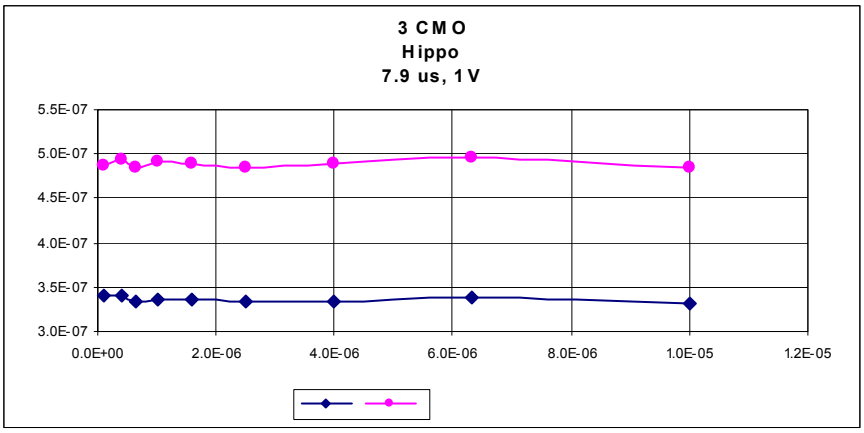
3 CMO
Hippo
7.9 us, 1 V
5.5E-07
5.0E-07
4.5E-07
4.0E-07
3.5E-07
3.0E-07
0.0E+00
2.0E-06
4.0E-06
6.0E-06
8.0E-06
1.0E-05
1.2E-05

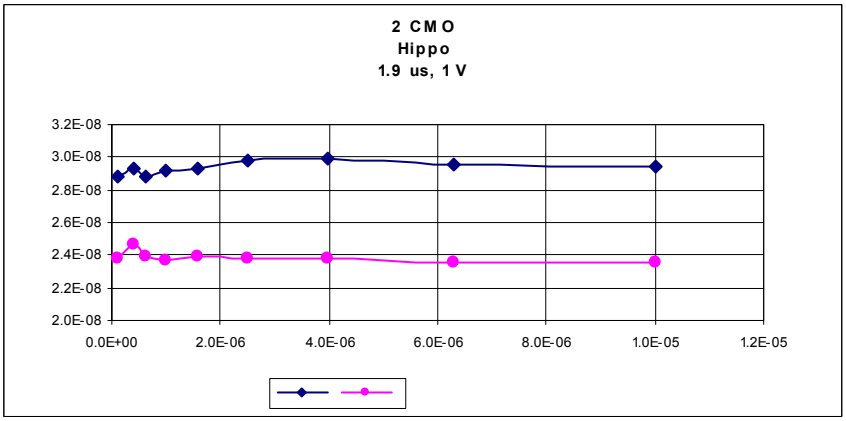
2 CMO
Hippo
1.9 us, 1 V
3.2E-08
3.0E-08
2.8E-08
2.6E-08
2.4E-08
2.2E-08
2.0E-08
0.0E+00
2.0E-06
4.0E-06
6.0E-06
8.0E-06
1.0E-05
1.2E-05

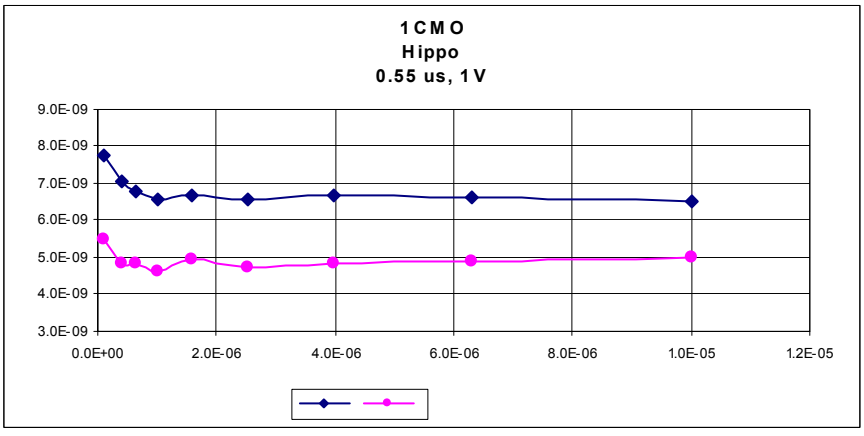
1 CMO
Hippo
0.55 us, 1 V
9.0E-09
8.0E-09
7.0E-09
6.0E-09
5.0E-09
4.0E-09
3.0E-09
0.0E+00
2.0E-06
4.0E-06
6.0E-06
8.0E-06
1.0E-05
1.2E-05

To view all the data for the cm01 and cm02 cores on one plot, I made a Log-log graph. Since 0 does not have a valid log, I set the square wave to have an off time of 10^{-7}.

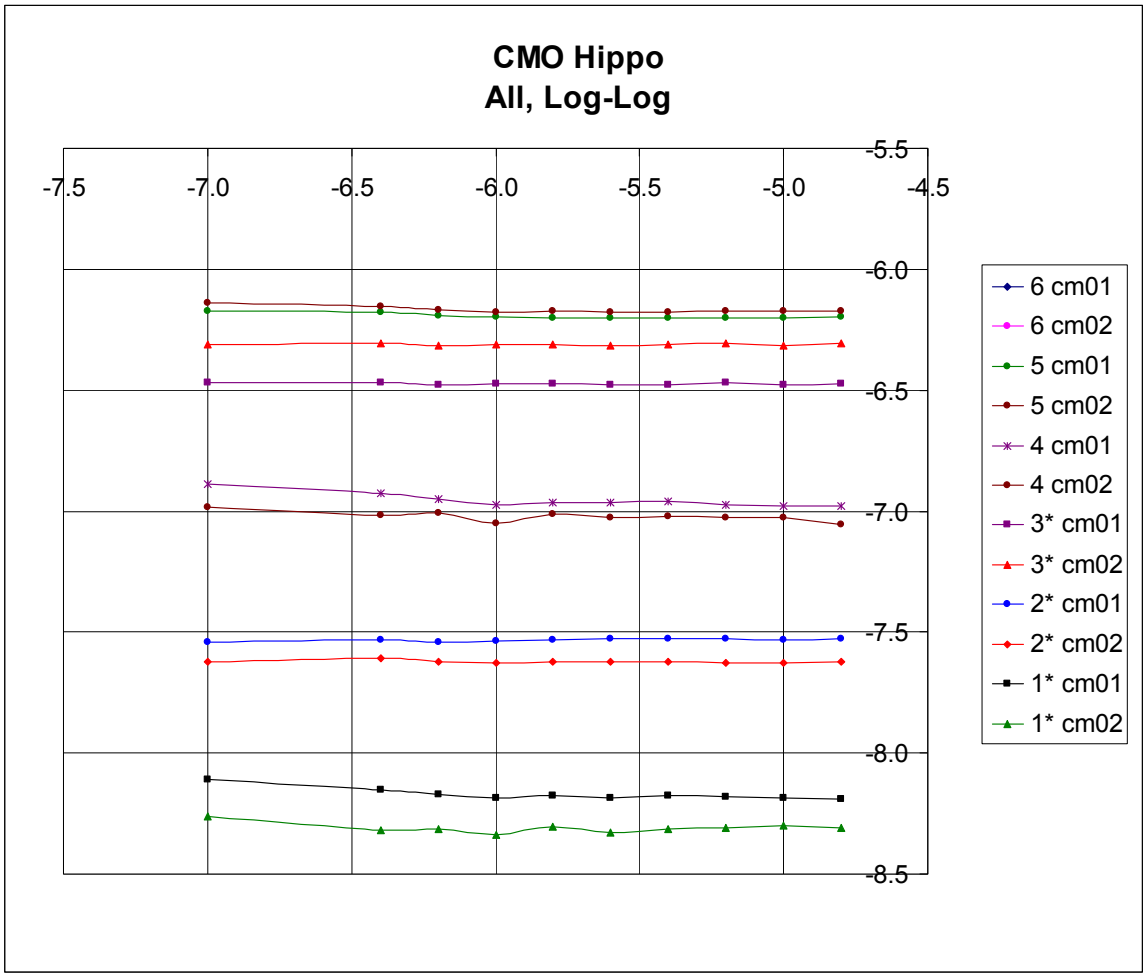

Appendix H
Drilled core data

One hypothesis for the off time loss was that the flux in the core might change state after the excitation is removed. With approximately zero nominal volts, the total flux would not be expected to change significantly, but the flux could migrate within the core from one region to another. The drilled core experiments showed that this hypothesis is not substantiated.

To test this hypothesis, a core was drilled through so that test windings could be inserted. Originally, it was planned to drill four holes from each direction (side to side and outside to inside).

A scheme was developed to allow intersecting wires to make an internal connection. If implemented, flux change (voltage) of any of 25 cross-sectional areas could be isolated.

Two more diagonal holes were planned from the outside, meeting within the core, to see if there was a helical component to the flux.

A vendor had promised to supply the drilled core for test, but was unable to perform, so John Harris had to make arrangements himself. Drilling proved to be much more difficult that thought, so the compromise was to drill two holes from each direction and not to drill the diagonal holes.

Time and budget constraints also prevented taking data with intersecting wires.

Drilled core test sets

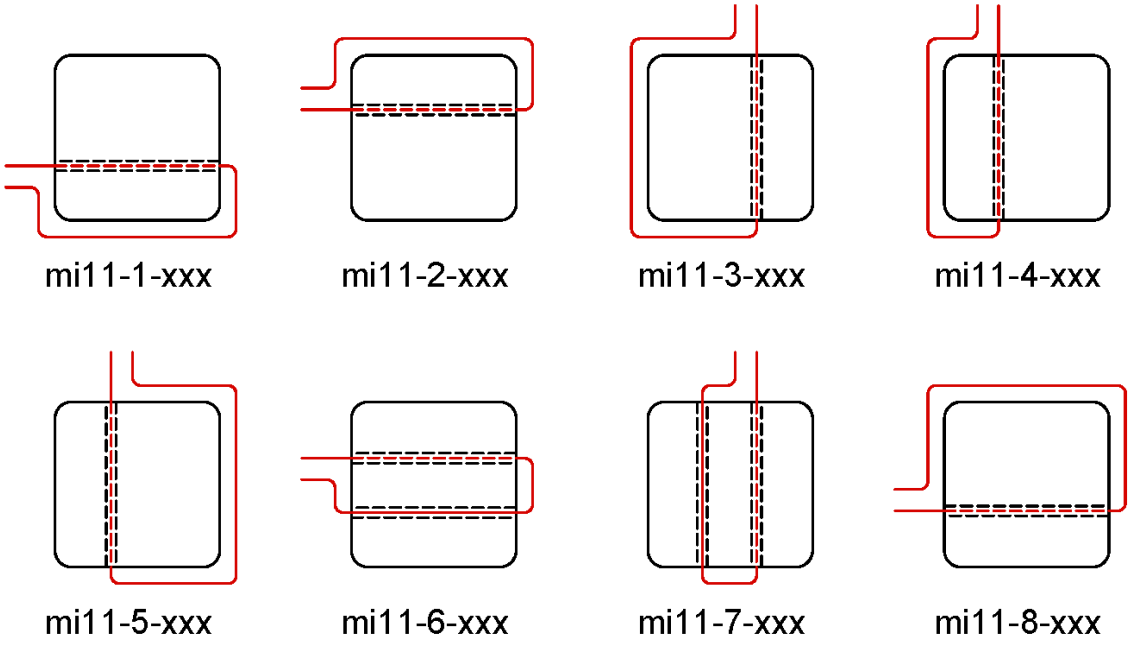

The sets mi11-1-xxx through mi11-8-xxx are the tests on the drilled cores, with probe wires as shown above. In the views, the center of the toroid is below the core, so the top of each sketch is the outside diameter. Horizontal symmetry was assumed, so mi11-4-xxx was not duplicated for the opposite edge. This proved to be an unfortunate decision, as the fluxes of the vertical sections do not add up and I cannot tell why.

Eight sets of data were taken, 131 runs each. Fortunately, the excitation of runs having the same last 3 digits is the same, precisely the same, as closely as can be measured. It is therefore possible to take data from different sets having the same last three digits, and make meaningful comparisons and calculations.

Although the sets are not identified on the graph below, the excitation voltage, the pulse width t_1, and the off time t_0 allow the points to be identified.

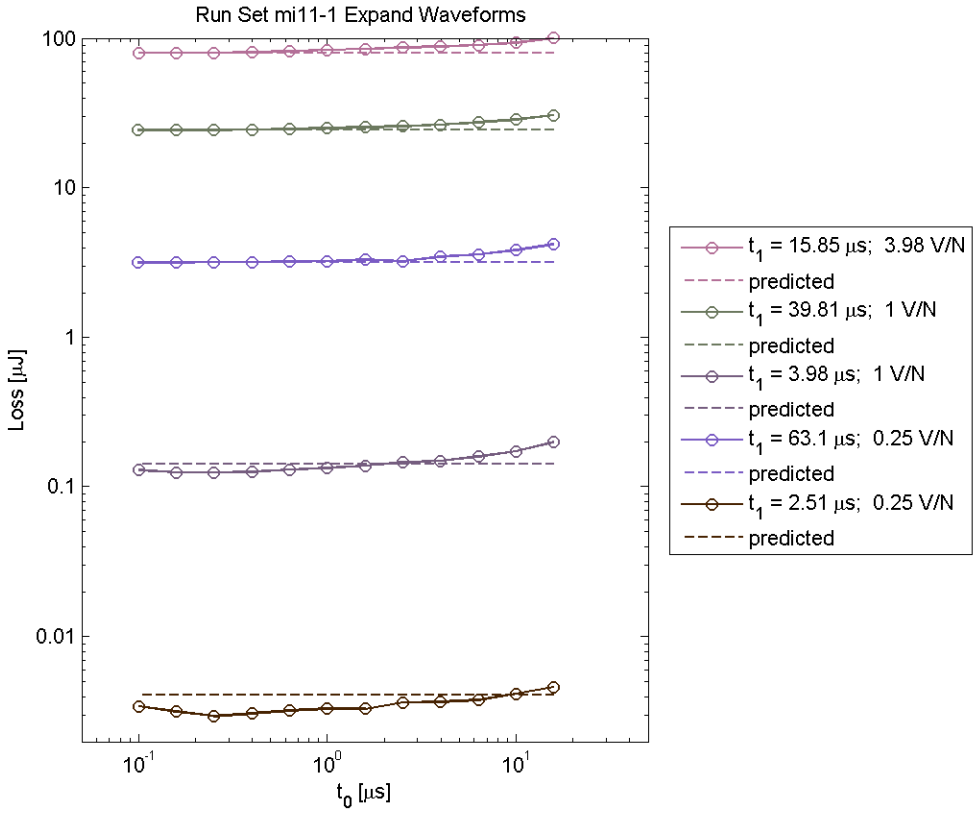

The run Mi11-X-104 excitation is Vi = 0.98 V/n, on time t_1 = 3.92 us, off time t_0 = 4.01 us the period P = 15.85 us. It is therefore the fourth point from the end on the third curve above.

The run Mi11-X-131 excitation is Vi = 3.91 V/n, on time t_1 = 15.78 us, the off time t_0 = 15.72 us the period P = 63 us. It is therefore the last point on the top curve above.

The graphs below show the excitation voltage, current, flux and the hysteresis loop for mi11-X-104 test runs. The graphs use component electrical engineering terms, volts, current and volt-seconds. Conventionally, the curves would be factored by the turns. For the flux graph and the hysteresis loop, the flux and mmf would be factored additionally by the magnetic equivalent dimensions and converted to magnetic parameters.

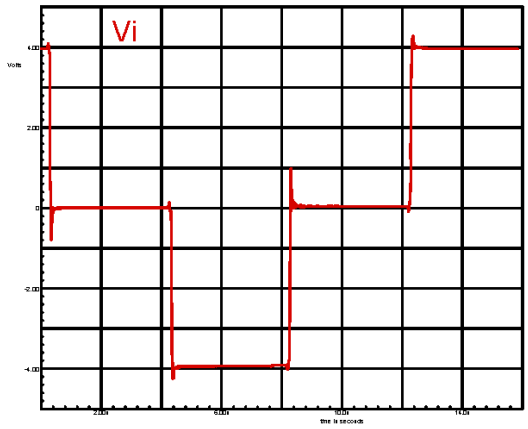

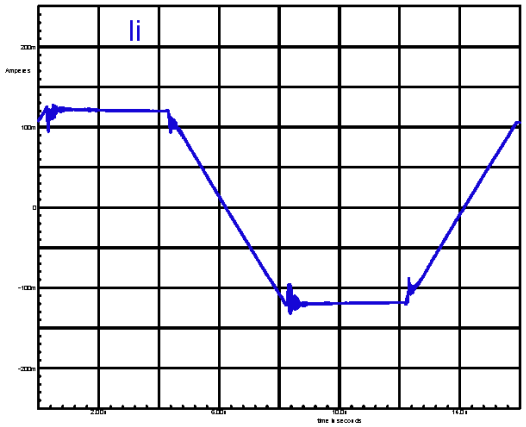

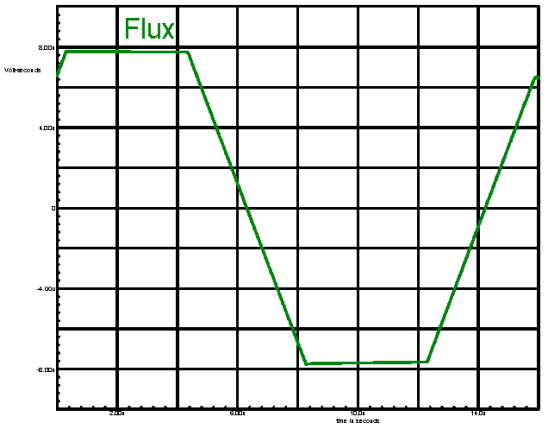

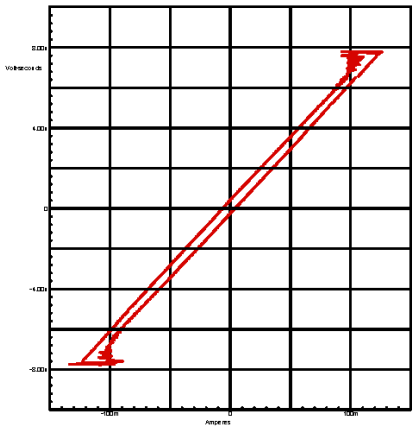

For power calculations, none of that conversion is necessary. This simplifies the loss estimation, and avoids the errors of multiple conversions using unfamiliar parameters.

The first graph below uses SPICE to sum the voltage of the probe windings of the vertical slices and to compare the sum to the volts per turn of the main sense winding. The match is fairly good, but some error can be seen, and it cannot be explained with the available data.

The second graph compares the voltages of the probe windings to each other. There is no reason for the voltage of the inner vertical slice to be higher, steady-state, so likely it has larger area.

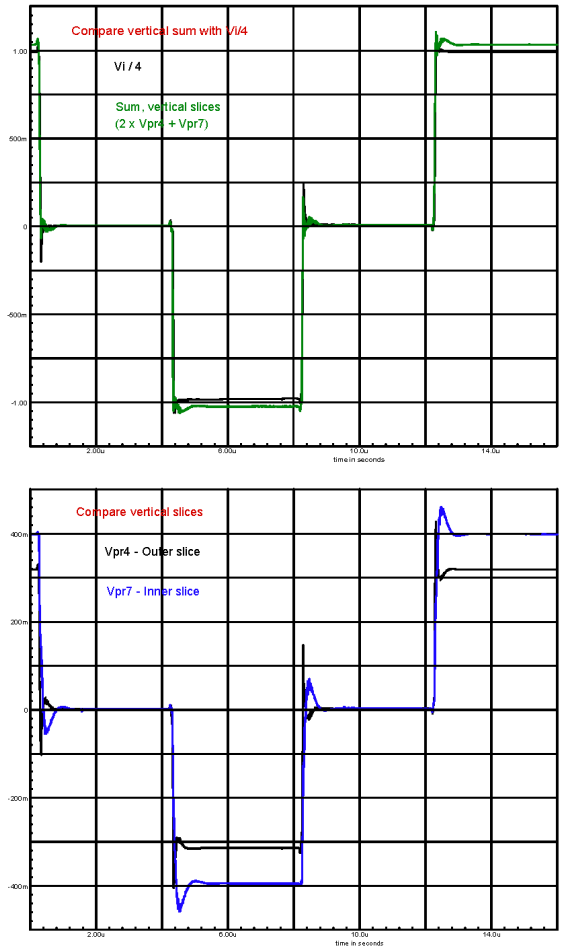

The vertical slices refer to runs mi11-4-104 and mi11-7-104. In taking the sum, the data from mi11-4-104 was doubled, as there is no data for the "third slice", with reference to the core sections shown above.

The first graph below uses SPICE to sum the voltages of the probe windings of the horizontal slices and to compare the sum to the volts per turn of the main sense winding. The match is so good that the curves are indistinguishable.

The second graph compares the voltages of the probe windings. It is not expected that the probe voltage of the central probe would be somewhat grater than the probe voltage of the inner winding, steady-state, so likely it has larger area.

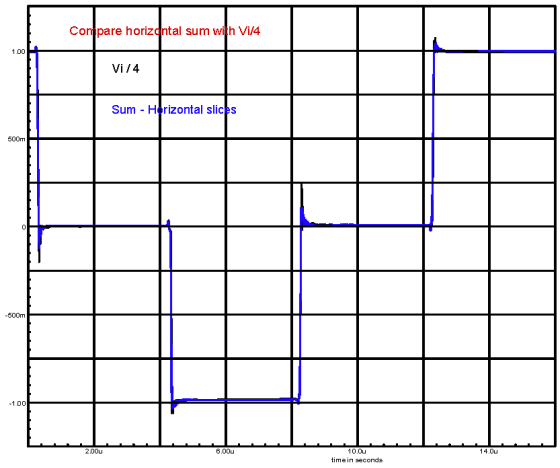

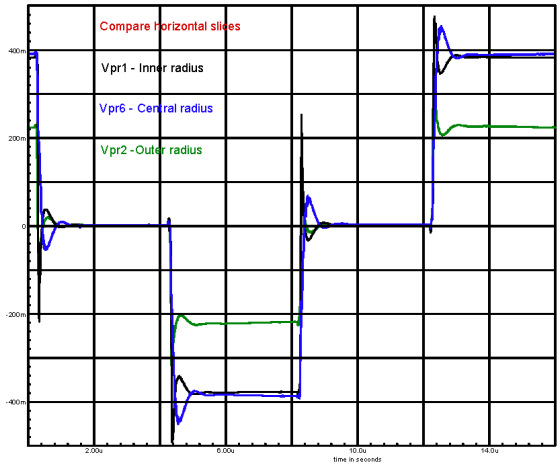

The horizontal slices refer to runs mi11-1-104, mi11-6-104 and mi11-2-104.

The graphs below show the excitation voltage, current, flux and the hysteresis loop for mi11-X-131 test runs. The graphs use component electrical engineering terms, volts, current and volt-seconds.

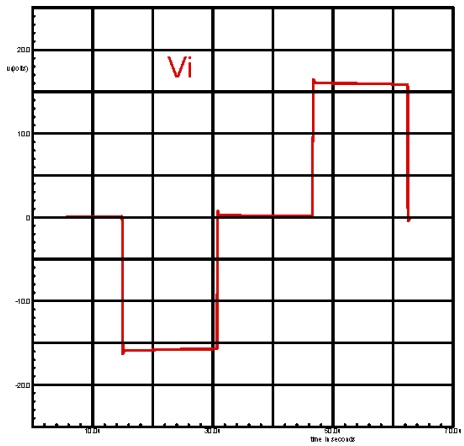

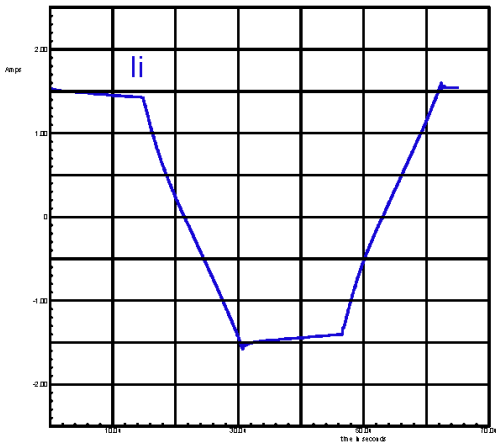

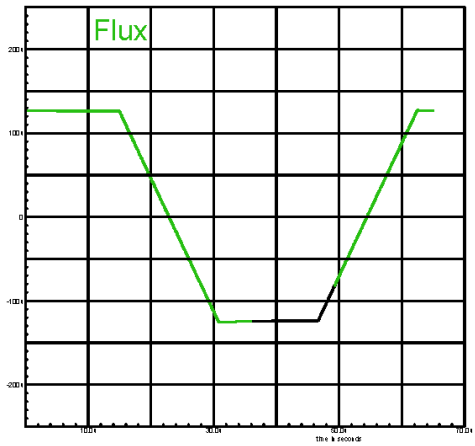

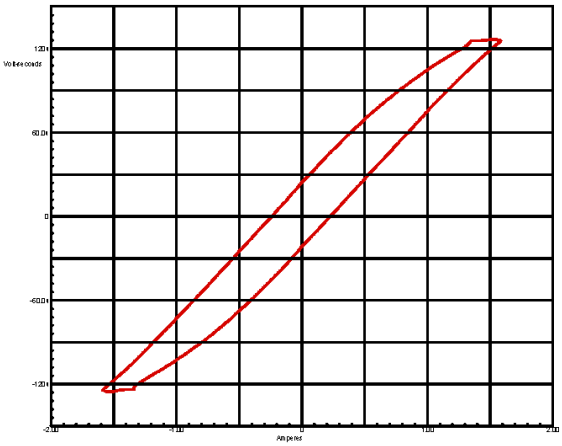

The current and voltage during the off time are shown below with expanded scale. As can be seen in the graphs on the previous page, the current ramp is quite small and the voltage is very low. The small voltage is positive and the current is negative, so that is power out of the core, but the amount of power is too small to account for the off time loss phenomena.

Two loss components are visible. A short exponential reduction in current is followed by a long linear ramp. The latter is probably the very small IR drop of the circuit resistance and the circulating current. The initial exponential current drop probably accounts for most of the lost energy as a reduction of ½ I^2L. The red reference lines were added in CAD.

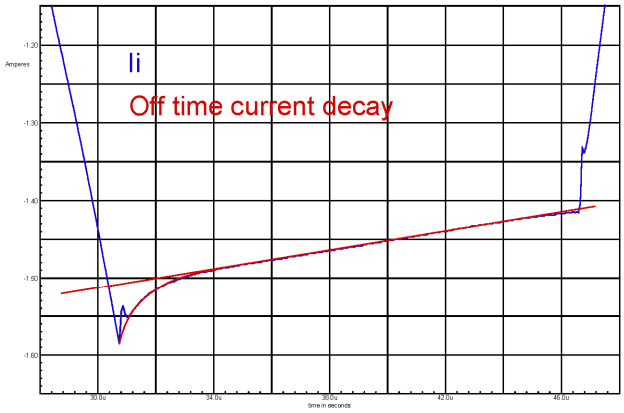

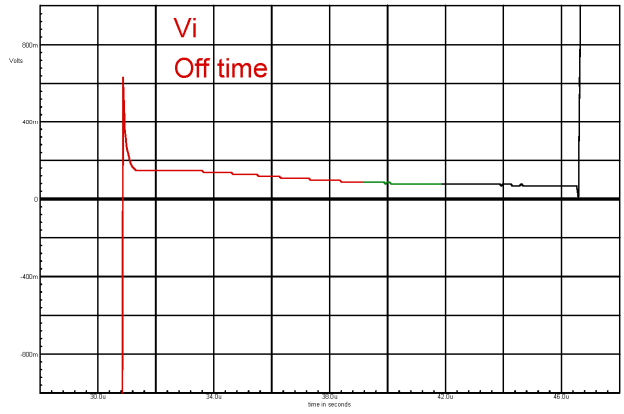

The flux changes revealed by the embedded windings do not appear to be a significant factor in explaining the off time loss phenomena. They are small, and the timing is not consistent.

The first graph below uses SPICE to sum the voltages of the probe windings of the vertical slices and compares the sum to the volts per turn of the main sense winding. The vertical slices refer to runs mi11-4-131 and mi11-7-131, with reference to the core sections shown above. In taking the sum, the data from mi11-4-131 was doubled, as there is no data for the "third slice". The match is pretty good, and the explanation for the bump in the middle is probably that the waveform had to be derived. An attempt to derive the "third slice" as the difference between mi11-5-131 and mi11-7-131 does not seem to work, and there is reason to believe that the embedded probe data for the double slice probe windings in mi11-3-131.csv, mi11-5-131.csv and mi11-8-131.csv are not correct.

The second graph compares the voltages of the probe windings to each other. There is no reason for the voltage of the inner slice to be higher, steady-state, so likely it has larger area.

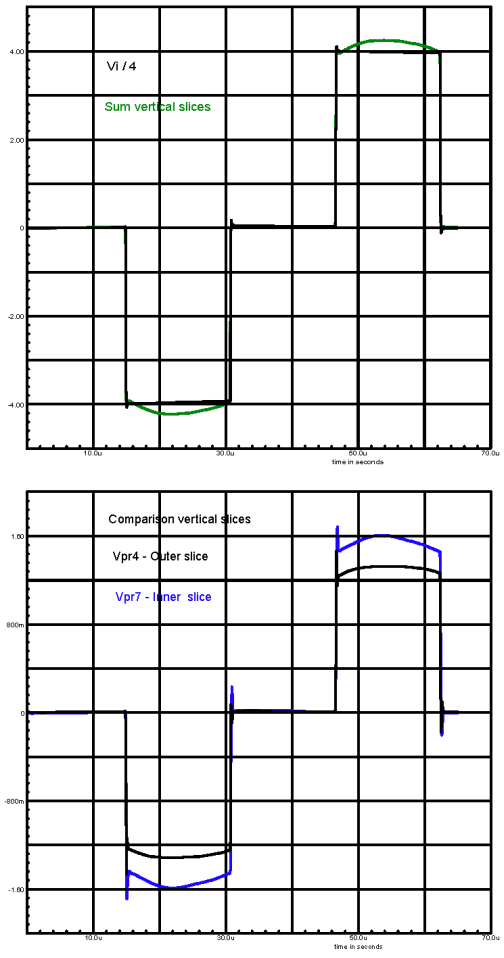

The first graph below uses SPICE to sum the voltages of the probe windings of the horizontal slices and compares it to the sum to the volts per turn of the main sense winding. The match is so good that the curves are indistinguishable.

The second graph compares the voltages of the probe windings to each other. From the mi11-X-104 data above, it is likely that the central slice has larger area, but its bump up in voltage while the voltage of outer slice goes down is unexpected. Note that the flux goes through zero half way through the pulse. The respective voltages are differences in $d\phi/dt$, so it is apparent that the flux distribution is different at low flux.

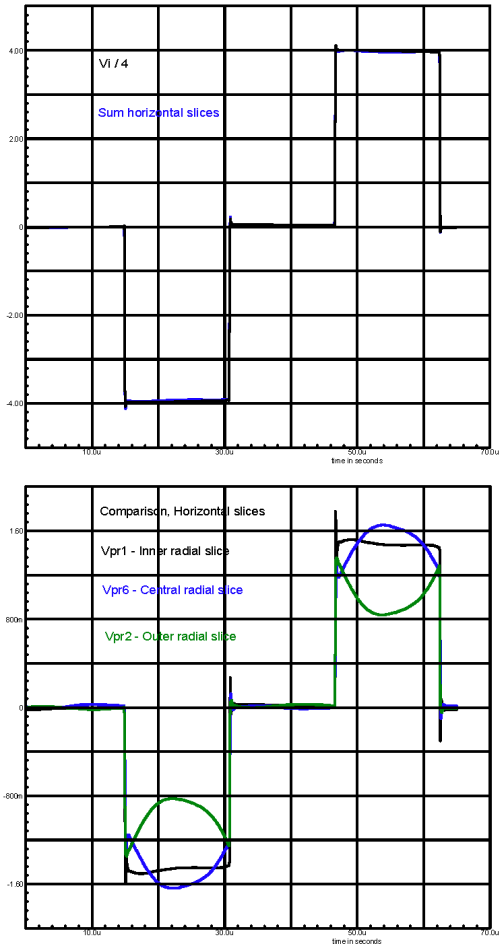

The horizontal slices refer to runs mi11-1-131, mi11-6-131 and mi11-2-131.

The graphs below show the probe winding voltages during the off time, the first graph showing the vertical slices and the second graph showing the horizontal slices.

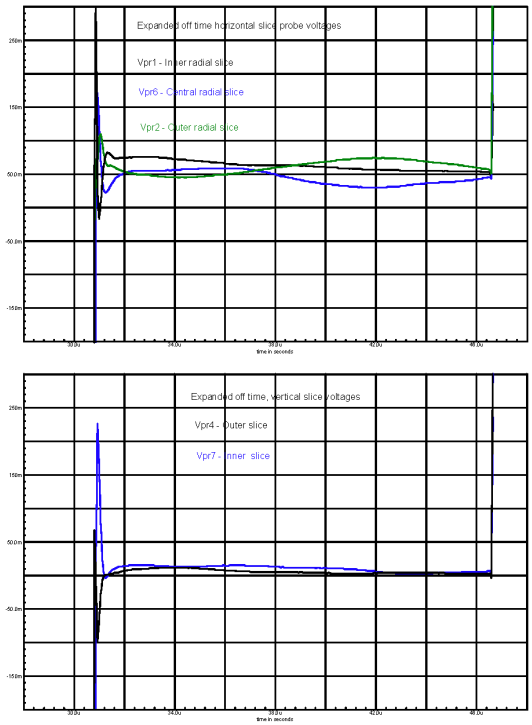

The voltages are extremely small and the timing is inconsistent with their being a significant factor in the explanation of the off time losses.

Appendix I –Simple SPICE model

This section narrates "cook book" style how to make a simple SPICE model of a magnetic core.

Start- with the model of Appendix D, The SPICE Tool, with the three voltage sources "Vi", "Ii" and "Flux." As explained in Appendix D, set up the PWL file for each voltage source and import the data from the Excel Tool.

```
mi01-3-093
```

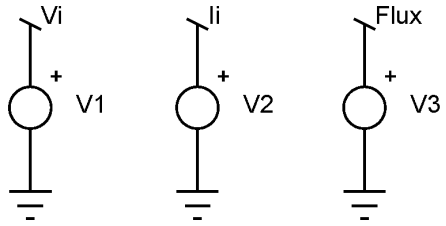

If the voltages are displayed using the scope utility, we can see the input voltage Vi, the input current Ii, and the flux in volt-seconds:

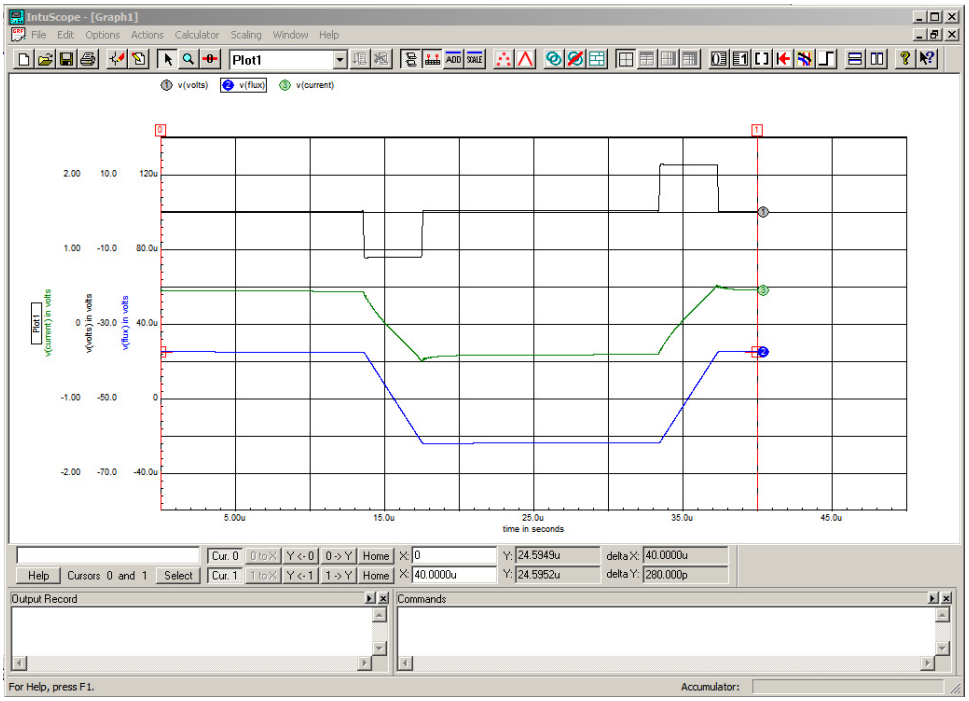

To begin building the SPICE model, add an inductor, and connect it to Vi using a terminal.

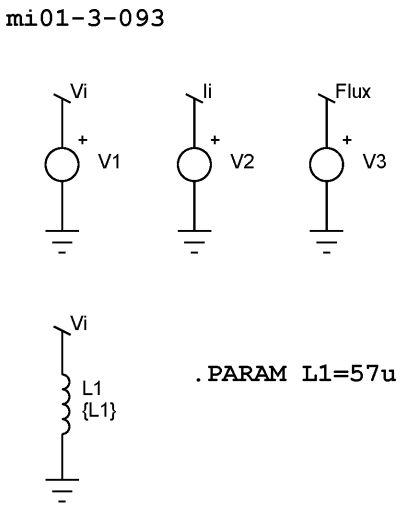

Note that I set the value of the inductor L1 to {L1}, and created a .PARAM statement to set its value. This is unimportant, just my preference. The value of L1 was set by trial and error.

Run the SPICE model, and display the currents Ii and i(L1)

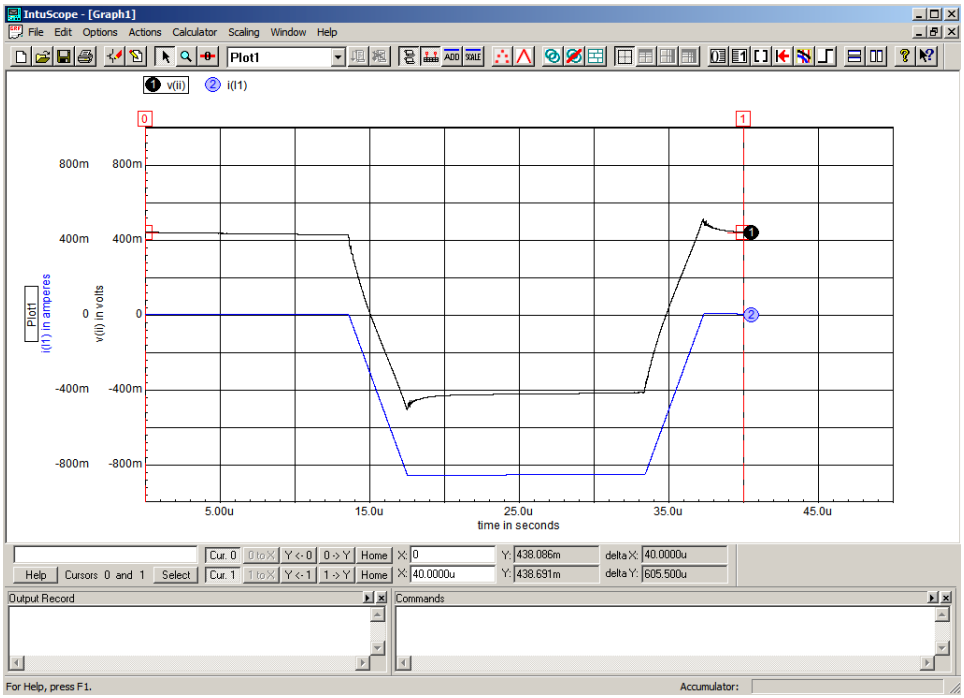

Note the current offset. The exact value can be read from the cursor at the bottom of the screen. This must be added as an "initial condition" for the inductor L1.

mi01-3-093

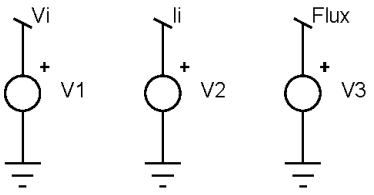

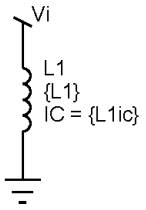


```
.PARAM L1=57u L1ic=438.1m
.PARAM P=39.5u
```

I added as a .PARAM {L1ic} = 438.1 m. I also added a .PARAM P=39.5u. {P} is the period, and can be used to set the run time in the Simulation Setup.

Now the currents look like this:

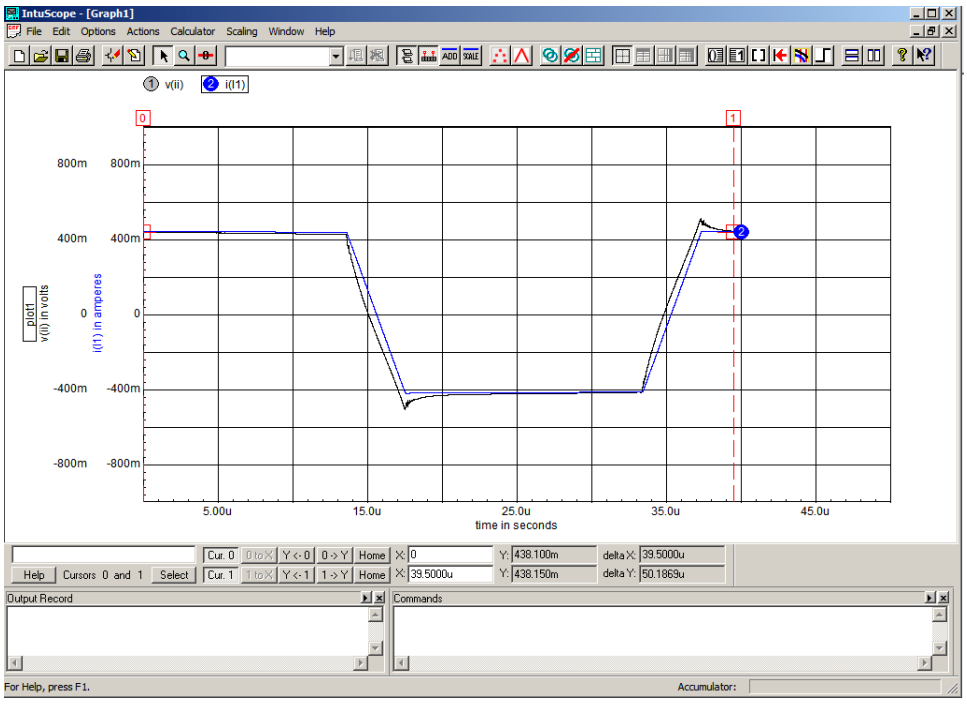

Next, I added another voltage source set at 0 V and named it "Vt," to measure current, a SPICE recommended procedure. I also added a behavioral voltage source with a ground and a terminal "Dif". The formula for the behavioral voltage source is v(Ii) – i(Vt). SPICE does not care that I am subtracting a current from a voltage; it just uses the values of each. This allows me to see how good the model is as I add components.

The objective is to get the model current i(Vt) close to the measured input current v(Ii) using the same excitation voltage v(Vi).

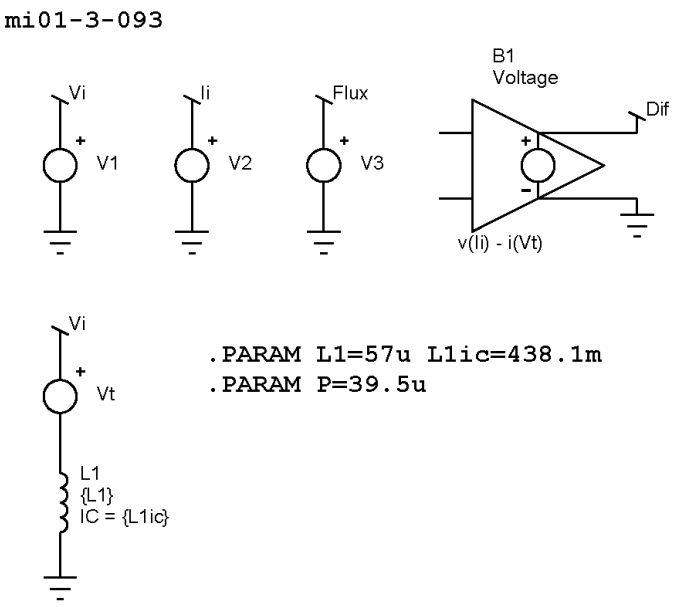

Running it, I can see the following;

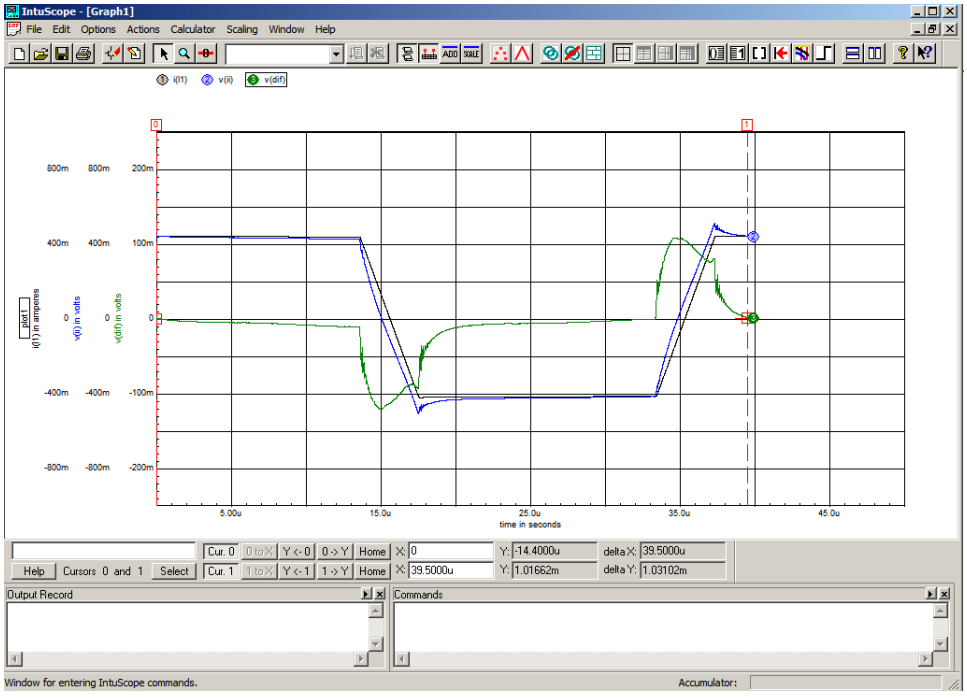

The scale factors of the traces can be set in the SPICE oscilloscope. The scale of Dif is 4 times, so errors are easier to see, but in particular, the vertical distance between the sloped lines is very hard to visualize. Dif shows a much greater error there than is apparent to the eye.

To move more quickly and combine some steps, note the gentle slope of Dif on the left. This is current decay during the off time, and suggests some series resistance. By trial and error, I added {R1} = 0.12. Note also the steep sides of the Dif. This suggests a parallel resistance, and I added {R2} = 500, again by trial and error.

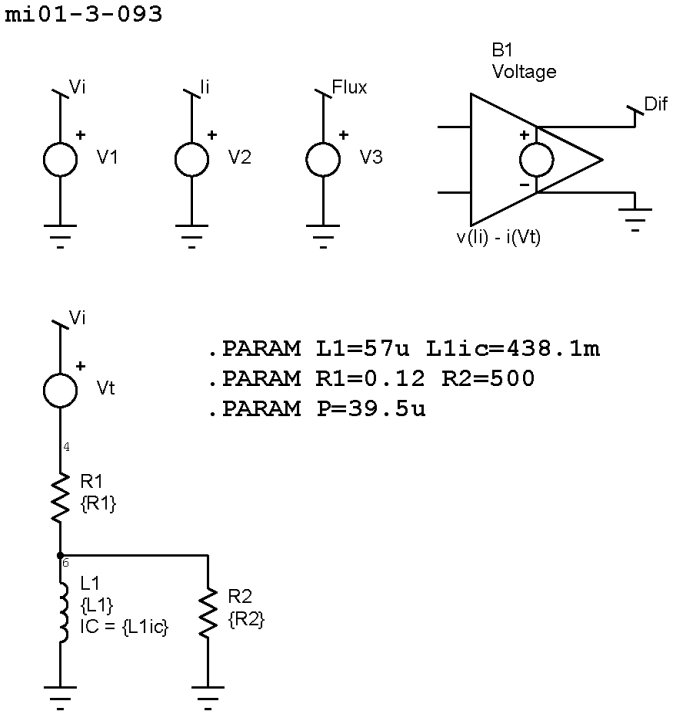

The model is improved somewhat. The Dif error is about 25 % less than it was:

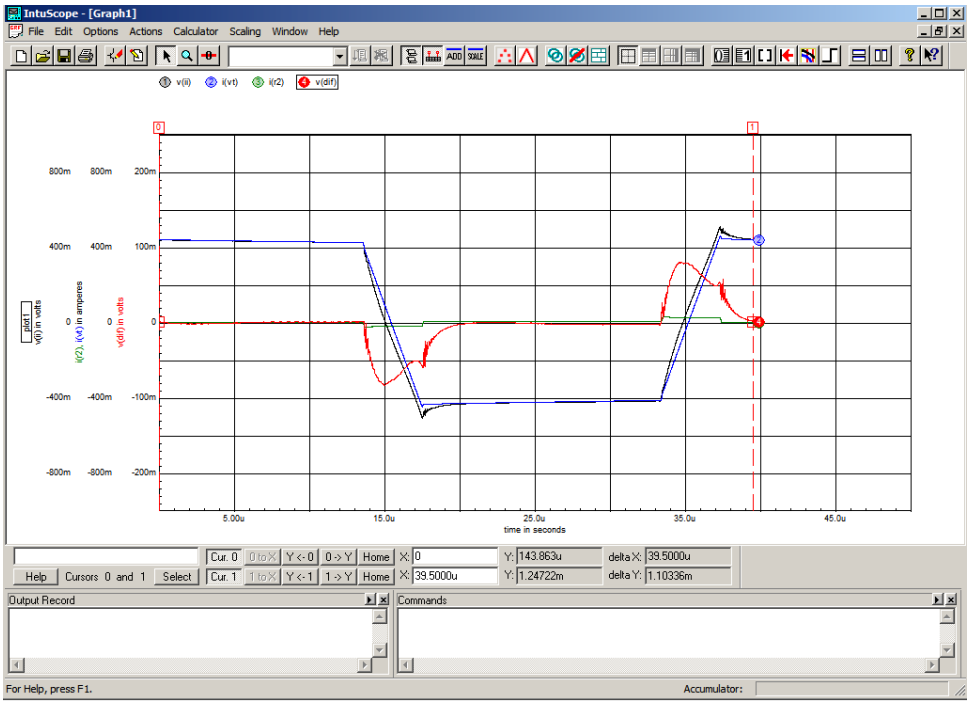

Note that the slight slope error on the left is now gone. The contribution of R2 is small, but it can be seen as the green trace, i(R2).

There is an exponential current increase as the excitation voltage is applied, and an exponential current decrease after the voltage is removed. This can be seen in the v(Ii) trace, but much more clearly in the Dif trace. A series R-L circuit is added, {R3} = 180 and {L2} = 80u.

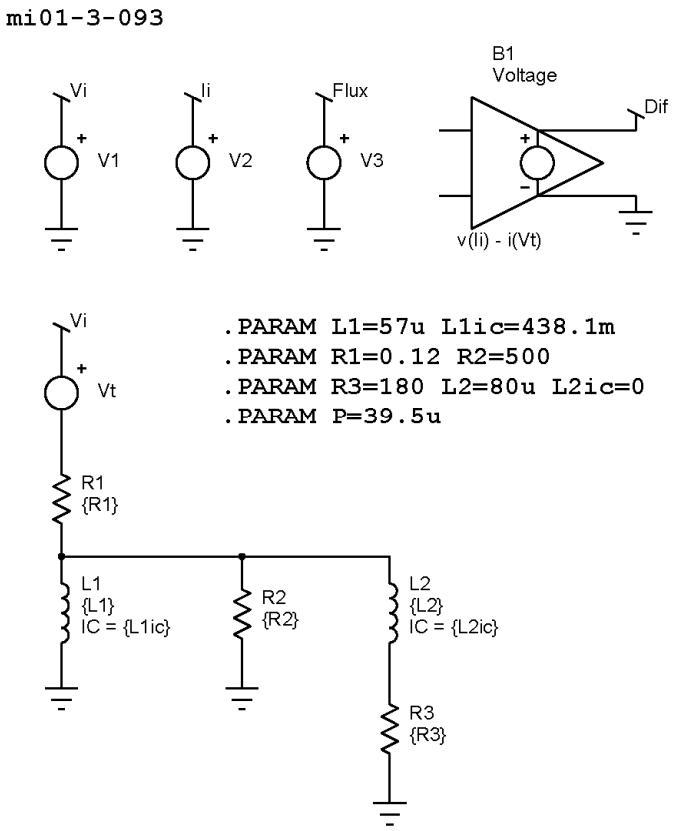

Now the currents can be compared again:

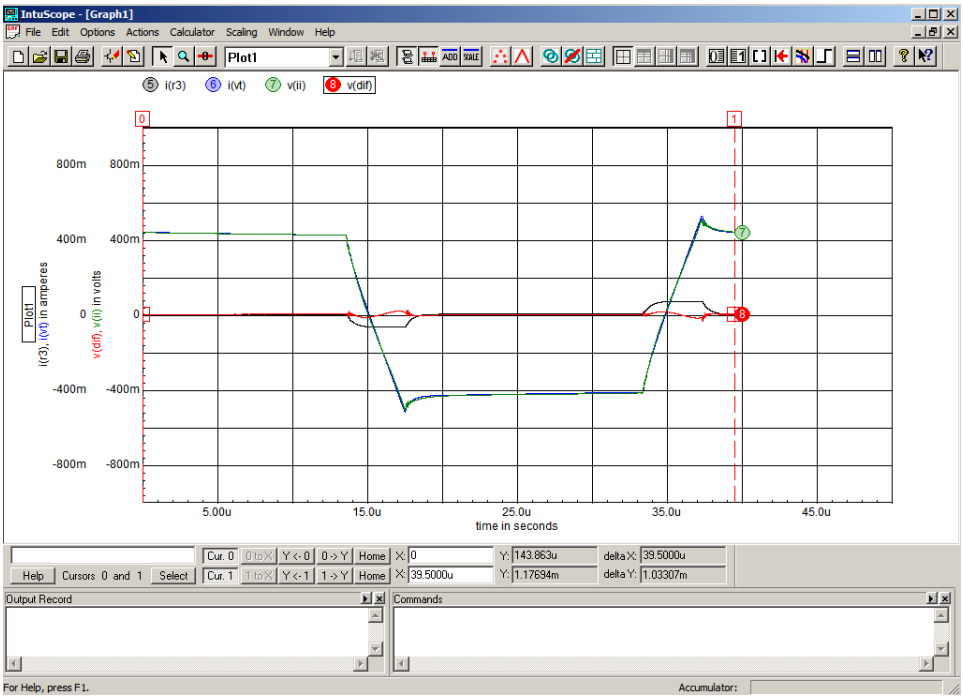

In this picture, the Dif current is shown at the same scale as the model current. I have also shown the contribution of the R-L circuit by displaying i(R3). The match is now fairly good. Notice that the error in the Dif current is not zero, but has nearly equal area above and below 0. There will be a slight error in the shape of the hysteresis loop, but the area within it should be quite close. This can be measured in CAD using the function to measure the area enclosed by a line. Unless scaled rigorously or converted, the area units in CAD will be nonsense, but their relative values are useful for comparison.

With SPICE, the hysteresis loop uses the current as the x-axis, and they are different for the real and modeled hysteresis loops. You could use flux as the x-axis and display both currents vertically, but then the image has to be rotated, flipped and rescaled to look right. I prefer to copy it twice into CAD and do the comparison there.

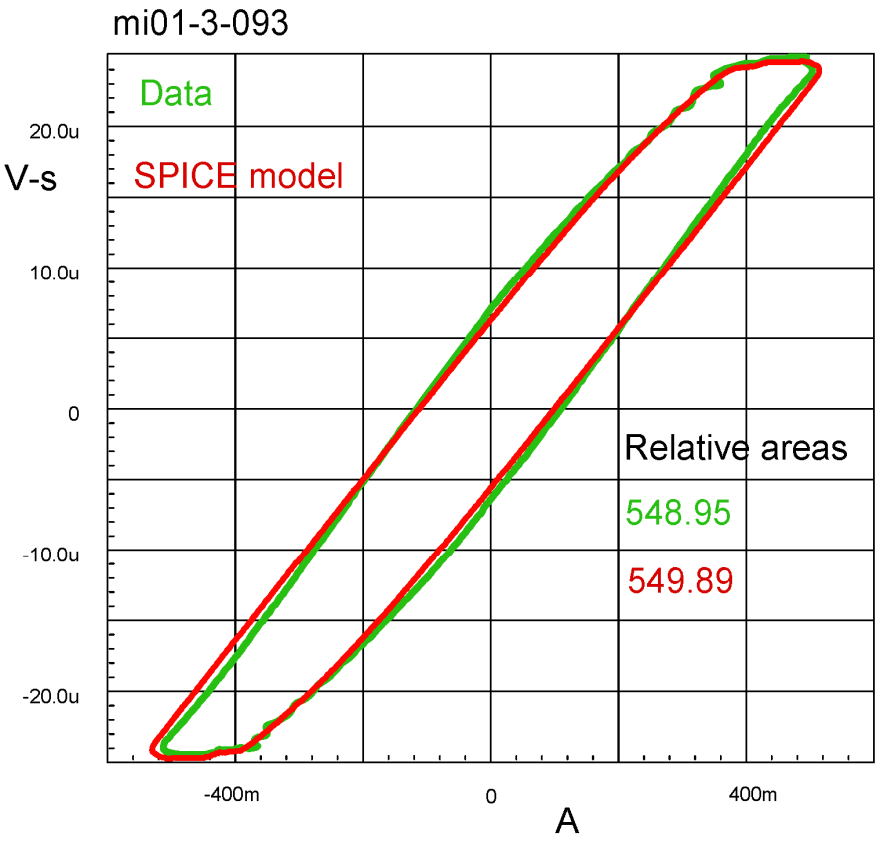

Improving the SPICE model further requires running different waveforms on the model as will be shown below. The parameters can be modified iteratively and new parallel branches can be added to refine the model as much as desired. Manually, this becomes an exercise like the game " Whac-A-Mole," but it is expected that a viable calibration routine can be found with further testing and experience. The temptation to over-refine the model should be avoided–at some point the added accuracy will have diminishing returns and may be dominated by other variables such as lot-to-lot variations.

Some additions to the SPICE model are worthwhile. A behavioral voltage source B3 calculates the loss as the total of the I^2R losses of the resistors. A behavioral voltage source B4 calculates the total stored energy as ½ I^2L for the inductors. The energy lost is calculated in the behavioral current source B7 and the capacitor C3 as the integral of the loss. The total energy is calculated in the behavioral voltage source B9 as the sum of the stored energy and the lost energy.

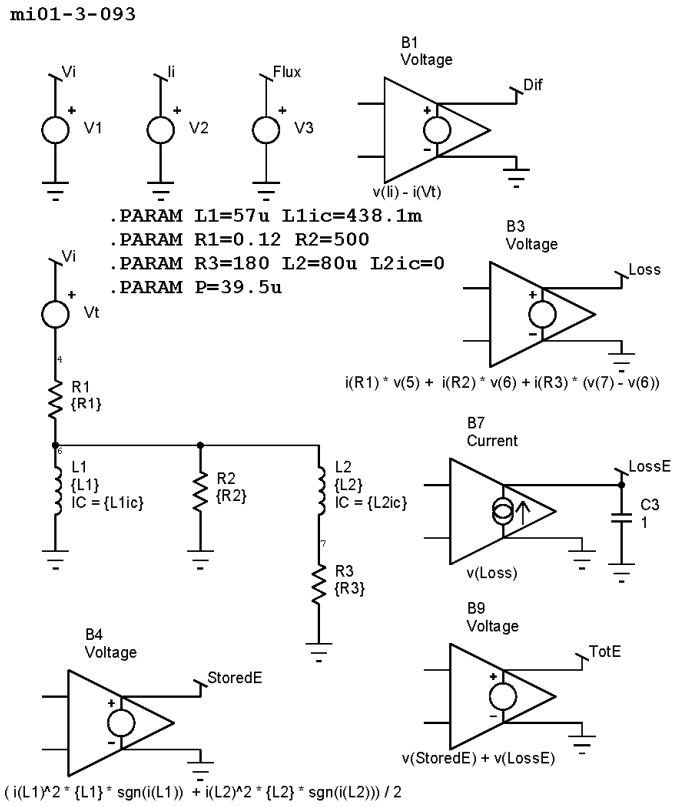

The picture below shows the input voltage Vi and the loss. Note that this is not the same as the Pi shown on the Excel Tool–it is the loss calculated in the model resistances. The loss never goes to zero and persists after the voltage is removed.

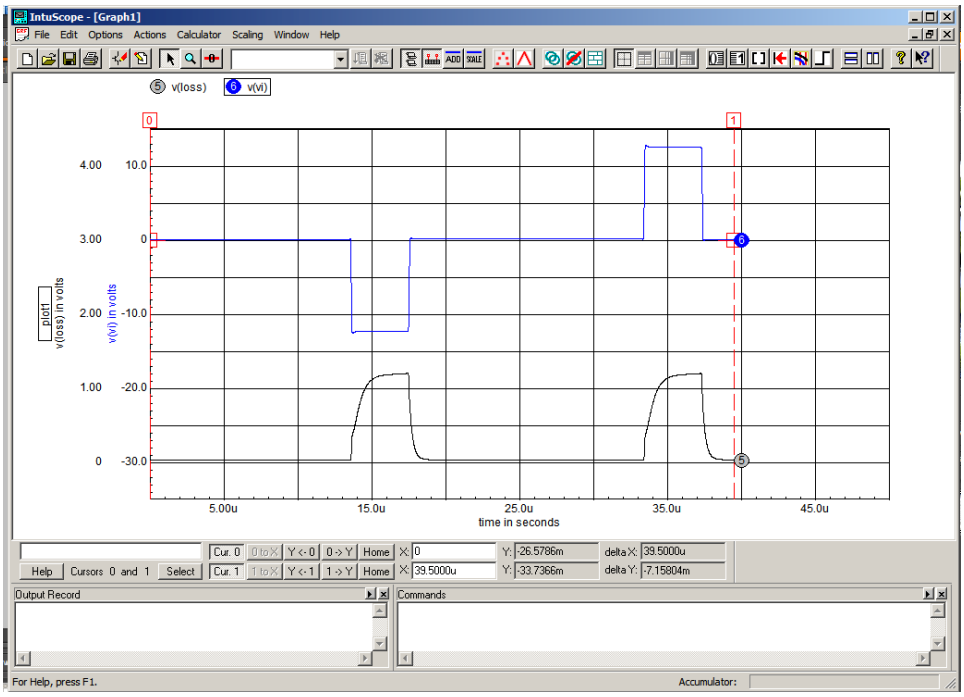

The graph below shows the energy loss, the energy stored and the total energy over the cycle in hte model. The energy loss should equal the energy calculated in the Excel Tool, and it is quite good. The value from the graph can be seen at the bottom as Cur 1 Y = 9.18u. From the Excel Tool, the energy is 9.16E-6 J. This close match exists only because the model is running with the same excitation conditions that were used to make the model.

The energy stored must be equal at the beginning and the end of the cycle if conditions model steady state conditions with a repetitive waveform. The initial stored energy is determined by the inductors and the initial currents specified for them.

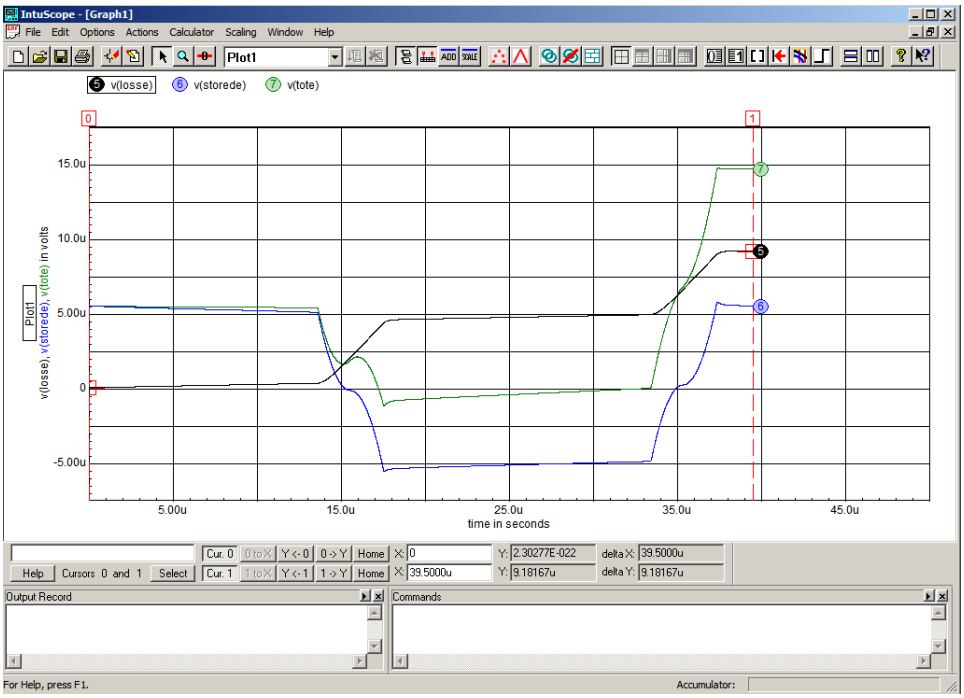

This model allows an estimation of the stored and dissipated energy throughout the cycle. However, before being too pleased, it is necessary to remember that the model is just that, a curve fitting technique, with fudge factors as the component values to get a reasonably good curve fit at the simulated conditions.

Using the model with other waveforms

Ideally, the model would accurately predict the current with other excitation levels and waveforms.

To compare the model using other waveforms, the Excel Tool is updated with the .csv data of the new waveform. This immediately updates the files in the SPICE model as well. However, the period {P} and the initial currents {L1ic} and L2ic} have to be set for the new curve. The data selected is mi01-3-156, a "Hippo curve" with an off-time of 15.8 µs and Vi of 12.5 V. The graph below is copied and pasted from the Excel Tool.

mi01-3-156

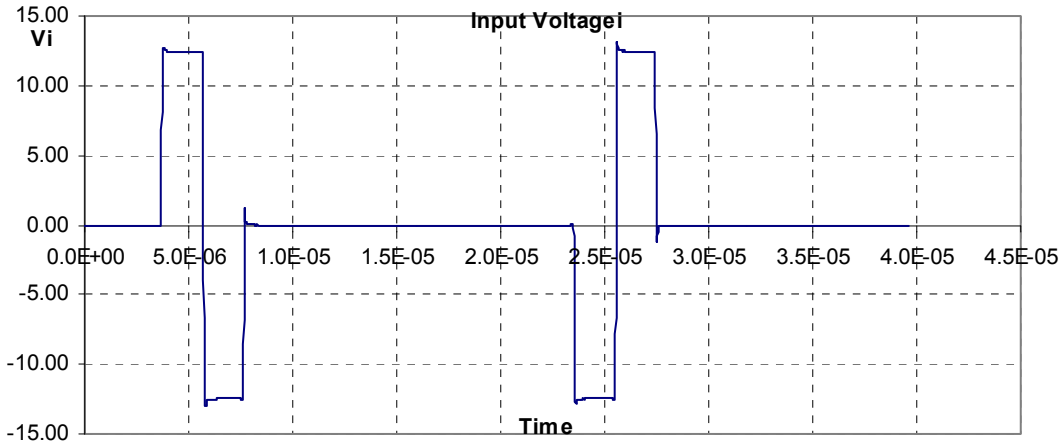

The input current v(Ii) from the .csv data and the model current i(Vt) are shown with the Dif error current. The errors are significant.

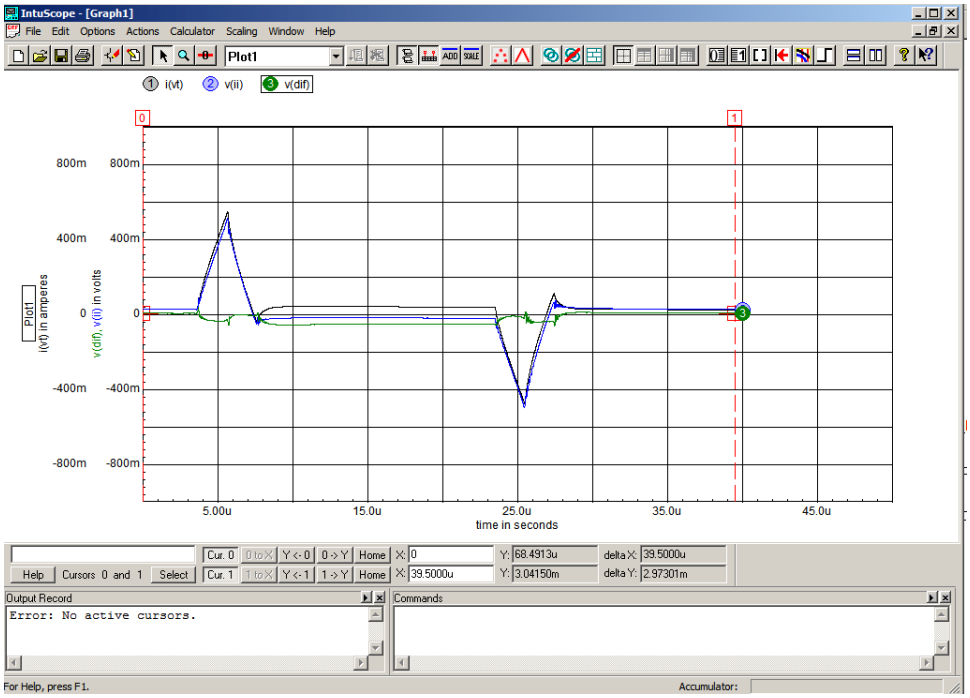

The hysteresis curve for the model vs the data is shown below. The blue hysteresis loop is from the SPICE model and the black hysteresis loop is using the .csv data input current, both with the .csv input flux as the vertical axis. By taking the ratio of the areas inside the hysteresis loops, we find that the model estimates the loss about 12 percent low.

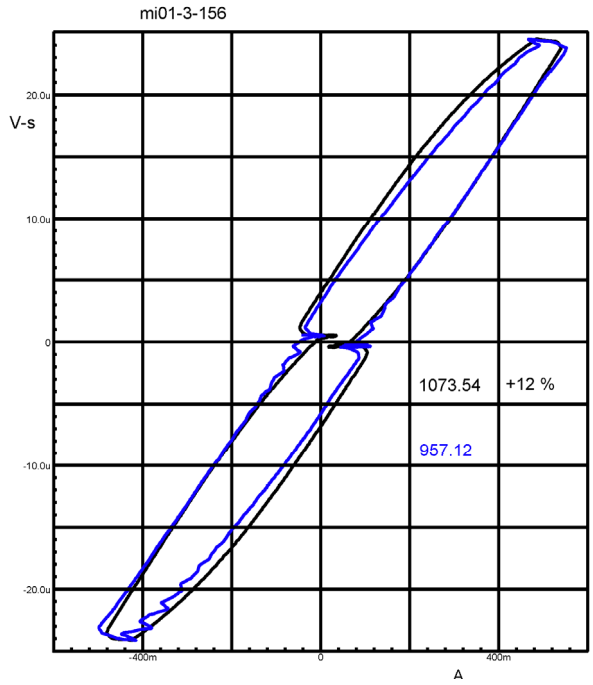

Three more examples are shown below.

Expanded excitation, with an off-time of 4.2 µs and Vi of 5 V.

mi01-3-069

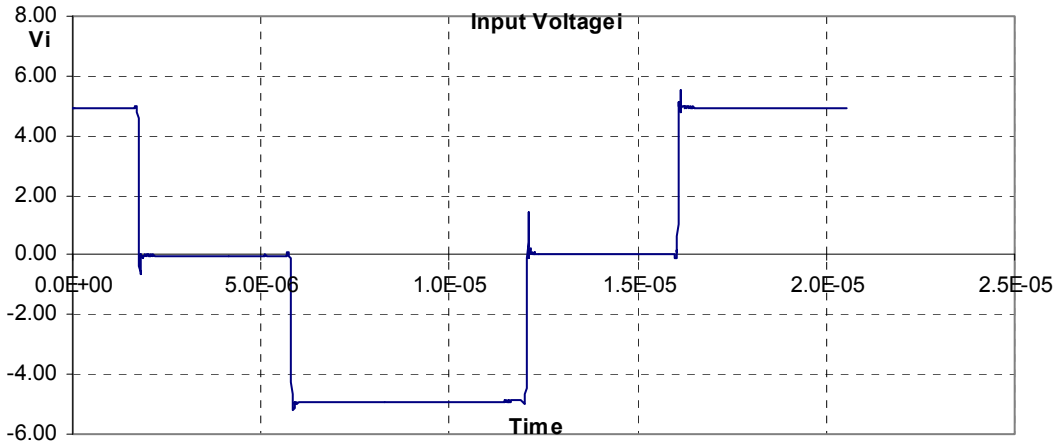

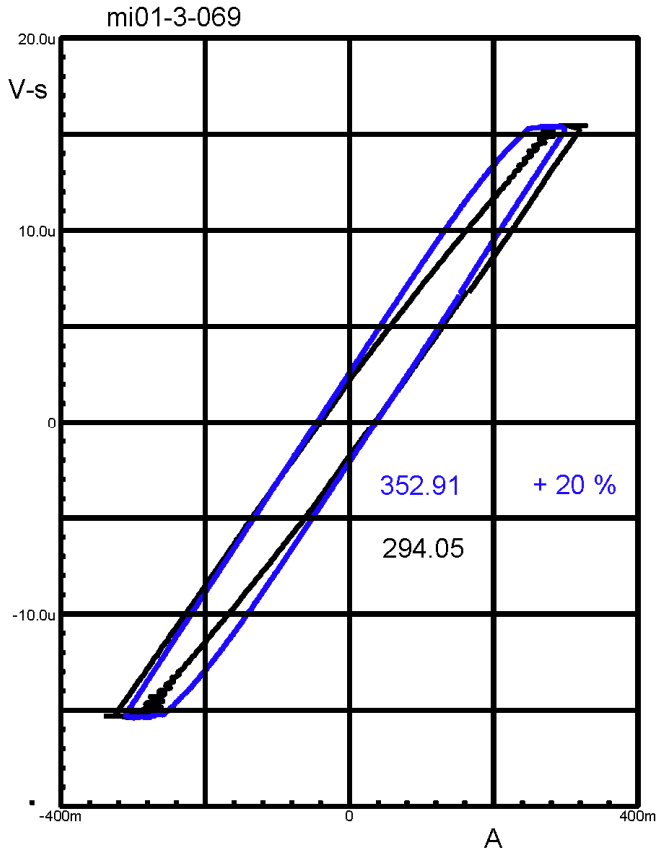

Expanded excittion, with an off-time of 0.125 µs.

mi01-3-082

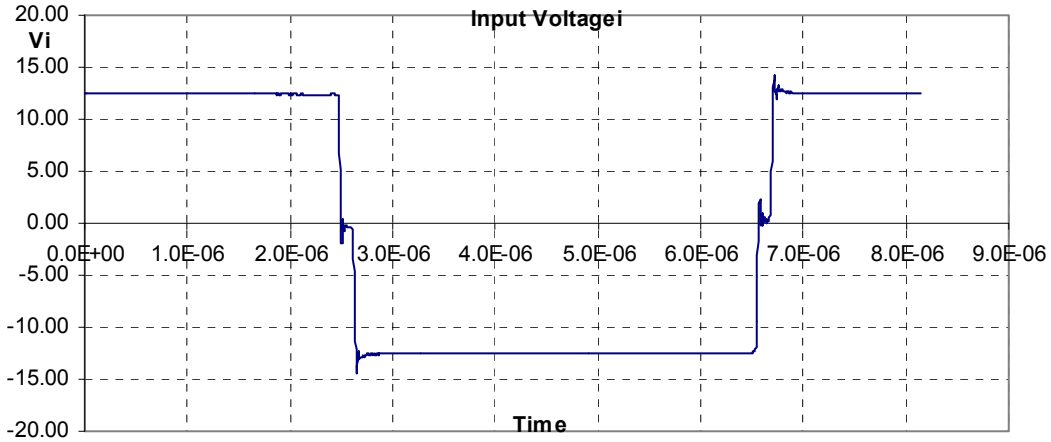

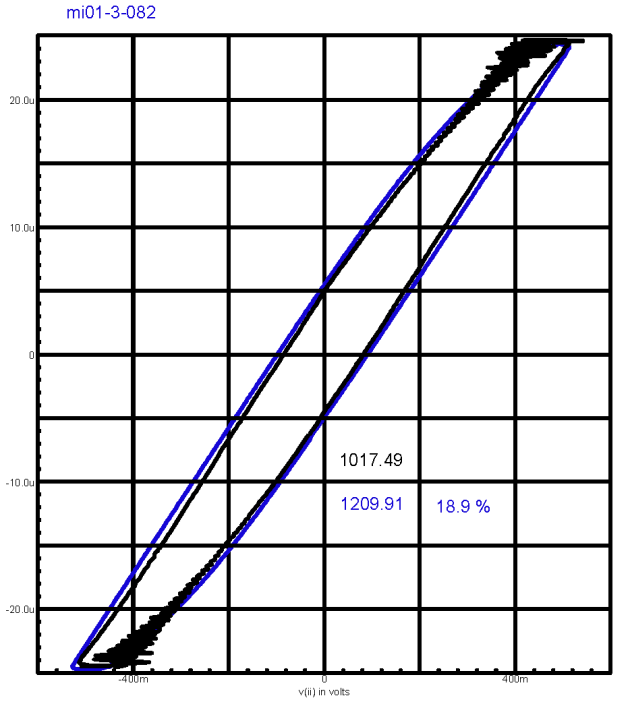

Expanded excitation, with an off-time of 0.67 µs.

mi01-3-086

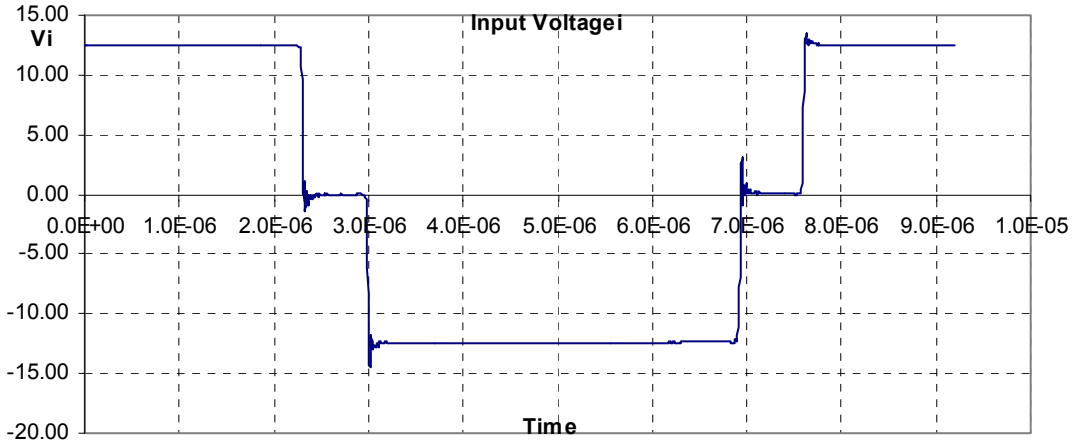

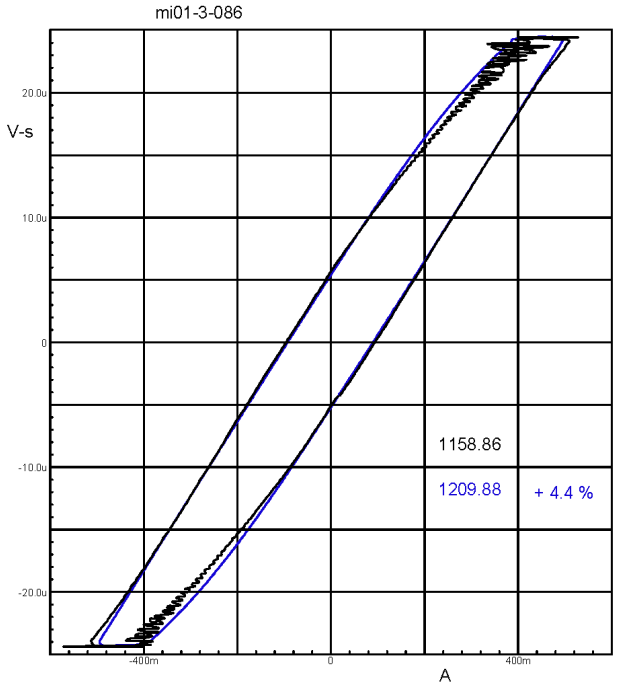

References

[1] *User-friendly Data for Magnetic Core Loss Calculations*, Edward Herbert, Canton, CT. November 10, 2008. This document is in Appendix A, and can be downloaded from http://www.psma.com/coreloss/eh1.pdf

[2] *Improved Core Loss Calculation for Magnetic Components Employed in Power Electronic Systems*, APEC 2011, J. Mühlethaler*, J. Bielay†, J. W. Kolar*, and A. Ecklebez‡, *Power Electronic Systems Laboratory, ETH Zurich, †Laboratory for High Power Electronic Systems, ETH Zurich, ‡ABB Switzerland Ltd., Corporate Research, Baden-Dättwil, Switzerland.

[3] Dr. Sullivan presented a paper at APEC2010, *Core Loss Predictions for General PWM Waveforms from a Simplified Set of Measured Data*

Patent status

This technology may be covered by patents or patents pending.